

**T H E   U N I V E R S I T Y   O F   T U L S A**  
**T H E   G R A D U A T E   S C H O O L**

**N E W   W E L L   T E S T I N G   A P P L I C A T I O N S**  
**O F**  
**T H E   P R E S S U R E   D E R I V A T I V E** /

**by**  
**Mustafa Onur**

**A dissertation submitted in partial fulfillment of**  
**the requirements for the degree of Doctor of Philosophy**  
**in the Discipline of Petroleum Engineering**  
**The Graduate School**  
**The University of Tulsa**  
**1989**

THE UNIVERSITY OF TULSA  
THE GRADUATE SCHOOL

NEW WELL TESTING APPLICATIONS  
OF  
THE PRESSURE DERIVATIVE

A DISSERTATION  
APPROVED FOR THE DISCIPLINE OF  
PETROLEUM ENGINEERING

By Dissertation Committee

Albert C. Reynolds Jr., Chairperson  
~~John S. ...~~  
~~...~~  
~~...~~  
~~...~~

## ABSTRACT

**Onur, Mustafa (Doctor of Philosophy in Petroleum Engineering)**

**New Well Testing Applications of The Pressure Derivative**

**(245 pp. - Chapter V)**

**Directed by Dr. Albert C. Reynolds, Jr.**

**(350 words)**

Type curves based on pressure derivatives have become highly popular for analyzing well test data. This work presents new derivative type curves based on a new derivative group which is equal to the dimensionless pressure group divided by its logarithmic derivative with respect to dimensionless time group. One major advantage of these type curves is that the type-curve match of field pressure/pressure-derivative data with the new derivative type curves is accomplished by moving the field data plot in only the horizontal direction. This type-curve match fixes time match-point values. The pressure change versus time data is then matched with the dimensionless pressure solution to determine pressure match-point values. Well/reservoir parameters can then be estimated in the standard way. This two step type-curve matching procedure increases the likelihood of obtaining a unique match. Moreover, the unique correspondence between the ordinate of the field data plot and the new derivative type curves should prove useful in determining whether given field data actually represents the well/reservoir model assumed by a selected type curve solution. It is also shown that the basic idea used in constructing the type curves can be used to ensure that proper semilog straight lines are chosen when analyzing pressure data by semilog methods. Analysis of both drawdown and buildup data is considered and actual field cases are analyzed using the new derivative type curves and the semilog identification method.

This work also presents new methods based on the pressure derivative to analyze buildup data obtained at a well (fractured or unfractured) produced to pseudosteady-state prior to shut-in. By using a method of analysis based on the pressure derivative, it is shown that a well's drainage area at the instant of shut-in and the flow capacity can be computed directly from buildup data even in cases where conventional semilog straight lines are not well-defined. By using the estimate of drainage area obtained from the derivative analysis, one can construct a modified semilog plot of pressure buildup data versus time which properly accounts for producing time effects.

## ACKNOWLEDGEMENTS

I wish to express my sincere appreciation to my advisor, Dr. Albert Reynolds, for his guidance and support throughout the course of this study. The constructive comments of the Dissertation Committee, Dr. R. Cerro, Dr. D. Doty, Dr. O. Shoham and Dr. Macias-Chapa are deeply appreciated.

The financial support of the Ministry of Education of Turkey and partial assistanships provided by the University of Tulsa are gratefully acknowledged. Funds for computer time were provided by the University of Tulsa.

Finally, I wish to thank my parents and my wife for their moral support and encouragement throughout my studies in the United States. Without their sacrifices, my success would not have been possible.

This dissertation is dedicated to my loving wife Ayşegül Onur and to my daughter Berfin Onur for their endless patience and understanding.

## TABLE OF CONTENTS

	<u>Page</u>
TITLE PAGE . . . . .	i
APPROVAL PAGE . . . . .	ii
ABSTRACT . . . . .	iii
ACKNOWLEDGMENTS . . . . .	v
TABLE OF CONTENTS . . . . .	vi
LIST OF TABLES . . . . .	x
LIST OF FIGURES . . . . .	xi
CHAPTER I INTRODUCTION . . . . .	1
CHAPTER II NEW PRESSURE-DERIVATIVE GROUP . . . . .	6
2.1 Definitions . . . . .	6
2.2 Theory . . . . .	7
2.3 Numerical Differentiation of Pressure-Time Data . . . . .	10
CHAPTER III APPLICATIONS OF NEW PRESSURE-DERIVATIVE GROUP . . . . .	19
3.1 New Type Curves For Well Test Analysis . . . . .	19
3.1.1 Line Source solution . . . . .	20
3.1.2 Wellbore Storage and Skin; Unfractured Well . . . . .	24
3.1.3 Planar Fractures; Drawdown . . . . .	32
3.1.4 Planar Fractures; Buildup . . . . .	39
3.1.5 Planar Fractures with Wellbore Storage . . . . .	50
3.1.6 Finite-Conductivity Fractures . . . . .	58
3.1.7 Unfractured Well in a Closed Bounded Reservoir;	

## TABLE OF CONTENTS (Continued)

	<u>Page</u>
Constant Rate Production . . . . .	71
3.1.8 Planar Fractured Well in a Closed Bounded Reservoir . . . . .	76
3.1.8.1 Constant Rate Production . . . . .	76
3.1.8.2 Constant Pressure Production . . . . .	82
3.2 Identification of Semilog Straight Lines . . . . .	90
3.2.1 Composite Reservoir . . . . .	90
3.2.2 Naturally Fractured Reservoir . . . . .	96
3.3 Example Applications . . . . .	103
3.3.1 Wellbore Storage and Skin; Buildup Example . . . . .	103
3.3.2 Wellbore Storage and Skin; Drawdown Example . . . . .	106
3.3.3 Infinite-Conductivity Fracture; Buildup Example . . . . .	117
3.3.4 Finite-Conductivity Fracture; Drawdown Example . . . . .	123
3.3.5 Finite-Conductivity Fracture; Buildup Example . . . . .	127

CHAPTER IV ANALYSIS OF PRESSURE BUILDUP DATA USING THE PRESSURE DERIVATIVE . . . . .	135
4.1 Assumptions and Definitions . . . . .	137
4.2 General Buildup Solution . . . . .	139
4.3 Unfractured Wells . . . . .	142
4.3.1 Single Well in a Closed Reservoir . . . . .	144

TABLE OF CONTENTS (Continued)

	<u>Page</u>
4.3.2 Analysis Procedure . . . . .	153
4.3.3 Well Located in an Infinite Multi-Well Pattern . . . . .	158
4.3.4 Multi-Well System in a Closed Bounded Reservoir . . . . .	163
4.4 Fractured Wells . . . . .	177
4.4.1 Single Well in a Closed Reservoir . . . . .	177
4.4.2 Analysis Procedure . . . . .	183
4.4.3 Well Located in an Infinite Multi-Well Pattern . . . . .	186
4.5 Wellbore Storage and Skin Effects . . . . .	191
4.6 Field Example . . . . .	199
CHAPTER V CONCLUSIONS . . . . .	206
NOMENCLATURE . . . . .	209
REFERENCES . . . . .	213
APPENDIX A - SHORT AND LONG TIME APPROXIMATIONS PLANAR FRACTURES; DRAWDOWN . . . . .	222
APPENDIX B - SHORT AND LONG TIME APPROXIMATIONS PLANAR FRACTURES; BUILDUP . . . . .	227
APPENDIX C - DERIVATIONS OF EQS. 3.1.116 THROUGH 3.1.118 CONSTANT PRESSURE PRODUCTION . . . . .	231
APPENDIX D - DERIVATIONS OF EQS. 3.2.11 THROUGH 3.2.13 COMPOSITE RESERVOIR . . . . .	234
APPENDIX E - DERIVATION OF BUILDUP PRESSURE EQUATION FOR A WELL LOCATED IN A MULTI-WELL	



TABLE OF CONTENTS (Continued)

	<u>Page</u>
SYSTEM . . . . .	237
APPENDIX F - BUILDUP RESPONSE OF A FINITE-CONDUCTIVITY VERTICALLY FRACTURED WELL DURING BILINEAR FLOW REGIME . . . . .	243

## LIST OF TABLES

<u>Table</u>	<u>Page</u>
2.3.1 Reservoir/Well Parameters; Test 1 of Ref. 6 . . . . .	13
2.3.2 Comparison of Numerical Differentiation Techniques; Test 1 of Ref. 6 . . . . .	14
3.3.1 Wellbore Storage and Skin; Drawdown Example, Ref. 81 - Reservoir/Well Parameters . . . . .	108
3.3.2 Wellbore Storage and Skin; Drawdown Example, Ref. 81 - Pressure and Derivative Versus Time Data . . . . .	110
3.3.3 Infinite-Conductivity Fracture; Buildup Example, Ref. 18 - Reservoir/Well Parameters . . . . .	118
3.3.4 Infinite-Conductivity Fracture; Buildup Example, Ref. 18 - Pressure and Derivative Versus Time Data . . . . .	119
3.3.5 Finite-Conductivity Fracture; Drawdown Example, Ref. 20 - Reservoir/Well Parameters . . . . .	124
3.3.6 Finite-Conductivity Fracture; Drawdown Example, Ref. 20 - Pressure and Derivative Versus Time Data . . . . .	125
3.3.7 Finite-Conductivity Fracture; Buildup Example, Ref. 83 - Pseudopressure and Derivative Versus Time Data . . . . .	130
4.3.1 Departure Times and Starting Times of Pseudosteady-State Flow for Various Closed Single-Well Drainage Shapes . . . . .	155
4.3.2 Well/Reservoir Cases Considered for Results of Figs. 4.3.8 and 4.3.9 . . . . .	171
4.6.1 Reservoir/Well Parameters; Field Example . . . . .	200
4.6.2 Pressure and Derivative Versus Time Data . . . . .	201

## LIST OF FIGURES

<u>Figure</u>	<u>Page</u>
2.3.1 Comparison of Numerical Differentiation Techniques; Test 1 of Ref. 6 . . . . .	18
3.1.1 New Line Source Solution Type Curve . . . . .	22
3.1.2 Bourdet <i>et al.</i> 's Wellbore Storage and Skin Type Curve . . . . .	26
3.1.3 New Wellbore Storage and Skin Type Curve Based on $p_{wD}$ and $p_{wD}/(2p'_{wD})$ . . . . .	28
3.1.4 New Wellbore Storage and Skin Type Curve Including Two Derivative Groups . . . . .	31
3.1.5 New Uniform-Flux Fracture Type Curve Including $p_{wD}$ , $p_{wD}/(2p'_{wD})$ and $2p'_{wD}/p_{wD}$ . . . . .	35
3.1.6 New Infinite-Conductivity Fracture Type Curve Including $p_{wD}$ , $p_{wD}/(2p'_{wD})$ and $2p'_{wD}/p_{wD}$ . . . . .	37
3.1.7 Comparison of Uniform-Flux and Infinite-Conductivity Fractured Well Solutions . . . . .	38
3.1.8 Effect of Producing Time on Correlation of Buildup Data With Uniform-Flux Drawdown Type Curve . . . . .	45
3.1.9 Effect of Producing Time on Correlation of Buildup Data With Infinite-Conductivity Drawdown Type Curve . . . . .	46
3.1.10 New Buildup Type Curve Based on $\tilde{p}_{sD}$ and $\tilde{p}_{sD}/(2\tilde{p}'_{sD})$ - Uniform-Flux Fracture . . . . .	48
3.1.11 New Type Curve Including $p_{wD}$ and $p'_{wD}$ ; Uniform-Flux Fracture With Wellbore Storage . . . . .	52
3.1.12 New Type Curve Including $p_{wD}$ and $p'_{wD}$ ; Infinite-Conductivity Fracture With Wellbore Storage . . . . .	53
3.1.13 New Type Curve Based on $p_{wD}/(2p'_{wD})$ - Uniform-Flux Fracture	

## LIST OF FIGURES (Continued)

<u>Figure</u>	<u>Page</u>
With Wellbore Storage . . . . .	55
3.1.14 New Type Curve Based on $p_{wD}/(2p'_{wD})$ - Infinite-Conductivity Fracture With Wellbore Storage . . . . .	56
3.1.15 Finite-Conductivity Fractured Well Geometry - Plan View . . . . .	59
3.1.16 Wong <i>et al.</i> 's Finite-Conductivity Fractured Well Type Curve . . . . .	62
3.1.17 New Finite-Conductivity Fractured Well Type Curve Based on $p_{wD}/(2p'_{wD})$ Versus $C_{fD}^2 t_{x_fD}$ . . . . .	66
3.1.18 Finite-Conductivity Type Curve Based on $p_{wD}$ and $p'_{wD}$ Versus $t_{x_fD}$ . . . . .	68
3.1.19 Finite-Conductivity Type Curve Based on $p_{wD}/(2p'_{wD})$ Versus $t_{x_fD}$ . . . . .	69
3.1.20 Finite-Conductivity Type Curve Based on Effective Wellbore Radius . . . . .	70
3.1.21 Type Curve Based on $p_{wD}$ and $p_{wD}/(2p'_{wD})$ ; Unfractured Well in Closed Square Reservoir . . . . .	74
3.1.22 New Uniform-Flux Type Closed Square Reservoir; Constant Rate Production . . . . .	77
3.1.23 New Infinite-Conductivity Type Closed Square Reservoir; Constant Rate Production . . . . .	78
3.1.24 Uniform-Flux Type Curve for Simultaneous Matching of Pressure and Pressure Derivative Data . . . . .	83
3.1.25 Infinite-Conductivity Type Curve for Simultaneous Matching of Pressure and Pressure Derivative Data . . . . .	84
3.1.26 New Uniform-Flux Type Curve - Closed Square Reservoir; Constant Pressure Production . . . . .	87
3.1.27 New Infinite-Conductivity Type Curve - Closed Square Reservoir; Constant Pressure Production . . . . .	88

## LIST OF FIGURES (Continued)

<u>Figure</u>	<u>Page</u>
3.1.28 Uniform-Flux Type Curve for Simultaneous Matching of Rate and Rate Derivative Data . . . . .	91
3.1.29 Infinite-Conductivity Type Curve for Simultaneous Matching of Rate and Rate Derivative Data . . . . .	92
3.2.1 Composite Reservoir Geometry-Plan View . . . . .	94
3.2.2 Pressure/Pressure-Derivative Group Solution for a Composite Reservoir . . . . .	97
3.2.3 Pressure/Pressure-Derivative Group Solution for a Naturally Fractured Reservoir - Unsteady-State Model . . . . .	100
3.2.4 Pressure/Pressure-Derivative Group Solution for a Naturally Fractured Reservoir - Pseudosteady-State Model . . . . .	103
3.3.1 Type-Curve Match of Pressure/Pressure-Derivative Data - Wellbore Storage and Skin; Buildup Example . . . . .	104
3.3.2 Type-Curve Match of Pressure Change Data - Wellbore Storage and Skin; Buildup Example . . . . .	105
3.3.3 Effect of Producing Time - Wellbore Storage and Skin; Buildup Example . . . . .	107
3.3.4 Type-Curve Match of Pressure/Pressure-Derivative Data - Wellbore Storage and Skin; Drawdown Example . . . . .	111
3.3.5 Semilog Plot of $\Delta p / (2\Delta p')$ Versus Time - Wellbore Storage and Skin; Drawdown Example . . . . .	112
3.3.6 Semilog Plot of Pressure Change, $\Delta p$ , Versus Time - Wellbore Storage and Skin; Drawdown Example . . . . .	113
3.3.7 Attempted Type-Curve Match of Pressure/Pressure-Derivative Data Using Parameter values of Ref. 82 . . . . .	115
3.3.8 Type-Curve Match of Pressure Data - Wellbore Storage and Skin;	

## LIST OF FIGURES (Continued)

<u>Figure</u>	<u>Page</u>
Drawdown Example . . . . .	116
3.3.9 Pressure and Two Sets of Pressure/Pressure-Derivative Data - Infinite-Conductivity Fracture; Buildup Example . . . . .	120
3.3.10 Type-Curve Match of Pressure/Pressure-Derivative Data - Infinite-Conductivity Fracture; Buildup Example . . . . .	121
3.3.11 Type-Curve Match of Buildup Pressure Data - Infinite-Conductivity Fracture . . . . .	122
3.3.12 Type-Curve Match of Pressure/Pressure-Derivative Data - Finite- Conductivity Fracture; Drawdown Example . . . . .	126
3.3.13 Type-Curve Match of Pressure and Derivative Data - Finite- Conductivity Fracture; Drawdown Example . . . . .	128
3.3.14 Attempted Type-Curve Match of Pseudopressure/Pseudopressure- Derivative Data - Finite-Conductivity Fracture; Buildup Example . . . . .	132
3.3.15 Attempted Type-Curve Match of Pseudopressure and Derivative Data . . . . .	134
4.2.1 System of Producing Wells in a Closed Bounded Reservoir . . . . .	140
4.2.2 Infinite Multi-Well Pattern . . . . .	143
4.3.1 Effect of Producing Time on Derivative Response; Single Well in a Closed Bounded Reservoir . . . . .	146
4.3.2 Effect of Well Location on Derivative Response; Single Well in a Closed Bounded Reservoir . . . . .	148
4.3.3 Comparison of Conventional and Modified MDH Semilog Slopes . . . . .	150
4.3.4 Comparison of Conventional and Modified MDH Plots . . . . .	152
4.3.5 Effect of Producing Time on Pressure Response; Single Well in an Infinite Multi-Well Pattern . . . . .	161

## LIST OF FIGURES (Continued)

<u>Figure</u>	<u>Page</u>
4.3.6 Two-Well System; Closed Square Reservoir . . . . .	168
4.3.7 Influence of Individual Well Rates on Derivative Response . . . . .	170
4.3.8 Effect of Number of Wells and Well Location on Pressure Response . . . . .	172
4.3.9 Effect of Number of Wells and Well Location on Derivative Response . . . . .	173
4.3.10 Two-Well System; Closed 2 : 1 Rectangular Reservoir . . . . .	175
4.3.11 Effect of Parameter $\alpha_1$ on Derivative Response . . . . .	176
4.4.1 Effect of Penetration Ratio, $L_{x_f}/\sqrt{A_1}$ , on Derivative Response; Uniform-Flux Fracture . . . . .	180
4.4.2 Effect of Penetration Ratio, $L_{x_f}/\sqrt{A_1}$ , on Derivative Response; Infinite-Conductivity Fracture . . . . .	181
4.4.3 Log-Log Plot of Derivative Response Versus Shut-in Time; Uniform-Flux Fracture . . . . .	184
4.4.4 Correlation of Modified Buildup Response With Drawdown Solution; Infinite-Conductivity Fracture . . . . .	187
4.4.5 Derivative Response in an Infinite Multi-Well Pattern; Uniform-Flux Fracture . . . . .	190
4.5.1 Effect of Wellbore Storage on Derivative Response; Closed Square Reservoir . . . . .	194
4.5.2 Effect of Wellbore Storage and Skin on Derivative Response; Closed Square Reservoir . . . . .	196
4.5.3 Effect of Drainage Area and Wellbore Storage on Derivative Response; Closed Square Reservoir . . . . .	197
4.6.1 Preliminary Type-Curve Match of Pressure/Pressure-Derivative Data; Field Example . . . . .	202

**LIST OF FIGURES (Continued)**

<u>Figure</u>	<u>Page</u>
4.6.2 Cartesian Plot of Derivative of Shut-in Pressure; Field Example .	203
4.6.3 Semilog Plot of Shut-in Pressure and Corrected Shut-in Pressure; Field Example . . . . .	205



## CHAPTER I

### INTRODUCTION

Recently, well test analysis methods incorporating the pressure derivative (time rate of change of pressure) have been used extensively for analyzing well test data. Specifically, type curves based on pressure derivatives have become a highly popular method in identifying the most appropriate theoretical reservoir/well model (and the flow regimes) exhibited by well test data and in determining reservoir/well parameters. Moreover, it has been shown that pressure derivative, as an interpretation method, is a valuable tool for determining some of the reservoir parameters which cannot be obtained from type curve analysis or from the conventional semilog analysis of well test pressure data. The main objective of this work is two-fold: (i) to develop new procedures for constructing type curves utilizing the pressure derivative, which further simplify the interpretation of well test data; and (ii) to present new analysis procedures based on the pressure derivative which can be applied to problems where type curve analysis or conventional semilog analysis of pressure data is not appropriate.

To the best of our knowledge, type curves based on pressure derivatives were first presented in the petroleum engineering literature by Tiab and Crichlow<sup>1</sup> who used the pressure derivative (time rate of change of pressure) to aid in fault detection and presented type curves based on the derivative of dimensionless pressure for a well located near a multiple-sealing-fault system and for a well located in a closed rectangular bounded reservoir, and by Tiab and Kumar<sup>2</sup> who presented type curves based on the derivative of dimensionless pressure for analyzing well test data obtained at an interference well. Previously, Hurst<sup>3</sup> and others<sup>4,5</sup> had used the pressure derivative in water influx calculations. Since the appearance of Refs. 1 and

2, several authors have presented type curves based on pressure derivatives. For example, Bourdet *et al.* presented derivative type curves for wellbore storage and skin problems<sup>6</sup> and for naturally fractured reservoirs<sup>7,8</sup>, Wong *et al.*<sup>9</sup> presented conceptually similar type curves for finite-conductivity fractures, and Suresh and Tiab<sup>10</sup> presented derivative type curves for analyzing well test pressure buildup data obtained at a well located at the center of a uniform-flux or infinite-conductivity planar fracture. Yeh and Reynolds<sup>11</sup> presented both pressure and pressure-derivative type curves for analyzing pressure data obtained at a restricted-entry well. Typically, these derivative type curves represent a graph (usually log-log) of dimensionless pressure (or a dimensionless pressure group) and the derivative of dimensionless pressure (or a constant times the derivative of dimensionless pressure) versus dimensionless time (or a dimensionless time group). Such type curves have two main advantages over conventional type curves based on a graph of dimensionless pressure versus dimensionless time. First, a graph of the derivative of dimensionless pressure often has more character (curvature); hence, it is easier to obtain a unique, well-defined type-curve match of field data with derivative type curves. Second, such type curves usually involve a graph of both the dimensionless pressure and the derivative of dimensionless pressure; thus, in analyzing field data, one must match simultaneously both the measured pressure change and the derivative of the measured pressure change, which further enhances the likelihood of obtaining a well-defined type-curve match and a consistent analysis.

In this work, an alternate method to constructing type curves that are based on a new combination of pressure and its derivative is presented. Essentially, the new method involves plotting both dimensionless pressure and dimensionless pressure divided by the logarithmic derivative of dimensionless pressure, which is called the pressure/pressure-derivative group throughout in this work, versus dimensionless time. In Chapter II, we formulate the basic idea of the new pressure/pressure-derivative group and show that when using type curves based on this new group, type curve matching of field pressure/pressure-derivative data is accomplished by moving the field data plot only in horizontal direction; thus, this procedure not only

simplifies the type-curve matching process, but also is advantageous in determining whether given field data are representative of the solution assumed by a particular type-curve solution. In addition, it is shown that the new pressure/pressure-derivative group can be used effectively to identify proper semilog straight line(s) when pressure data is analyzed by conventional semilog methods. In Chapter II, we also present some of the numerical differentiation methods used to obtain pressure derivatives from the measured pressure-time data and compare these methods in regard to obtaining smooth pressure derivatives.

We demonstrate that the pressure/pressure-derivative group established in Chapter II can be used to construct new type curves for a broad range of problems encountered in well testing. In Chapter III, the basic procedure is used to construct new type curves for classical line source solution (or Theis<sup>12</sup> solution), for classical wellbore storage and skin problems<sup>13,14,15,16</sup>, for a well intercepted by a planar (uniform-flux or infinite-conductivity) fracture<sup>17-19</sup>, and for finite-conductivity fractured wells<sup>20-24</sup>. These type curves are constructed using the solutions based on single phase flow of a slightly-compressible fluid of constant viscosity. The type curves are presented for both infinite-acting reservoirs and closed bounded reservoirs, and for a well produced either at a constant rate or at a constant pressure. In Chapter III, we also investigate the validity of using new drawdown type curves to analyze buildup data and delineate the conditions under which buildup data can be analyzed by using such type curves. The applicability of semilog straight line identification using the pressure/pressure-derivative group is demonstrated in Chapter III for composite reservoirs<sup>25-28</sup> and for naturally fractured reservoirs<sup>29-33</sup>. At the end of Chapter III, analyses of actual field data cases are presented to illustrate the advantages associated with the use of new type curves and the applicability of the new pressure/pressure-derivative group for identifying the proper semilog straight line exhibited by actual field data.

In Chapter IV, we present new applications of the pressure derivative method for analyzing the pressure buildup data obtained at a well located in a system of wells draining a closed bounded reservoir. Both fractured and unfractured wells

are considered. As is well known, Miller-Dyes-Hutchinson<sup>34</sup> (MDH) and Matthews-Brons-Hazebroek<sup>35</sup> (MBH) procedures are the ones which are commonly used to compute the average reservoir pressure from a buildup test. However, these procedures for estimating average reservoir pressure require knowledge of the well's drainage area and the Dietz<sup>36</sup> shape factor, and also assume that one can identify the proper semilog straight line on a conventional semilog plot (Horner<sup>37</sup> or MDH) of buildup pressure data. By using a method of analysis based on the pressure derivative, it is shown that the drainage area of the well (at the instant of shut-in) and the flow capacity (permeability-thickness product) can be computed directly from the derivative of pressure buildup data even in cases where it is difficult to identify a well-defined semilog straight line on a conventional semilog analysis of pressure buildup data. By using the estimates obtained from this derivative analysis procedure, it is shown that one can construct a modified semilog plot of pressure buildup data versus the shut-in time, which properly accounts for producing time effects. This modified semilog plot can be used to obtain estimates of the skin factor and the average pressure, and checks on the estimate of flow capacity obtained by our derivative analysis technique. In Chapter IV, we also present a second method for estimating well's drainage area from pressure buildup data. The second method relies on the fact that during buildup, the well's shut-in pressure increases to a maximum and then decreases due to interference from neighboring producing wells. It is shown that the derivative of shut-in pressure at the point where the shut-in pressure is maximum is equal to zero and that the maximum shut-in pressure and the time at which it occurs can be utilized to compute the well's drainage area and the average reservoir pressure. We also investigate the validity of these methods to analyze pressure buildup data influenced by wellbore storage and skin effects and delineate the conditions under which such pressure buildup data can be analyzed by these methods to determine the well's drainage area and the permeability-thickness product. At the end of Chapter IV, we present the analysis of an actual well-test pressure buildup data to illustrate the use of new pressure-derivative analysis procedures suggested in this work.

The foundational work on the new pressure/pressure-derivative group used to construct new type curves for well test analysis presented in this work was first presented publicly in a paper submitted to the SPE (Society of Petroleum Engineers) in Feb, 1987; see Ref. 38, (later published in the March 1988 issue of SPEFE; Society of Petroleum Engineers Formation Evaluation). Since that time another paper; see Ref. 39, which has presented type curves using the same pressure/pressure-derivative group for analyzing well test data obtained at a horizontal well, was presented at the 1987 California Regional Meeting. Later our work was applied to construct new type curves for a well intercepted by a vertical finite-conductivity fracture and to aid in the identification of semilog straight lines; these results were presented at the 1987 SPE Annual Fall Meeting; see Ref. 40. At the same meeting another paper (Ref. 41) presented type curves for wellbore storage and skin problems based on a similar combination of the pressure/pressure-derivative group and discussed the conditions under which those type curves can be used to analyze the pressure buildup data influenced by wellbore storage and skin effects.

The work presented here on new analysis procedures based on the pressure derivative for analyzing pressure buildup data obtained at a well located in a system of wells draining a closed bounded reservoir was first publicly presented at the 1988 SPE Annual Fall Meeting; see Ref. 42.

## CHAPTER II

### NEW PRESSURE-DERIVATIVE GROUP

In this chapter, a new pressure-derivative group for constructing new type curves is formulated. This new pressure-derivative group involves the dimensionless pressure change divided by its logarithmic derivative. It is shown that when using type curves based on this pressure/pressure-derivative group, the vertical scale of these type curves is automatically aligned with the vertical scale of the corresponding field pressure/pressure-derivative data; thus, type-curve matching of field data can be accomplished by moving the field data plot only in horizontal direction. This automatic alignment of vertical scales simplifies type-curve matching and also is advantageous for determining whether the field data actually represents the solution assumed by a given type curve. Moreover, it is shown that this pressure/pressure-derivative group can be used to ensure that proper semilog straight lines are chosen when analyzing well test pressure data by conventional semilog methods.

As described in the preceding paragraph, the new pressure/pressure-derivative group involves the derivative of pressure with respect to time; and therefore, the construction of this group from a given measured pressure versus time data requires numerical differentiation of such data. We document some of the numerical differentiation methods to obtain pressure derivatives from measured pressure-time data and compare these methods with regard to obtaining reliable smooth pressure-derivative data by applying them to real well test data.

#### 2.1 Definitions

The purpose of this section is to present some of the basic definitions that will be used in the formulation of the new pressure/pressure-derivative group. All

definitions are given in oil field units and assume single phase flow of a slightly-compressible fluid of constant viscosity.

The dimensionless wellbore pressure drop for a well producing at a constant rate, dimensionless time based on wellbore radius, dimensionless time based on fracture-half length, and dimensionless time based on drainage area are defined, respectively, by

$$p_{wD} = \frac{kh [p_i - p_{wf}(t)]}{141.2qB\mu}, \quad (2.1.1)$$

$$t_D = \frac{2.637 \times 10^{-4} kt}{\phi c_t \mu r_w^2}, \quad (2.1.2)$$

$$t_{x_f D} = \frac{2.637 \times 10^{-4} kt}{\phi c_t \mu L_{x_f}^2}, \quad (2.1.3)$$

and

$$t_{AD} = \frac{2.637 \times 10^{-4} kt}{\phi c_t \mu A}. \quad (2.1.4)$$

In Eqs. 2.1.2 through 2.1.4,  $t$  is in hours.

Since the new pressure/pressure-derivative group proposed in this work involves the derivative of dimensionless pressure with respect to the natural logarithm of dimensionless time, we use  $p'_{wD}$  to denote this logarithmic derivative; that is,

$$p'_{wD} = \frac{dp_{wD}}{d \ln t_D}. \quad (2.1.5)$$

From the chain rule, it follows that Eq. 2.1.5 is equivalent to:

$$p'_{wD} = t_D \frac{dp_{wD}}{dt_D}. \quad (2.1.6)$$

## 2.2 Theory

In this section, the theory of the new pressure/pressure-derivative group that motivated us to generate new type curves for well test analysis is presented.

From Eq. 2.1.6, it follows that the constants making time (in hours) dimensionless may be canceled from the logarithmic derivative and thus,

$$p'_{wD} = \frac{dp_{wD}}{d \ln t_D} = \frac{dp_{wD}}{d \ln t_{e,D}} = \frac{dp_{wD}}{d \ln t_{AD}} = \frac{dp_{wD}}{d \ln t}. \quad (2.2.1)$$

We let  $\Delta p$  (in psi) denote the pressure change during the test (for drawdown test;  $\Delta p = p_i - p_{wf}$ ) and define  $\Delta p'$  by

$$\Delta p' = \frac{d\Delta p}{d \ln t} = t \frac{d\Delta p}{dt}, \quad (2.2.2)$$

where the second equality of Eq. 2.2.2 follows directly from the chain rule. From Eqs. 2.1.1-2.1.6 and 2.2.2, it follows easily that

$$\frac{p_{wD}}{2p'_{wD}} = \frac{\Delta p}{2\Delta p'}, \quad (2.2.3)$$

that is, the vertical scale on a plot  $\Delta p/(2\Delta p')$  versus real time  $t$  is identical to the vertical scale on a plot of  $p_{wD}/(2p'_{wD})$  versus dimensionless time  $t_D$  (or,  $t_{e,D}$ , or,  $t_{AD}$ ) and thus, when using type curves based on the left side of Eq. 2.2.3, type-curve matching of the pressure/pressure-derivative data will require moving the field data plot in only the horizontal direction. This is one major advantage that the new type curves to be presented in the next chapter have over previous type curves based on pressure derivatives. Previous type curves (see Refs. 1, 2, and 6-11) incorporating pressure derivatives require both horizontal and vertical movement of the field data plot in order to obtain a type-curve match. Since the vertical scale of type curves based on the group given by the left side of Eq. 2.2.3 is always automatically aligned with the vertical scale on a plot of  $\Delta p/(2\Delta p')$ , such type curves should also be advantageous in determining whether given field data is representative of the type curve chosen for analysis; i.e., a log-log plot of  $\Delta p/(2\Delta p')$  versus  $t$  should prove useful in selecting the most appropriate reservoir/well model to be used for analysis.

Although we have chosen to use the group  $p_{wD}/(2p'_{wD})$  in preparing most of the type curves of interest, other similar groups, as illustrated in Chapter III,



can be used. For example, the inverse of the group defined by the left side of Eq. 2.2.3; that is,  $2p'_{wD}/p_{wD}$ , the group that eliminates 2 from denominator of left side of Eq. 2.2.3; that is,  $p_{wD}/p'_{wD}$  (or its inverse) could also be used. It should be noted that the vertical scale of type curves based on a particular group chosen is automatically aligned with the vertical scale of corresponding field data plot. Therefore, each of these type curves will have the same advantages as do type curves based on  $p_{wD}/(2p'_{wD})$ . However, the motivation for the specific group used is aesthetic - it allows one to correlate the pressure/pressure-derivative group with the dimensionless pressure during radial or pseudoradial flow. For example, during plane radial flow, it is well known that the dimensionless pressure drop is given by

$$p_{wD} = \frac{1}{2} [\ln t_D + 0.80907] + s, \quad (2.2.4)$$

where  $s$  is the skin factor due to damage or stimulation around the wellbore. Differentiating Eq. 2.2.4 with respect to  $\ln t_D$  and multiplying the resulting equation by 2 gives

$$2p'_{wD} = 1, \quad (2.2.5)$$

and hence, during radial flow, the following equation will apply:

$$p_{wD} = \frac{p_{wD}}{2p'_{wD}} = \frac{1}{2} [\ln t_D + 0.80907] + s. \quad (2.2.6)$$

Eq. 2.2.6 indicates that the dimensionless group,  $p_{wD}/(2p'_{wD})$ , and the dimensionless pressure,  $p_{wD}$  will be identical functions of time during radial flow and that both dimensionless groups will be given by the well known semilog straight line equation. The same result, as shown later in this work, will apply during pseudoradial flow exhibited by a vertically fractured well.

Other important and useful feature of the pressure/pressure-derivative group defined by Eq. 2.2.3 follows directly from Eq. 2.2.6. Specifically, using Eqs. 2.1.2 and 2.2.3, Eq. 2.2.6 can be rewritten as

$$\frac{\Delta p}{2\Delta p'} = 1.151 \left[ \log t + \log \left( \frac{k}{\phi c_t \mu r_w^2} \right) - 3.23 \right] + s; \quad (2.2.7)$$

that is, a semilog plot of  $\Delta p/(2\Delta p')$  versus  $t$  will always exhibit a semilog straight line with slope equal to 1.151 during plane radial flow; i.e., when Eq. 2.2.6 applies. It is important to note that this observation holds regardless of the values of reservoir parameters and thus, a semilog plot of  $\Delta p/(2\Delta p')$  versus  $t$  should prove useful in identifying proper semilog straight line(s) when analyzing field data. If such a plot identifies a semilog straight line (or lines), then conventional semilog analysis methods can be applied with confidence to determine reservoir parameters. The same result (Eq. 2.2.7 with the skin factor defined suitably) applies during the pseudoradial flow regime for a restricted entry-well<sup>11,43</sup> and for the pseudoradial flow regime for fractured wells<sup>17-20</sup>.

### 2.3 Numerical Differentiation of Pressure-Time Data

Here, we present some of the numerical differentiation techniques to obtain pointwise pressure derivatives from measured pressure versus time data. It is not the intention of this work to develop new techniques for differentiating pressure-time data or to study numerical analysis aspects of these techniques; rather the objective is to show which differentiation methods can be used to obtain reliable smooth pressure derivative data. In this regard, three numerical differentiation techniques have been considered. In the first technique, the pressure derivative data (time rate of change of pressure change; i.e.,  $d\Delta p/dt$ ) is obtained by fitting a moving Lagrange interpolating polynomial through each five successive data points,  $(t, \Delta p)$ , and then differentiating this polynomial at the central data point. Here, this technique is referred to as the five-point formula. In the second technique, the pressure derivative data,  $d\Delta p/dt$ , is obtained by fitting a moving Lagrange interpolating polynomial through each three successive data points and then differentiating this polynomial at the central point. Here, this technique is referred to as the three-point formula. In the third technique, the pressure derivative data is computed by fitting a moving least squares quadratic through each five successive data points and then differentiating this quadratic at the central point. The details of these techniques can be found in any numerical analysis book; for example, see Refs. 44-46.

After obtaining the derivative of pressure with respect to time  $t$ , the logarithmic pressure derivative data,  $d\Delta p/d\ln t$ , at the point of interest is obtained by using the basic chain rule; that is,

$$\Delta p'_i = \left( \frac{d\Delta p}{d\ln t} \right)_i = t_i \left( \frac{d\Delta p}{dt} \right)_i, \quad (2.3.1)$$

where "i" represents the point where the pressure derivative is computed.

While working with the actual field data, derivative data is often noisy (oscillatory). Ref. 47 has suggested a procedure for obtaining smooth pressure derivative data when using a differentiation formula given by

$$\Delta p'_i = \frac{t_i}{(\delta t_i + \delta t_{i+1})} \left[ \frac{\delta p_{i+1}}{\delta t_{i+1}} \delta t_i + \frac{\delta p_i}{\delta t_i} \delta t_{i+1} \right], \quad (2.3.2)$$

where  $\delta p_{i+1}$ ,  $\delta p_i$ ,  $\delta t_{i+1}$ , and  $\delta t_i$  are defined, respectively, by

$$\delta p_{i+1} = \Delta p_{i+1} - \Delta p_i, \quad (2.3.3)$$

$$\delta p_i = \Delta p_i - \Delta p_{i-1}, \quad (2.3.4)$$

$$\delta t_{i+1} = t_{i+1} - t_i, \quad (2.3.5)$$

and

$$\delta t_i = t_i - t_{i-1}. \quad (2.3.6)$$

Here, subscript  $i$  represents the central data point, subscript  $i - 1$  represents the data point to the left of central point and subscript  $i + 1$  represents the data point to the right of central point. It should be noted that the differentiation formula used by Ref. 47 (Eq. 2.3.2) is as same as the differentiation formula obtained by fitting a Lagrange interpolating polynomial through each successive three data points and differentiating this polynomial at the central data point; i.e., the three-point Lagrange formula; see Eq. 5.18 of Ref. 45. Smoothing procedure of Ref. 47 is based on a parameter  $L$  which is defined as:

$$L = \min \left\{ \ln \left( \frac{t_{i+1}}{t_i} \right), \ln \left( \frac{t_i}{t_{i-1}} \right) \right\}; \quad (2.3.7)$$

that is,  $L$  defines a minimum distance based on the logarithmic time scale between the left and right points of the central time points where the derivative is computed and is a dimensionless parameter. The basic idea of this parameter is to smooth out noise by using points further away from the point at which the pressure derivative is computed; that is, by applying the differentiation formula given by Eq. 2.3.2 subject to condition given by Eq. 2.3.7. They recommended choosing  $L$  between 0.1 and 0.5 and noted that it may be necessary to use different values of  $L$  for different intervals of given pressure-time data. Although this procedure can be used to obtain smooth pressure derivative data, we have found that determining an appropriate value of  $L$  may require a trial and error procedure.

Working with a simulated pressure-time data, we have found that all of the techniques described above produce accurate and nonoscillatory pressure-derivative data. However, it has been our experience that, when working with actual pressure-time data, the third technique (least squares quadratic) produces much smoother pressure derivative data than do other two techniques and its use is much simpler than the procedure suggested by Bourdet *et al.*<sup>47</sup>. Therefore, throughout this work, we have used this “least squares quadratic” technique to differentiate pressure-time data.

In the following, we apply three numerical differentiation techniques described above to an actual field data set and compare these techniques with regard to obtaining smooth pressure derivatives. The field example considered here is buildup test 1 of Ref. 6. Relevant reservoir/well parameters are given in Table 2.3.1. The analysis of this field buildup data will be presented in Chapter III. Since the producing time prior to shut-in is shorter than the maximum shut-in time considered, we differentiate buildup pressure data with respect to Agarwal’s equivalent time<sup>48</sup> which is defined as:

$$t_c = \frac{t_p \Delta t}{(t_p + \Delta t)}, \quad (2.3.8)$$

where  $t_p$  is the producing time prior to shut-in, and  $\Delta t$  is the shut-in time. Table 2.3.2 presents the recorded pressure change,  $\Delta p$ , and the logarithmic derivative

**Table 2.3.1**  
**Reservoir/Well Parameters; Test 1 of Ref. 6**

Porosity (percent) . . . . .	0.25
Thickness (ft) . . . . .	107
Wellbore Radius (ft) . . . . .	0.29
System Compressibility (1/psi) . . . . .	4.2E-06
Viscosity of Fluid (cp) . . . . .	2.5
Formation Volume Factor (RB/STB) . . . . .	1.06
Production Rate Prior to Shut-in (STB/D) . . . . .	174
Flowing Pressure at the Instant of Shut-in (psi) . . . . .	3086.33
Producing Time (hrs) . . . . .	15.33

Table 2.2.2

Comparison of Numerical Differentiation Techniques; Test 1 of Ref. 6

Shut-in Time $\Delta t$ (Hours)	Equivalent Time $t_e$ (Hours)	Pressure Change $\Delta p$ (psi)	Logarithmic Derivative of Pressure $\Delta p'$ (psi)		
			Three-Point Formula	Least Squares Quadratic	Five-Point Formula
8.3333E-03	8.3288E-03	7.4800E+00	5.9830E+00	6.1160E+00	-
1.2500E-02	1.2490E-02	1.0220E+01	9.3381E+00	9.4940E+00	9.2737E+00
1.6667E-02	1.6649E-02	1.3700E+01	1.3454E+01	1.3071E+01	1.3614E+01
2.0833E-02	2.0805E-02	1.6940E+01	1.6873E+01	1.6853E+01	1.6882E+01
2.5000E-02	2.4959E-02	2.0440E+01	2.0252E+01	1.9940E+01	2.0382E+01
2.9167E-02	2.9111E-02	2.3680E+01	2.2723E+01	2.3087E+01	2.2572E+01
3.3333E-02	3.3261E-02	2.6920E+01	2.5977E+01	2.3126E+01	2.6445E+01
3.7500E-02	3.7408E-02	3.0160E+01	2.8978E+01	2.2877E+01	2.3593E+01
4.5833E-02	4.5697E-02	3.3150E+01	2.7670E+01	2.7654E+01	2.6519E+01
5.0000E-02	4.9837E-02	3.6150E+01	3.7081E+01	3.1785E+01	3.8278E+01
5.8333E-02	5.8112E-02	4.2630E+01	4.7221E+01	4.4896E+01	4.8451E+01
6.6667E-02	6.6378E-02	4.9590E+01	4.9045E+01	5.0238E+01	4.8542E+01
7.5000E-02	7.4635E-02	5.4840E+01	5.3005E+01	6.2083E+01	4.9842E+01
8.3333E-02	8.2883E-02	6.1310E+01	7.7419E+01	7.1714E+01	7.9554E+01
9.5833E-02	9.5238E-02	7.5620E+01	8.8837E+01	8.2718E+01	9.4905E+01
1.0833E-01	1.0757E-01	8.4350E+01	7.1737E+01	8.6728E+01	6.5492E+01
1.2083E-01	1.1989E-01	9.2060E+01	8.9855E+01	8.0870E+01	9.3624E+01
1.3333E-01	1.3218E-01	1.0279E+02	8.5221E+01	8.7698E+01	8.6978E+01
1.4583E-01	1.4446E-01	1.0791E+02	7.8863E+01	9.4754E+01	7.0545E+01
1.6250E-01	1.6080E-01	1.1963E+02	1.1054E+02	1.0302E+02	1.1565E+02
1.7917E-01	1.7710E-01	1.3035E+02	1.1926E+02	1.1983E+02	1.1903E+02
1.9583E-01	1.9336E-01	1.4156E+02	1.2905E+02	1.2841E+02	1.2931E+02
2.1250E-01	2.0960E-01	1.5204E+02	1.3689E+02	1.3529E+02	1.3714E+02
2.2917E-01	2.2579E-01	1.6274E+02	1.4109E+02	1.4299E+02	1.4236E+02
2.5000E-01	2.4599E-01	1.7446E+02	1.4903E+02	1.5531E+02	1.4423E+02
2.9167E-01	2.8622E-01	2.0088E+02	1.7598E+02	1.7535E+02	1.7956E+02
3.3333E-01	3.2624E-01	2.2382E+02	1.9265E+02	1.9453E+02	1.9191E+02
3.7500E-01	3.6005E-01	2.4801E+02	2.1256E+02	2.0425E+02	2.1600E+02
4.1667E-01	4.0564E-01	2.6994E+02	2.0864E+02	2.1474E+02	2.0606E+02
4.5833E-01	4.4503E-01	2.8865E+02	2.1624E+02	2.2344E+02	2.1328E+02
5.0000E-01	4.8421E-01	3.0811E+02	2.4110E+02	2.4048E+02	2.4135E+02
5.4168E-01	5.2319E-01	3.2757E+02	2.6511E+02	2.4955E+02	2.7166E+02
5.8333E-01	5.6195E-01	3.4750E+02	2.4798E+02	2.5824E+02	2.4355E+02
6.2500E-01	6.0052E-01	3.6172E+02	2.5330E+02	2.6310E+02	2.4939E+02
6.6667E-01	6.3888E-01	3.7993E+02	2.8306E+02	2.5636E+02	2.9412E+02
7.0833E-01	6.7705E-01	3.9564E+02	2.4375E+02	2.7483E+02	2.3716E+02
7.5000E-01	7.1502E-01	4.0786E+02	2.5863E+02	2.7297E+02	2.4929E+02
8.1250E-01	7.7160E-01	4.3230E+02	2.9844E+02	2.7814E+02	3.1532E+02
8.7500E-01	8.2775E-01	4.5101E+02	2.5825E+02	2.8229E+02	2.4822E+02

Table 2.3.2 (Cont'd)

Comparison of Numerical Differentiation Techniques; Test 1 of Ref. 6

Shut-in Time $\Delta t$ (Hours)	Equivalent Time $t_e$ (Hours)	Pressure Change $\Delta p$ (psi)	Logarithmic Derivative of Pressure $\Delta p'$ (psi)		
			Three-Point Formula	Least Squares Quadratic	Five-Point Formula
9.3750E-01	8.8347E-01	4.6722E+02	2.7398E+02	2.6979E+02	2.7589E+02
1.0000E-00	9.3876E-01	4.8542E+02	2.7826E+02	2.7927E+02	2.7764E+02
1.0625E-00	9.9363E-01	4.9990E+02	2.8373E+02	2.8572E+02	2.8184E+02
1.1250E-00	1.0481E-00	5.1662E+02	3.0104E+02	2.8966E+02	3.0567E+02
1.1875E-00	1.1021E-00	5.3108E+02	2.8861E+02	2.8087E+02	2.9194E+02
1.2500E-00	1.1558E-00	5.4482E+02	2.5331E+02	2.6627E+02	2.4770E+02
1.3125E-00	1.2090E-00	5.5453E+02	2.4756E+02	2.6329E+02	2.4121E+02
1.3750E-00	1.2618E-00	5.6652E+02	2.8117E+02	2.6375E+02	2.5964E+02
1.4375E-00	1.3143E-00	5.7799E+02	2.6345E+02	2.6802E+02	2.6482E+02
1.5000E-00	1.3663E-00	5.8748E+02	2.4773E+02	2.5693E+02	2.4216E+02
1.6250E-00	1.4693E-00	6.0594E+02	2.2742E+02	2.3240E+02	2.2855E+02
1.7500E-00	1.5707E-00	6.1919E+02	2.1067E+02	2.2380E+02	2.0526E+02
1.8750E-00	1.6707E-00	6.3293E+02	2.2474E+02	2.0810E+02	2.2871E+02
2.0000E-00	1.7692E-00	6.4590E+02	2.0836E+02	2.0145E+02	2.1042E+02
2.2500E-00	1.9620E-00	6.6338E+02	1.6284E+02	1.6327E+02	1.6060E+02
2.3750E-00	2.0564E-00	6.7086E+02	1.5046E+02	1.5373E+02	1.4994E+02
2.5000E-00	2.1495E-00	6.7711E+02	1.4025E+02	1.4528E+02	1.3703E+02
2.7500E-00	2.3317E-00	6.8832E+02	1.4046E+02	1.4001E+02	1.4003E+02
3.0000E-00	2.5090E-00	6.9878E+02	1.3898E+02	1.3110E+02	1.4233E+02
3.2500E-00	2.6815E-00	7.0773E+02	1.1507E+02	1.3254E+02	1.0726E+02
3.5000E-00	2.8494E-00	7.1347E+02	1.3368E+02	1.3266E+02	1.3497E+02
3.7500E-00	3.0130E-00	7.2317E+02	1.5018E+02	1.2715E+02	1.5929E+02
4.0000E-00	3.1723E-00	7.2964E+02	1.0737E+02	1.0872E+02	1.0688E+02
4.2500E-00	3.3275E-00	7.3387E+02	6.4245E+01	7.3077E+01	6.0351E+01
4.5000E-00	3.4788E-00	7.3562E+02	4.0763E+01	5.6544E+01	3.4258E+01
4.7500E-00	3.6264E-00	7.3737E+02	5.6315E+01	5.9062E+01	5.5288E+01
5.0000E-00	3.7703E-00	7.4012E+02	7.9610E+01	7.3095E+01	8.2359E+01
5.2500E-00	3.9107E-00	7.4336E+02	8.7166E+01	7.9242E+01	9.0465E+01
5.5000E-00	4.0478E-00	7.4631E+02	7.4572E+01	7.8805E+01	7.2621E+01
5.7500E-00	4.1816E-00	7.4837E+02	7.2122E+01	7.2575E+01	7.2177E+01
6.0000E-00	4.3122E-00	7.5086E+02	7.0514E+01	6.1552E+01	7.4801E+01
6.2500E-00	4.4399E-00	7.5261E+02	5.1683E+01	4.4603E+01	4.8306E+01
7.2500E-00	4.9222E-00	7.5445E+02	3.9156E+01	3.3518E+01	3.7575E+01
7.7500E-00	5.1476E-00	7.5668E+02	4.3295E+01	3.8598E+01	4.2407E+01
8.2500E-00	5.3636E-00	7.5819E+02	4.1517E+01	4.2043E+01	4.1535E+01
8.7500E-00	5.5705E-00	7.5994E+02	4.0822E+01	3.8158E+01	4.1792E+01
9.2500E-00	5.7690E-00	7.6118E+02	3.3245E+01	3.9084E+01	3.0728E+01
9.7500E-00	5.9596E-00	7.6219E+02	4.0199E+01	3.6457E+01	4.2096E+01
1.0250E+01	6.1428E-00	7.6368E+02	3.7654E+01	3.6512E+01	3.7742E+01

Table 2.3.2 (Cont'd)

Comparison of Numerical Differentiation Techniques; Test 1 of Ref. 6

Shut-in Time $\Delta t$ (Hours)	Equivalent Time $t_e$ (Hours)	Pressure Change $\Delta p$ (psi)	Logarithmic Derivative of Pressure $\Delta p'$ (psi)		
			Three-Point Formula	Least Squares Quadratic	Five-Point Formula
1.0750E+01	6.3189E-00	7.6442E+02	3.2206E+01	3.5134E+01	3.1259E+01
1.1250E+01	6.4884E-00	7.6543E+02	3.3949E+01	3.4272E+01	3.3606E+01
1.1750E+01	6.6517E-00	7.6617E+02	3.6542E+01	3.6264E+01	3.6875E+01
1.2250E+01	6.8090E-00	7.6718E+02	3.8365E+01	3.6895E+01	3.6797E+01
1.2750E+01	6.9607E-00	7.6792E+02	3.6512E+01	3.4916E+01	3.7359E+01
1.3250E+01	7.1071E-00	7.6874E+02	3.0551E+01	3.2917E+01	3.0588E+01
1.3750E+01	7.2485E-00	7.6917E+02	2.7637E+01	3.1901E+01	2.5427E+01
1.4500E+01	7.4517E-00	7.7017E+02	3.2702E+01	3.0803E+01	3.4278E+01
1.5250E+01	7.6449E-00	7.7092E+02	3.0226E+01	3.2139E+01	2.9473E+01
1.6000E+01	7.8289E-00	7.7166E+02	3.2510E+01	3.2539E+01	3.2509E+01
1.6750E+01	8.0043E-00	7.7241E+02	3.4826E+01	3.2394E+01	3.5911E+01
1.7500E+01	8.1716E-00	7.7315E+02	3.0985E+01	3.3543E+01	2.9703E+01
1.8250E+01	8.3315E-00	7.7366E+02	3.3603E+01	3.0288E+01	3.5365E+01
1.9000E+01	8.4844E-00	7.7440E+02	2.7783E+01	2.8225E+01	2.7135E+01
1.9750E+01	8.6308E-00	7.7466E+02	2.3218E+01	3.1882E+01	1.9803E+01
2.0500E+01	8.7710E-00	7.7516E+02	4.0280E+01	3.1351E+01	4.2936E+01
2.1250E+01	8.9055E-00	7.7591E+02	3.9266E+01	3.4290E+01	4.1555E+01
2.2250E+01	9.0764E-00	7.7641E+02	2.6716E+01	2.8704E+01	2.5361E+01
2.3250E+01	9.2385E-00	7.7689E+02	2.1331E+01	2.4706E+01	1.9635E+01
2.4250E+01	9.3924E-00	7.7715E+02	2.4516E+01	2.7003E+01	2.3762E+01
2.5250E+01	9.5388E-00	7.7766E+02	3.3758E+01	2.6978E+01	3.6625E+01
2.6250E+01	9.6780E-00	7.7816E+02	2.5913E+01	2.8893E+01	2.5075E+01
2.7250E+01	9.8108E-00	7.7840E+02	2.3881E+01	2.7685E+01	2.2018E+01
2.8500E+01	9.9682E-00	7.7890E+02	3.0249E+01	2.8188E+01	-



of pressure change,  $\Delta p'$ , for each of three techniques as functions of shut-in time,  $\Delta t$ , and equivalent time,  $t_e$ . Here the pressure change,  $\Delta p$ , and the logarithmic derivative of pressure change,  $\Delta p'$ , are defined, respectively, by

$$\Delta p = p_{ws} - p_{wf,s}, \quad (2.3.9)$$

and

$$\Delta p' = \frac{d\Delta p}{d \ln t_e}, \quad (2.3.10)$$

where  $p_{ws}$  represents the recorded shut-in pressure and  $p_{wf,s}$  represents the pressure at the instant of shut-in.

Figure 2.3.1 shows a log-log graph of the logarithmic derivative obtained from three-point formula, five-point formula and least squares quadratic technique versus the shut-in time. The data points shown by triangle, square and circle, respectively, represent the logarithmic derivatives obtained from three point-formula, five-point formula and least squares quadratic technique. It is apparent from the results of Fig. 2.3.1 that the logarithmic derivatives obtained by differentiating a least squares quadratic lie between the derivatives obtained from three-point and five-point formulas and much smoother than those obtained from three-point and five point formulas.

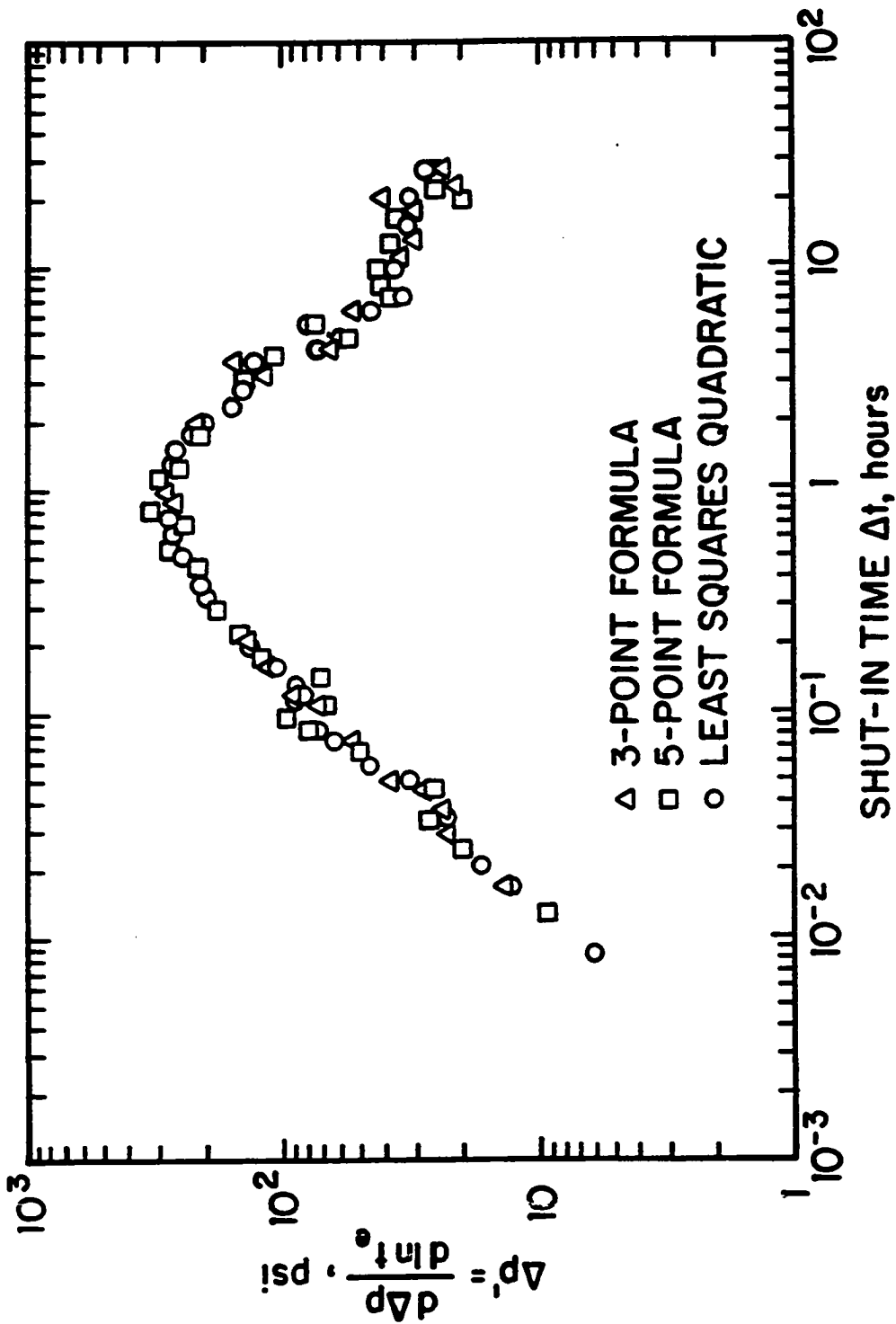


Fig. 2.3.1 - Comparison of Numerical Differentiation Techniques; Test 1 of Ref. 6

## CHAPTER III

### APPLICATIONS OF NEW PRESSURE-DERIVATIVE GROUP

In the previous chapter, we formulated the basic idea for a new pressure-derivative group. The purpose of this chapter is to demonstrate two important applications of this new group to well testing problems. As a first application, we present new type curves based on this group for a broad range of problems encountered in well test analysis. As a second application, it is shown that this group can be used to identify proper semilog straight lines when analyzing field data. In this regard, identification of proper semilog straight lines by using this group are demonstrated for nonhomogeneous reservoirs such as composite and naturally fractured reservoirs. At the end of this chapter, we include the analyses of actual field well test data by using new type curves presented in this chapter.

#### 3.1 New Type Curves For Well Test Analysis

In this section, new type curves based on the pressure/pressure-derivative group are constructed for the classical line source solution, for classical wellbore storage and skin problems, for planar fractured wells and for finite-conductivity fractured wells. Type curves are presented for a well produced at either a constant rate or a constant wellbore pressure. Both closed bounded reservoirs and infinite reservoirs have been considered. These type curves are constructed so that vertical scale of the type curves is automatically aligned with the vertical scale of the corresponding field data plot and thus, the type-curve matching of field data plot is accomplished by moving the field data plot only in horizontal direction. This type-curve match fixes

the correspondence between the time scales; i.e., determines the time match-point values, and then the conventional type-curve matching of dimensionless pressure is performed by the vertical movement of the field pressure data plot. Type curves presented here not only can be used to analyze buildup data prior to the time when producing time effects<sup>48,49</sup> become important, but also can be used to analyze draw-down and buildup data obtained from gas wells provided the proper combination of pseudopressure<sup>50</sup> and time or pseudotime<sup>51</sup> is employed; see Refs. 52 and 53.

### 3.1.1 Line Source Solution

In this subsection, a new type curve for analyzing well test data obtained at an interference well is presented. This type curve was constructed by using line source solution of Theis<sup>12</sup>, which assumes single phase flow of a slightly-compressible fluid of constant viscosity to a well produced at a constant rate in an infinite homogeneous-isotropic reservoir.

The dimensionless pressure drop solution at any point in an infinite reservoir due to production of a well of infinitesimally small radius (line source well) at a constant rate was derived by Theis<sup>12</sup> and is given by

$$p_D = -\frac{1}{2}\text{Ei} \left[ -\frac{r_D^2}{4t_D} \right], \quad (3.1.1)$$

where Ei denotes the exponential-integral function; i.e.,

$$-\text{Ei}(-x) = \int_x^{\infty} \frac{e^{-u}}{u} du, \quad (3.1.2)$$

$p_D$  denotes the dimensionless pressure drop which is defined as

$$p_D = \frac{kh [p_i - p(r,t)]}{141.2qB\mu}, \quad (3.1.3)$$

and  $t_D/r_D^2$  denotes the dimensionless time group defined as

$$t_D/r_D^2 = \frac{2.637 \times 10^{-4} kt}{\phi c_t \mu r^2}. \quad (3.1.4)$$

Here,  $r_D$  denotes the dimensionless radial distance; i.e.,  $r_D = r/r_w$  where  $r$  is the radial distance between wells.

Differentiating Eq. 3.1.1 with respect to the natural logarithm of  $t_D/r_D^2$  gives

$$p'_D = \frac{dp_D}{d \ln(t_D/r_D^2)} = \frac{1}{2} \exp \left[ -\frac{r_D^2}{4t_D} \right]. \quad (3.1.5)$$

It follows easily from Eqs. 2.2.3, 3.1.1 and 3.1.5 that

$$\frac{p_D}{2p'_D} = \frac{\Delta p}{2\Delta p'} = -\frac{1}{2} \exp \left( \frac{r_D^2}{4t_D} \right) \text{Ei} \left[ -\frac{r_D^2}{4t_D} \right]. \quad (3.1.6)$$

As is well known<sup>54</sup>, for  $t_D/r_D^2 \geq 25$ , Eq. 3.1.1 can be approximated by

$$p_D = \frac{1}{2} \left[ \ln \left( \frac{t_D}{r_D^2} \right) + 0.80907 \right]. \quad (3.1.7)$$

When Eq. 3.1.7 applies, it can be easily shown that the following equations apply:

$$2p'_D = 1, \quad (3.1.8)$$

and

$$\begin{aligned} p_D &= \frac{p_D}{2p'_D} = \frac{\Delta p}{2\Delta p'} = \frac{1}{2} \left[ \ln \left( \frac{t_D}{r_D^2} \right) + 0.80907 \right] \\ &= 1.151 \left[ \log t + \log \left( \frac{kh}{\phi c_t h \mu r^2} \right) - 3.23 \right]. \end{aligned} \quad (3.1.9)$$

Figure 3.1.1 shows a log-log plot of the  $p_D$ ,  $p'_D$  and  $p_D/(2p'_D)$  versus  $t_D/r_D^2$  solutions. The solutions  $p_D$ ,  $p'_D$  and  $p_D/(2p'_D)$  shown in Fig. 3.1.1 were obtained by using Eqs. 3.1.1, 3.1.5, and 3.1.6, respectively. The solid curve through circular data points represents the type curve based on the dimensionless pressure,  $p_D$ , which is commonly used to analyze the pressure data obtained at an interference well, the dashed curve represents the type curve based on the logarithmic pressure-derivative,  $p'_D$ , and the solid curve represents the type curve based on the new pressure/pressure-derivative group,  $p_D/(2p'_D)$ . An inspection of results of Fig. 3.1.1 shows that, for values of dimensionless time group  $t_D/r_D^2 \geq 25$ , the  $p_D/(2p'_D)$  solution coincides with the  $p_D$  solution as expected from Eq. 3.1.9. To the best of our knowledge, Eq. 3.1.6 were first presented by Chow<sup>55</sup> in the ground-water hydrology literature. However, he did not consider any type curve application of the  $p_D/(2p'_D)$  function in analyzing interference test data. Specifically, Chow

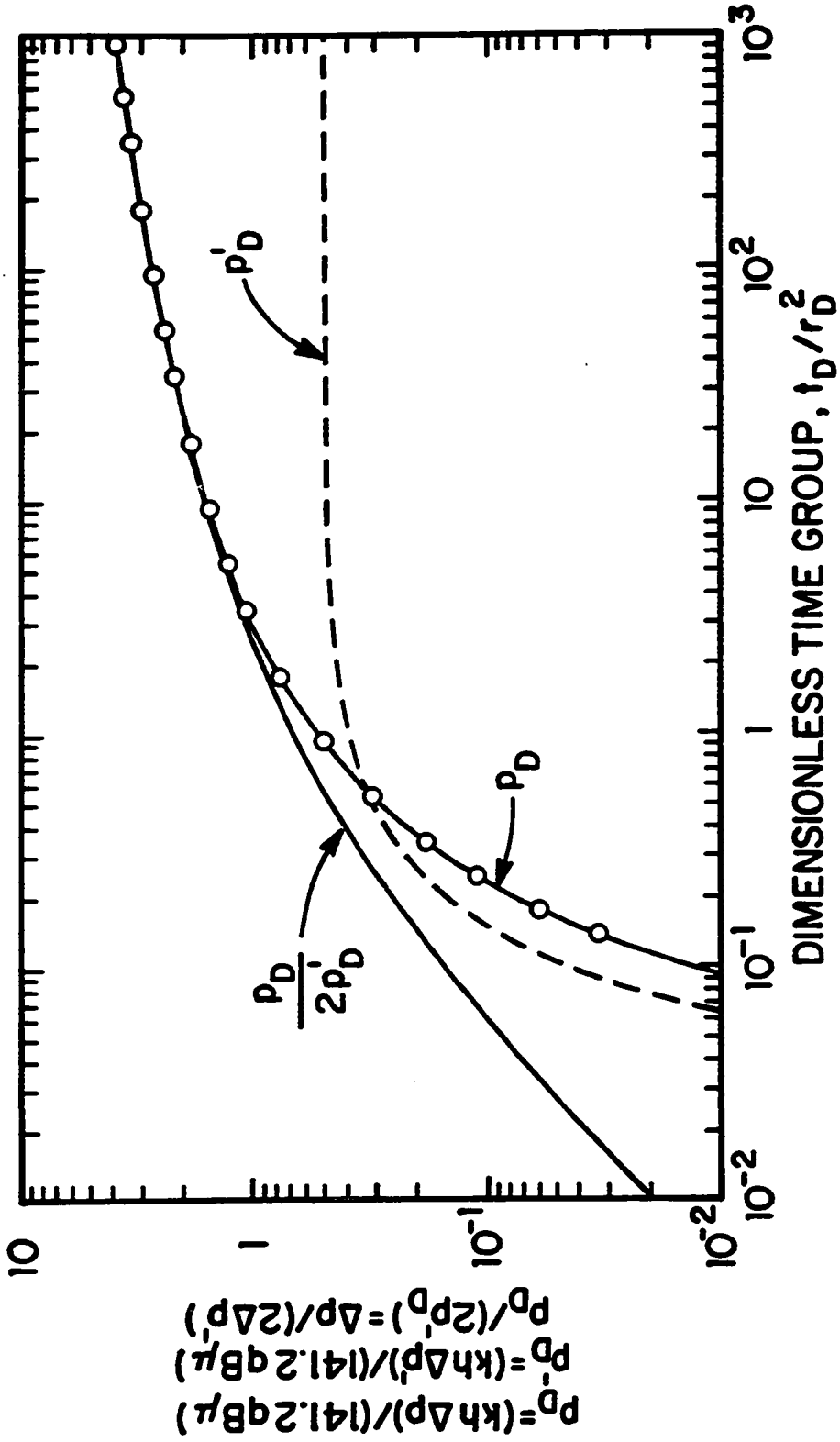


Fig. 3.1.1 - New Line Source Solution Type Curve

wrote down the equation for  $p_D/p'_D$  based on the line source solution and used the resulting equation to develop graphical methods for analyzing interference test data for cases where the pressure data obtained at an interference well do not exhibit the semilog straight line predicted by Eq. 3.1.7. However, as is well known, in cases where wellbore storage and skin effects exist at the active well (producing well)<sup>56</sup> or the wellbore storage and skin effects exist at both the active well and the observation well (interference well)<sup>57</sup>, the early time interference well test data does not obey the solution given by Eq. 3.1.1 (or, Eq. 3.1.6), and thus in general, Chow's graphical methods based on Eq. 3.1.6 cannot be used to determine reservoir parameters, transmissibility  $kh/\mu$  and storativity  $\phi c_t h$ . As we showed in Chapter II, the  $p_D/(2p'_D)$  group can be used to generate a type curve, as shown in Fig. 3.1.1, which can be used not only for analyzing early time interference test data to obtain reservoir parameters but also for determining whether such an interference data is actually representative of the line source solution on which the type curves of Fig. 3.1.1 are based. Therefore, the approach taken in this work is radically different from the approach taken in Ref. 55.

The type curves presented in Fig. 3.1.1 can be used to analyze the well test data obtained at an interference well by the following procedure: (i) Make a log-log plot on tracing paper of  $\Delta p (= p_i - p(r, t))$ ,  $\Delta p'$  and  $\Delta p/(2\Delta p')$  versus  $t$  using the basic scales of the type curve shown in Fig. 3.1.1; (ii) Because the vertical scale of the field  $\Delta p/(2\Delta p')$  plot is identical to the vertical scale of  $p_D/(2p'_D)$  solution, match the field data plot of  $\Delta p/(2\Delta p')$  with the type curve based on  $p_D/(2p'_D)$  solution by moving the data plot only in the horizontal direction. This step will determine whether field data is representative of the solution on which type curve of Fig. 3.1.1 is based. If a good type-curve match of field data is obtained with the type curve based on  $p_D/(2p'_D)$  solution, then this type-curve match of field data plot fixes the correspondence between the time scales of the type curve and the field data, and determines the time match-point values,  $(t)_M$  and  $(t_D/r_D^2)_M$ , where here, and throughout this work, the subscript  $M$  refers to a match-point value; (iii) Perform a simultaneous match of the field data plot of  $\Delta p$ -vs- $t$  and  $\Delta p'$ -vs- $t$  with

the type curves based on  $p_D$  and  $p'_D$  solutions by moving the field data plot only in the vertical direction. This simultaneous type-curve match of the  $\Delta p$  and  $\Delta p'$  data determines the pressure match-point values,  $(\Delta p)_M$  and  $(p_D)_M$ ; (iv) Using the pressure match-point values, determine the permeability-thickness product from

$$kh = \frac{141.2qB\mu(p_D)_M}{(\Delta p)_M}, \quad (3.1.10)$$

and using the time match-point values, determine the porosity-compressibility-thickness product from the following equation:

$$\phi c_t h = \frac{2.637 \times 10^{-4} kh(t)_M}{\mu r^2 (t_D/r_D^2)_M}. \quad (3.1.11)$$

Although the line source solution type curves represented by the log-log plots of  $p_D$  and  $p'_D$  versus  $t_D/r_D^2$  in Fig. 3.1.1 are not new; for example, see Refs. 2 and 54, to the best of our knowledge, the type curve of Fig. 3.1.1 which incorporates the  $p_D/(2p'_D)$  solution has not been presented previously. Although adding the  $p_D/(2p'_D)$  solution or the  $p'_D$  solution as a type curve in Fig. 3.1.1 does not provide great advantages over the type curve based on the dimensionless pressure solution,  $p_D$ , in analyzing well test data obtained at an interference well operating under single phase flow conditions, using the basic idea presented in this work, Peres *et al.*<sup>58</sup> has recently shown that type curves based on the pseudopressure/pseudopressure-derivative group for analyzing interference well test data obtained under multiphase flow conditions provide great advantages over the type curve based on only the pseudopressure in obtaining a unique match of the field data and in determining whether given interference well test data can be analyzed by the type curves of Fig. 3.1.1 which are based on the single phase flow solution.

### 3.1.2 Wellbore Storage and Skin; Unfractured Well

Here, new type curves for classical wellbore storage and skin problems are presented. The type curves were obtained by numerically inverting the Laplace space analytical solution of Agarwal *et al.*<sup>14</sup> (Eq. 8 of Ref. 14) using the Stehfest<sup>59</sup>



algorithm. Type curves presented here are based on the same assumption as those of Refs. 6, 14, 15, and 16; that is, flow of a slightly-compressible fluid of constant viscosity to a well of radius  $r_w$  in an infinite reservoir.

The motivation for the new wellbore storage and skin type curves follows. During the time when the dimensionless pressure drop and its logarithmic derivative is controlled by wellbore storage effects, it is well known<sup>6,14,15,16</sup> that

$$p_{wD} = p'_{wD} = \frac{t_D}{C_D}, \quad (3.1.12)$$

where  $C_D$  denotes the dimensionless wellbore storage constant defined by

$$C_D = \frac{5.615C}{2\pi\phi c_t r_w^2 h}. \quad (3.1.13)$$

Throughout  $C$  denotes the wellbore storage coefficient in RB/psi. Similarly, it is also well known that during the time period when the wellbore storage effects become negligible, the dimensionless pressure drop and its logarithmic derivative are given by the following equations:

$$p_{wD} = \frac{1}{2} [\ln(t_D) + 0.80907] + s, \quad (3.1.14)$$

and

$$p'_{wD} = \frac{1}{2}. \quad (3.1.15)$$

Here,  $s$  is the skin factor. From fundamental results of Earlougher and Kersh<sup>15</sup> and Refs. 16 and 6, it is also known that the dimensionless pressure drop  $p_{wD}$  and its logarithmic derivative  $p'_{wD}$  as functions of  $t_D/C_D$  can be correlated in terms of  $C_D \exp(2s)$  for  $C_D \exp(2s) \geq 10^2$  and  $s \geq 0$ . The type curves of Bourdet *et al.*<sup>6</sup> shown in Fig. 3.1.2 are based on this correlation. Note that solid curves and dashed curves, respectively, represent log-log plots of  $p_{wD}$  versus  $t_D/C_D$  and  $p'_{wD}$  versus  $t_D/C_D$  as a function of  $C_D \exp(2s)$ .

Although new wellbore storage skin and skin type curves presented in this work are based on this underlying correlation as those of Ref. 6, as discussed

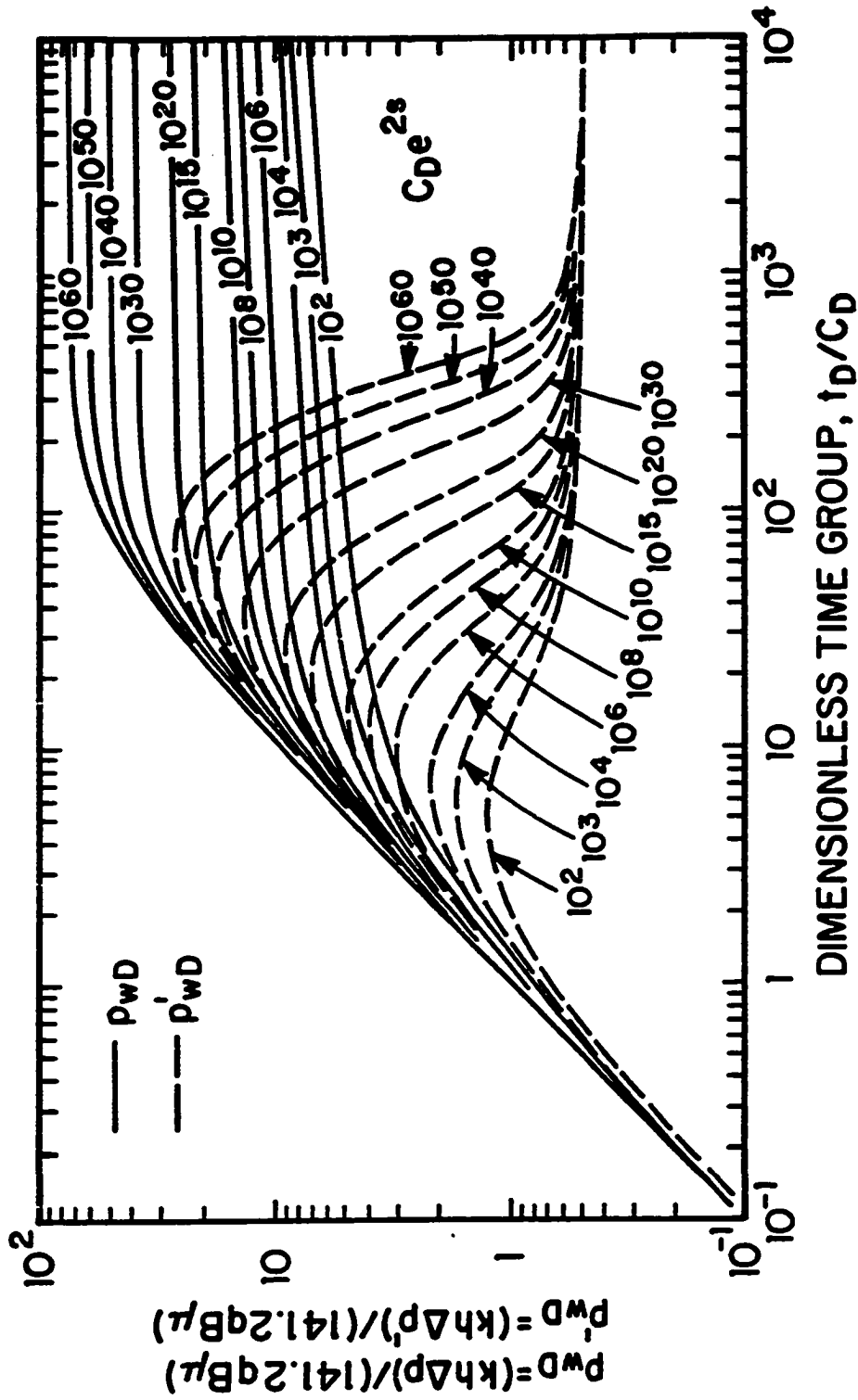


Fig. 3.1.2 - Bourdet et al.'s Wellbore Storage and Skin Type Curve

earlier, we utilize a different combination of the pressure and the pressure derivative. Specifically, when Eq. 3.1.12 holds, it is easy to see that

$$\frac{p_{wD}}{2p'_{wD}} = \frac{\Delta p}{2\Delta p'} = \frac{1}{2}, \quad (3.1.16)$$

and when Eq. 3.1.14 (or, equivalently, Eq. 3.1.15) applies, it can be easily shown that

$$\frac{p_{wD}}{2p'_{wD}} = \frac{\Delta p}{2\Delta p'} = p_{wD} = \frac{1}{2} \left[ \ln \left( \frac{t_D}{C_D} \right) + 0.80907 + \ln [C_D \exp(2s)] \right]. \quad (3.1.17)$$

Based on the basic correlation of Refs. 15, 16, 6 discussed earlier, it is clear that  $p_{wD}$  and  $p_{wD}/(2p'_{wD})$  graphed versus  $t_D/C_D$  can be correlated in terms of the parameter  $C_D \exp(2s)$  and this observation provides the motivation for new wellbore storage and skin type curves shown in Fig. 3.1.3 for various values of the parameter  $C_D \exp(2s)$ . Note, as predicted by Eq. 3.1.17, the dimensionless pressure  $p_{wD}$  coincides with the pressure/pressure-derivative  $p_{wD}/(2p'_{wD})$  at all times subsequent to the beginning of semilog straight line. More specifically, the semilog straight line (Eq. 3.1.17) begins at the time when the  $p_{wD}/(2p'_{wD})$  solution for a given value of  $C_D \exp(2s)$  joins the  $p_{wD}$  solution for the same value of  $C_D \exp(2s)$ . As mentioned previously, this is one aesthetic advantage of the particular pressure-derivative group used in construction of the type curves of Fig. 3.1.3.

During wellbore storage dominated flow, the graph of  $p_{wD}$  displays the characteristic unit slope line on log-log coordinates (see Eq. 3.1.12) and the graph of  $p_{wD}/(2p'_{wD})$  is flat and equal to 0.5 as predicted by Eq. 3.1.16. Clearly, type curves of Fig. 3.1.3 indicate that if all measured pressure data corresponds to the wellbore storage dominated flow period, type-curve match of field data with the type curves of Fig. 3.1.3 will not be unique in regard to obtaining the parameter  $C_D \exp(2s)$  and the reservoir permeability. In this case, one can only obtain the wellbore storage coefficient  $C$  from the unit slope line in the standard way<sup>54</sup>. One of the advantages of type curves of Fig. 3.1.3 is that one can easily identify when nonunique results are possible. Note that the character (curvature) of type curves

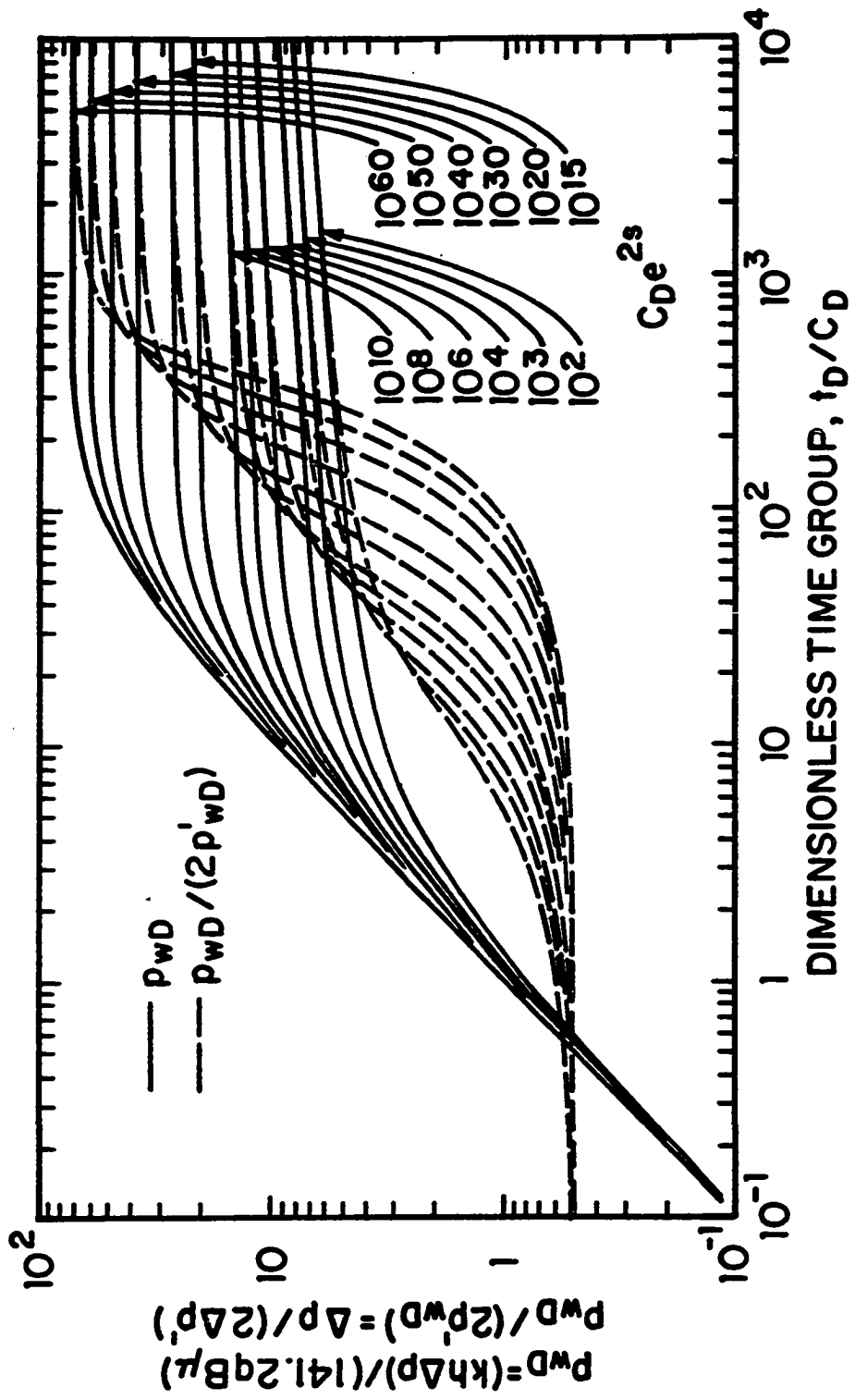


Fig. 3.1.3 - New Wellbore Storage and Skin Type Curve Based on  $p_{wD}$  and  $p_{wD}/(2p_{wD})$

of Fig. 3.1.3 is as great as for the corresponding type curves of Fig. 3.1.2 during the transitional period between wellbore storage dominated flow (Eq. 3.1.16) and radial flow (Eq. 3.1.17). Thus, it appears that the new type curves shown in Fig. 3.1.3 have the same advantages as the Bourdet *et al.*<sup>6</sup> type curves with regard to obtaining a unique match; however, as shown in the following, the procedure for using type curves of Fig. 3.1.3 is different.

Again letting  $\Delta p$  denote the pressure change during the test ( $\Delta p = p_i - p_{wf}$  for drawdown) and letting  $\Delta p'$  denote the logarithmic derivative defined by Eq. 2.2.2, we recommend preparing a log-log plot of both  $\Delta p$  and  $\Delta p/(2\Delta p')$  versus time on the same sheet of tracing paper. As established earlier, since the vertical scale on a plot of  $\Delta p/(2\Delta p')$  versus  $t$  is automatically aligned with the vertical scale on a plot of  $p_{wD}/(2p'_{wD})$  versus  $t_D/C_D$ , type-curve matching of the field data plot of  $\Delta p/(2\Delta p')$  will require moving the field data plot in only the horizontal direction; thus, it should be relatively easy to obtain a good match. The type-curve match of field pressure/pressure-derivative data will determine an estimate of  $(C_D \exp(2s))_M$  from the specific  $p_{wD}/(2p'_{wD})$  type curve matched and will determine time match-point values;  $(t)_M$  and  $(t_D/C_D)_M$ . Once time match-point values are determined, the field data plot should be moved vertically to obtain a match of  $\Delta p$  versus  $t$  with the  $p_{wD}$ -vs- $t_D/C_D$  curve corresponding to the value of  $C_D \exp(2s)$  obtained from the match of  $\Delta p/(2\Delta p')$  data. This match will determine the pressure match-point values as  $(\Delta p)_M$  and  $(p_{wD})_M$ , and then one can estimate the permeability-thickness product from these pressure match-point values using the following equation:

$$kh = \frac{141.2qB\mu (p_{wD})_M}{(\Delta p)_M}, \quad (3.1.18)$$

and the wellbore storage coefficient from the time match-point values using the following equation:

$$C = \frac{0.000295kh (t)_M}{\mu (t_D/C_D)_M}. \quad (3.1.19)$$

At this point, one can compute the dimensionless wellbore storage coefficient  $C_D$  from Eq. 3.1.13 using the value of  $C$  obtained from Eq. 3.1.19 and the skin factor

from the value of the  $C_D \exp(2s)$  associated with the curve matched as

$$s = \frac{1}{2} \ln \left[ \frac{(C_D \exp(2s))_M}{C_D} \right]. \quad (3.1.20)$$

It should be noted that, the preceding procedure uses the match of pressure/pressure-derivative data only to fix correspondence between the horizontal ( $t$  and  $t_D/C_D$ ) scales and to determine the value of  $C_D \exp(2s)$ ; however, if the wellbore storage constant  $C$  can be estimated before type curve matching - for example, from the unit slope line in the standard way - then the permeability-thickness product can be computed from the time match-point values; i.e., from the obvious rearrangement of Eq. 3.1.19. In either procedure, the type curve match obtained can be checked by converting the  $\Delta p$  data to dimensionless form by using Eq. 2.1.1 and then checking to see if both dimensionless pressure data and the pressure/pressure-derivative data can be simultaneously matched with the type curves (based on both  $p_{wD}$  and  $p_{wD}/(2p'_{wD})$ ) previously matched.

We believe the preceding procedure using the type curves of Fig. 3.1.3 will prove at least as viable as the procedure for using Fig. 3.1.2. Moreover, the fact that the vertical scale of the derivative data,  $\Delta p/(2\Delta p')$ , is always automatically aligned with the vertical scale of the derivative type curves is a distinct advantage not only in type-curve matching process but also in providing an indication of whether field data actually is representative of the solution on which all wellbore storage and skin type curves are based.

Finally, as noted in Chapter II, one can also prepare type curves as shown in Fig. 3.1.4, which shows log-log plots of  $p_{wD}/(2p'_{wD})$  (solid curves with solid data points),  $(2p'_{wD})/p_{wD}$  (dashed curves with solid data points), and  $p_{wD}$  (solid curves with open data points) versus  $t_D/C_D$  for three values of  $C_D \exp(2s)$ . Because the  $(2p'_{wD})/p_{wD}$  solutions are simply rearrangements of the corresponding  $p_{wD}/(2p'_{wD})$  solutions, adding the  $(2p'_{wD})/p_{wD}$  solutions has no theoretical advantage. In cases where we have matched field data by hand and the derivative data are noisy (oscillatory); however, having both groups on type curves seems to enhance visually our ability to obtain a good match. To use the type curves of Fig. 3.1.4, one plots

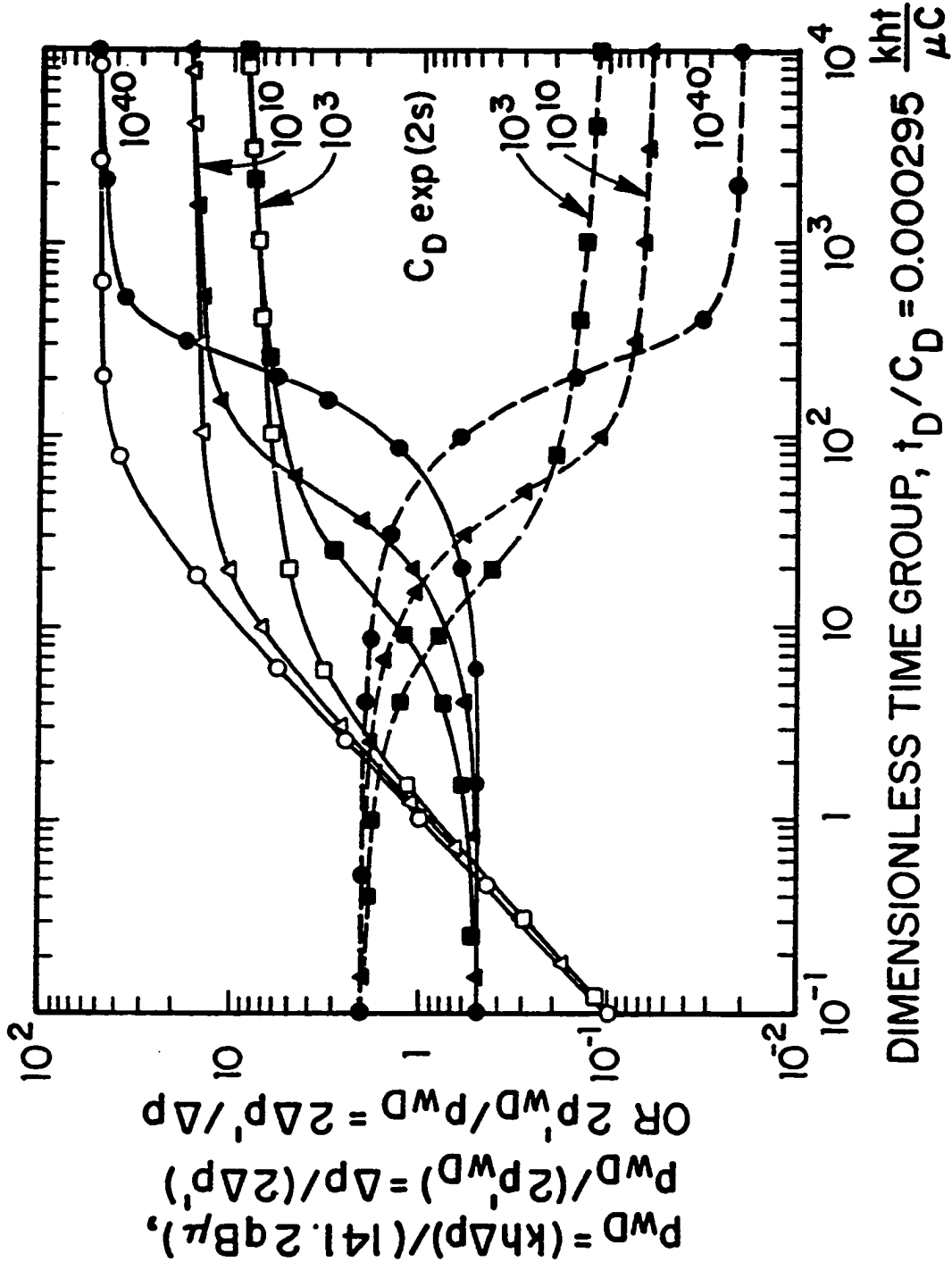


Fig. 3.1.4 - New Wellbore Storage and Skin Type Curve Including Two Derivative Groups

$\Delta p/(2\Delta p')$ ,  $(2\Delta p')/\Delta p$ , and  $\Delta p$  versus  $t$  on tracing paper. Because the vertical scale is the same for the two sets of derivative data and for the type curve, one first matches the two sets of derivative data by moving the field data plot only in the horizontal direction. Once the two sets of derivative data are matched simultaneously, the match fixes the correspondence between the horizontal scales of the field data plot and that of the type curve ( $t$  and  $t_D/C_D$ ) and determines the value of  $C_D \exp(2s)$  from the two type curves matched. The plot of  $\Delta p$  versus  $t$  is then matched to the  $p_{wD}$ -vs- $t_D/C_D$  curve corresponding to the value of  $C_D \exp(2s)$  obtained from the match of two sets of derivative data. These pressure data are matched by moving the field pressure data only in the vertical direction, and the parameters are estimated as discussed previously. Note that in this procedure, three sets of data are matched to three type curves in Fig. 3.1.4; to have a consistent match, the three curves matched must all be associated with the same value of  $C_D \exp(2s)$ .

### 3.1.3 Planar Fractures; Drawdown

Here, new type curves based on the ideas presented previously are given for a well intercepted by a planar fracture (uniform-flux or infinite-conductivity). The discussion in this part is restricted to the infinite-acting period when the wellbore pressure response is not affected by the reservoir drainage boundary. Moreover, it is restricted to the cases where the well is produced at a constant rate from a single layer homogeneous reservoir of uniform thickness with the height of the vertical fracture equal to the formation thickness, and there exists no wellbore storage and skin effects.

In the discussion of type curves for fractured wells,  $p'_{wD}$  represents the logarithmic derivative of  $p_{wD}$  with respect to the dimensionless time  $t_{x,D}$  (see Eq. 2.1.3); i.e.,

$$p'_{wD} = \frac{dp_{wD}}{d \ln t_{x,D}}; \quad (3.1.21)$$

however, from Eq. 2.2.1, this derivative is identical to the logarithmic derivative



with respect to  $t_D$  (see Eq. 2.1.2) and is also the same as the logarithmic derivative with respect to real time  $t$ .

The solution of the dimensionless pressure drop at well intercepted by a planar fracture in an infinite reservoir was derived by Gringarten *et al.*<sup>17</sup> and is given by

$$p_{wD} = \frac{1}{2} \sqrt{\pi t_{x_f D}} \left[ \operatorname{erf} \left( \frac{1-x_D}{2\sqrt{t_{x_f D}}} \right) + \operatorname{erf} \left( \frac{1+x_D}{2\sqrt{t_{x_f D}}} \right) \right] - \left( \frac{1-x_D}{4} \right) \operatorname{Ei} \left[ -\frac{(1-x_D)^2}{4t_{x_f D}} \right] - \left( \frac{1+x_D}{4} \right) \operatorname{Ei} \left[ -\frac{(1+x_D)^2}{4t_{x_f D}} \right], \quad (3.1.22)$$

where "erf" denotes the error function; i.e.,

$$\operatorname{erf}(x) = \frac{2}{\sqrt{\pi}} \int_0^x \exp(-u^2) du, \quad (3.1.23)$$

and Ei denotes the exponential integral given by Eq. 3.1.2. In Eq. 3.1.22,  $x_D$  denotes the point at which the dimensionless pressure drop is computed, and is defined as

$$x_D = \frac{x}{L_{x_f}}. \quad (3.1.24)$$

As shown by Ref. 17, the dimensionless wellbore pressure drop for a uniform-flux fracture is obtained from Eq. 3.1.22 by setting  $x_D = 0$ , whereas the dimensionless wellbore pressure drop for an infinite-conductivity fracture is obtained from Eq. 3.1.22 by setting  $x_D = 0.732$ .

Differentiating the dimensionless pressure drop given by Eq. 3.1.22 with respect to  $\ln t_{x_f D}$  gives

$$p'_{wD} = \frac{\sqrt{\pi t_{x_f D}}}{4} \left[ \operatorname{erf} \left( \frac{1-x_D}{2\sqrt{t_{x_f D}}} \right) + \operatorname{erf} \left( \frac{1+x_D}{2\sqrt{t_{x_f D}}} \right) \right]. \quad (3.1.25)$$

With Eqs. 3.1.22 and 3.1.25, as shown in Appendix A, we can establish the following short time and long time asymptotic formulas:

$$\lim_{t_{x_f D} \rightarrow 0} \frac{p_{wD}}{\sqrt{\pi t_{x_f D}}} = 1, \quad (3.1.26)$$

$$\lim_{t_{x_f D} \rightarrow \infty} \frac{p_{wD}}{0.5 [\ln(t_{x_f D}) + c]} = 1, \quad (3.1.27)$$

$$\lim_{t_{x,D} \rightarrow 0} \frac{2p'_{wD}}{\sqrt{\pi t_{x,D}}} = 1, \quad (3.1.28)$$

and

$$\lim_{t_{x,D} \rightarrow \infty} 2p'_{wD} = 1. \quad (3.1.29)$$

In Eq. 3.1.27,  $c = 2.80907$  for a uniform-flux fracture and  $c = 2.20$  for an infinite-conductivity fracture.

From Eqs. 3.1.26 and 3.1.28, it follows that for sufficiently small values of  $t_{x,D}$ , the following approximations are valid:

$$p_{wD} = 2p'_{wD} = \sqrt{\pi t_{x,D}}, \quad (3.1.30)$$

and

$$\frac{p_{wD}}{2p'_{wD}} = \frac{\Delta p}{2\Delta p'} = 1, \quad (3.1.31)$$

where the justification of the first equality of Eq. 3.1.31 was established in Chapter II. From Eq. 3.1.31, it follows that

$$\frac{2p'_{wD}}{p_{wD}} = \frac{2\Delta p'}{\Delta p} = 1. \quad (3.1.32)$$

It should be noted that Eqs. 3.1.30 through 3.1.32 apply during the linear flow period. Similarly, it follows from Eqs. 3.1.27 and 3.1.29 that for sufficiently large values of  $t_{x,D}$ ,

$$p_{wD} = \frac{p_{wD}}{2p'_{wD}} = \frac{\Delta p}{2\Delta p'} = \frac{1}{2} [\ln(t_{x,D}) + c], \quad (3.1.33)$$

and

$$\frac{1}{p_{wD}} = \frac{2p'_{wD}}{p_{wD}} = \frac{2\Delta p'}{\Delta p} = \frac{1}{0.5 [\ln(t_{x,D}) + c]}. \quad (3.1.34)$$

Note that Eqs. 3.1.33 and 3.1.34 apply during pseudoradial flow.

Figure 3.1.5 shows a log-log plot of  $p_{wD}$ ,  $p_{wD}/(2p'_{wD})$ , and  $(2p'_{wD})/p_{wD}$  versus  $t_{x,D}$  for a well at the center of a uniform-flux fracture. An inspection of the results shows that for practical purposes linear flow occurs; that is, Eqs. 3.1.30 through 3.1.32 apply for  $t_{x,D} < 0.1$ . Similarly, pseudoradial flow occurs, that is, Eqs. 3.1.33 and 3.1.34 with  $c = 2.80907$  apply for  $t_{x,D} > 3$ . Note that the pressure/pressure-derivative group,  $p_{wD}/(2p'_{wD})$ , was chosen so that it correlates exactly with the dimensionless pressure  $p_{wD}$  during pseudoradial flow; see Fig. 3.1.5 and Eq. 3.1.33.

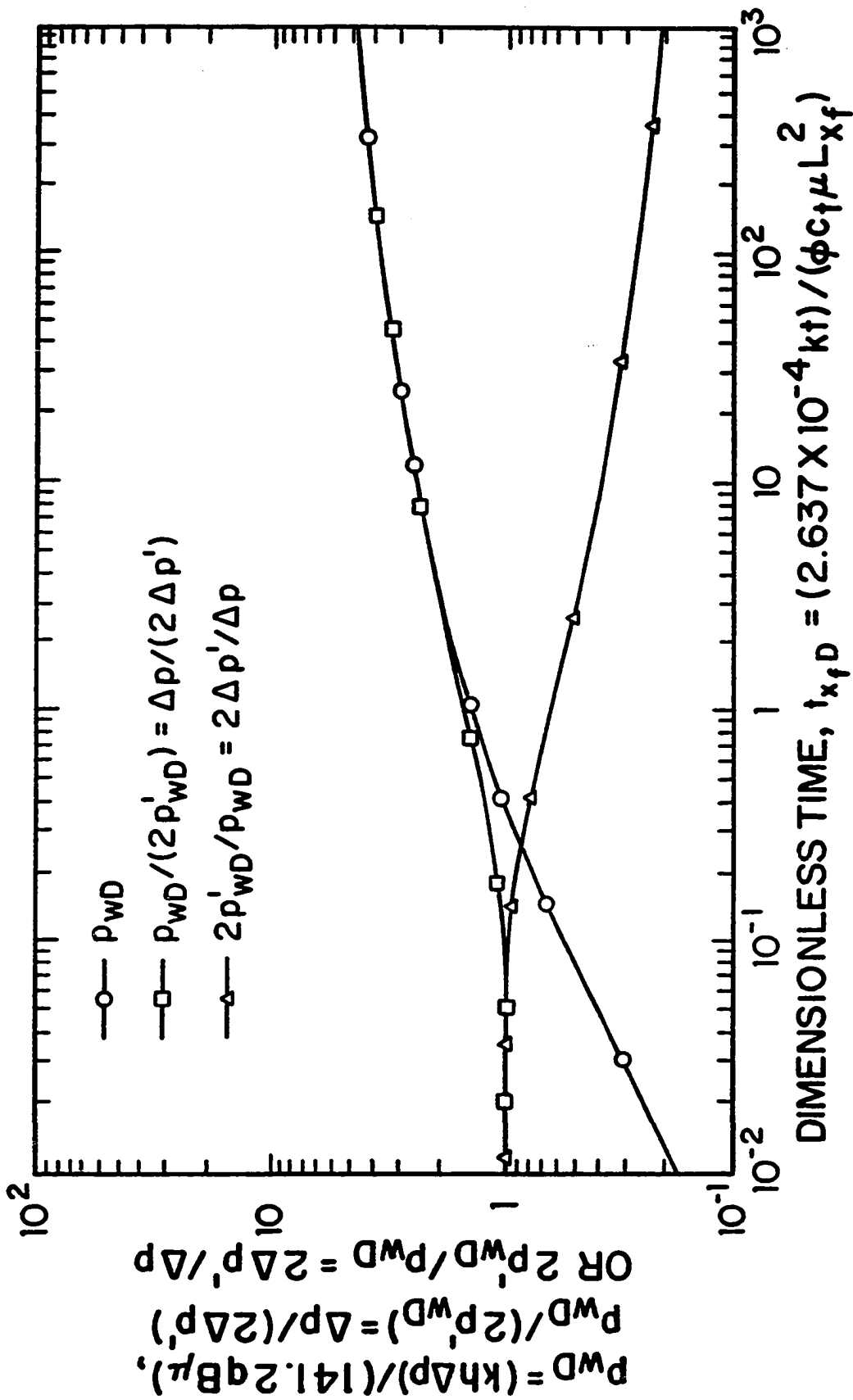


Fig. 3.1.5 - New Uniform-Flux Fracture Type Curve Including  $p_{wD}$ ,  $P_{wD}/(2p'_{wD})$  and  $2p'_{wD}/P_{wD}$

Similarly, Fig. 3.1.6 shows a log-log plot of  $p_{wD}$ ,  $p_{wD}/(2p'_{wD})$ , and  $(2p'_{wD})/p_{wD}$  versus  $t_{x,D}$  for the infinite-conductivity case. Computational results and an inspection of Fig. 3.1.6 indicate that linear flow (Eqs. 3.1.30 through 3.1.32) occurs only for  $t_{x,D} < 0.01$  and that pseudoradial flow (Eqs. 3.1.33 and Eqs. 3.1.34 with  $c = 2.20$ ) holds for  $t_{x,D} > 7$ .

Figure 3.1.7 presents a comparison of the uniform-flux and infinite-conductivity solutions. Fig. 3.1.7 shows a log-log plot  $p_{wD}$  and  $(2p'_{wD})/p_{wD}$  versus  $t_{x,D}$ . Note that uniform-flux and infinite-conductivity solutions are similar. However, the dimensionless pressure solution for the infinite-conductivity case falls slightly below the dimensionless pressure solution for the uniform-flux case, and the curvature of the two solutions in the time interval  $0.05 < t_{x,D} < 5$  is different. In Fig. 3.1.7, the cross on the  $(2p'_{wD})/p_{wD}$  solution (dashed curves) denotes the time when linear flow ends based on a 2% difference between the right and left sides of Eq. 3.1.32. On the basis of this criterion, linear flow for the infinite-conductivity solution ends before  $t_{x,D} = 10^{-2}$ . Also note that the  $(2p'_{wD})/p_{wD}$  solutions for the uniform-flux and infinite-conductivity solutions cross at  $t_{x,D} \approx 0.5$ .

Figures 3.1.5, 3.1.6 and 3.1.7 can be used as a type curve by the following procedure.

1. Make a log-log plot of  $\Delta p$ ,  $\Delta p/(2\Delta p')$ , and  $(2\Delta p')/\Delta p$  versus  $t$  on tracing paper by using the basic scale of the type curve.

2. Match the two sets of pressure/pressure-derivative data,  $\Delta p/(2\Delta p')$  and  $(2\Delta p')/\Delta p$  simultaneously with the two derivative type curves by moving the data plot in only the horizontal direction. This match fixes the time scale of the field data plot and the time scale of the type curve; that is, it determines the time match-point values,  $(t)_M$  and  $(t_{x,D})_M$ , where the subscript  $M$  refers to a match-point value.

3. Perform a type-curve match of the  $\Delta p$ -vs- $t$  data with the  $p_{wD}$ -vs- $t_{x,D}$  type curve by moving the field data plot only in the vertical direction. (The correspondence between the time scales has already been determined in Step 2.) This type-curve match of pressure data yields the pressure match-point values,  $(\Delta p)_M$  and  $(p_{wD})_M$ .

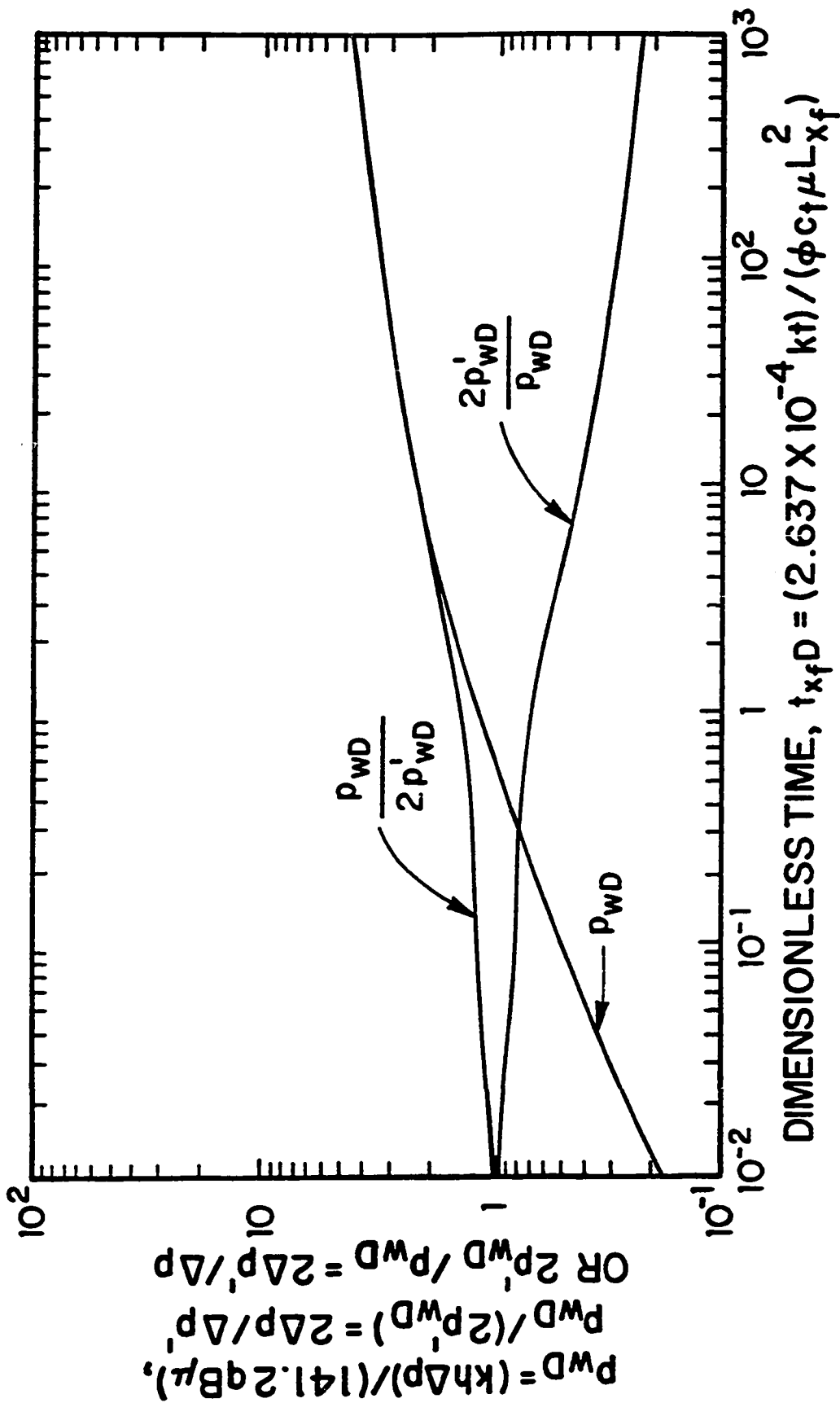


Fig. 3.1.6 - New Infinite-Conductivity Fracture Type Curve Including  $P_{wD}$ ,  $P_{wD} / (2P'_{wD})$  and  $2P'_{wD} / P_{wD}$

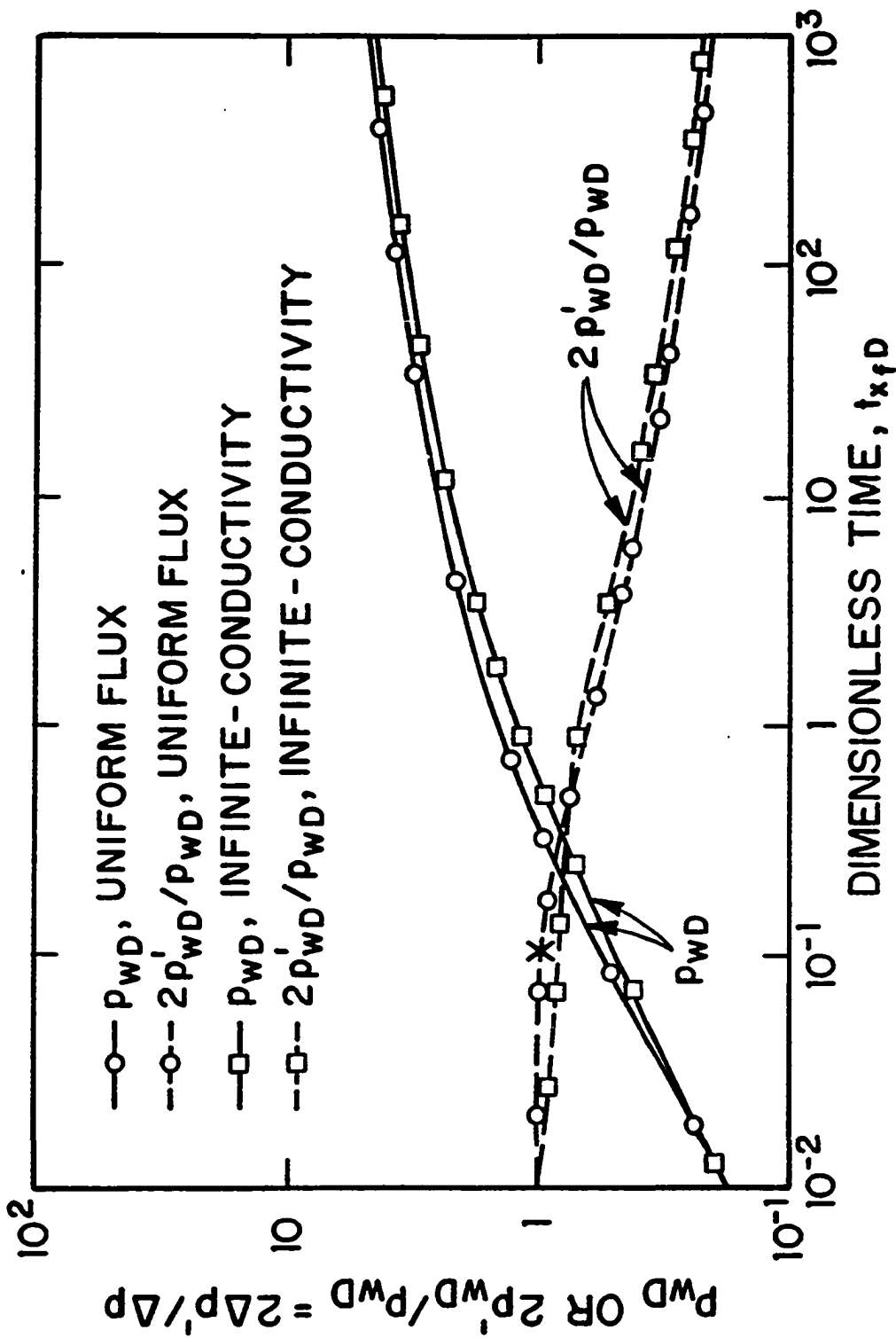


Fig. 3.1.7 - Comparison of Uniform-Flux and Infinite-Conductivity Fractured Well Solutions

4. Using the pressure match-point values, determine the permeability from

$$k = \frac{141.2qB\mu(p_{wD})_M}{h(\Delta p)_M} \quad (3.1.35)$$

Using the time match-point values, determine the fracture half-length from the following equation:

$$L_{x_f} = \sqrt{\frac{2.637 \times 10^{-4} k(t)_M}{\phi c_t \mu (t_{x_f D})_M}} \quad (3.1.36)$$

Although the uniform-flux and infinite-conductivity type curves represented by the log-log plots of  $p_{wD}$  versus  $t_{x_f D}$  in Figs. 3.1.5 and 3.1.6 are not new, to the best of our knowledge, the type curves of Figs. 3.1.5 and 3.1.6, which incorporates the two sets of derivative data, have not been presented previously. Adding the pressure/pressure-derivative solutions enhances the probability of obtaining a unique match, identifies when nonunique results are possible, and provides another means of checking whether the field data really represent the solution assumed by the type curves of Figs. 3.1.5 and 3.1.6 because the vertical scales of the two sets of field derivative data and the two pressure/pressure-derivative type curves are identical (see Eqs. 3.1.31 through 3.1.34). Again, note that the two derivative groups are simply rearrangements of the same basic solution and thus, from a theoretical viewpoint, it is sufficient to incorporate only one of the pressure/pressure-derivative type curves (either  $p_{wD}/(2p'_{wD})$  or  $(2p'_{wD})/p_{wD}$ ) on the basic type curve. When field data are matched by hand, however, having both pressure/pressure-derivative groups on the type curve seems to make performing a type curve-match easier from a visual viewpoint.

#### 3.1.4 Planar Fractures: Buildup

Here, we investigate the validity of using new drawdown type curves presented in the previous subsection to analyze the buildup data obtained at a planar fractured well and delineate the conditions under which such type curves can be used to analyze buildup data. It is shown that new drawdown type curves can be used to analyze buildup data prior to the time when producing time effects become

important. Moreover, it is shown that if producing time effects are important; i.e., buildup data cannot be analyzed by using new drawdown type curves, new buildup type curves can be constructed by using the basic pressure/pressure-derivative group to analyze such buildup data. Although results presented here are restricted to planar fractures, some of the specific conclusions obtained would be valid for other reservoir/well models.

We define two buildup pressure changes, namely,  $p_{sD}$  and  $\tilde{p}_{sD}$ , respectively, by

$$p_{sD} = \frac{kh(p_i - p_{ws})}{141.2qB\mu}, \quad (3.1.37)$$

and

$$\tilde{p}_{sD} = \frac{kh(p_{ws} - p_{wf,s})}{141.2qB\mu}, \quad (3.1.38)$$

where  $p_{ws}$  is the shut-in wellbore pressure and  $p_{wf,s}$  is the wellbore pressure at the instant of shut-in; that is, the final flowing wellbore pressure.

Suresh and Tiab<sup>10</sup> presented type curves for analyzing buildup data by plotting  $dp_{sD}/d\Delta t_{x,D}$  versus  $\Delta t_{x,D}$ , where  $\Delta t_{x,D}$  is the dimensionless shut-in time defined by

$$\Delta t_{x,D} = \frac{2.637 \times 10^{-4} k \Delta t}{\phi c_t \mu L_x^2}. \quad (3.1.39)$$

There are two disadvantages to such an approach. First, the buildup data plotted in this way cannot be correlated with the analogous derivative for the drawdown case; that is,  $dp_{wD}/dt_{x,D}$ . Second, even for large values of producing time, a different solution is obtained for each value of producing time (see Figs. 2 and 3 of Ref. 10). The approach taken in this work, however, is to use the logarithmic derivative and to examine the conditions under which the type curves of Figs. 3.1.5 and 3.1.6 can be used to analyze buildup data. This approach does not suffer from these two disadvantages. We begin with an outline of the theoretical background.

Throughout,  $t_p$  is the producing time in hours and  $t_{px,D}$  is the dimensionless producing time, which is defined by

$$t_{px,D} = \frac{2.637 \times 10^{-4} k t_p}{\phi c_t \mu L_x^2}. \quad (3.1.40)$$



Agarwal's equivalent time and dimensionless equivalent time are denoted by  $t_e$  and  $t_{eD}$ , respectively, and are defined, respectively, by

$$t_e = \frac{t_p \Delta t}{t_p + \Delta t}, \quad (3.1.41)$$

and

$$t_{eD} = \frac{t_{px,D} \Delta t_{x,D}}{t_{px,D} + \Delta t_{x,D}} = \frac{2.637 \times 10^{-4} k t_e}{\phi c_t \mu L_{x,D}^2}. \quad (3.1.42)$$

Throughout our discussion of buildup analysis,  $\Delta p$  denotes the change in the wellbore shut-in pressure during buildup; that is,

$$\Delta p = p_{ws} - p_{wf,s}. \quad (3.1.43)$$

In addition,  $\tilde{p}'_{sD}$  is the derivative of  $\tilde{p}_{sD}$  with respect to the natural logarithm of dimensionless equivalent time, and  $\Delta p'$  is the derivative of  $\Delta p$  with respect to the natural logarithm of equivalent time:

$$\tilde{p}'_{sD} = \frac{d\tilde{p}_{sD}}{d \ln(t_{eD})} = \frac{d\tilde{p}_{sD}}{d \ln t_e}, \quad (3.1.44)$$

and

$$\Delta p' = \frac{d\Delta p}{d \ln t_e}, \quad (3.1.45)$$

where the justification of the second equality of Eq. 3.1.44 is identical to the justification for Eq. 2.2.1. From the chain rule and Eq. 3.1.42, it follows easily that

$$\tilde{p}'_{sD} = \frac{\Delta t_{x,D} (t_{px,D} + \Delta t_{x,D})}{t_{px,D}} \frac{d\tilde{p}_{sD}}{d\Delta t_{x,D}} = \frac{\Delta t_{x,D}}{t_{eD}} \frac{d\tilde{p}_{sD}}{d \ln(\Delta t_{x,D})}, \quad (3.1.46)$$

From a well known superposition result, we have

$$\tilde{p}_{sD} = p_{wD}(\Delta t_{x,D}) + [-p_{wD}(t_{px,D} + \Delta t_{x,D}) + p_{wD}(t_{px,D})], \quad (3.1.47)$$

where each  $p_{wD}$  term on the right side of Eq. 3.1.47 represents drawdown solution (Eq. 3.1.22) evaluated at different values of dimensionless time. Replacing each  $p_{wD}$  term in Eq. 3.1.47 by the drawdown solution (Eq. 3.1.22) evaluated at the

appropriate value of dimensionless time and differentiating the resulting equation by use of Eq. 3.1.46 gives

$$\frac{\tilde{p}'_{sD}}{\sqrt{\pi t_{eD}}} = \frac{(\Delta t_{x_j D})^2}{4\sqrt{t_{eD} t_{eD}}} \left[ \frac{\sqrt{\Delta t_{x_j D}}}{\Delta t_{x_j D}} \left[ \operatorname{erf} \left( \frac{1-x_D}{2\sqrt{\Delta t_{x_j D}}} \right) + \operatorname{erf} \left( \frac{1+x_D}{2\sqrt{\Delta t_{x_j D}}} \right) \right] - \frac{\sqrt{t_{px_j D} + \Delta t_{x_j D}}}{(t_{px_j D} + \Delta t_{x_j D})} \left[ \operatorname{erf} \left( \frac{1-x_D}{2\sqrt{t_{px_j D} + \Delta t_{x_j D}}} \right) + \operatorname{erf} \left( \frac{1+x_D}{2\sqrt{t_{px_j D} + \Delta t_{x_j D}}} \right) \right] \right], \quad (3.1.48)$$

where  $x_D = 0.0$  for an uniform-flux fracture and  $x_D = 0.732$  for an infinite-conductivity fracture.

If  $\Delta t_{x_j D} \ll t_{px_j D}$  so that  $t_{eD} \approx \Delta t_{x_j D}$ , and the terms within the square brackets of Eq. 3.1.47 can be neglected, then Eq. 3.1.47 and Eq. 3.1.48 can be approximated by the following equations:

$$\tilde{p}_{sD} = p_{wD} (\Delta t_{x_j D}) = p_{wD} (t_{eD}), \quad (3.1.49)$$

and

$$\tilde{p}'_{sD} = \frac{dp_{wD}}{d \ln (\Delta t_{x_j D})} = \frac{dp_{wD}}{d \ln (t_{eD})}. \quad (3.1.50)$$

When Eqs. 3.1.49 and 3.1.50 apply, the dimensionless buildup pressure change,  $\tilde{p}_{sD}$ , and its logarithmic derivative,  $\tilde{p}'_{sD}$ , as a function of either  $\Delta t_{x_j D}$  or  $t_{eD}$  will correlate with the corresponding drawdown solutions, and in such cases, buildup data can be analyzed with the drawdown type curves shown in Figs. 3.1.5 and 3.1.6. On the other hand, if all  $p_{wD}$  terms in Eq. 3.1.47 can be represented by the semilog equation (Eq. 3.1.33 evaluated at the appropriate value of dimensionless time), then Eq. 3.1.47 reduces to

$$\tilde{p}_{sD} = \frac{1}{2} [\ln (t_{eD}) + c], \quad (3.1.51)$$

where  $c = 2.80907$  for an uniform-flux fracture and  $c = 2.20$  for an infinite-conductivity fracture. When Eq. 3.1.51 applies, the dimensionless buildup pressure change,  $\tilde{p}_{sD}$ , as a function of  $t_{eD}$  can be correlated exactly with the drawdown semilog equation (Eq. 3.1.33); however,  $\tilde{p}_{sD}$  as a function of  $\Delta t_{x_j D}$  will not agree

with the drawdown solution unless  $t_{eD} \approx \Delta t_{x,D}$ . Thus, following the ideas of Agarwal<sup>48</sup>, we expect that the buildup solution will correlate best with the drawdown solution when buildup solution is plotted versus equivalent time.

From Eq. 3.1.48, it can be shown that

$$\lim_{t_{eD} \rightarrow 0} \frac{2\tilde{p}'_{eD}}{\sqrt{\pi t_{eD}}} = 1, \quad (3.1.52)$$

and thus for sufficiently small values of shut-in time, the following approximation holds:

$$2\tilde{p}'_{eD} = \sqrt{\pi t_{eD}}. \quad (3.1.53)$$

For sufficiently small values of shut-in time,  $\tilde{p}_{eD}$  is also given by right side of Eq. 3.1.53; that is,

$$\tilde{p}_{eD} = \sqrt{\pi t_{eD}}; \quad (3.1.54)$$

therefore, it follows from Eqs. 3.1.53 and 3.1.54, for sufficiently small values of  $t_{eD}$ ,

$$\frac{\tilde{p}_{eD}}{2\tilde{p}'_{eD}} = \frac{\Delta p}{2\Delta p'} = 1, \quad (3.1.55)$$

and

$$\frac{2\tilde{p}'_{eD}}{\tilde{p}_{eD}} = \frac{2\Delta p'}{\Delta p} = 1. \quad (3.1.56)$$

Starting with Eqs. 3.1.47 and 3.1.48, it can be also shown that for sufficiently large values of  $\Delta t_{x,D}$ , the following approximations apply:

$$\lim_{t_{eD} \rightarrow t_{ps,D}} \tilde{p}_{eD}(t_{eD}) = p_{wD}(t_{px,D}), \quad (3.1.57)$$

and

$$\lim_{t_{eD} \rightarrow t_{ps,D}} 2\tilde{p}'_{eD} = 1. \quad (3.1.58)$$

Thus, it follows from Eqs. 3.1.57 and 3.1.58 that for sufficiently large values of  $\Delta t_{x,D}$ , the following approximation applies:

$$\frac{\tilde{p}_{eD}}{2\tilde{p}'_{eD}} = \tilde{p}_{eD}(t_{eD}) = p_{wD}(t_{px,D}). \quad (3.1.59)$$

Eq. 3.1.59 always holds in the limit; that is, as  $\Delta t_{x,D} \rightarrow \infty$ , or, equivalently, as  $t_{eD} \rightarrow t_{px,D}$  (see Eq. 3.1.42). Eq. 3.1.59 implies that the dimensionless buildup pressure/pressure-derivative group,  $\tilde{p}_{sD}(t_{eD})/[2\tilde{p}'_{sD}(t_{eD})]$ , will correlate with the dimensionless drawdown derivative group,  $p_{wD}(t_{x,D})/[2p'_{wD}(t_{x,D})]$ , at large values of shut-in time *if and only if*  $\tilde{p}_{sD}(t_{eD}) = p_{wD}(t_{x,D})/[2p'_{wD}(t_{x,D})]$  when  $t_{eD} = t_{px,D}$ , and this occurs only when Eqs. 3.1.33 and 3.1.51 hold. (The derivations of Eqs. 3.1.52 through 3.1.59 are presented in Appendix B.)

Figure 3.1.8 presents a comparison between the uniform-flux drawdown and buildup solutions for various values of the producing time,  $t_{px,D}$ . In Fig. 3.1.8, the solid curves represent the drawdown solutions of Fig. 3.1.5 and also represent the buildup solutions (plotted versus equivalent time) whenever the producing time satisfies  $t_{px,D} > 3$ . Solid data points represent the  $\tilde{p}_{sD}/(2\tilde{p}'_{sD})$  solutions and open data points are used for both the  $(2\tilde{p}'_{sD})/\tilde{p}_{sD}$  and  $\tilde{p}_{sD}$  solutions. As the producing time decreases below  $t_{px,D} = 3$ , the difference between the buildup and drawdown solutions increases. For the  $t_{px,D} = 1$  case shown by inverted triangles, the buildup solutions are reasonably close to the analogous drawdown solutions. When  $t_{px,D} = 0.1$ , however, there is a clear difference between the buildup and drawdown solutions. As shown by the results of Fig. 3.1.8, the  $\tilde{p}_{sD}/(2\tilde{p}'_{sD})$  solution always approaches  $\tilde{p}_{sD}$  when  $t_{eD}$  approaches  $t_{px,D}$ , which is the result predicted by Eq. 3.1.59. Note that this observation could be very useful in identifying the short producing time effects directly from the field data plot of  $\Delta p/(2\Delta p')$  versus equivalent time  $t_e$  due to the fact that  $\tilde{p}_{sD}/(2\tilde{p}'_{sD}) = \Delta p/(2\Delta p')$ . The results of Fig. 3.1.8 indicate that the the drawdown type curves of Fig. 3.1.5 (solid curves of Fig. 3.1.8) can be used to obtain a reasonably accurate analysis of buildup data provided that the producing time satisfies  $t_{px,D} \geq 1$  and buildup data are analyzed in terms of equivalent time. For shorter values of producing time, one can construct a specific buildup type curve for each value of producing time. In this regard, the buildup solutions represented by the open and solid data points on Fig. 3.1.8 would represent the buildup type curves for the  $t_{px,D} = 0.1$ .

Similarly, Fig. 3.1.9 presents a comparison between the infinite-conductivity

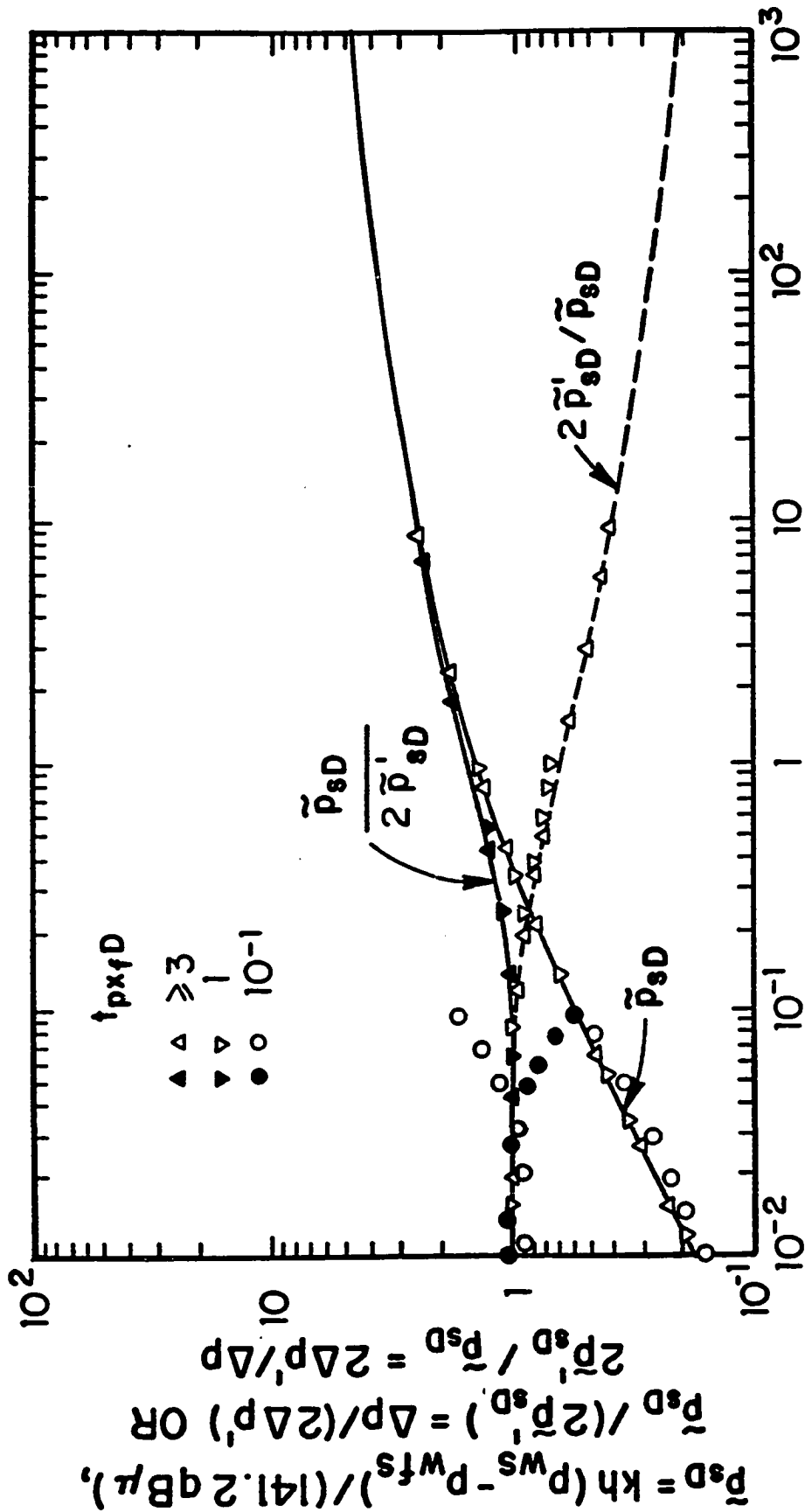


Fig. 3.1.8 - Effect of Producing Time on Correlation of Buildup Data With Uniform-Flux Drawdown Type Curve

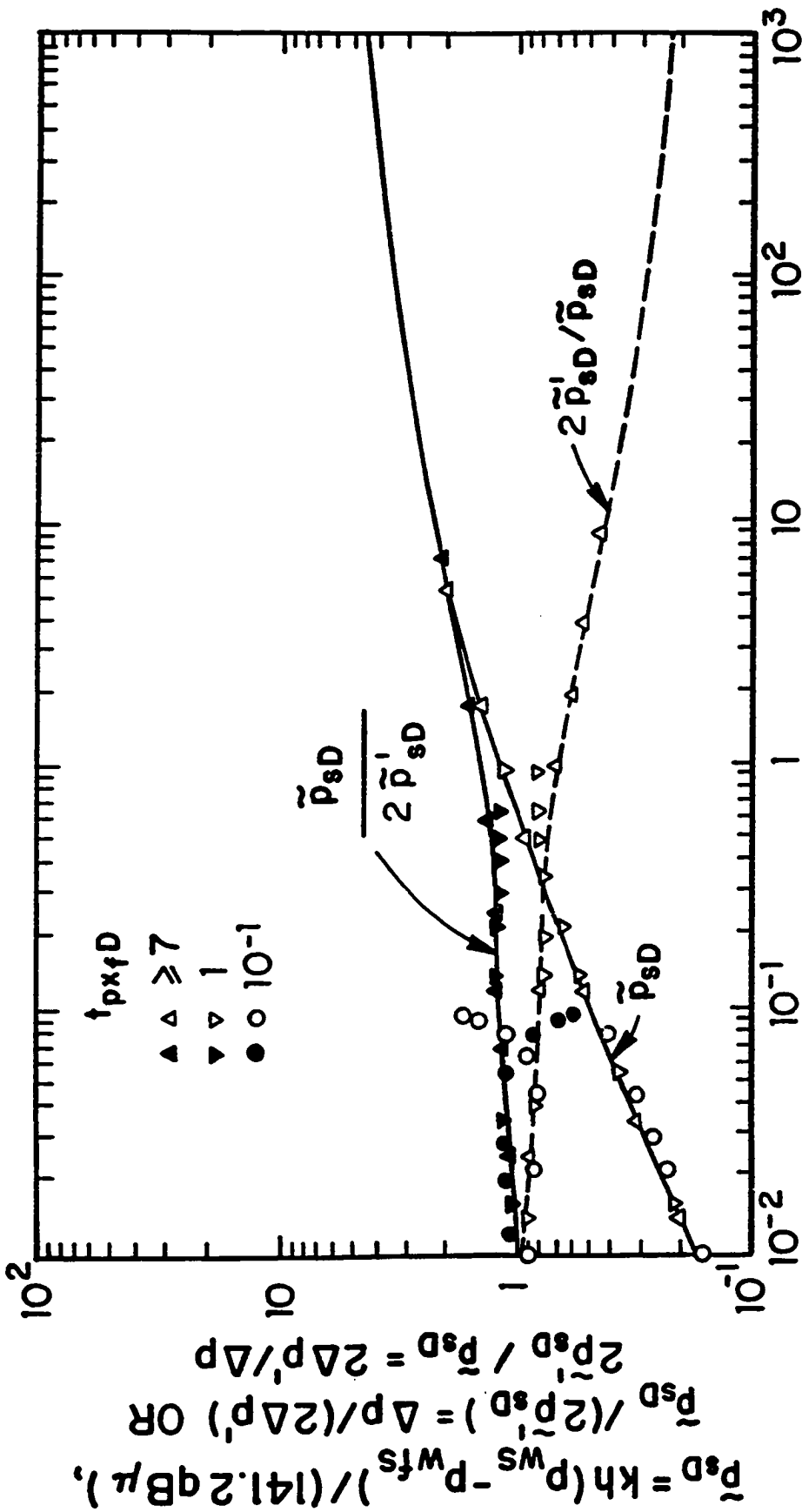


Fig. 3.1.9 - Effect of Producing Time on Correlation of Buildup Data With Infinite-Conductivity Drawdown Type Curve

drawdown and buildup solutions. From the Figs. 3.1.8 and 3.1.9, it is apparent that for a given value of producing time, the correlation between the buildup and drawdown solutions is slightly better for the uniform-flux case than for the infinite-conductivity case. For the infinite-conductivity case, computations indicate that the difference between buildup and drawdown solutions is negligible only if  $t_{px,D} \geq 7$ . Also note that for all values of producing time,  $\tilde{p}_{s,D}/(2\tilde{p}'_{s,D})$  approaches  $\tilde{p}_{s,D}$  as shut-in time increases, which indicates that the asymptotic formula of Eq. 3.1.59 also applies for the infinite-conductivity case.

Raghavan<sup>49</sup> constructed buildup type curves for analyzing buildup data from a well at the center of uniform-flux and infinite-conductivity fracture. The three lower curves in Fig. 3.1.10 represent his uniform-flux type curves for three specific values of producing time,  $t_{px,D}$ , 0.1, 0.5, and 1.0. Note that a different buildup solution,  $\tilde{p}_{s,D}$ , is obtained for each value of producing time and that the buildup pressure change  $\tilde{p}_{s,D}$  is plotted versus  $\Delta t_{x,D}$  not equivalent time  $t_{eD}$ . The curve through solid circular data points of Fig. 3.1.10 represents the corresponding drawdown solution,  $p_{wD}(t_{x,D})$  (Eq. 3.1.22 with  $x_D = 0$ ). The inherent problem in attempting to use these type curves is that all buildup curves have a similar character (curvature) and thus it is usually possible to match buildup data with more than one curve when producing time effects are important; i.e., when the buildup and drawdown solutions differ significantly. To determine which buildup curves should be used to match given field data requires that one know the dimensionless producing time,  $t_{px,D}$ , which cannot be computed directly. Comparing Figs. 3.1.8 and 3.1.10, we see that the buildup pressure change,  $\tilde{p}_{s,D}$ , will correlate with the drawdown solution,  $p_{wD}(t_{x,D})$ , for a longer period of time when the buildup pressure change is plotted in terms of equivalent time,  $t_{eD}$ , instead of  $\Delta t_{x,D}$ . In Fig. 3.1.10, the dimensionless pressure/pressure-derivative group  $\tilde{p}_{s,D}/(2\tilde{p}'_{s,D}) [= \Delta p/(2\Delta p')]$  is also plotted versus the dimensionless shut-in time,  $\Delta t_{x,D}$  for each value of the producing time. Note that here,  $\tilde{p}'_{s,D}$  is the logarithmic derivative of  $\tilde{p}_{s,D}$  with respect to equivalent time  $t_{eD}$  not with respect to  $\Delta t_{x,D}$  and thus, during buildup, the pseudoradial flow regime starts when  $\tilde{p}_{s,D}$  and  $\tilde{p}_{s,D}/(2\tilde{p}'_{s,D})$  solutions coincide for a given value of

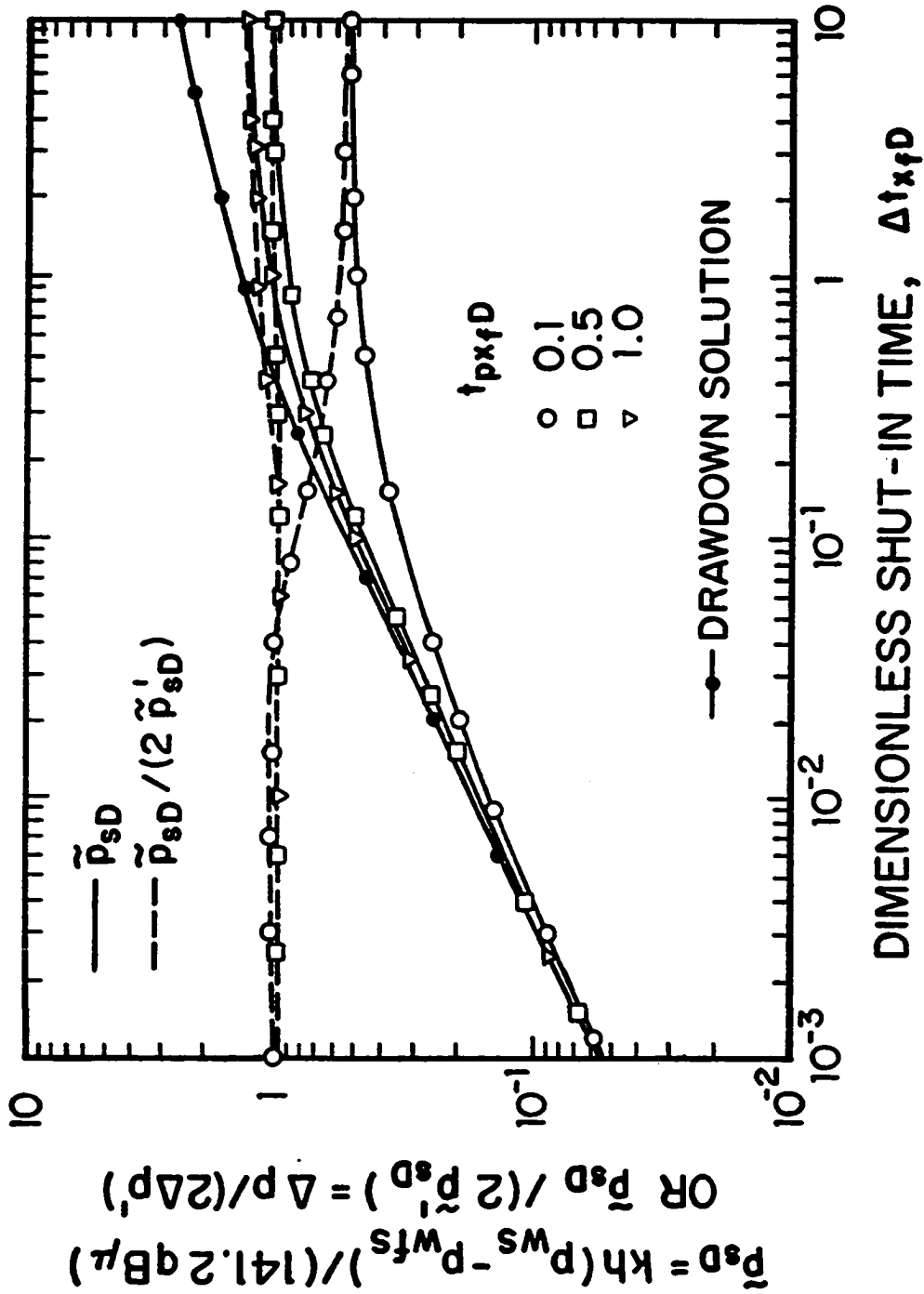


Fig. 3.1.10 - New Buildup Type Curve Based on  $\tilde{p}_{s,D}$  and  $\tilde{p}'_{s,D} / (2\tilde{p}'_{s,D})$ ; Uniform-Flux Fracture



the producing time. Because, as mentioned earlier, type-curve matching of this pressure/pressure-derivative group requires only that we move the field data plot in the horizontal direction, it was thought that adding this group to Raghavan's type curve, which is based on only the buildup pressure change, would enhance one's ability to obtain a unique match. The results of Fig. 3.1.10 show that this is the case if sufficient buildup data are available. The results also indicate that if all buildup data correspond to  $\Delta t_{x,D} < 0.1$ , then it will not be possible to determine a unique time match point by type-curve matching the pressure/pressure-derivative data. (This result is not surprising because for  $\Delta t_{x,D} < 0.1$ , all buildup data reflect linear flow.) On the other hand, the results of Fig. 3.1.10, as well as other computations not shown, indicate that if buildup data are available throughout the time range  $10^{-2} \leq \Delta t_{x,D} \leq 2$ , then one may be able to obtain a unique match of the pressure/pressure-derivative data. If so, the match of derivative data determines time match-point values,  $(\Delta t_{x,D})_M$  and  $(\Delta t)_M$ , and the value of producing time  $t_{px,D}$  from the specific curve matched. One then matches the buildup pressure data ( $\Delta p$ -vs- $\Delta t$ ) plot by moving these data only vertically until a match with the  $\tilde{p}_{s,D}$  curve corresponding to the value of  $t_{px,D}$  is obtained. This determines the values of permeability and fracture half-length by the standard computational procedure.

Before closing this section, we note that if the producing time is sufficiently greater than the maximum shut-in time considered, then the buildup data plotted along the lines mentioned above can be analyzed using the drawdown type curves presented in this work. However, if the producing time is less than the maximum shut-in time considered, then the use of Agarwal's equivalent time may significantly compress the span of data available, as observed in Figs. 3.1.8 and 3.1.9, and may even lead one to ignore the possibility of semilog analysis in some cases where a semilog straight line actually exists; see Rosato *et al.*<sup>24</sup>, Soliman<sup>60</sup> and Ozkan *et al.*<sup>61</sup>. In such cases, the use of the pressure/pressure-derivative group can be extremely useful in identifying the semilog straight line as follows.

For sufficiently large values of shut-in time so that pseudoradial flow prevails during buildup; that is,  $p_{wD}(\Delta t_{x,D})$  and  $p_{wD}(\Delta t_{x,D} + t_{px,D})$  terms in Eq. 3.1.47

can be represented by the semilog equation (Eq. 3.1.33 evaluated at the appropriate value of dimensionless time), Eq. 3.1.47 can be written as

$$\tilde{p}_{eD} = \frac{1}{2} \ln(t_{eD}) + p_{wD}(t_{pxfD}) - \frac{1}{2} \ln(t_{pxfD}). \quad (3.1.60)$$

Differentiating Eq. 3.1.60 with respect to  $\ln(t_{eD})$  and multiplying the resulting equation by 2 gives

$$2\tilde{p}'_{eD} = 1. \quad (3.1.61)$$

Dividing Eq. 3.1.60 by Eq. 3.1.61 gives

$$\frac{\tilde{p}_{eD}}{2\tilde{p}'_{eD}} = \frac{\Delta p}{2\Delta p'} = \tilde{p}_{eD} = 1.151 \log(t_{eD}) + p_{wD}(t_{pxfD}) - 1.151 \log(t_{pxfD}); \quad (3.1.62)$$

that is, regardless of value of the producing time  $t_{pxfD}$ , if pseudoradial (or radial) flow prevails during buildup, the pressure/pressure-derivative group will identify the semilog straight line on a semilog plot of  $\Delta p/(2\Delta p')$  versus  $t_e$ . However, as mentioned earlier, if the producing time is much shorter than the maximum shut-in time considered, then the use of equivalent time will significantly compress the span of data available. In such cases, a Cartesian plot of  $\Delta p/(2\Delta p')$  versus  $\ln t_e$  can be used to visually expand the span of data available in identifying the semilog straight line. If such a plot identifies a semilog straight line, then desired reservoir parameters can be obtained from the dimensional analogue of Eq. 3.1.60 in the conventional manner. We also note that as  $t_{eD}$  approaches to  $t_{pxfD}$ , Eq. 3.1.62 reduces to Eq. 3.1.59.

### 3.1.5 Planar Fractures With Wellbore Storage

In this section, new type curves are constructed for a well with wellbore storage effects intercepted by a planar fracture (either uniform-flux or infinite-conductivity) in an infinite reservoir. These type curves are generated using the well known superposition result of van Everdingen and Hurst<sup>13</sup>; that is,

$$\bar{p}_{wD} = \frac{u\bar{p}_D}{u[1 + C_{xfD}u^2\bar{p}_D]}, \quad (3.1.63)$$

where  $u$  represents the Laplace transform variable with respect to the dimensionless time,  $t_{x,D}$ . In Eq. 3.1.63  $\bar{p}_{wD}$  and  $\bar{p}_D$ , respectively, represent the Laplace space solutions for the dimensionless wellbore pressure drop for a well produced at a constant rate with wellbore storage effects and without wellbore storage effects. Here,  $C_{x,D}$  denotes the dimensionless wellbore storage constant based on fracture half-length and is defined by

$$C_{x,D} = \frac{5.615C}{2\pi c_i h L_{x_f}^2}, \quad (3.1.64)$$

where  $C$  denotes the wellbore storage coefficient in RB/psi. The  $p_{wD}$ ,  $dp_{wD}/dt_{x,D}$  and  $p_{wD}/(2p'_{wD})$  solutions were generated by using the Laplace space analytical solution of Fraim and Lee<sup>62</sup> (see Eq. 3.1.115),  $\bar{p}_D$  in Eq. 3.1.63, and then numerically inverting Eq. 3.1.63 using the Stehfest<sup>59</sup> algorithm.

Previously, type curves based on the dimensionless pressure,  $p_{wD}$ , were presented for an infinite-conductivity fractured well influenced by wellbore storage effects by Ramey and Gringarten<sup>63</sup> and for a uniform-flux fractured well influenced by wellbore storage effects by Raghavan<sup>64</sup>. Here, we present the type curves which incorporates both the pressure derivative,  $p'_{wD}$ , and the pressure/pressure-derivative,  $p_{wD}/(2p'_{wD})$ , solutions for a planar fractured well influenced by wellbore storage effects.

Figures 3.1.11 and 3.1.12 show uniform-flux and infinite-conductivity type curves, respectively, based on both the dimensionless pressure,  $p_{wD}$ , and its logarithmic derivative,  $p'_{wD}$  versus dimensionless time,  $t_{x,D}$ , for a well influenced by wellbore storage effects. In Figs. 3.1.11 and 3.1.12, the solid curves represent log-log plots of  $p_{wD}$  versus  $t_{x,D}$  and dashed curves represent log-log plots of  $p'_{wD}$  versus  $t_{x,D}$  for various values of the dimensionless wellbore storage coefficient  $C_{x,D}$ . The solid and dashed curves through circular data points represent the solutions without wellbore storage effects; that is,  $C_{x,D} = 0$ . An inspection of results of Figs. 3.1.11 and 3.1.12 indicates that during wellbore storage dominated flow; that is at early times, both the dimensionless pressure and its logarithmic derivative display a unit

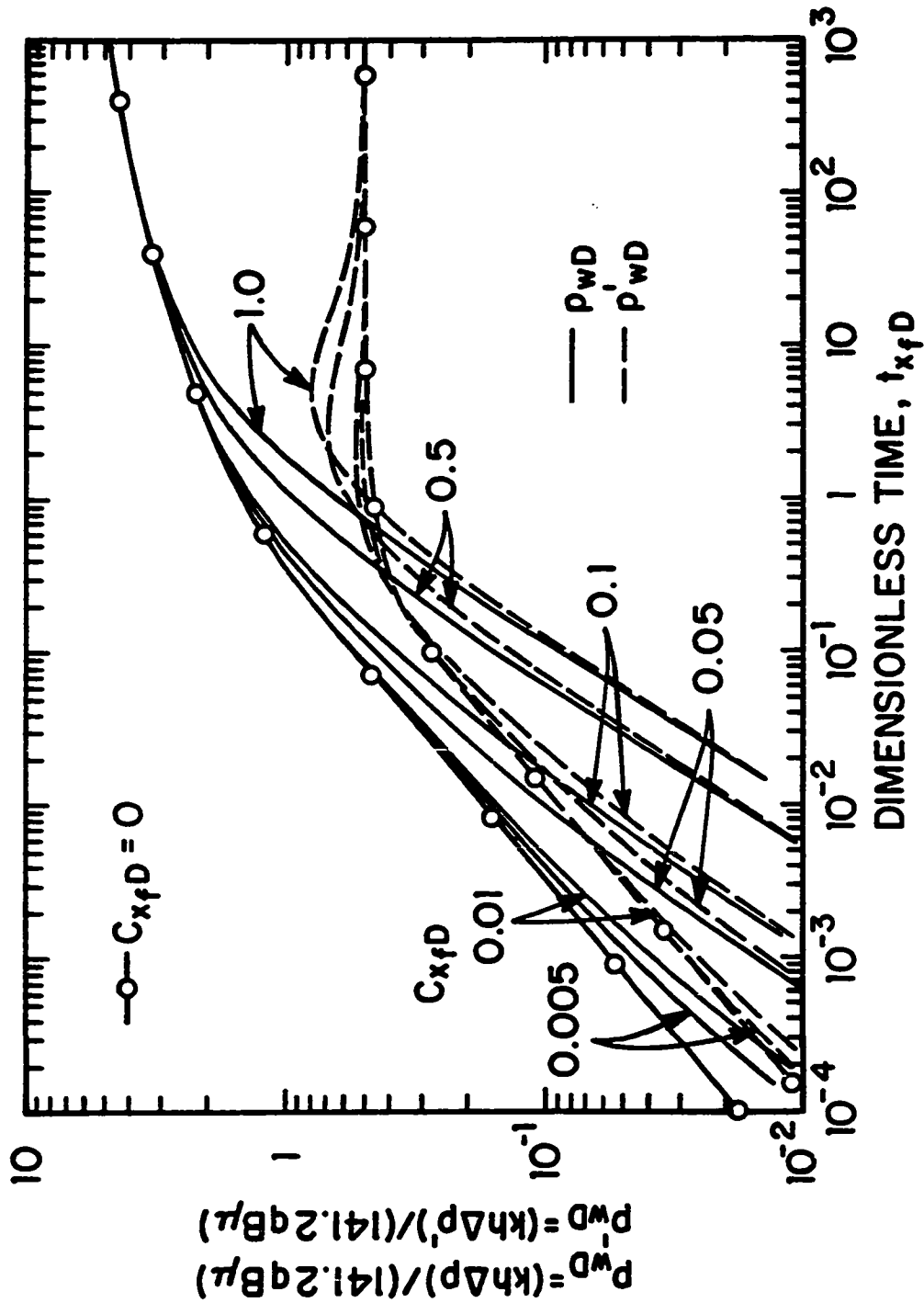


Fig. 3.1.11 - New Type Curve Including  $p_{wD}$  and  $p_{wD}'$ ; Uniform-Flux Fracture With Wellbore Storage

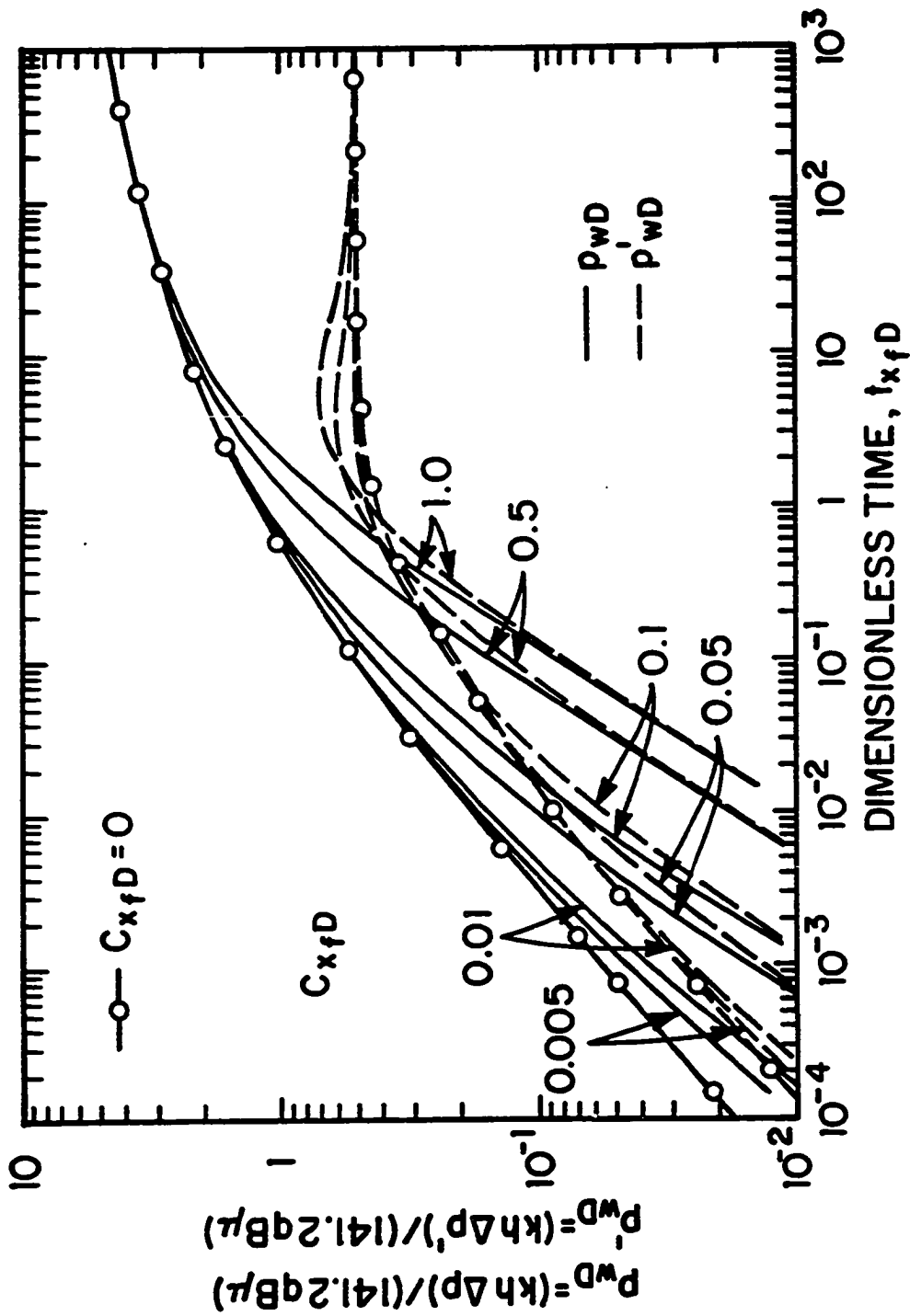


Fig. 3.1.12 - New Type Curve Including  $p_{wD}$  and  $p'_{wD}$ ; Infinite-Conductivity Fracture With Wellbore Storage

slope line predicted by the following relation:

$$p_{wD} = p'_{wD} = \frac{t_{x_f D}}{C_{x_f D}}. \quad (3.1.65)$$

Note that the same result was obtained for unfractured wells (see section 3.1.2) during the time period that wellbore storage controls the pressure response. At late times ( $t_{x_f D} \geq 100$ ), for all values of dimensionless wellbore storage constants considered in Figs. 3.1.11 and 3.1.12, wellbore storage effects no longer controls the pressure response; that is, pseudoradial flow prevails. When pseudoradial flow prevails, the following equations apply:

$$p_{wD} = \frac{1}{2} [\ln(t_{x_f D}) + c], \quad (3.1.66)$$

and

$$p'_{wD} = 0.5. \quad (3.1.67)$$

In Eq. 3.1.66,  $c = 2.80907$  for an uniform-flux fracture and  $c = 2.2$  for an infinite-conductivity fracture. It should be also noted from Figs. 3.1.11 and 3.1.12 that for large values of dimensionless wellbore storage constant during the transition time period from wellbore storage dominated flow to the pseudoradial flow, linear flow period is obscured because both the dimensionless pressure and its logarithmic derivative do not display the half slope line predicted by Eq. 3.1.30.

Figures 3.1.13 and 3.1.14, respectively, show new uniform-flux and infinite-conductivity type curves based on the derivative group,  $p_{wD}/(2p'_{wD})$ , versus the dimensionless time,  $t_{x_f D}$ , in log-log coordinates for the same values of dimensionless wellbore storage coefficient considered in Figs. 3.1.11 and 3.1.12. In Figs. 3.1.13 and 3.1.14, again the solid curve through circular data points represents the solution without wellbore storage effects; i.e.,  $C_{x_f D} = 0$ . In general, the character (curvature) of the curves are quite good with regard to obtaining a well-defined type-curve match of field data plot of  $\Delta p/(2\Delta p')$  versus  $t$ . However, at early times and for values  $C_{x_f D} \geq 0.01$ , the graph of  $p_{wD}/(2p'_{wD})$  is flat and equals 0.5, which indicates that in this interval, a unique match of field data plot with the type curves

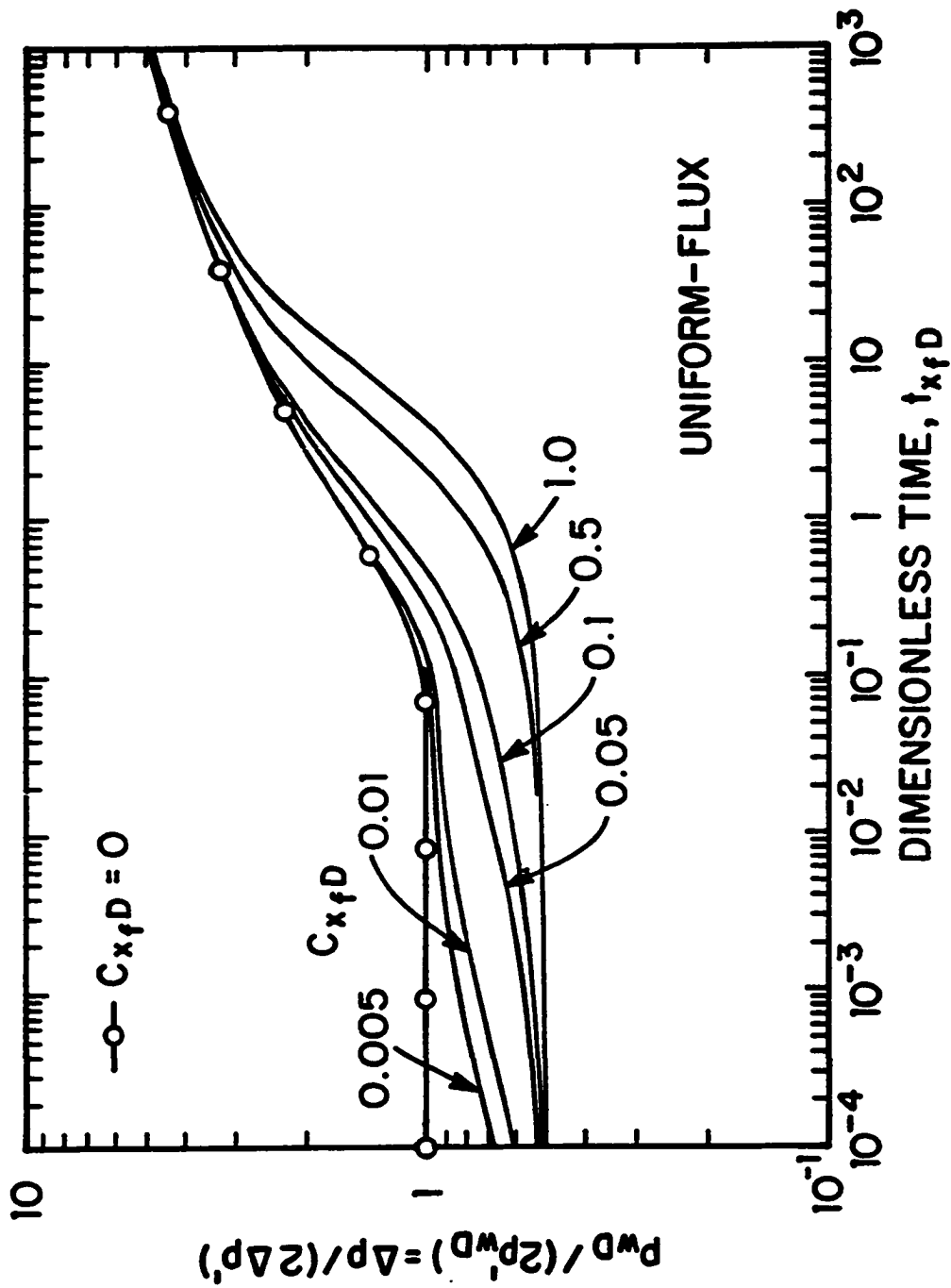


Fig. 3.1.13 - New Type Curve Based on  $p_{wD} / (2p'_{wD})$ ; Uniform-Flux Fracture With Wellbore Storage

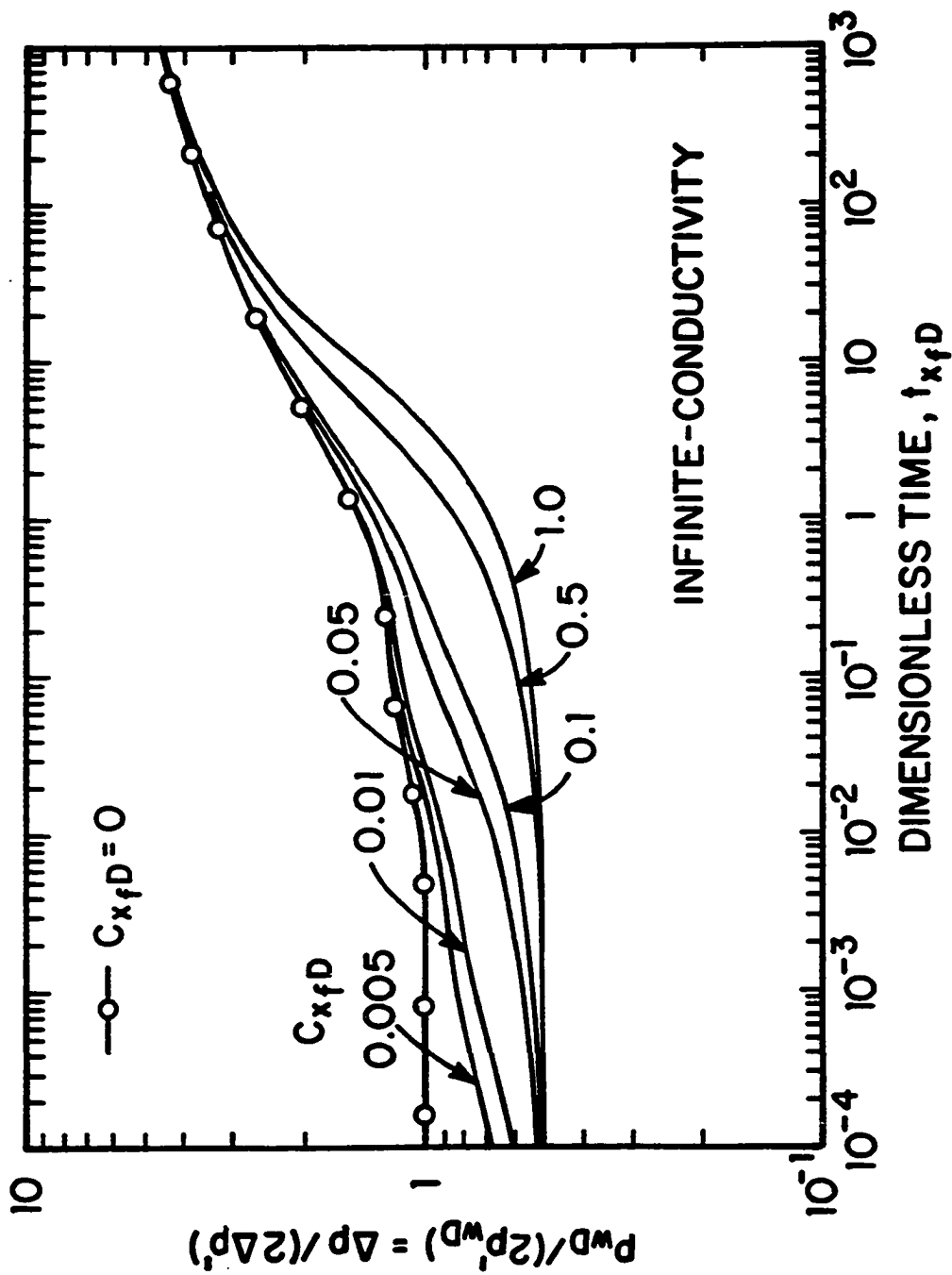


Fig. 3.1.14 - New Type Curve Based on  $p_{wD}/(2p'_{wD})$ ; Infinite-Conductivity Fracture With Wellbore Storage



of Figs. 3.1.13 and 3.1.14 is not possible for determining reservoir permeability and fracture half-length. If the field data are available beyond this interval, then a unique match of field data plot of  $\Delta p/(2\Delta p')$  is possible for determining reservoir parameters and fracture half-length. When wellbore storage effects no longer dominate the  $p_{wD}/(2p'_{wD})$  solution, the  $p_{wD}/(2p'_{wD})$  solution for a given value of  $C_{x,D}$  merges with the associated pressure/pressure-derivative solution without wellbore storage effects; that is,  $p_{wD}/(2p'_{wD})$  solution corresponding to a value of  $C_{x,D} = 0$  (solid curves with circular data points in Figs. 3.1.13 and 3.1.14). Note that each curve merges to the curve corresponding to  $C_{x,D} = 0$  at a different time depending on the value of  $C_{x,D}$ . Also note that the linear flow regime does not exist for large values of  $C_{x,D}$ ; that is,  $p_{wD}/(2p'_{wD})$  never equals 1. Given the solution for a particular value of  $C_{x,D}$ , pseudoradial flow exists when the following equation holds:

$$\frac{p_{wD}}{2p'_{wD}} = \frac{1}{2} [\ln(t_{x,D}) + c]. \quad (3.1.68)$$

The type curves of Figs. 3.1.13 and 3.1.14 can be extremely useful in analyzing well test data obtained at fractured well influenced by wellbore storage effects and in identifying the flow regimes exhibited by the field data. In using the type curves of Figs. 3.1.11 through 3.1.14, one first matches the pressure/pressure-derivative plotted as  $\Delta p/(2\Delta p')$  versus  $t$  with the appropriate type curve [ $p_{wD}/(2p'_{wD})$ ] shown in Figs. 3.1.13 and 3.1.14 by the standard procedure described earlier; i.e., by the horizontal movement of the field data plot only. This type-curve match of the  $\Delta p/(2\Delta p')$  data will give an estimate of  $C_{x,D}$  from the specific type curve matched, and the time match points will fix the correspondence between  $t$  and  $t_{x,D}$ . Once this correspondence is fixed, one prepares a log-log plot of  $\Delta p$  and  $\Delta p'$  versus  $t$  on a tracing paper using the basic scale of type curves shown in Figs. 3.1.11 and 3.1.12 and matches both  $\Delta p$  and  $\Delta p'$  versus  $t$  simultaneously with the  $p_{wD}$  and  $p'_{wD}$  versus  $t_{x,D}$  type curve corresponding to value of  $C_{x,D}$  obtained from the previous match by a vertical movement of field data plot. At this point, one can estimate the permeability from the pressure match-point values, fracture half-length from

the time match-point values, and the value of wellbore storage coefficient from the value of  $C_{e,D}$  associated with the curve matched; i.e., once the pressure match-point values are obtained, the parameters are estimated by the standard procedure<sup>64,65</sup>.

### 3.1.6 Finite-Conductivity Fractures

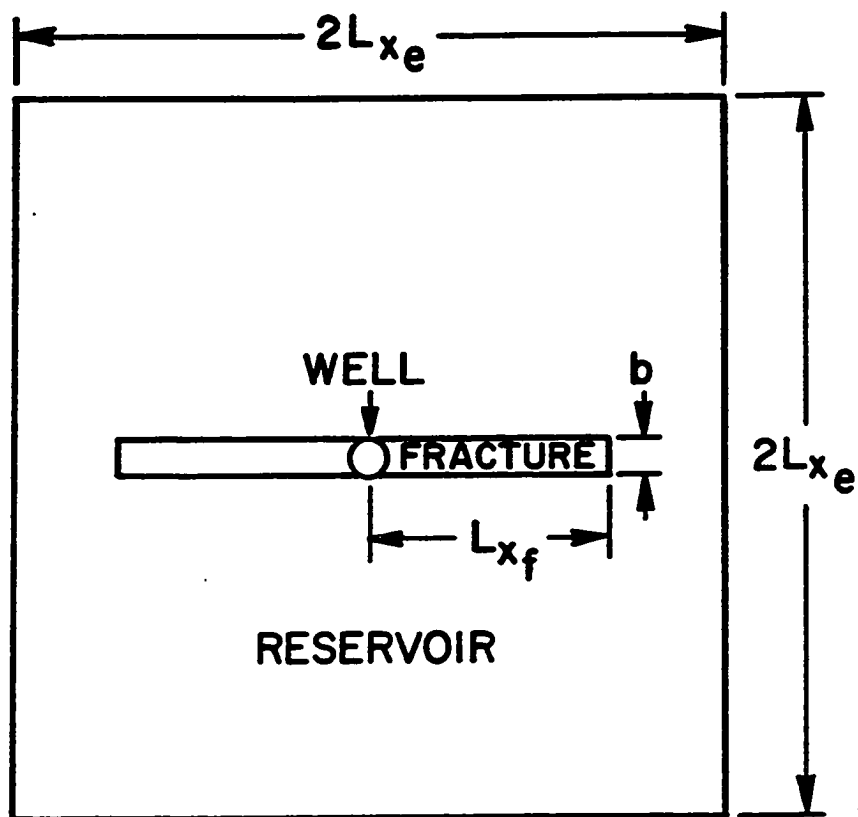
In this section, we consider finite-conductivity fractures and present new type curves based for analyzing well test data obtained at a well intercepted by a finite-conductivity vertical fracture. All results presented in this section assume constant rate production, no wellbore storage effects, negligible fracture storage, negligible fracture damage, and a single layer homogeneous reservoir of uniform thickness with the height of the vertical fracture equal to the formation thickness. A plan view of the reservoir/fracture system is shown in Fig. 3.1.15. Although Fig. 3.1.15 depicts a square drainage region, we present only results for the infinite-acting period so the outer reservoir boundaries have no influence on the wellbore pressure response for the time periods considered. (Fig. 3.1.15 would also depict the reservoir/fracture system for the uniform-flux and infinite-conductivity solutions considered in the previous sections provided we let the fracture width  $b$  approach zero to obtain a planar fracture.) All results presented here were generated via a numerical simulator written by Bennett<sup>65</sup>.

For finite-conductivity fractures, the dimensionless fracture conductivity is defined by

$$C_{fD} = \frac{k_f b}{k L_{xf}}, \quad (3.1.69)$$

where  $k_f$  and  $b$ , respectively, denote the permeability in the fracture and the width of the fracture.

As is well known, for the infinite-acting period, there exist three distinct flow regimes of practical interest that may be exhibited by the wellbore pressure response, bilinear flow which was discovered by Cinco-L. and Samaniego<sup>22</sup> (also see Refs. 9, 23 and 24), pseudolinear flow, Refs. 9, 21, 24 and 66, and pseudoradial flow, Refs. 9, 20-24 and 66. During bilinear flow, the dimensionless wellbore pressure



**Fig. 3.1.15 - Finite-Conductivity Fractured Well Geometry - Plan View**

drop is given by

$$p_{wD} = \frac{\pi t_{x_fD}^{1/4}}{\Gamma(5/4)\sqrt{2C_{fD}}}, \quad (3.1.70)$$

where  $\Gamma$  denotes the gamma function. The pressure response during pseudolinear and pseudoradial flow, respectively, is given by

$$p_{wD} = \sqrt{\pi t_{x_fD}} + \frac{\pi}{3C_{fD}}, \quad (3.1.71)$$

and

$$\begin{aligned} p_{wD} &= \frac{1}{2}(\ln(t_{x_fD}) + 0.80907) + \ln\left(\frac{L_{x_f}}{r_w}\right) + s_f \\ &= \frac{1}{2}(\ln(t_D) + 0.80907) + s_f. \end{aligned} \quad (3.1.72)$$

From the results of Refs. 24 and 66, pseudolinear flow as described by Eq. 3.1.71 occurs provided that  $C_{fD} \geq 15$ . (For  $5 \leq C_{fD} < 15$ , an equation similar to Eq. 3.1.71 applies provided the constant  $\pi/3$  in Eq. 31 is decreased; see Ref. 24.) In Eq. 3.1.72,  $s_f$  denotes the skin factor due to the existence of a fracture and is related to the effective wellbore radius  $r'_w$  and the fracture half-length by

$$r'_w = r_w e^{-s_f} = \frac{L_{x_f}}{n}, \quad (3.1.73)$$

where  $n$  is a parameter whose value depends on  $C_{fD}$ ; see, for example, Refs. 20 and 57. (For an infinite-conductivity fracture,  $n = 2$  and for a uniform-flux fracture,  $n = c$ ; see Ref. 17) From Eqs. 3.1.73 and 3.1.72, it follows easily that, during pseudoradial flow,

$$\begin{aligned} p_{wD} &= \frac{1}{2}(\ln(t_{x_fD}) + 0.80907) + \ln(n) = \\ &= \frac{1}{2}(\ln(t_{Dr'_w}) + 0.80907) \end{aligned} \quad (3.1.74)$$

where, as noted previously, the value of  $n$  is determined by the value of  $C_{fD}$ . In Eq. 3.1.74,  $t_{Dr'_w}$  denotes dimensionless time based on the effective wellbore radius  $r'_w$ ; that is,

$$t_{Dr'_w} = \frac{2.637 \times 10^{-4} kt}{\phi c_t (r'_w)^2}. \quad (3.1.75)$$

As is well known<sup>20,21</sup>,  $p_{wD}$  is a unique function of  $t_{x,D}$  and  $C_{fD}$  during the infinite-acting period. Note this is the expected result based on Eqs. 3.1.70, 3.1.71 and 3.1.72. Based on this result, several authors have presented type curves for analyzing well-test pressure data obtained at a well intercepted by a finite-conductivity vertical fracture. In particular, Refs. 20 and 21 presented type curves as log-log plots of  $p_{wD}$  versus  $t_{x,D}$  with each curve corresponding to a specific value of  $C_{fD}$ . (The type curves of Refs. 20 and 21 assume a single-layer reservoir with the fracture height equal to the formation thickness and the well in the center of the fracture, but the results of Refs. 68-71 indicate that the type curves are applicable for more general conditions.) Subsequent to the work of Refs. 20 and 21, Cinco-L. and Samaniego-V.<sup>22</sup> presented the solutions (type-curves) as log-log graphs of  $C_{fD}p_{wD}$  versus  $C_{fD}^2 t_{x,D}$  with each curve corresponding to a specific value of  $C_{fD}$ . Wong *et al.*<sup>9</sup> added the pressure derivative solutions (dashed curves in Fig. 3.1.16) to these type curves to obtain the complete type curves shown in Fig. 3.1.16 which are discussed in more detail later. Finally, Rosato *et al.*<sup>23</sup> prepared type curves as log-log plots of  $p_{wD}$  versus  $t_{x,D}/C_{fD}^2$ . The type curves of Ref. 22 (dimensionless pressure solutions shown as solid curves in Fig. 3.1.16) as well as the type curves of Ref. 23 correlate solutions for all values of  $C_{fD}$  during bilinear flow.

Superficially, it appears that the type curves of Refs. 20, 21 and 23 have an advantage if a prefracture estimate of flow capacity,  $kh$ , is known since, in this case, measured  $\Delta p$  data can be converted to dimensionless form using Eq. 2.1.1. A log-log plot of this  $p_{wD}$  versus  $t$  data can then be type-curve matched by moving this data only in the horizontal direction. Such a procedure simplifies the type curve matching procedure but does not resolve the problem of a nonunique match in all cases. In fact, one of the significant advantages of the Wong *et al.*<sup>9</sup> type curves is that their method of plotting makes it clear when nonunique results are possible.

The basis for the type curves of Ref. 22 (pressure solutions represented by solid curves in Fig. 3.1.16) can be seen as follows. Multiplying Eq. 3.1.70 by  $C_{fD}$  and

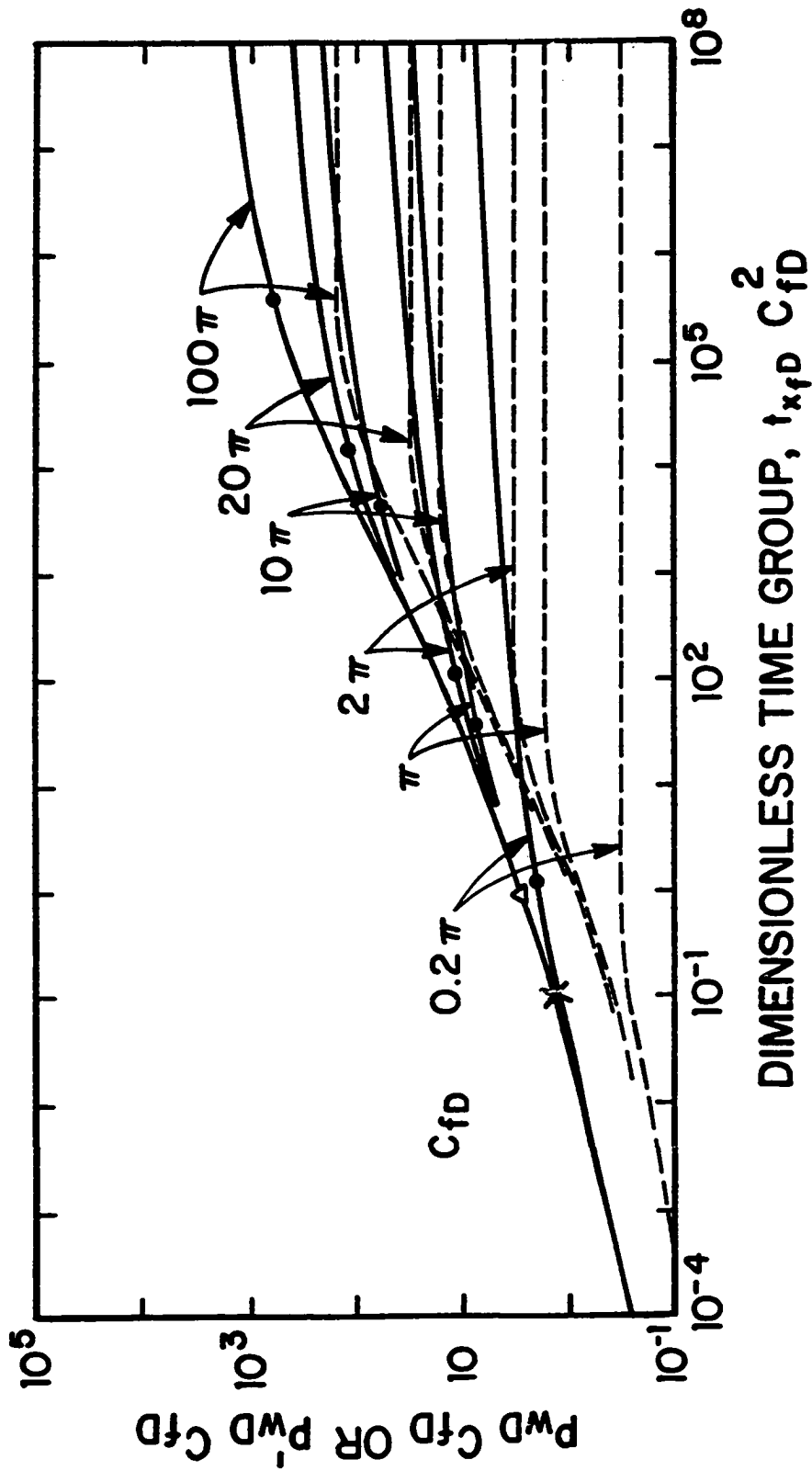


Fig. 3.1.16 - Wong *et al.*'s Finite-Conductivity Fractured Well Type Curve

rearranging the resulting equation gives

$$C_{fD}p_{wD} = \frac{\pi}{\Gamma(5/4)\sqrt{2}} \left( C_{fD}^2 t_{x,D} \right)^{1/4}. \quad (3.1.76)$$

By multiplying Eq. 3.1.71 by  $C_{fD}$ , we obtain

$$C_{fD}p_{wD} = \sqrt{\pi C_{fD}^2 t_{x,D}} + \frac{\pi}{3}. \quad (3.1.77)$$

Eqs. 3.1.76 and 3.1.77 indicate that solutions for all values of  $C_{fD}$  can be combined to obtain a single-curve during both the bilinear and pseudolinear flow regimes provided that solutions are graphed as  $C_{fD}p_{wD}$  versus  $C_{fD}^2 t_{x,D}$ .

Taking logarithmic derivatives of Eqs. 3.1.76 and 3.1.77 with respect to  $t_{x,D}$ , respectively, gives

$$C_{fD}p'_{wD} = \frac{\pi}{4\sqrt{2}\Gamma(5/4)} \left( t_{x,D} C_{fD}^2 \right)^{1/4}, \quad (3.1.78)$$

during bilinear flow and

$$C_{fD}p'_{wD} = \frac{\sqrt{\pi}}{2} \left( t_{x,D} C_{fD}^2 \right)^{1/2}, \quad (3.1.79)$$

during pseudolinear flow. Note that Eqs. 3.1.78 and 3.1.79 indicate that during both bilinear flow and pseudolinear flow, derivative solutions for all values of  $C_{fD}$  can be combined into a single-curve by plotting these solutions as  $C_{fD}p'_{wD}$  versus  $t_{x,D}C_{fD}^2$ .

Figure 3.1.16 displays the type curves of Wong *et al.*<sup>9</sup>. In Fig. 3.1.16, the solid curves and dashed curves, respectively, represent graphs of  $p_{wD}C_{fD}$  and  $p'_{wD}C_{fD}$  versus  $t_{x,D}C_{fD}^2$ . The point on the solid curve labeled with a cross corresponds to the time at which  $t_{x,D}C_{fD}^2 = 0.1$  which corresponds to the approximate time at which bilinear flow ends for  $C_{fD} \geq 3$  according to the results of Ref. 22. (For  $C_{fD} < 3$ , formulas for the ending time of bilinear flow are more complicated; see Ref. 22.) According to the results of Ref. 66, pseudolinear flow, Eq. 3.1.71, begins approximately at the time corresponding to  $t_{x,D}C_{fD}^2 = 1$  which corresponds to the point labeled with an open triangle in Fig. 3.1.16. Points labeled with solid circles

in Fig. 3.1.16 correspond to the approximate time at which pseudoradial flow begins for the various values of  $C_{fD}$ . Note for  $C_{fD} \geq 10\pi$ , all  $p_{wD}C_{fD}$  solutions correlate (lie on the same curve) for  $t_{x_fD} < 10^3$  and all corresponding  $p'_{wD}C_{fD}$  solutions lie on the top dashed curve for  $t_{x_fD} < 10^2$  as expected based on the discussion given previously. This indicates that if  $C_{fD} \geq 10\pi$  and all pressure data corresponds to  $t_{x_fD}C_{fD}^2 < 10^2$ , then it will not be possible to determine  $C_{fD}$  directly from the type curve match obtained using the type curves of Fig. 3.1.16 even though the type curve match will be unique. However, if prefracture estimates of  $k$  and  $h$  are available, a complete analysis is still possible as discussed later.

If all measured pressure data corresponds to the bilinear flow period, there exists no reliable procedure to determine fracture half-length. However, if prefracture estimates of  $k$  and  $h$  are known, one can obtain fracture conductivity  $k_f b$  from a fourth root of time plot and a lower bound for  $L_{x_f}$  and an upper bound for  $C_{fD}$  can be obtained; see Refs. 9, 22 and 23.

To use the type curves of Fig. 3.1.16, one prepares a log-log plot of  $\Delta p$  and  $\Delta p'$  versus  $t$  on tracing paper using the scales of the type curve, and then simultaneously matches pressure and pressure derivative data with the type curve of Fig. 3.1.16. Under ideal circumstances, one obtains a unique match which gives the match point values:  $(\Delta p)_M$  and  $(p_{wD}C_{fD})_M$ ;  $(\Delta p')_M$  and  $(p'_{wD}C_{fD})_M$ ;  $(t_M)$  and  $(t_{x_fD}C_{fD}^2)_M$  and also gives the value of  $(C_{fD})_M$  corresponding to the the  $C_{fD}$  value associated with the pressure and pressure derivative curves matched. Here, the subscript  $M$  denotes a match point value. The value of flow capacity,  $kh$ , can be determined from the obvious rearrangement of the following equation:

$$\frac{kh}{141.2qB\mu} (C_{fD})_M = \frac{(p_{wD}C_{fD})_M}{\Delta p_M}, \quad (3.1.80)$$

and then assuming that the reservoir thickness  $h$  is known, the permeability  $k$  can be determined. The fracture half-length can be determined by taking square roots in the following equation:

$$L_{x_f}^2 = \frac{t_M (C_{fD})_M^2}{(t_{x_fD}C_{fD}^2)_M} \frac{2.637 \times 10^{-4} k}{\phi c_i \mu}. \quad (3.1.81)$$



If a unique type curve match is obtained, but the value of  $C_{fD}$  cannot be determined from the match as discussed previously, then a complete analysis is still possible provided prefracture estimates of  $k$  and  $h$  are available. In this case, one computes  $(C_{fD})_M$  from the obvious rearrangement of Eq. 3.1.80 and then still computes  $L_{x_f}$  with Eq. 3.1.81. After the values of  $C_{fD}$ ,  $k$  and  $L_{x_f}$  have been determined, one can estimate the value of  $k_f b$  from Eq. 3.1.69. Once  $C_{fD}$  has been determined, one can determine the value of  $n$  (see Refs. 67 and 20) and then one can estimate the value of the skin factor  $s_f$  due to the existence of the fracture by taking the natural logarithm of Eq. 3.1.73 and solving the resulting equation for  $s_f$ . However, this value of  $s_f$  is meaningful only at times subsequent to the beginning of pseudoradial flow.

From Eqs. 3.1.76 and 3.1.78, it follows that

$$\frac{p_{wD}}{2p'_{wD}} = 2, \quad (3.1.82)$$

during bilinear flow. From Eqs. 3.1.77 and 3.1.79, it follows easily that

$$\frac{p_{wD}}{2p'_{wD}} = 1 + \left[ \frac{\sqrt{\pi}}{3\sqrt{C_{fD}^2 t_{x_f D}}} \right], \quad (3.1.83)$$

during pseudolinear flow. Similarly, during pseudoradial flow,

$$\frac{p_{wD}}{2p'_{wD}} = p_{wD} = 1.151(\log(t_{Dx_f}) + 0.351 + \log(n^2)). \quad (3.1.84)$$

Figure 3.1.17 presents a semilog type curve motivated by the results of Eqs. 3.1.82 and 3.1.83. Note that for practical purposes Eq. 3.1.82 applies for  $t_{x_f D} C_{fD}^2 \leq 10^{-1}$  provided that  $C_{fD} \geq 3$ . The open triangle on Fig. 3.1.17 corresponds to the time where  $t_{x_f D} C_{fD}^2 = 1$  which represents the time at which pseudolinear flow begins for  $C_{fD} \geq 15$ ; see Ref. 66. Note that the term in square braces on the right side of Eq. 3.1.83 is not negligible at this time; in fact, this term does not ever become completely negligible unless  $C_{fD}$  is very large. Note that the uniform-flux and infinite-conductivity fracture solutions are also shown on Fig. 3.1.17 where we have used  $C_{fD} = 100\pi$  for the infinite-conductivity case and  $C_{fD} = 4.4$  for the

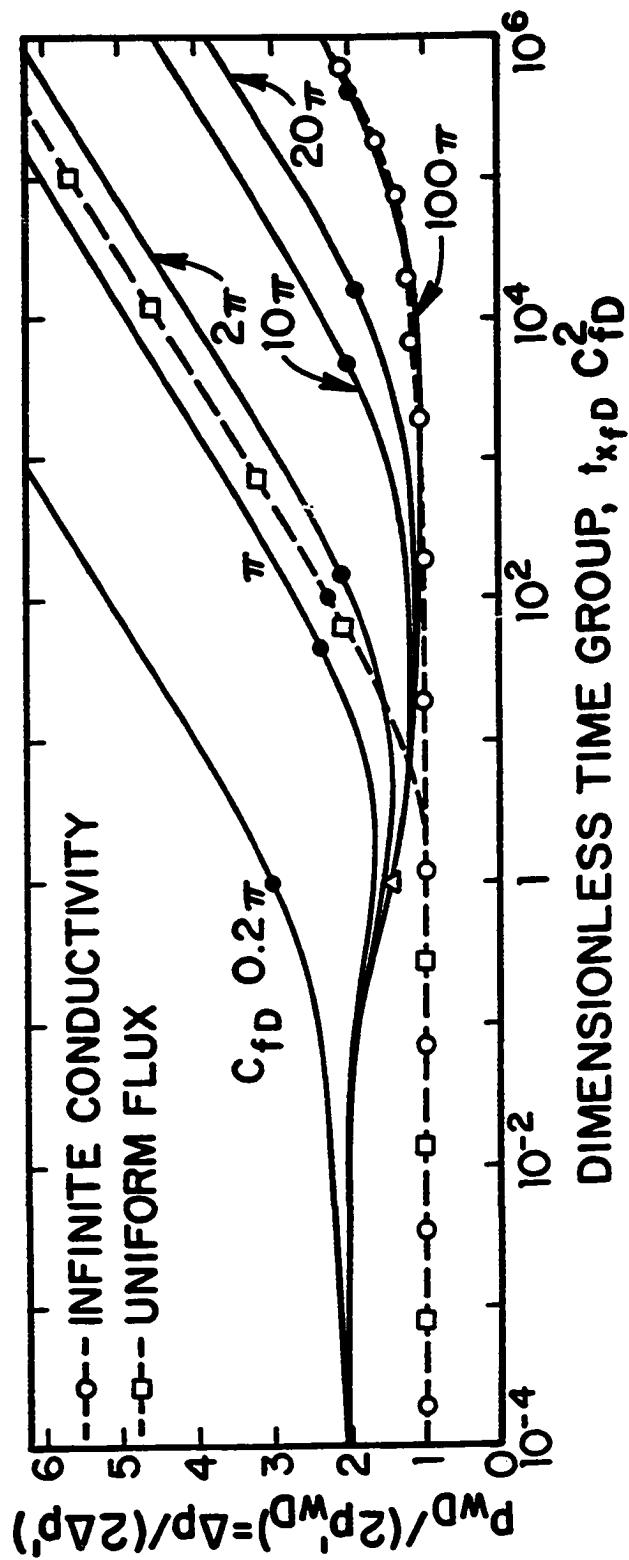


Fig. 3.1.17 - New Finite-Conductivity Fractured Well Type Curve Based on  $p_{wD}/(2p'_{wD})$  Versus  $C_{fD}^2 t_{x_f D}$

uniform-flux case. The solid circular data points on Fig. 3.1.17 correspond to the approximate time at which pseudoradial flow (Eq. 3.1.84) begins. The advantages of the semilog type curve of Fig. 3.1.17 is similar to the advantages of the type curves of Figs. 3.1.1, 3.1.3, 3.1.5, 3.1.6, 3.1.13 and 3.1.14. Specifically, the type curve allows us to identify flow regimes, allows us to determine if measured pressure data actually does correspond to a finite-conductivity fracture and simplifies the type curve matching procedure since  $\Delta p/(2\Delta p')$  versus  $t$  data is moved only in the horizontal direction in order to obtain a type-curve match using Fig. 3.1.17. From such a type curve match, one can determine how to complete the analysis. This type curve match should clearly indicate whether data corresponding to bilinear, pseudolinear and pseudoradial flow are available. Given sufficient data, this type-curve match will indicate whether analysis should be based on the uniform-flux solution, the infinite-conductivity solution, or the finite-conductivity solutions for a particular value of  $C_{fD}$ . The type-curve match will also fix the correspondence between  $t$  and  $t_{Dx}, C_{fD}^2$ ; that is, determine the time match-point values so that data can then be type-curve matched with the type curves of Fig. 3.1.16 by moving data only in the vertical direction. In fact, if  $k$  and  $h$  are known from a prefracture test and  $C_{fD}$  is determined by type-curve matching with Fig. 3.1.17, then a complete analysis can be obtained from this match. Here, one would determine  $L_x$ , from Eq. 3.1.81 and then proceed as discussed previously.

Although we prefer the mode of graphing used in Fig. 3.1.16 because it correlates solutions during the bilinear and pseudolinear flow regimes, it is possible to present type curves in other ways. For example, Figs. 3.1.18 and 3.1.19 present type curves along the lines of Refs. 20 and 21. Fig. 3.1.18 shows the type curve where we have added the pressure derivative,  $p'_{wD}$ , to the original type curves based on dimensionless pressure,  $p_{wD}$ . Similarly, Fig. 3.1.19 shows the type curve where the pressure/pressure-derivative group,  $p_{wD}/(2p'_{wD})$  is plotted against the dimensionless time,  $t_{x,D}$ . It is also possible to prepare type curves as log-log plots of  $p_{wD}$  and  $p'_{wD}$  versus  $t_{D,r'_w}$  as shown in Fig. 3.1.20. These type curves correlate all solutions during the pseudoradial flow regime. (To the best of our knowledge,

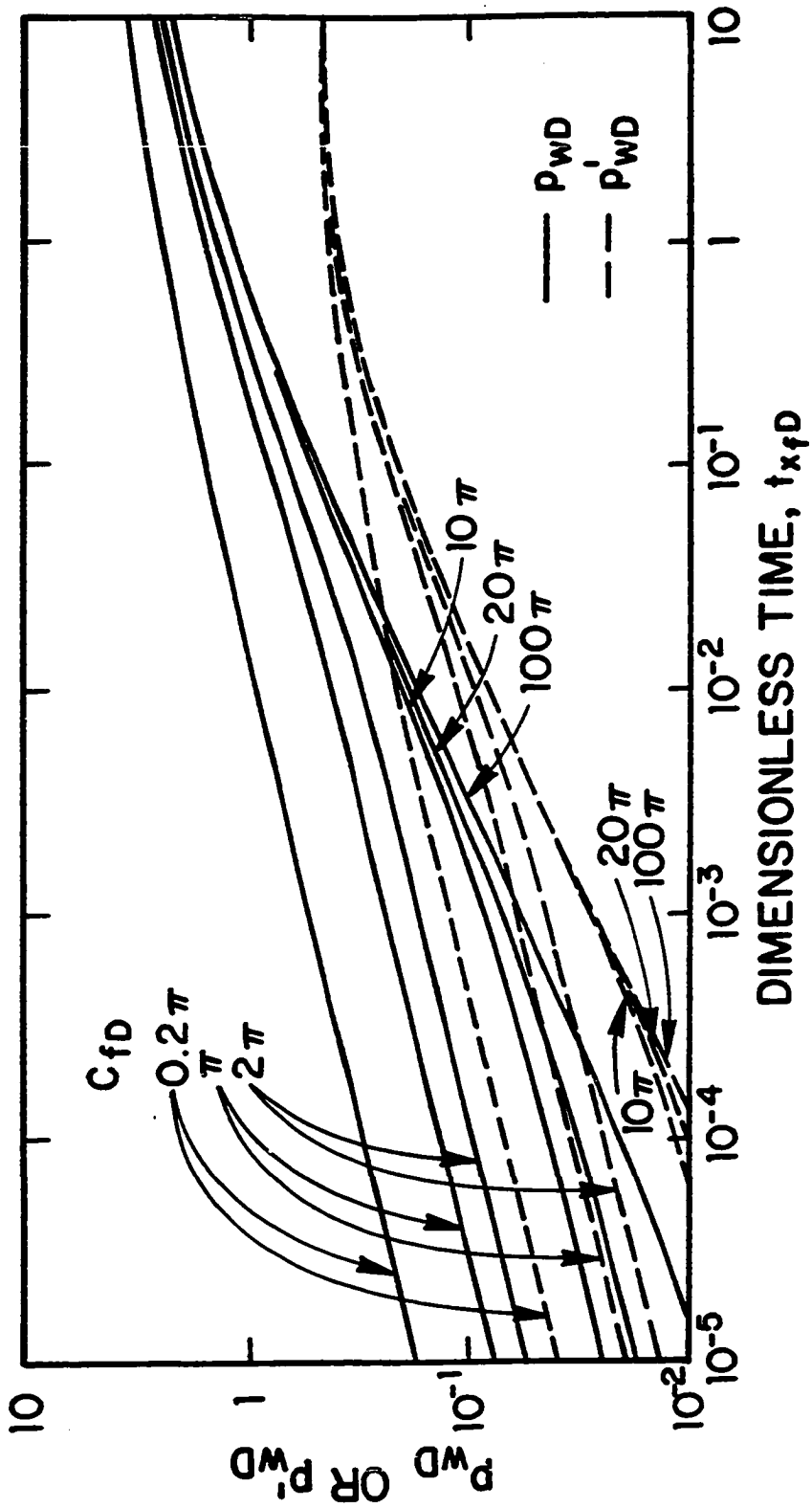


Fig. 3.1.18 - Finite-Conductivity Type Curve Based on  $p_{wD}$  and  $p'_{wD}$  Versus  $t_{xfD}$

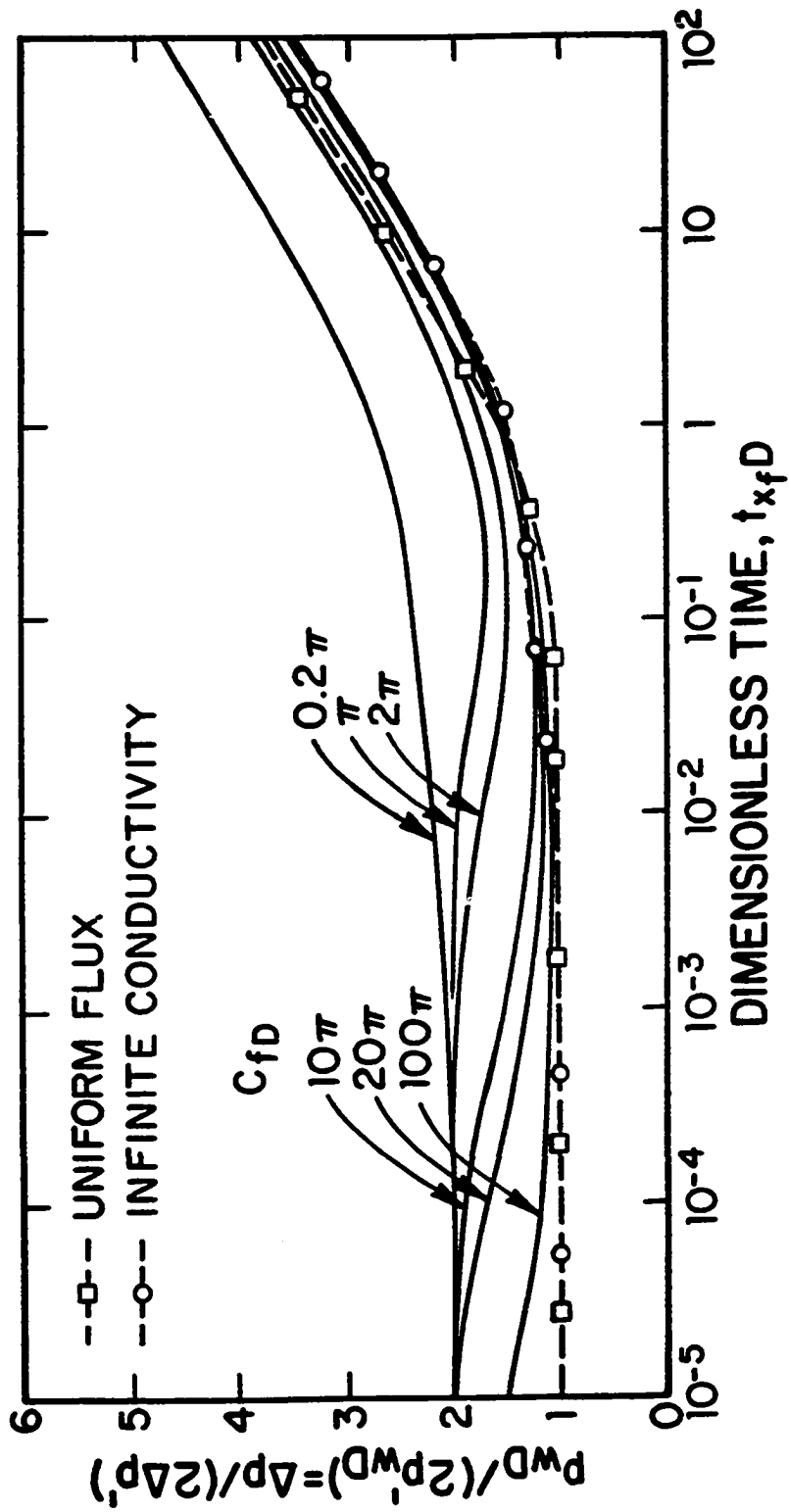


Fig. 3.1.19 - Finite-Conductivity Type Curve Based on  $p_{wD}/(2p'_{wD})$  Versus  $t_{x_f} D$

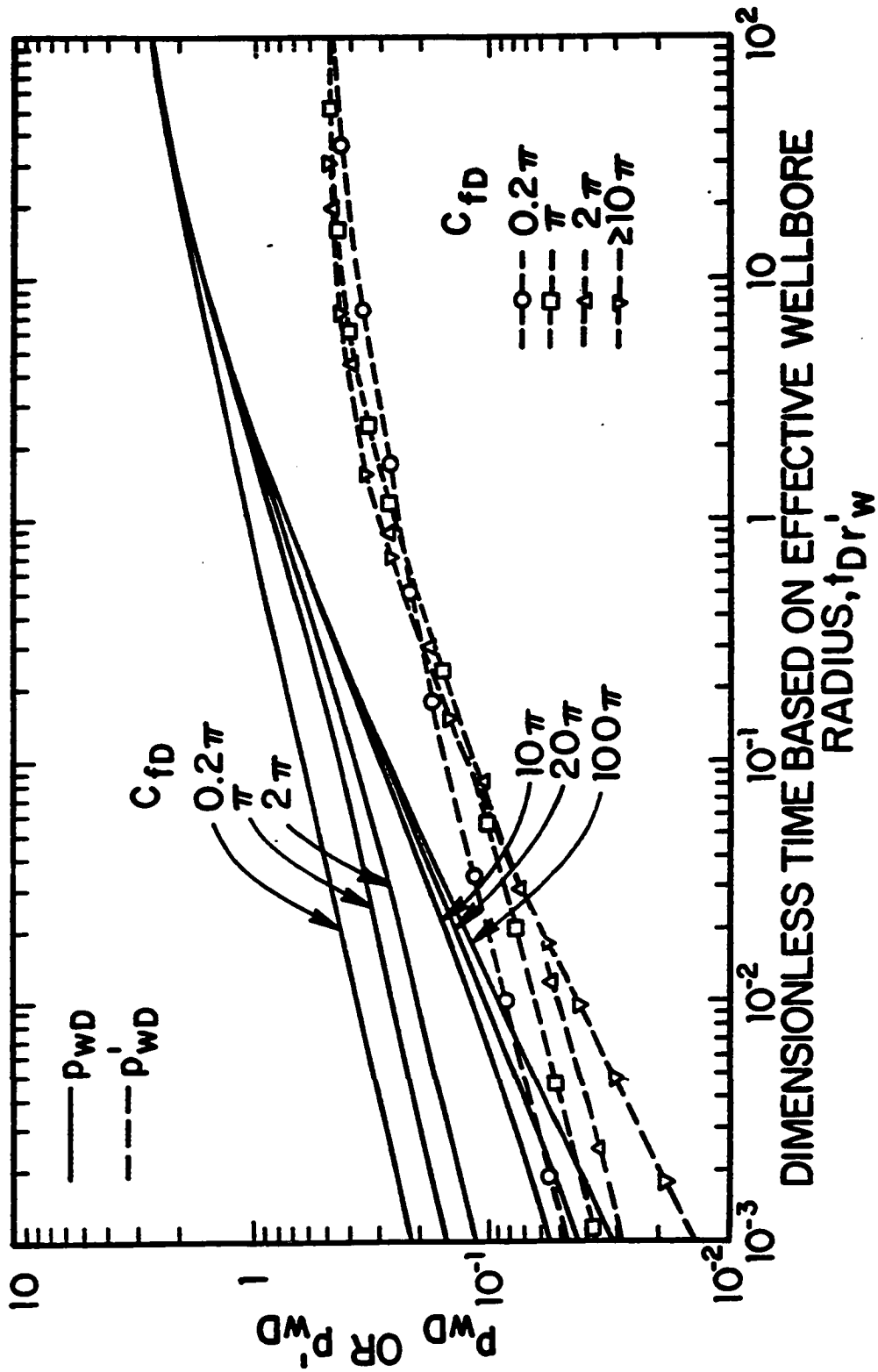


Fig. 3.1.20 - Finite-Conductivity Type Curve Based on Effective Wellbore Radius

the type curves of Figs. 3.1.17, 3.1.18, 3.1.19 and 3.1.20 have not been presented previously.)

### 3.1.7 Unfractured Well in a Closed Bounded Reservoir: Constant Rate Production

Here, we present new type curves using the basic ideas presented previously for the case where an unfractured well is located at the center of a close bounded square reservoir. All results assume constant rate production from a line source well, and no wellbore storage and skin effects. Type curves were obtained using the solution based on superposition and the method of images<sup>35,72,73</sup>. Although we only generate type curves for analyzing well test data obtained at a well located in a closed bounded square reservoir, type curves can be constructed for other geometric shapes and well locations by using the solution procedure described in Ref. 73. These type curves can then be used to analyze field data along the same lines presented in the following for a well at the center of a closed square.

As is well known, for an unfractured well in a closed bounded reservoir, there exist two distinct flow regimes which can be exhibited by the wellbore pressure response; radial flow and pseudosteady-state flow. During radial flow, the dimensionless pressure drop and its logarithmic derivative are given by the following well known equations:

$$p_{wD} = \frac{1}{2} [\ln(t_D) + 0.80907], \quad (3.1.85)$$

and

$$p'_{wD} = \frac{1}{2}. \quad (3.1.86)$$

During pseudosteady-state flow period; that is, the time period that the physical no-flow boundaries of reservoir control the well pressure response, the dimensionless well pressure drop and its logarithmic derivative are given, respectively, by

$$p_{wD}(t_D) = 2\pi t_{AD} + \frac{1}{2} \ln \left( \frac{4A}{e^{\gamma} C_A r_w^2} \right), \quad (3.1.87)$$

and

$$p'_{wD} = \frac{dp_{wD}}{d \ln(t_D)} = \frac{dp_{wD}}{d \ln(t_{AD})} = 2\pi t_{AD}, \quad (3.1.88)$$

where  $t_D$  and  $t_{AD}$ , respectively, denote the dimensionless time based on wellbore radius  $r_w$  (Eq. 2.1.2) and the dimensionless time based on well's drainage area  $A$  (Eq. 2.1.4). The relation between  $t_D$  and  $t_{AD}$  follows directly from Eqs. 2.1.2 and 2.1.4 as

$$t_{AD} = \left( \frac{r_w}{\sqrt{A}} \right)^2 t_D. \quad (3.1.89)$$

In Eq. 3.1.88,  $C_A$  ( $= 30.8828$  for a well at the center of a closed square drainage region) is the Dietz shape factor<sup>36</sup>, and  $\gamma$  ( $= 0.57722$ ) is the Euler's constant.

Type curves based on the pressure derivative for analyzing well test data obtained at a well located in a closed bounded rectangular reservoir were first presented by Tiab and Chriehlow<sup>1</sup>. Type curves of Ref. 1 were based on a plot of the Cartesian derivative,  $dp_{wD}/dt_{DA}$ , versus dimensionless time  $t_{AD}$ . Later, Proano and Lilley<sup>74</sup> presented type curves based on both the dimensionless pressure  $p_{wD}$  and the logarithmic derivative of pressure change,  $dp_{wD}/d\ln(t_{AD})$  ( $= dp_{wD}/d\ln t_D$ ), for analyzing well test data obtained at a well influenced by wellbore storage and skin effects in a closed bounded reservoir. As mentioned earlier, the approach taken in this work for constructing derivative type curves is different from those of Refs. 1 and 74. Our approach is to use the pressure/pressure-derivative group in generating type curves which will further simplify interpretation and analysis of well test data obtained at a well located in a closed bounded reservoir.

The motivation for the new type curves follows. During radial flow; that is, When Eqs. 3.1.85 and 3.1.86 apply, it can be easily shown that

$$\frac{p_{wD}}{2p'_{wD}} = p_{wD} = \frac{1}{2} [\ln(t_D) + 0.80907]. \quad (3.1.90)$$

Similarly, during pseudosteady-state flow; that is, when Eqs. 3.1.87 and 3.1.88 apply, the following equation holds:

$$\frac{p_{wD}}{2p'_{wD}} = \frac{1}{2} + a(t_{AD}), \quad (3.1.91)$$

where  $a(t_{AD})$  is given by

$$a(t_{AD}) = \frac{1}{8\pi t_{AD}} \ln \left[ \frac{4A}{e^{\gamma} C_A r_w^2} \right] \quad (3.1.92)$$



If  $t_{AD}$  is sufficiently large so that  $a(t_{AD})$  is negligible compared to 0.5 in Eq. 3.1.91, then Eq. 3.1.91 reduces to

$$\frac{p_{wD}}{2p'_{wD}} = \frac{\Delta p}{2\Delta p'} = \frac{1}{2}. \quad (3.1.93)$$

Figure 3.1.21 shows new type curves for a well in the center of a closed (no-flow outer boundaries) square reservoir. The solid curves represent the log-log plots of  $p_{wD}$  versus  $t_D$  and the dashed curves represent the log-log plots of  $p_{wD}/(2p'_{wD})$  versus  $t_D$  for various values of the parameter  $\sqrt{A}/r_w$ . Points labeled with a solid circle on the dimensionless pressure/pressure-derivative solutions for a given value of  $\sqrt{A}/r_w$  denote the time when pseudosteady-state flow begins according to the criterion that pseudosteady-state flow begins at the earliest time such that left and right sides of Eq. 3.1.88 differ no more than 5%. The curve labeled with an infinity sign on Fig. 3.1.21 represents the infinite-acting solution given by Eq. 3.1.85. Note that during the infinite-acting period,  $p_{wD}$  and  $p_{wD}/(2p'_{wD})$  solutions are identical (see Eq. 3.1.90). Thus, for the infinite-acting solution (solid curve labeled by infinity sign in Fig. 3.1.20),  $p_{wD}$  coincides with  $p_{wD}/(2p'_{wD})$  at all times. However, when no-flow boundaries of the reservoir start to influence the well response, both the  $p_{wD}$  and  $p_{wD}/(2p'_{wD})$  solution diverge from the infinite-acting solution (curve labeled with an infinity sign). Moreover, for a given particular value of  $\sqrt{A}/r_w$ , the  $p_{wD}/(2p'_{wD})$  solution approaches asymptotically the value of 0.5 as predicted by Eq. 3.1.93. Note that the character (curvature) of curves representing the  $p_{wD}/(2p'_{wD})$  group is very good compared to the character of curves representing the  $p_{wD}$  solution, and thus, adding the  $p_{wD}/(2p'_{wD})$  solutions should enhance one's ability to obtain a well-defined match of field data and to identify the flow regimes exhibited by actual field data.

The procedure using the type curves of Fig. 3.1.21 is identical to procedure discussed earlier. Once the time match-point, pressure match-point values and the parameter  $\sqrt{A}/r_w$  are obtained from the type-curve match of field data with a particular type curve of Fig. 3.1.20, one can determine the flow capacity using the

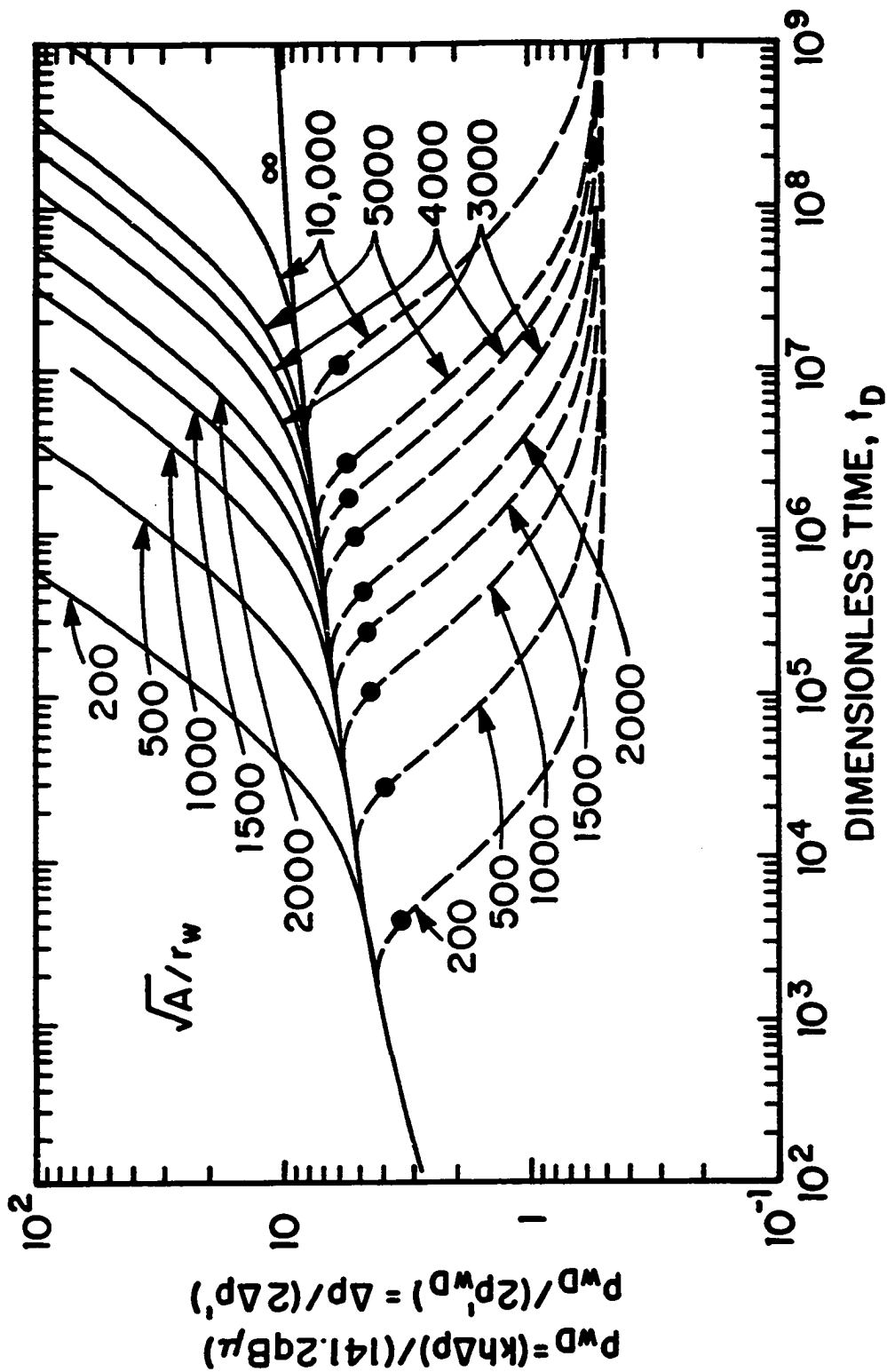


Fig. 3.1.21 - Type Curve Based on  $p_{wD}$  and  $p_{wD}/(2p'_{wD})$ ; Unfractured Well in Closed Square Reservoir

pressure match-point values from

$$kh = \frac{141.2qB\mu(p_{wD})_M}{(\Delta p)_M}, \quad (3.1.94)$$

and the porosity-compressibility-thickness product using the time-match point values from

$$\phi c_i h = \frac{2.637 \times 10^{-4} kh(t)_M}{\mu r_w^2 (t_D)_M}. \quad (3.1.95)$$

The well's drainage area can be determined using the value of  $\sqrt{A}/r_w$  obtained from the specific type curve matched in Fig. 3.1.20 as

$$A = \left( \frac{\sqrt{A}}{r_w} \right)_M^2 r_w^2. \quad (3.1.96)$$

Note that if all field data corresponds to infinite acting period (radial flow period), then the value of the parameter  $\sqrt{A}/r_w$  cannot be determined from the type-curve match of field data. In this case, one can only obtain a lower bound for well's drainage area from Eq. 3.1.96.

As a final remark, we note that the  $p_{wD}$  and  $p_{wD}/(2p'_{wD})$  solutions shown in Fig. 3.1.21 assume no damage or no stimulation around the wellbore, that is, assume that the skin factor is zero. However, the type curves of Fig. 3.1.21 can be used to analyze nonzero skin cases provided the effective wellbore radius concept<sup>75</sup> is used. The effective wellbore radius is defined by

$$r'_w = r_w \exp(-s), \quad (3.1.97)$$

where  $s$  is the skin factor due to damage or stimulation around the wellbore. If  $t_D$  (Eq. 2.1.2) is replaced by  $t_{Dr'_w}$  (Eq. 3.1.75) and  $\sqrt{A}/r_w$  is replaced by  $\sqrt{A}/r'_w$ , then one can use the type curves of Fig. 3.1.20 to analyze the field data influenced by skin effect with the same procedure discussed earlier for the case where field data is not influenced by skin effect. In this case, one will still use Eq. 3.1.94 to determine the value of flow capacity. However, the effective wellbore radius,  $r'_w$ , should be computed from time match-point values, provided that  $\phi c_i h$  product is known, as

$$r'_w = \sqrt{\frac{2.637 \times 10^{-4} kh(t)_M}{\phi c_i h \mu (t_{Dr'_w})_M}}. \quad (3.1.98)$$

After obtaining  $r'_w$  from Eq. 3.1.98 one can determine both the skin factor  $s$  from the obvious rearrangement of Eq. 3.1.97 and the well's drainage area from Eq. 3.1.96 with  $r_w$  replaced by  $r'_w$ .

### 3.1.8 Planar Fractured Well in a Closed Bounded Reservoir

In this section, we consider the case where a planar (uniform-flux or infinite-conductivity) fractured well in the center of a closed (no-flow boundaries) square drainage region as depicted by Fig. 3.1.15 with  $b = 0$ . We consider both the case where the well is produced at a constant rate and the case where the well is produced at a constant wellbore pressure. The area of the square drainage region (see Fig. 3.1.15) is given by

$$A = 4L_{xe}^2, \quad (3.1.99)$$

where  $L_{xe}$  represents the distance from the well to the external boundary in both the  $x$  and  $y$  directions. The fracture is assumed to lie along the  $x$  axis; i.e., the fracture is parallel to two sides of the square drainage region.

In the discussion of constant pressure production case,  $q_D$  denotes the dimensionless well rate defined as

$$q_D(t_{x,D}) = \frac{141.2q(t)B\mu}{kh(p_i - p_{wf})}, \quad (3.1.100)$$

and  $q'_D$  denotes the logarithmic derivative of dimensionless rate  $q_D$  with respect to  $t_{x,D}$ ; i.e.,

$$q'_D = \frac{dq_D}{d \ln(t_{x,D})} = \frac{dq_D}{d \ln(t_D)} = \frac{dq_D}{d \ln(t_{AD})} = \frac{dq_D}{d \ln t}. \quad (3.1.101)$$

Here,  $q(t)$  is the well production rate measured at the surface as a function of time in STB/D and  $p_{wf}$  is the bottom-hole pressure. The equalities of Eq. 3.1.101 follow from the results of Chapter II.

#### 3.1.8.1 Constant Rate Production

Figures 3.1.22 and 3.1.23 show uniform-flux and infinite-conductivity type curves, respectively, for a well in the center of a closed square drainage region.

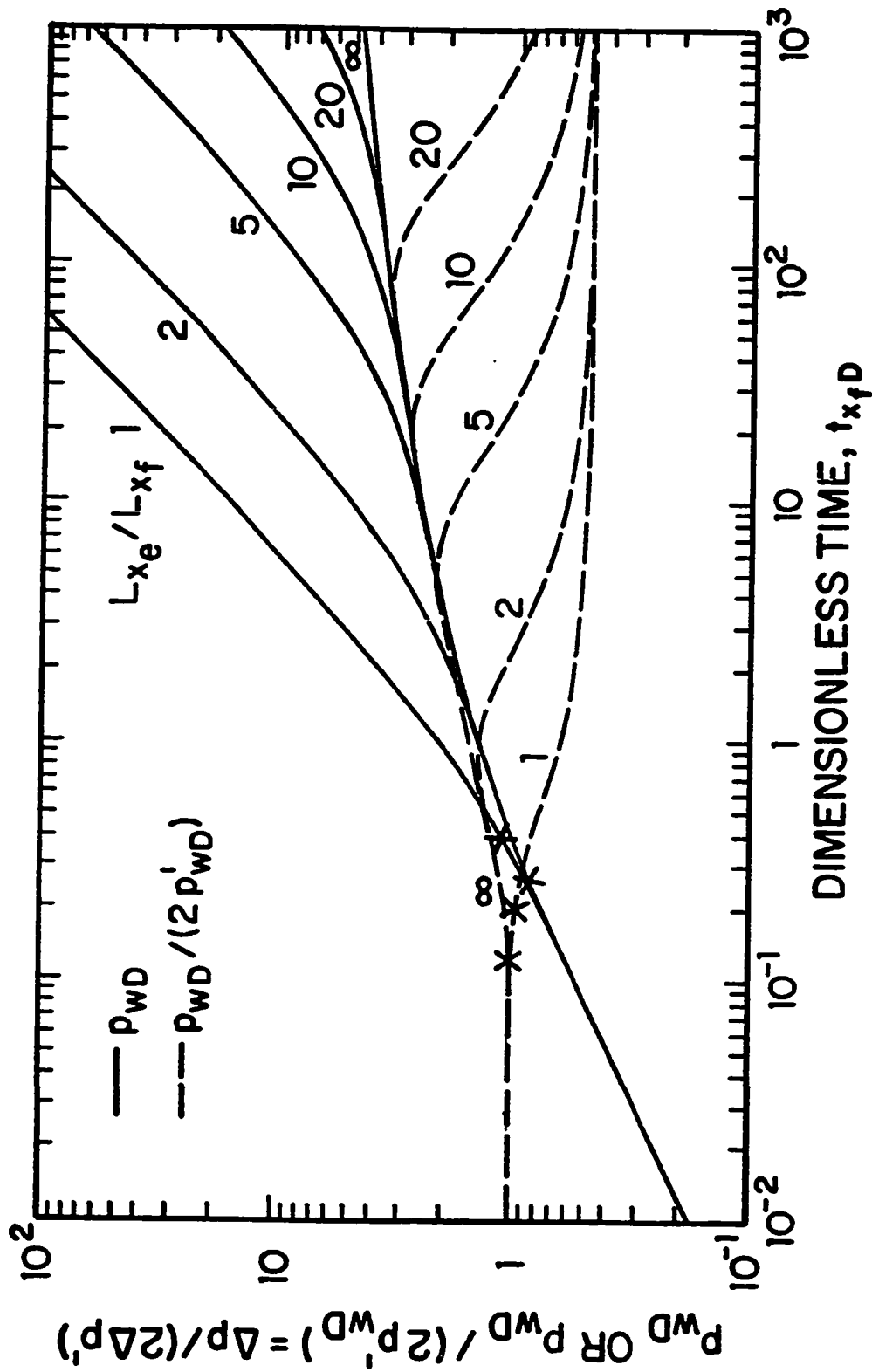


Fig. 3.1.22 - New Uniform-Flux Type Curve - Closed Square Reservoir; Constant Rate Production

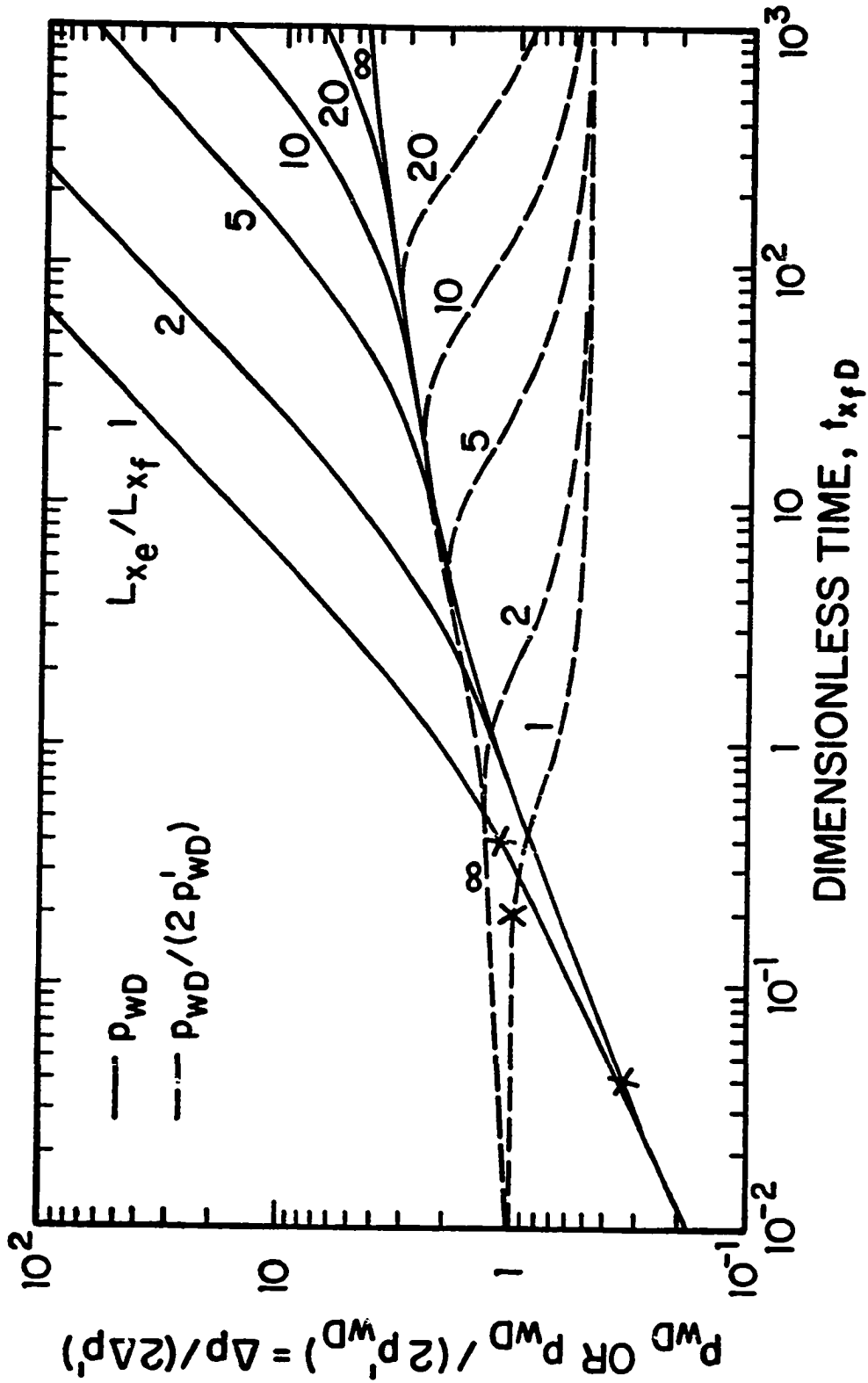


Fig. 3.1.23 - New Infinite-Conductivity Type Curve - Closed Square Reservoir; Constant Rate Production

The  $p_{wD}$  versus  $t_{x_jD}$  solutions shown in Figs. 3.1.22 and 3.1.23 were constructed by use of Gringarten *et al.*'s<sup>17</sup> solution (also see Gringarten<sup>19</sup>); that is,

$$p_{wD} = 2\pi \int_0^{t_{AD}} \left[ 1 + 2 \sum_{n=1}^{\infty} \exp(-4n^2\pi^2\tau) \right] \left[ 1 + 2 \sum_{n=1}^{\infty} \exp(-4n^2\pi^2\tau) \frac{\sin(n\pi L_{x_j}/L_{x_e})}{n\pi L_{x_j}/L_{x_e}} \cos(n\pi x_D L_{x_j}/L_{x_e}) \right] d\tau, \quad (3.1.102)$$

where  $t_{AD}$  represents the dimensionless time based on drainage area of square region and  $x_D$  denotes the point where the well pressure is computed;  $x_D = 0$  for uniform-flux and  $x_D = 0.732$  for infinite-conductivity. The  $p_{wD}/(2p'_{wD})$  solutions were constructed using Eq. 3.1.102 and its logarithmic derivative; i.e.,

$$p'_{wD} = 2\pi t_{AD} \left[ 1 + 2 \sum_{n=1}^{\infty} \exp(-4n^2\pi^2 t_{AD}) \right] \left[ 1 + 2 \sum_{n=1}^{\infty} \exp(-4n^2\pi^2 t_{AD}) \frac{\sin(n\pi L_{x_j}/L_{x_e})}{n\pi L_{x_j}/L_{x_e}} \cos(n\pi x_D L_{x_j}/L_{x_e}) \right]. \quad (3.1.103)$$

The solid curves represent log-log plots of  $p_{wD}$  versus  $t_{x_jD}$  and the dashed curves represent log-log plots of  $p_{wD}/(2p'_{wD})$  versus  $t_{x_jD}$  for various values of the penetration ratio  $L_{x_e}/L_{x_j}$ . Points labeled with a cross on the dimensionless-pressure solutions of Figs. 3.1.22 and 3.1.23 denote the time at which linear flow ends according to criterion that linear flow ends at the earliest time such that the left and right sides of Eq. 3.1.30 differ by 2%. Similarly, points labeled with a cross on the  $p_{wD}/(2p'_{wD})$  solutions denote the time at which linear flow ends according to the criterion that linear flow ends at the earliest time at which the left and right terms of Eq. 3.1.31 differ by 2%. Different criteria for the end of linear flow (or more generally, for the beginning or end of any flow regime) give different times. Note that linear flow lasts longest when  $L_{x_e}/L_{x_j} = 1$  because in this case linear flow continues until the reservoir boundary influences the wellbore pressure response.

The curves labeled with an infinity sign on Figs. 3.1.22 and 3.1.23 represent the infinite-acting solutions discussed previously in Section 3.1.3. Pseudoradial flow (Eq. 3.1.33) begins at the time when the  $p_{wD}/(2p'_{wD})$  solution for a given value of

$L_{x_e}/L_{x_f}$  merges with the associated infinite-acting dimensionless pressure solution. Note that pseudoradial flow does not exist for all values of the  $L_{x_e}/L_{x_f}$ . Given the solutions for a particular value of  $L_{x_e}/L_{x_f}$ , for practical purposes, pseudosteady-state flow begins when these solutions diverge from the corresponding infinite-acting solution. The time at which pseudosteady-state flow begins may be approximated by  $t_{AD} = 0.1$ , or, equivalently, by

$$t_{x_f,D} = 0.4 \left( \frac{L_{x_e}}{L_{x_f}} \right)^2. \quad (3.1.104)$$

Eq. 3.1.104 follows directly from the relation between  $t_{AD}$  and  $t_{x_f,D}$ ; that is,

$$t_{x_f,D} = \frac{A}{L_{x_f}^2} t_{AD} = \frac{4L_{x_e}^2}{L_{x_f}^2} t_{AD}. \quad (3.1.105)$$

When pseudosteady-state flow prevails; that is when  $t_{AD} \geq 0.1$ , it is well known<sup>19</sup> that the following equation applies:

$$p_{wD} = 2\pi t_{AD} + \frac{1}{2} \ln \left( \frac{4A}{e^{\gamma} C_f L_{x_f}^2} \right), \quad (3.1.106)$$

where  $C_f$  is the fractured well shape factor defined by Gringarten<sup>19</sup>. Differentiating Eq. 3.1.106 with respect to  $\ln(t_{x_f,D})$  and multiplying the resulting equation by 2 gives

$$2p'_{wD} = 4\pi t_{AD}. \quad (3.1.107)$$

Furthermore, dividing Eq. 3.1.106 by Eq. 3.1.107, we obtain

$$\frac{p_{wD}}{2p'_{wD}} = 0.5 + a_f(t_{AD}), \quad (3.1.108)$$

where we define  $a_f(t_{AD})$  as

$$a_f(t_{AD}) = \frac{1}{8\pi t_{AD}} \ln \left[ \frac{4A}{e^{\gamma} C_f L_{x_f}^2} \right]. \quad (3.1.109)$$

Note that  $a_f$  is as same as the equation obtained for an unfractured well in a closed bounded reservoir provided that  $A/r_w^2$  replaced by  $A/L_{x_f}^2$  and  $C_A$  replaced by  $C_f$



in Eq. 3.1.92. In fact, if the effective wellbore radius concept can be used, then Eq. 3.1.109 can be rewritten as

$$a_f(t_{AD}) = \frac{1}{8\pi t_{AD}} \ln \left[ \frac{4A}{e^{\gamma} C_A (r'_w)^2} \right], \quad (3.1.110)$$

where  $C_A$  is the unfractured well shape factor for reservoir/well geometry under consideration and  $r'_w$  represents the effective wellbore radius which is given by

$$r'_w = \frac{L_{x_f}}{n}. \quad (3.1.111)$$

It should be noted that when Eqs. 3.1.109 and 3.1.110 are equivalent, there is a relationship between the unfractured well shape factor,  $C_A$ , and the fractured well shape factor,  $C_f$ . This relationship is given by the following equation:

$$C_f = \frac{C_A}{n^2}, \quad (3.1.112)$$

where  $n = e$  for an uniform-flux fractured well and  $n = 2$  for an infinite-conductivity fractured well. From the results of Refs. 19 and 65, we expect that Eq. 3.1.111 (or Eq. 3.1.112) will not be valid for all values of the penetration ratio,  $L_{x_e}/L_{x_f}$ . If Eq. 3.1.111 is not valid, then one should use equation Eq. 3.1.109 provided the shape factor  $C_f$  is determined from the tables of Ref. 19 as a function of  $L_{x_e}/L_{x_f}$ . As is established in the previous section on unfractured wells, as time gets sufficiently large so that  $a_f$  is negligible compared to 0.5 in Eq. 3.1.108, then Eq. 3.1.108 reduces to Eq. 3.1.93. From results of Figs. 3.1.21 and 3.1.22, it is apparent that for a given value of  $L_{x_e}/L_{x_f}$ , when  $t_{x_f D} \geq 0.4(L_{x_e}/L_{x_f})^2$ , the  $p_{wD}/(2p'_{wD})$  solution diverges from the infinite-acting solution and asymptotically approaches 0.5 as dimensionless time  $t_{x_f D}$  increases, which indicates that asymptotic formula of Eq. 3.1.93 also applies for the fractured well case.

The procedure using the type curves of Figs. 3.1.22 and 3.1.23 is identical to the procedure discussed for Fig. 3.1.21. The character of the curves representing the pressure/pressure-derivative group  $p_{wD}/(2p'_{wD})$  is quite good, particularly during

time period  $0.05 \leq t_{AD} \leq 1$ . Therefore, one should be able to obtain a good match of field data with type curves of Figs. 3.1.22 and 3.1.23.

Finally, we note that it is possible to construct type curves for fractured wells in the straightforward way; by plotting both  $p_{wD}$  and  $p'_{wD}$  versus  $t_{xjD}$ . The type curves obtained in this way for the uniform-flux and infinite-conductivity fracture cases are shown in Figs. 3.1.24 and 3.1.25, respectively. The advantage of these type curves, as mentioned earlier, is that one can perform a simultaneous match of both  $\Delta p$  and  $\Delta p'$  versus time  $t$  data.

### 3.1.8.2 Constant Pressure Production

Here, we consider the case where a planar fractured well located in the center of a closed bounded square reservoir is produced at a constant wellbore pressure. All results presented in this section are generated by using the well known result given by van Everdingen and Hurst<sup>13</sup>, that is,

$$\bar{q}_D(u) \bar{p}_{wD}(u) = \frac{1}{u^2}, \quad (3.1.113)$$

where  $u$  is the Laplace transform variable with respect to dimensionless time  $t_{xjD}$ . Here,  $\bar{p}_{wD}$  represents the Laplace space solution of the dimensionless pressure for the constant production rate case, that is, the Laplace space solution of Eq. 3.1.102, and  $\bar{q}_D$  represents the Laplace space solution for the dimensionless rate defined by Eq. 3.1.100. for constant pressure production case. It follows from Eq. 3.1.113 that the dimensionless flow rate  $q_D$  can be generated by numerically inverting the following equation:

$$\bar{q}_D(u) = \frac{1}{u^2 \bar{p}_{wD}(u)}, \quad (3.1.114)$$

using the Stehfest algorithm provided that the Laplace space solution of dimensionless pressure  $p_{wD}$  (see Eq. 3.1.102) for the constant rate production case is available. Recently, the Laplace transform of the dimensionless pressure solution  $p_{wD}$  (Eq. 3.1.102) was presented by Fraim and Lee<sup>62</sup> and is given by

$$\bar{p}_{wD}(u) = \frac{2\pi}{u} \left[ \frac{1}{4\sqrt{u}L_{xe}/L_{xf}} \coth(\sqrt{u}L_{xe}/L_{xf}) + \right.$$

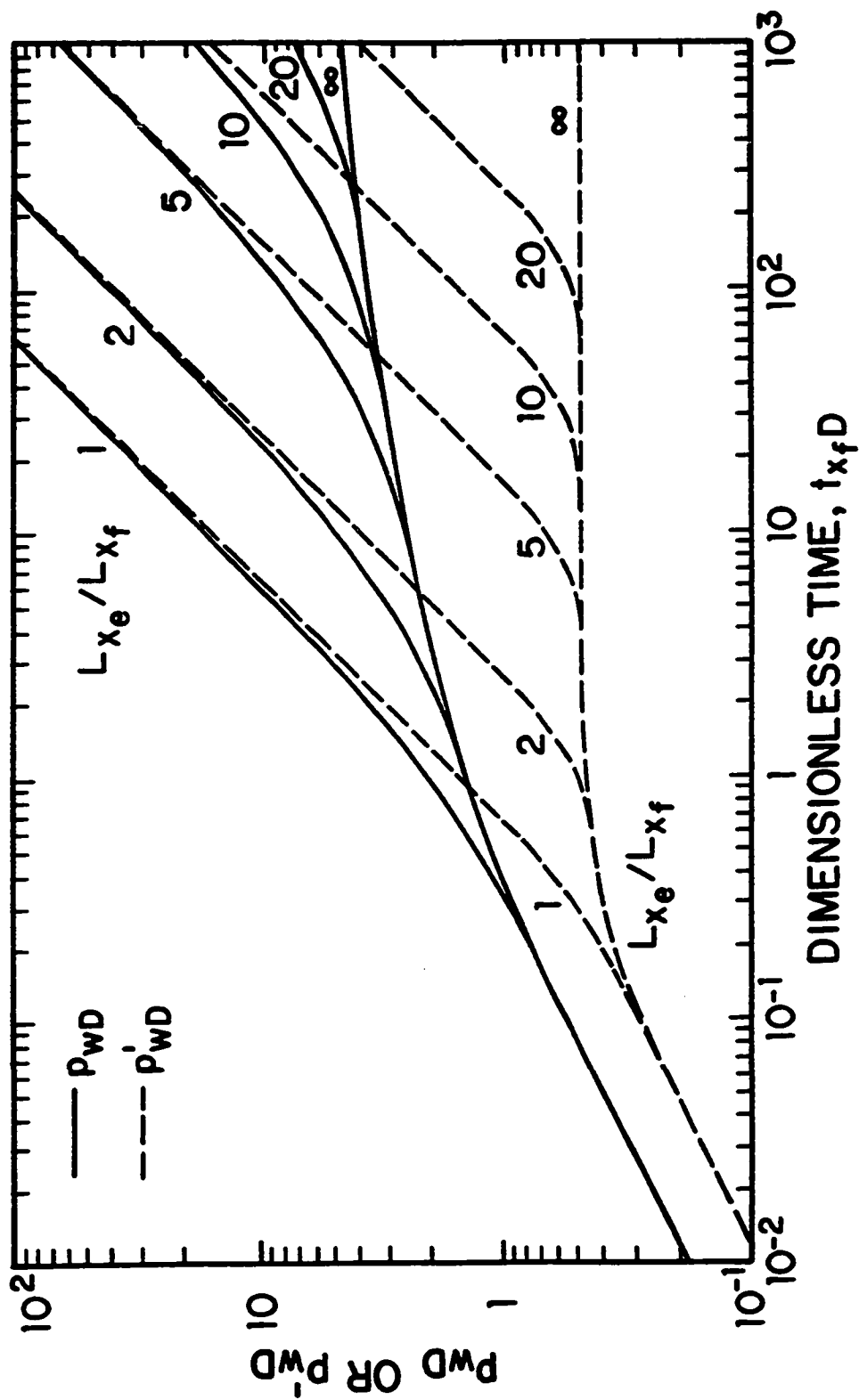


Fig. 3.1.24 - Uniform-Flux Type Curve Simultaneous Matching of Pressure and Pressure Derivative Data

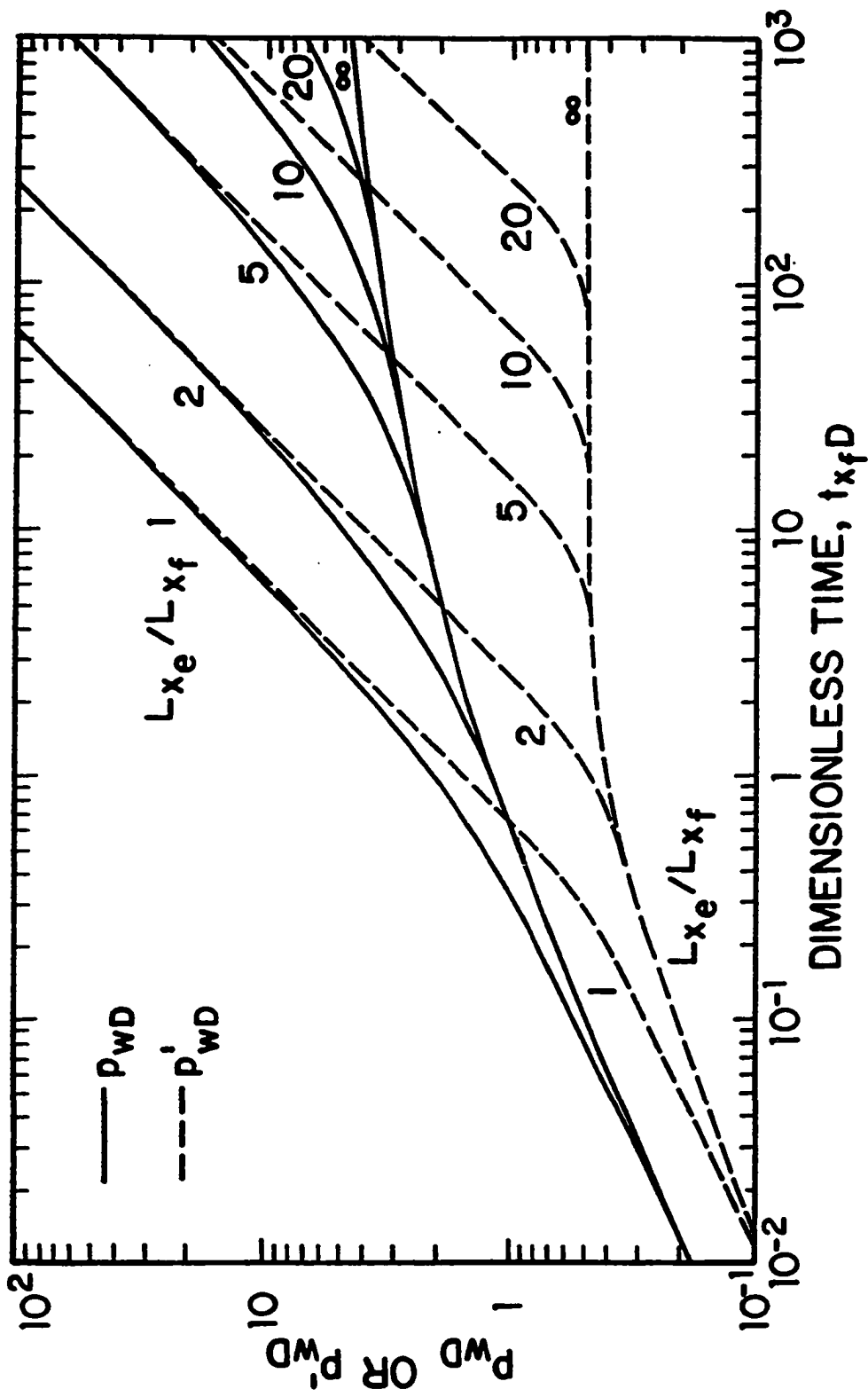


Fig. 3.1.25 - Infinite-Conductivity Type Curve Simultaneous Matching of Pressure and Pressure Derivative Data

$$\sum_{n=1}^{\infty} \sin(n\pi L_{x_f}/L_{x_e}) \frac{\cos(n\pi x_D L_{x_f}/L_{x_e}) \coth\left(2\sqrt{(L_{x_e}/L_{x_f})^2 u + n^2 \pi^2}\right)}{n\pi L_{x_f}/L_{x_e} \cdot 2\sqrt{(L_{x_e}/L_{x_f})^2 u + n^2 \pi^2}} \quad (3.1.115)$$

Previously, type curves based on the dimensionless rate  $q_D$  for an infinite-conductivity fractured well produced at a constant pressure were presented by Ref. 76. Here, we present type curves which incorporate the logarithmic derivative of dimensionless rate;  $q'_D$  and the logarithmic derivative of dimensionless rate divided by the dimensionless rate; that is,  $-2q'_D/q_D$ , for analyzing well rate data obtained at a fractured well produced at a constant wellbore pressure.

For a planar fractured well produced at a constant pressure, the dimensionless flow rate  $q_D$  exhibits three distinct flow regimes, namely, linear flow regime during which the production rate declines linearly with time, pseudoradial flow regime during which production rate declines semi-logarithmically with time, and the boundary dominated flow regime during which rate declines exponentially with time. As shown in Appendix C, during linear flow regime, the dimensionless rate is given by

$$q_D(t_{x_f D}) = \frac{2}{\pi} \frac{1}{\sqrt{\pi t_{x_f D}}} \quad (3.1.116)$$

During pseudoradial flow and boundary-dominated flow, respectively, the following equations for the dimensionless rate apply:

$$q_D(t_{x_f D}) = \frac{1}{0.5[\ln(t_{x_f D}) + c]}, \quad (3.1.117)$$

where  $c = 2.80907$  for a uniform-flux fracture and  $c = 2.20$  for an infinite-conductivity fracture, and

$$q_D(t_{x_f D}) = \frac{1}{a_{cf}} \exp\left[\frac{-2\pi t_{AD}}{a_{cf}}\right], \quad (3.1.118)$$

where

$$a_{cf} = \frac{1}{2} \ln\left[\frac{4A}{c' C_f L_{x_f}^2}\right]. \quad (3.1.119)$$

Differentiating Eqs. 3.1.116 through 3.1.118 with respect to  $\ln(t_{x_f D})$  gives, respectively,

$$-q'_D = -\frac{1}{2} q_D(t_{x_f D}) = \frac{1}{\pi \sqrt{\pi t_{x_f D}}}, \quad (3.1.120)$$

$$-q'_D = -\frac{1}{2}q_D^2 (t_{x_f,D}) = \frac{1}{0.5 [\ln (t_{x_f,D}) + c]^2}, \quad (3.1.121)$$

and

$$-q'_D = \frac{2\pi t_{AD}}{a_{c_f}^2} \exp \left[ \frac{-2\pi t_{AD}}{a_{c_f}} \right]. \quad (3.1.122)$$

From Eq. 3.1.116, it follows that

$$-\frac{2q'_D}{q_D} = 1, \quad (3.1.123)$$

during linear flow. From Eqs. 3.1.116 and 3.1.120, it follows easily that

$$-\frac{2q'_D}{q_D} = q_D = \frac{1}{0.5 [\ln (t_{x_f,D}) + c]}, \quad (3.1.124)$$

during pseudoradial flow. From Eqs. 3.1.118 and 3.1.122 it follows that during boundary dominated flow, we obtain

$$-\frac{2q'_D}{q_D} = \frac{4\pi t_{AD}}{a_{c_f}}. \quad (3.1.125)$$

Figures 3.1.26 and 3.1.27 show uniform-flux and infinite-conductivity type curves, respectively, for a well in the center of a closed square drainage region. The solid curves represent log-log plots of  $q_D$  versus  $t_{x_f,D}$  and the dashed curves represent log-log plots of  $-(2q'_D)/q_D$  versus  $t_{x_f,D}$  for various values of the penetration ratio  $L_{x_e}/L_{x_f}$ . As in the case of type curves of Figs. 3.1.22 and 3.1.23, the curves labeled with infinity sign represent the infinite acting solutions; i.e., the solutions for the time period when the outer boundaries of reservoir do not influence the well rate. Points labeled with a solid dot on the dimensionless rate solutions denote the approximate times at which left and right sides of Eq. 3.1.116 differ by more than 2%. Similarly, the points labeled with a solid dot on the  $-(2q'_D)/q_D$  solutions denotes the earliest time when linear flow ends based on a criterion that  $-(2q'_D)/q_D$  differs from one by more than 2%; see Eq. 3.1.123. As in the constant rate production case (see Figs. 3.1.22 and 3.1.23) different ending times are obtained for the  $q_D$  and  $-(2q'_D)/q_D$  solutions for the end linear flow regime, and also linear flow lasts longest when  $L_{x_e}/L_{x_f} = 1$  case. Pseudoradial flow begins at

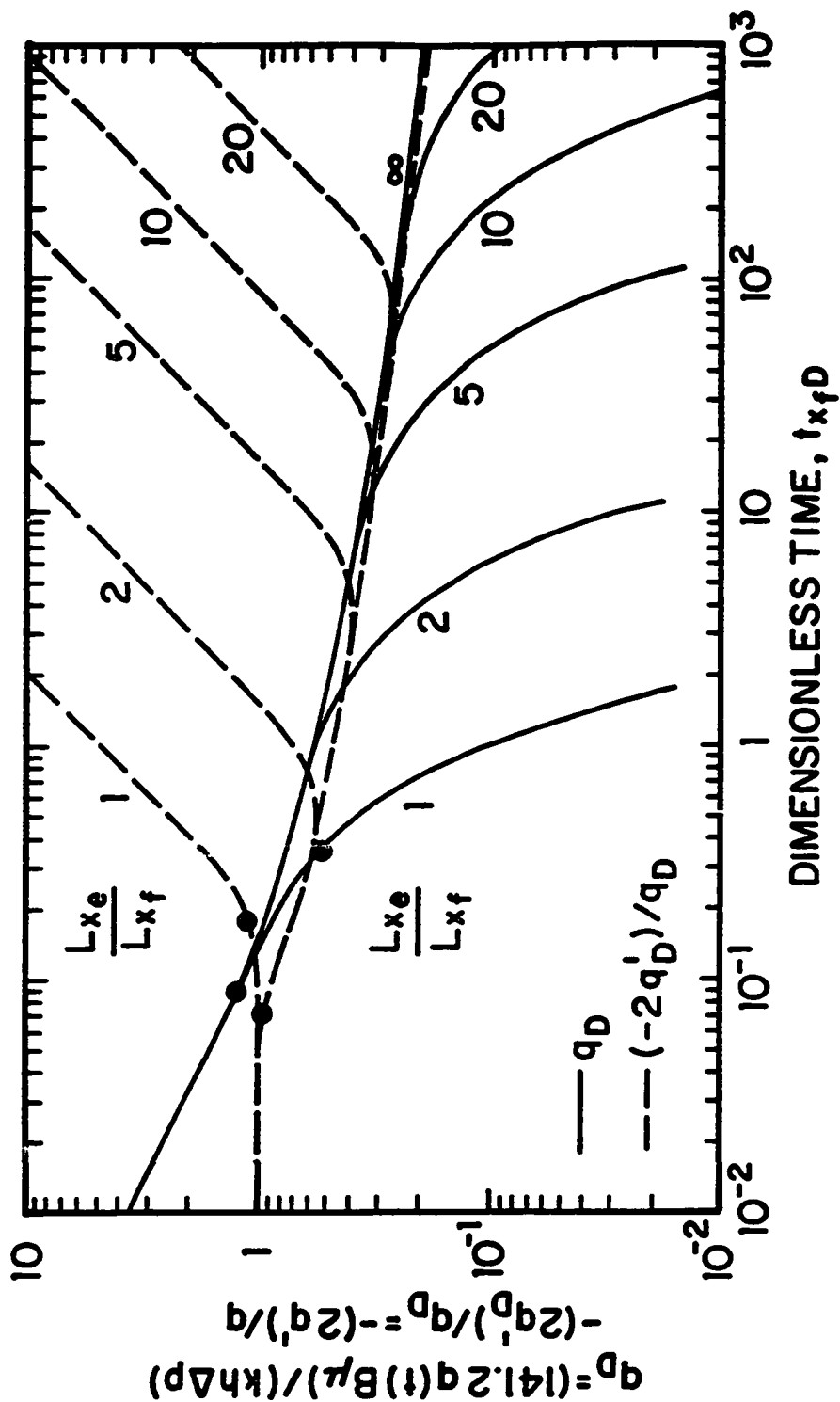


Fig. 3.1.26 - New Uniform-Flux Type Curve - Closed Square Reservoir; Constant Wellbore Pressure Production

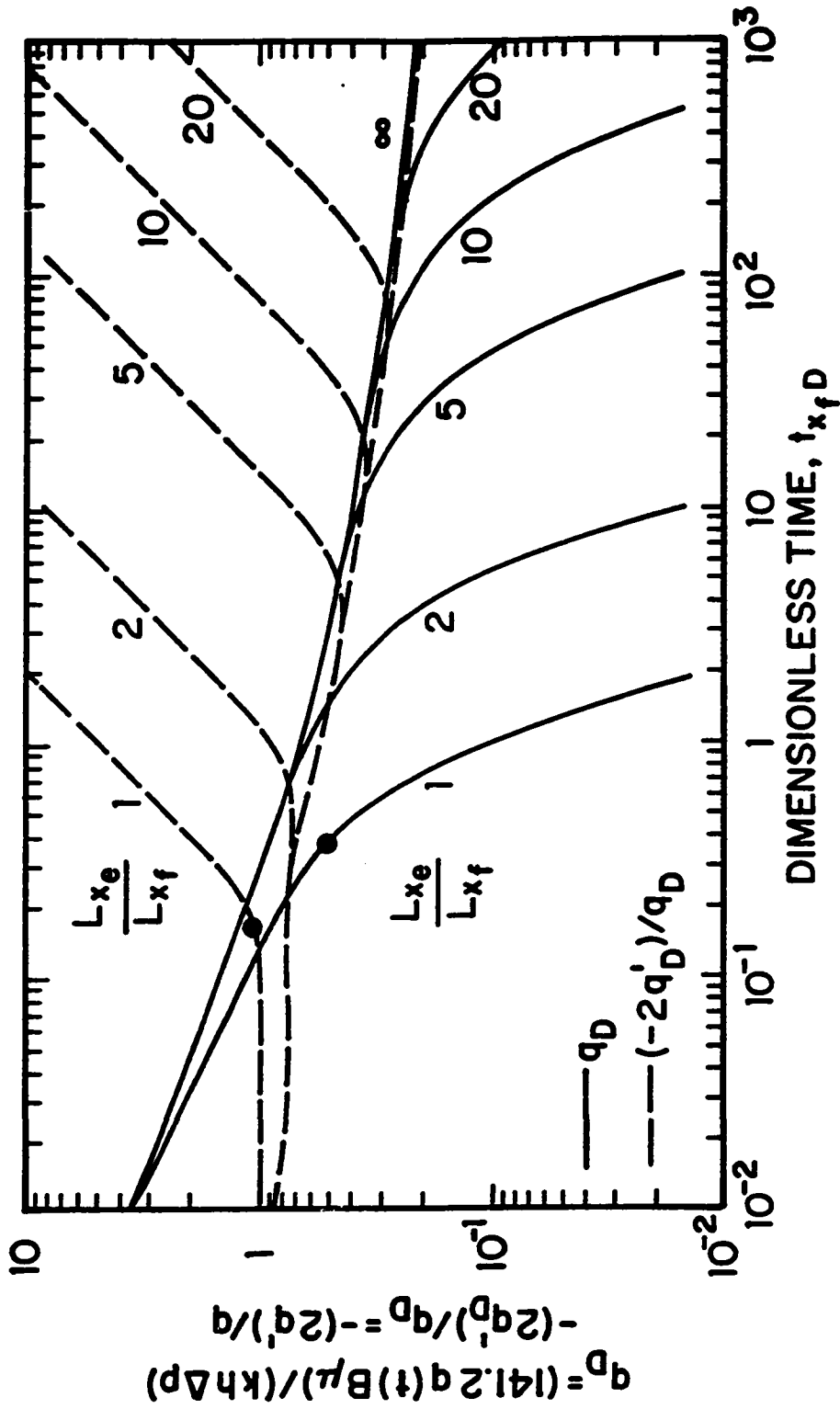


Fig. 3.1.27 - New Infinite-Conductivity Type Curve - Closed Square Reservoir;  
Constant Wellbore Pressure Production



the time when the  $-(2q'_D)/q_D$  solutions for a given value of  $L_{x_e}/L_{x_f}$  merge with the associated infinite-acting solutions as predicted by Eq. 3.1.124. In fact, this is the basic motivation of the specific group  $-(2q'_D)/q_D$  chosen to construct the type curves shown in Figs. 3.1.26 and 3.1.27. From results of Figs. 3.1.26 and 3.1.27, it is apparent that pseudoradial flow (Eq. 3.1.124) does not hold for all values of the penetration ratio  $L_{x_e}/L_{x_f}$ ; more specifically, pseudoradial flow exists only for the values of  $L_{x_e}/L_{x_f} \geq 10$ . Boundary-dominated flow for all practical purposes begins when both  $q_D$  and  $-(2q'_D)/q_D$  solutions diverge from the infinite-acting solutions for a given value of the penetration ratio  $L_{x_e}/L_{x_f}$ . The time at which boundary-dominated flow begins can be approximated by  $t_{AD} = 0.1$  and this approximation is valid for all values of  $L_{x_e}/L_{x_f}$  shown in Figs. 3.1.26 and 3.1.27. For values of  $t_{AD} > 0.1$  and a given the value of  $L_{x_e}/L_{x_f}$ , the  $-(2q'_D)/q_D$  solutions exhibit a unit slope line on log-log coordinates as predicted by Eq. 3.1.125.

By comparing the type curves generated for a well produced at a constant rate production case (see Figs. 3.1.22 and 3.1.23 in the previous subsection) with the type curves of Figs. 3.1.26 and 3.1.27 for the constant pressure production case, we note that linear flow regime ends earlier for the constant pressure production case and the pseudoradial flow regime exists for values of the penetration ratio  $L_{x_e}/L_{x_f} \geq 5$  for the constant rate production case, whereas pseudoradial flow for the constant pressure production case applies only for values of  $L_{x_e}/L_{x_f} \geq 10$ . However, for all practical purposes, the boundary dominated flow starts at  $t_{AD} = 0.1$  for both modes of production.

The procedure for using the type curves of Figs. 3.1.26 and 3.1.27 is the same as the procedure using the type curves of Figs. 3.1.22 and 3.1.23. The only difference is that one makes a log-log plot on tracing paper of  $q$  and  $-(2q')/q$ , where  $q$  is the production rate and  $q'$  is the derivative of production rate with respect to  $\ln t$ , versus  $t$  using the basic scales of the type curves of Figs. 3.1.26 and 3.1.27. Then one proceeds with the standard procedure, as discussed earlier, to obtain a type-curve match of field data plot with the curves of Figs. 3.1.26 and 3.1.27. After obtaining time match-point values and rate match-point values, one computes the

permeability-thickness product from the rate match-point values as

$$kh = \frac{141.2B\mu(q)_M}{(p_i - p_{wf})(q_D)_M}, \quad (3.1.126)$$

and the fracture-half length from time match-point values using Eq. 3.1.36. If field data diverges from the infinite-acting solutions, one can determine the value of the penetration ratio,  $L_{xe}/L_{xf}$ , from the type-curve match of field data and then obtain the well's drainage area,  $A$ , from this value of  $L_{xe}/L_{xf}$ , using the following equation:

$$A = 4L_{xf}^2 \left( \frac{L_{xe}}{L_{xf}} \right)_M^2. \quad (3.1.127)$$

As in the case of constant rate production case, we present type curves to perform a simultaneous match of rate data  $q$  and its logarithmic derivative  $-q'$  data for constant pressure production case. Figs. 3.1.28 and 3.1.29 shows, respectively, uniform-flux and infinite-conductivity type curves based on the dimensionless rate  $q_D$  and its dimensionless logarithmic derivative,  $-q'_D$  as functions of  $L_{xe}/L_{xf}$ , and  $t_{xf}D$ .

### 3.2 Identification of Semilog Straight Lines

As shown in Chapter II, for plane radial flow in a homogeneous reservoir, a semilog plot of  $\Delta p/(2\Delta p')$  versus  $t$  will exhibit a straight line of slope 1.151 (see Eq. 2.2.7), and this slope will be independent of reservoir properties. Although Eq. 2.2.7, in general, cannot be used to do computational analysis, the preceding observation based on Eq. 2.2.7 allows one to identify the time period if the proper semilog straight line (Eq. 2.2.4) exists. One can then analyze the well pressure data for this time period using standard semilog analysis methods. The objective of this section is to illustrate the validity of this semilog line identification method for nonhomogeneous reservoirs such as composite and naturally fractured reservoirs.

#### 3.2.1 Composite Reservoir

Results are based on the analytical solution for a line source well producing at a constant rate in a composite infinite-acting reservoir composed of two layers. A

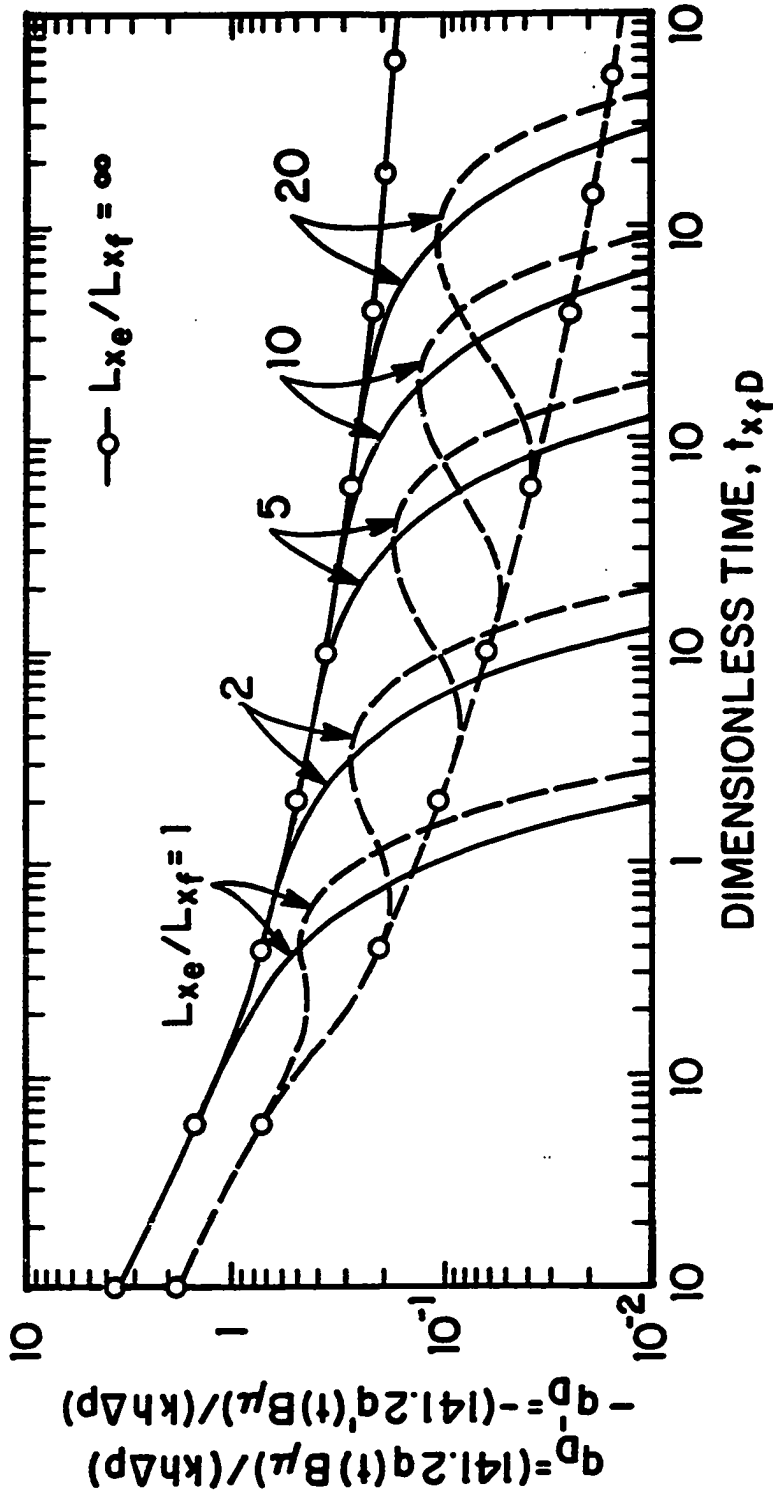


Fig. 3.1.28 - Uniform-Flux Type Curve Simultaneous Matching of Rate and Rate Derivative Data

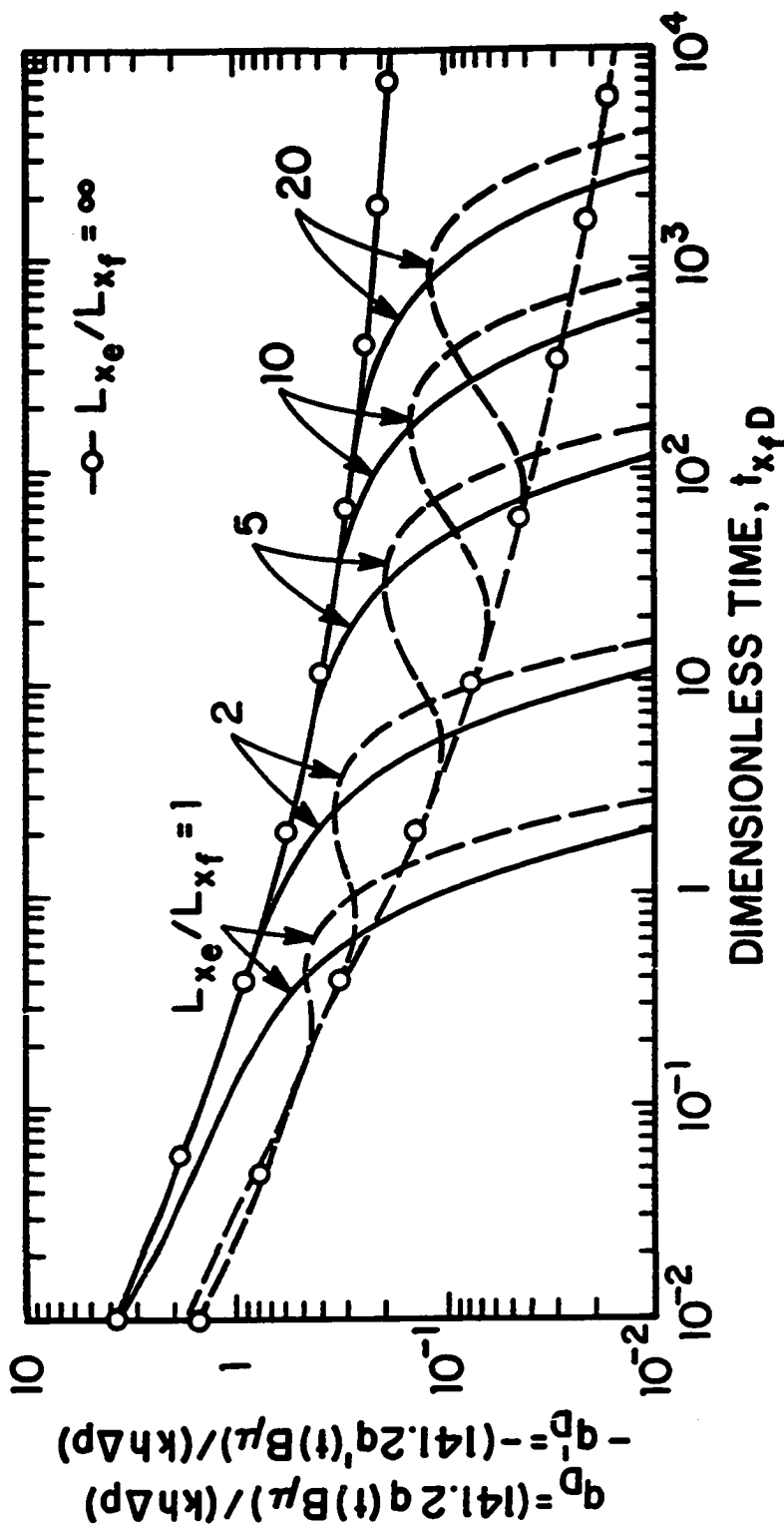


Fig. 3.1.29 - Infinite-Conductivity Type Curve Simultaneous Matching of Rate and Rate Derivative Data

plan view of the composite reservoir geometry is given in Fig. 3.2.1. The solid circle in the center represents the well which is produced at a constant rate. Although  $r_e$  is used to denote the external reservoir radius, all results presented here are for an infinite-acting reservoir, that is,  $r_e$  is infinitely large.

The analytical solution used is identical to the one given by Hurst<sup>35</sup>. The subscript  $j$  denotes zone  $j$  with zone 1 representing the inner zone and zone 2 representing the outer zone; specifically,  $k_1$  and  $\eta_1$ , respectively, represent the permeability and diffusivity of the inner zone;  $k_2$  and  $\eta_2$ , respectively, represent the permeability and diffusivity of the outer zone. The mobility of zone  $j$  is given by

$$\lambda_j = \frac{k_j}{\mu_j}, \quad \text{for } j = 1, 2. \quad (3.2.1)$$

The radius of the inner zone is  $r_s$  (see Fig. 3.2.1) and  $r_{sD}$  denotes its dimensionless analogue defined by

$$r_{sD} = \frac{r_s}{r_w}. \quad (3.2.2)$$

$\lambda_r$  and  $\eta_r$  are defined to denote the mobility ratio and the diffusivity ratio, respectively, by

$$\lambda_r = \frac{\lambda_1}{\lambda_2} = \frac{(k/\mu)_1}{(k/\mu)_2}, \quad (3.2.3)$$

and

$$\eta_r = \frac{\eta_1}{\eta_2} = \frac{[k/(\phi c_t \mu)]_1}{[k/(\phi c_t \mu)]_2}. \quad (3.2.4)$$

For simplicity, it is assumed that there is no wellbore storage effect and that the skin factor due to wellbore damage or stimulation is zero; nevertheless, the addition of a skin factor would not change the semilog slopes. Dimensionless pressure,  $p_{wD2}$ , and dimensionless time  $t_{D2}$  are defined in terms of the properties of the outer zone, respectively, as

$$p_{wD2} = \frac{k_2 h [p_i - p_{wf}]}{141.2 q B \mu_2}, \quad (3.2.5)$$

and

$$t_{D2} = \frac{2.637 \times 10^{-4} k_2 t}{\phi (c_t \mu)_2 r_w^2} = \frac{2.637 \times 10^{-4} \eta_2 t}{r_w^2}, \quad (3.2.6)$$

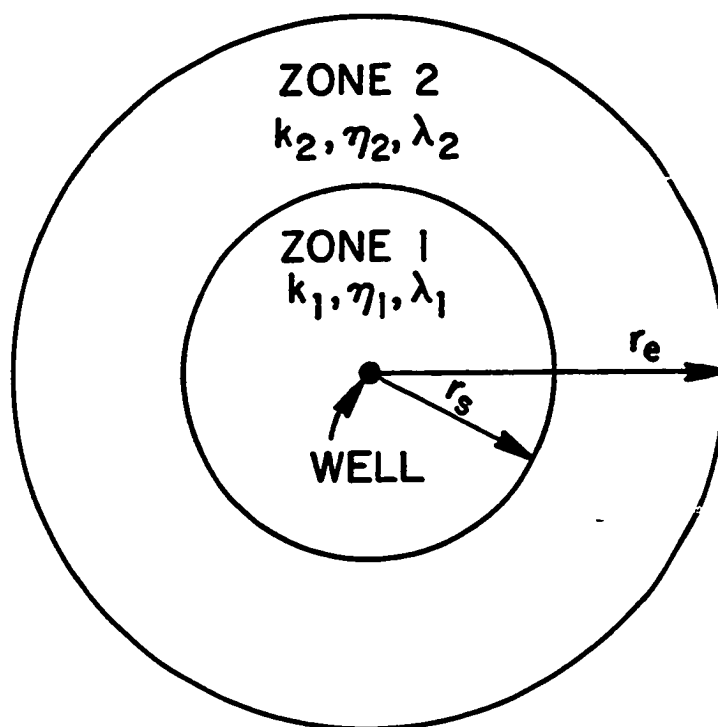


Fig. 3.2.1 - Composite Reservoir Geometry - Plan View

whereas,  $p_{wD1}$  denotes dimensionless pressure defined in terms of inner zone properties; that is,

$$p_{wD1} = \frac{k_1 h [p_i - p_{wf}]}{141.2 q B \mu_1}. \quad (3.2.7)$$

For this classical composite reservoir problem, it is well known that two semilog straight lines may exist. When the early semilog straight line reflecting the properties of the inner zone exists, it can be shown easily that the following three equations hold:

$$p_{wD1} = \lambda_r p_{wD2} = 1.151 \left[ \log (\eta_r t_{D2}) + 0.351 \right], \quad (3.2.8)$$

$$p'_{wD1} = \lambda_r p'_{wD2} = 0.5, \quad (3.2.9)$$

and

$$p_{wD1} = \frac{p_{wD2}}{2 p'_{wD2}} = \frac{\Delta p}{2 \Delta p'} = 1.151 \left[ \log (\eta_r t_{D2}) + 0.351 \right], \quad (3.2.10)$$

where  $p'_{wD1}$  and  $p'_{wD2}$ , respectively, denote the logarithmic derivative of  $p_{wD1}$  with respect to  $t_{D1}$  and the logarithmic derivative of  $p_{wD2}$  with respect to  $t_{D2}$ . Note Eq. 3.2.10 directly follows from Eqs. 3.2.8 and 3.2.9. During the time period when the second semilog straight line exists, the following equations apply:

$$p_{wD2} = 1.151 \left[ \log (t_{D2}) + 0.351 \right] + \left( \frac{\lambda_2}{\lambda_1} - 1 \right) \ln (r_{sD}), \quad (3.2.11)$$

$$p'_{wD2} = 0.5, \quad (3.2.12)$$

and

$$p_{wD2} = \frac{p_{wD2}}{2 p'_{wD2}} = \frac{\Delta p}{2 \Delta p'} = 1.151 \left[ \log (t_{D2}) + 0.351 \right] + \left( \frac{\lambda_2}{\lambda_1} - 1 \right) \ln (r_{sD}). \quad (3.2.13)$$

If the inner zone is considered to be a skin zone, then Hawkins' equation<sup>42</sup> for the skin factor follows from Eq. 3.2.13 without making the steady-state assumption that Hawkins used in his derivation. To the best of our knowledge, this observation

has not been presented previously. For completeness, the analytical derivations of Eqs. 3.2.11 through 3.2.13 are presented in Appendix D.

Figure 3.2.2 presents semilog plots of the  $\Delta p/(2\Delta p')$  solutions for two different values of the mobility and diffusivity ratios. Note in both cases semilog straight lines of slope 1.151 are obtained both at early and late times as predicted by Eqs. 3.2.10 and 3.2.13. Given corresponding field data, one would use the  $\Delta p/(2\Delta p')$  versus  $t$  plot to identify the semilog straight lines and the time periods where they exist, and then prepare a semilog plot of  $\Delta p$  versus  $t$ , determine the semilog slopes during the identified time periods and proceed with standard computations<sup>25-28</sup> for estimating the reservoir parameters.

### 3.2.2 Naturally Fractured Reservoir

Here, we first consider naturally fractured reservoir which is based on the the slab model of Kazemi<sup>29</sup> and de Swaan-O<sup>30</sup>. This model assumes that matrix is divided by a set of parallel, equally spaced horizontal fractures and that unsteady-state fluid transfer occurs from the matrix system to the fracture system. Results presented here were obtained using the Laplace analytical solution of Serra *et al.*<sup>33</sup> for a well produced at a constant rate in a naturally fractured infinite-reservoir which is based on the slab model of Refs. 29 and 30. As in the case of a composite reservoir, for simplicity, we do not consider wellbore storage and skin effects.

Dimensionless pressure,  $p_{wfD}$ , and dimensionless time,  $t_{fD}$ , are defined in terms of the intrinsic properties of the fracture system, respectively, as

$$p_{wfD} = \frac{k_f h_{ft} [p_i - p_{wf}]}{141.2qB\mu}, \quad (3.2.14)$$

and

$$t_{fD} = \frac{2.637 \times 10^{-4} k_f t}{(\phi c_t)_f \mu r_w^2}. \quad (3.2.15)$$

Dimensionless matrix storativity,  $\omega'$ , and dimensionless fracture transfer coefficient,  $\lambda'$ , are defined, respectively, by

$$\omega' = \frac{\phi_m c_m h_{mt}}{\phi_f c_f h_{ft}}, \quad (3.2.16)$$



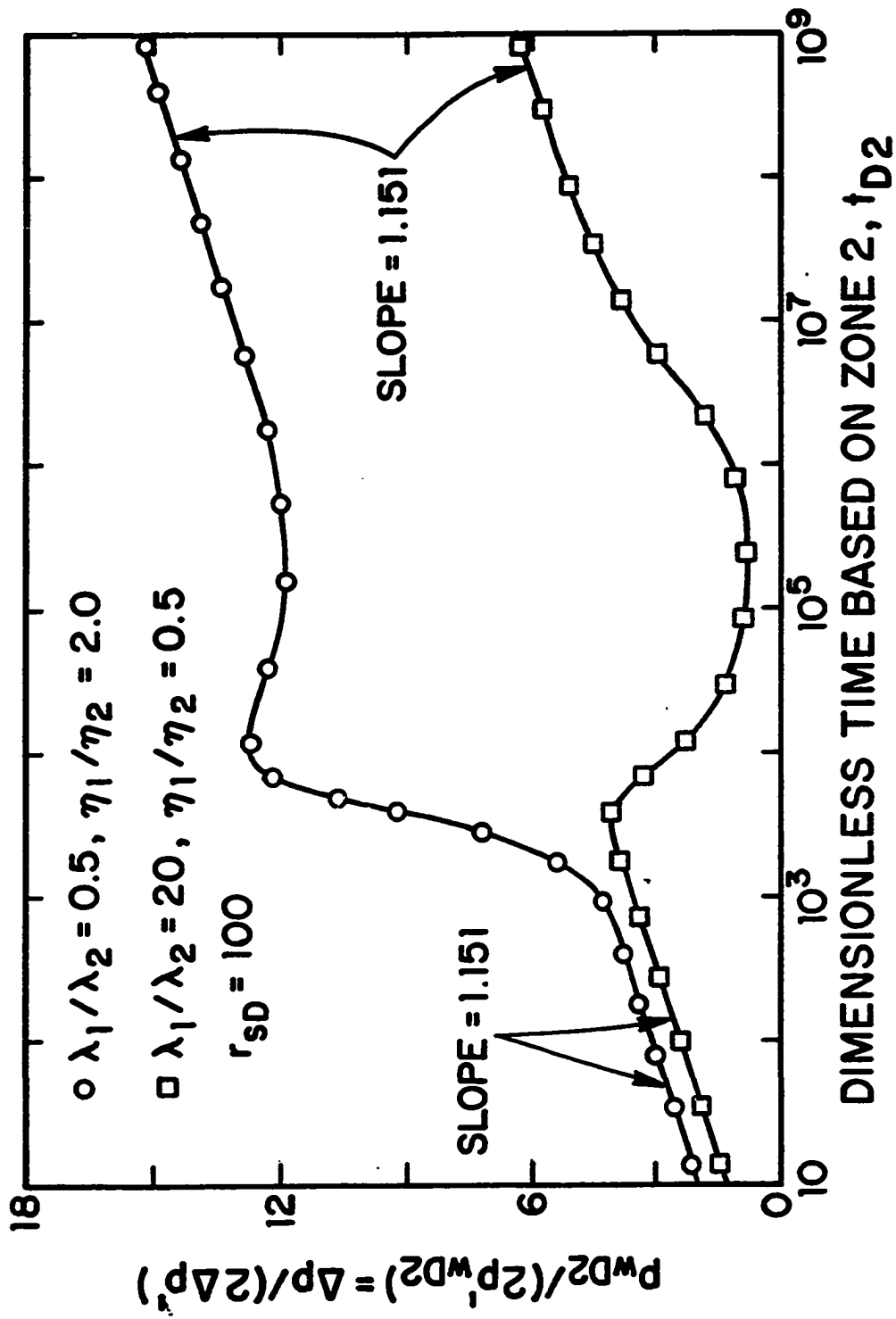


Fig. 3.2.2 - Pressure/Pressure-Derivative Group Solution for a Composite Reservoir

and

$$\lambda' = 12 \left( \frac{k_m h_{mt}}{k_f h_{ft}} \right) \left( \frac{r_w^2}{h_m^2} \right). \quad (3.2.17)$$

In Eqs. 3.2.14 through 3.2.16, the subscripts  $f$  and  $m$  refer, respectively, to fracture and matrix properties, and  $h_{ft}$  and  $h_{mt}$  represent the total thickness of the matrix and fracture systems, respectively; see Ref. 33.

For this naturally fractured reservoir model, it is well known that a semilog plot of wellbore pressure response,  $\Delta p$ , versus  $t$  may exhibit three semilog straight lines. When the early-time semilog straight line reflecting the properties of the fracture system exists, as is well known<sup>29-33</sup>, the dimensionless well pressure drop  $p_{w,D}$  is given by

$$p_{w,D} = 1.151 [\log(t_{fD}) + 0.351], \quad (3.2.18)$$

Differentiating Eq. 3.2.18 with respect to  $\ln(t_{fD})$  gives

$$p'_{w,D} = \frac{dp_{w,D}}{d \ln(t_{fD})} = \frac{1}{2} \quad (3.2.19)$$

and dividing Eq. 3.2.18 by Eq 3.2.19 multiplied by 2 gives

$$p_{w,D} = \frac{p_{w,D}}{2p'_{w,D}} = \frac{\Delta p}{2\Delta p'} = 1.151 [\log(t_{fD}) + 0.351], \quad (3.2.20)$$

When the intermediate-time semilog straight line reflecting the both the properties of fracture system and matrix system exists, the well pressure drop,  $p_{w,D}$ , is given by<sup>33,77</sup>

$$p_{w,D} = 0.5756 \left[ \log(t_{fD}) + 0.452 - \log\left(\frac{\lambda'\omega'}{3}\right) \right]. \quad (3.2.21)$$

Using Eq. 3.2.21, it is trivial to show that the following equations hold:

$$p'_{w,D} = \frac{1}{4}, \quad (3.2.22)$$

and

$$\begin{aligned} \frac{p_{w,D}}{2p'_{w,D}} &= \frac{\Delta p}{2\Delta p'} = p_{w,D} = 1.151 [\log(t_{fD}) \\ &+ 0.452 - \log\left(\frac{\lambda'\omega'}{3}\right)]. \end{aligned} \quad (3.2.23)$$

Similarly, during the late-time period when the third semilog straight line exists, the well dimensionless pressure drop  $p_{w,D}$  is given by<sup>29-33</sup>,

$$p_{w,D} = 1.151 [\log(t_{fD}) + 0.351 - \log(1 + \omega')]. \quad (3.2.24)$$

It follows directly from Eq. 3.2.24 that when the third semilog straight line exists, the following equations also apply:

$$p'_{w,D} = \frac{1}{2}, \quad (3.2.25)$$

and

$$\begin{aligned} \frac{p_{w,D}}{2p'_{w,D}} = \frac{\Delta p}{2\Delta p'} = p_{w,D} &= 1.151 [\log(t_{fD}) \\ &+ 0.351 - \log(1 + \omega')]. \end{aligned} \quad (3.2.26)$$

Figure 3.2.3 shows semilog plots of the  $p_{w,D}/(2p'_{w,D}) [= \Delta p/(2\Delta p')]$  solutions versus  $t_{fD}$  for these different values of the fracture transfer coefficient  $\lambda'$  for the value of  $\omega' = 1000$ . From results of Fig. 3.2.3, it is apparent that semilog straight lines of slope 1.151 as predicted by Eqs. 3.2.20, 3.2.23 and 3.2.26 are obtained at early, intermediate and late times only for the case where  $\lambda' = 10^{-9}$ . For the cases where  $\lambda' = 10^{-6}$  and  $\lambda' = 10^{-3}$ , only the intermediate-time and late-time semilog straight lines as given by Eqs. 3.2.23 and 3.2.26 are obtained. Therefore, if given corresponding field data plot of  $\Delta p/(2\Delta p')$  versus  $t$  identifies semilog straight lines of slope 1.151 and time periods when they exist, then one can proceed with the standard procedures described by Ref. 33 for determining fracture and matrix properties from a conventional semilog plot of  $\Delta p$  versus  $t$ .

For completeness, we briefly consider naturally fractured reservoir model of Barenblatt *et al.*<sup>78</sup> and Warren and Root<sup>79</sup> in which pseudosteady-state fluid transfer from matrix system to fracture system is assumed. Note that the naturally fractured reservoir model of Kazemi<sup>29</sup> and de Swaan-O<sup>30</sup> discussed above assumes unsteady-state fluid transfer from the matrix system to the fracture system.

As is well known<sup>79,80</sup>, for this naturally fractured reservoir model, a semilog plot of well pressure response,  $\Delta p$ , versus  $t$  may exhibit two semilog straight lines,

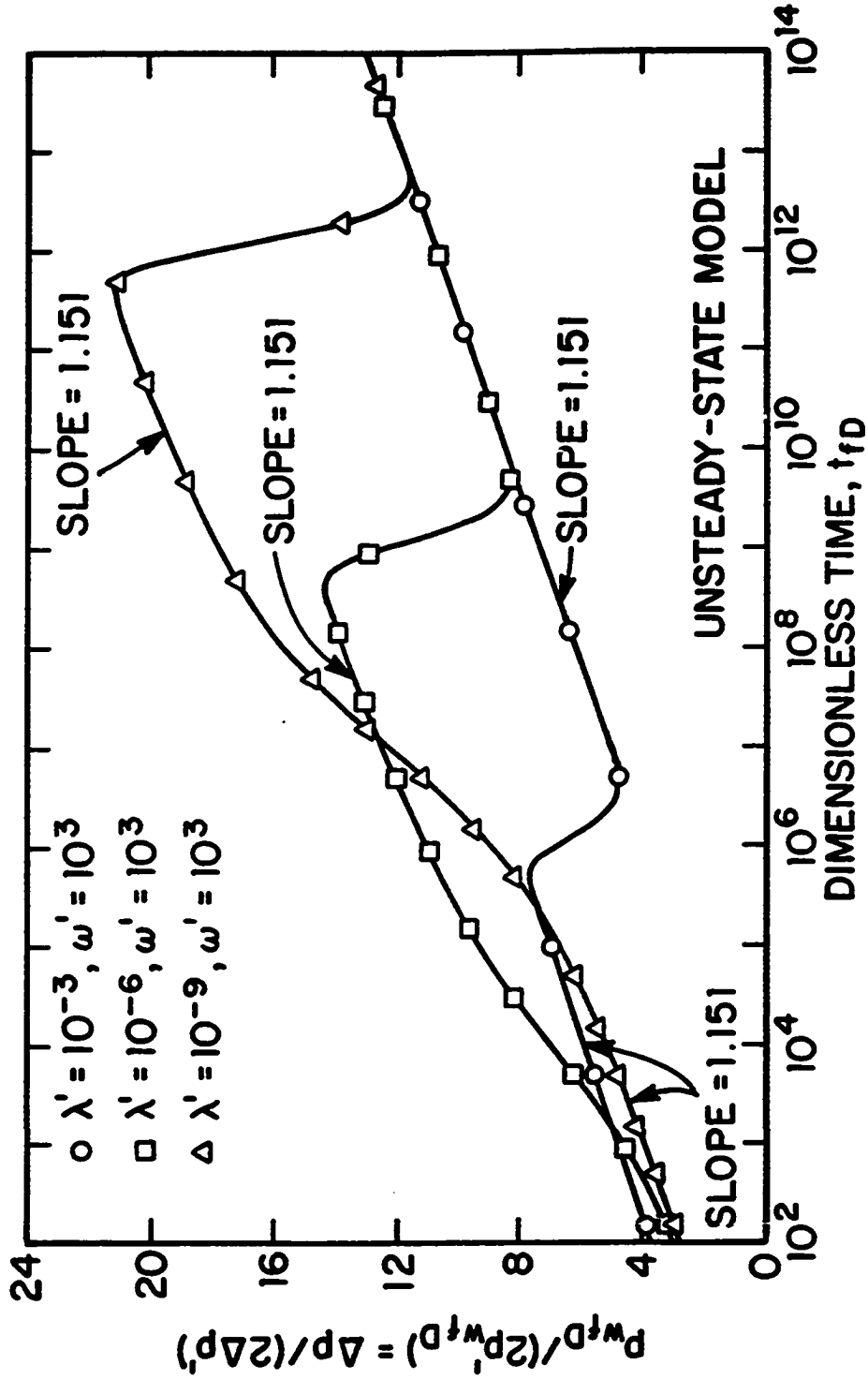


Fig. 3.2.3 - Pressure/Pressure-Derivative Group Solution for a Naturally Fractured Reservoir - Unsteady-State Model

namely, the early-time semilog straight line and the late-time semilog straight line. When the early-time semilog straight line exists, the dimensionless well pressure drop,  $p_{w,D}$ , its logarithmic derivative,  $p'_{w,D}$ , and the pressure/pressure-derivative group,  $p_{w,D}/(2p'_{w,D})$ , respectively, are given by Eqs. 3.2.18, 3.2.19 and 3.2.20. When the late-time semilog straight line exists,  $p_{w,D}$ ,  $p'_{w,D}$  and  $p_{w,D}/(2p'_{w,D})$  are given, respectively, by Eqs. 3.2.24, 3.2.25 and 3.2.26. We should note that in this naturally fractured reservoir model, the intermediate-time semilog straight line which exists for some values of  $\omega'$  in naturally fractured reservoir model of Refs. 29 and 30 with slope of 0.5756 (see Eqs. 3.2.21-3.2.23) does not exist and this is the basic difference in wellbore pressure response of the two naturally fractured reservoir models.

Figure 3.2.4 shows log-log plots of  $p_{w,D}/(2p'_{w,D}) [= \Delta p/(2\Delta p')]$  solutions versus  $t_{fD}$  for same values of  $\lambda'$  and  $\omega'$  considered in Fig. 3.2.3. Results shown in Fig. 3.2.4 were generated using the Laplace analytical solution of Bourdet and Gringarten<sup>80</sup> which is based on the naturally fractured reservoir model of Refs. 78 and 79. An inspection of the results of Figs. 3.2.3 and 3.2.4 indicate that the  $p_{w,D}/(2p'_{w,D})$  solutions identify both the early-time and late-time semilog straight lines of slope 1.151 if ever they exist for given the same values of  $\omega'$  and  $\lambda'$  for both naturally fractured reservoir models. However, in the intermediate time period, as clearly seen from results of Figs. 3.2.3 and 3.2.4, the  $p_{w,D}/(2p'_{w,D})$  solutions exhibit completely a different behavior for the naturally fractured reservoir model under consideration. For this time period, in the unsteady-state model (see Fig. 3.2.3), the  $p_{w,D}/(2p'_{w,D})$  solutions exhibit a semilog straight line of slope 1.151, whereas in the pseudosteady-state model (see Fig. 3.2.4) the  $p_{w,D}/(2p'_{w,D})$  solutions increase to a maximum and then decrease. Therefore, given corresponding field data plot of  $\Delta p/(2\Delta p')$  versus  $t$  not only identifies the appropriate naturally fractured reservoir model (either unsteady-state or pseudosteady-state model) exhibited by the field data but also determines the proper semilog straight lines and time periods when they exist.

As a final remark, we note that one can use Fig. 3.2.3, Fig. 3.2.4 and similar

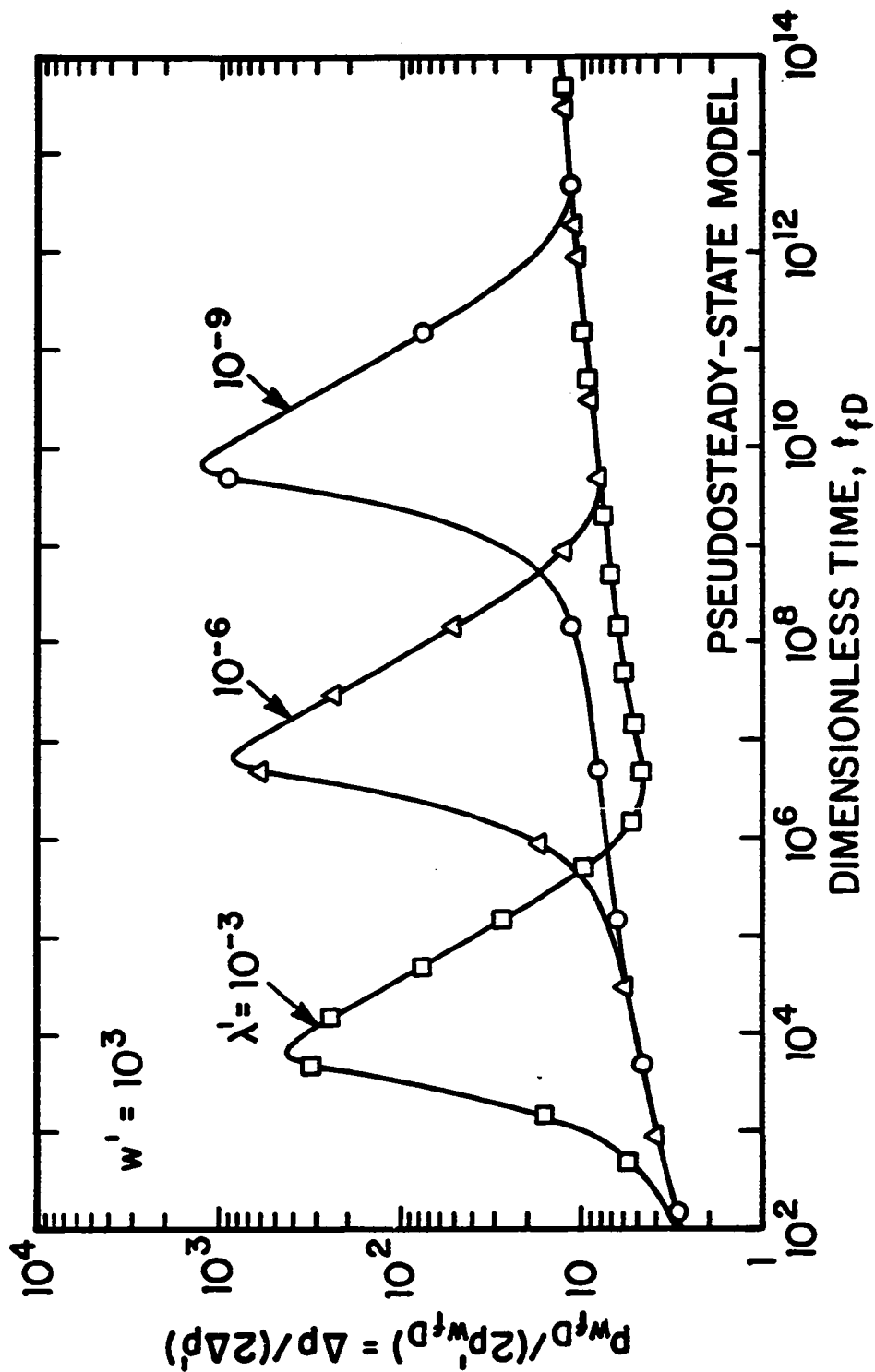


Fig. 3.2.4 .. Pressure/Pressure-Derivative Group Solution for a Naturally Fractured Reservoir - Pseudosteady-State Model

figures generated for different values of parameters  $\lambda'$  and  $\omega'$  for type-curve matching purposes in analyzing the well test data obtained at a well producing at a constant rate in a naturally fractured reservoir in the standard way discussed earlier.

### 3.3 Example Applications

This section considers the analyses of five field test data using the new type curves presented in the previous chapters. The first two examples considered pertain to cases where the pressure data are influenced by wellbore storage and skin effects. The third, fourth and fifth examples are for hydraulically fractured wells.

#### 3.3.1 Wellbore Storage and Skin; Buildup Example

The example presented here is Test 1 of Ref. 6. The relevant reservoir/well parameters and recorded shut-in pressure change,  $\Delta p$ , and derivative data,  $\Delta p'$ , were presented, respectively, in Tables 2.3.1 and 2.3.2. Fig. 3.3.1 presents type curve matches of log-log plots of  $\Delta p/(2\Delta p')$  versus  $\Delta t$  (circular data points) and  $\Delta p/(2\Delta p')$  versus Agarwal's equivalent time  $t_e$  (square data points) obtained using the type curves of the form shown in Fig. 3.1.3. The solid curves on Fig. 3.3.1 represent the drawdown type curves with which we matched the two plots of  $\Delta p/(2\Delta p')$ . It is apparent from Fig. 3.3.1 that as shut-in time increases beyond 10 hours, the two modes of plotting,  $\Delta p/(2\Delta p')$ -vs- $\Delta t$  and  $\Delta p/(2\Delta p')$ -vs- $t_e$ , give different traces. Recall that in this type curve matching procedure, the data plot is moved only in the horizontal direction. Thus, the matches shown in Fig. 3.3.1 clearly indicate that the field data is influenced by wellbore storage and skin effects. The determined match-point values for the case where  $\Delta p/(2\Delta p')$  data plotted versus  $\Delta t$  are  $[C_D \exp(2s)]_M = 5 \times 10^9$ ,  $(t_D/C_D)_M = 0.135$  and  $(\Delta t)_M = 0.01$  hours. Then, by moving the pressure data ( $\Delta p$  versus  $\Delta t$ ) only in the vertical direction, a type curve match with the  $p_{wD}$  versus  $t_D/C_D$  solution corresponding to  $C_D \exp(2s) = 5 \times 10^9$  was obtained giving the following match point values;  $(p_{wD})_M = 1.9$  and  $\Delta p = 100$  psi. (This match is shown in Fig. 3.3.2.) By using the standard computational procedures given in section 3.1.2, the following estimates were obtained from the

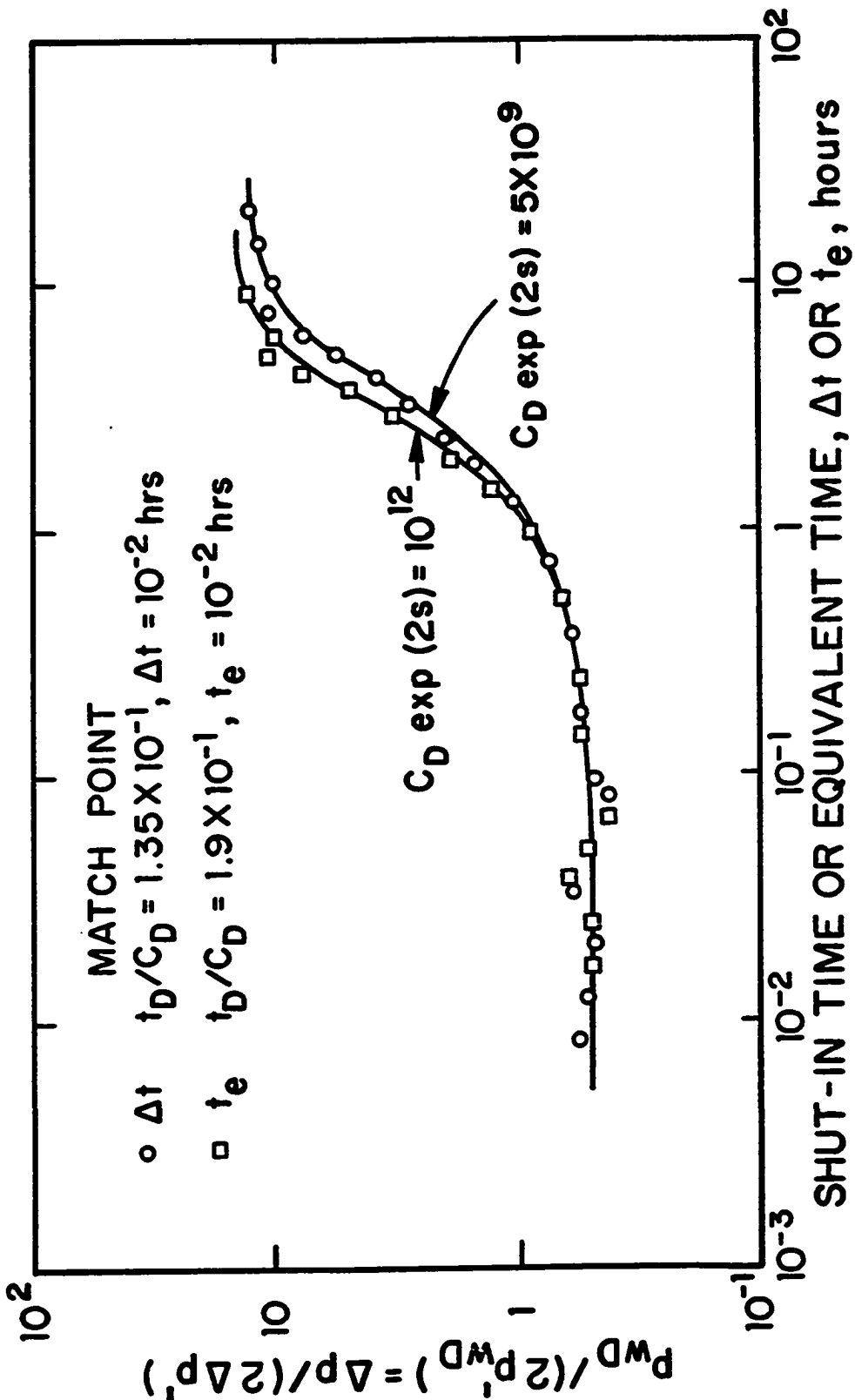


Fig. 3.3.1 - Type-Curve Match of Pressure/Pressure-Derivative Data - Wellbore Storage and Skin; Buildup Example



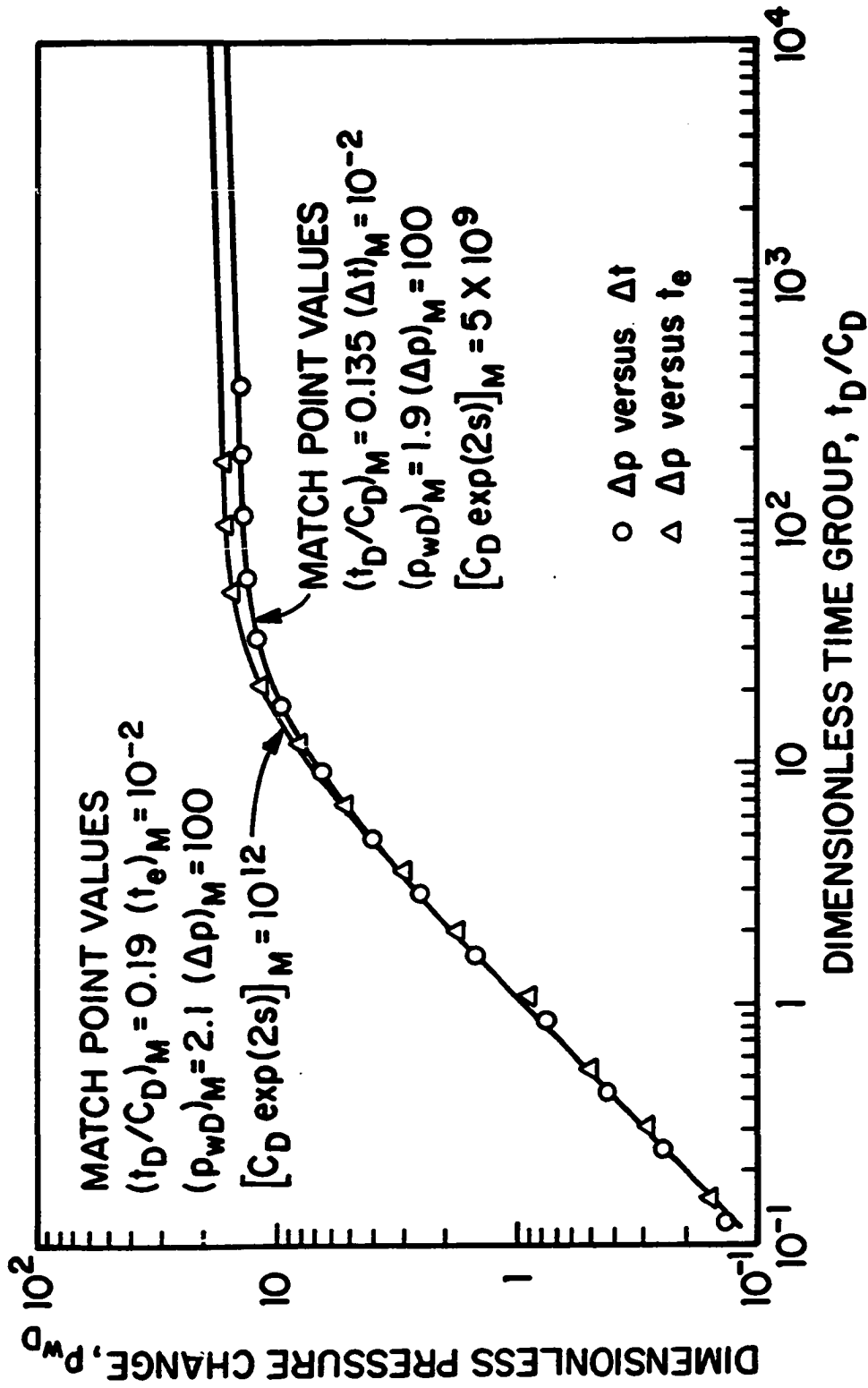


Fig. 3.3.2 - Type-Curve Match of Pressure Change Data - Wellbore Storage and Skin; Buildup Example

match point values;  $k = 10.95$  md,  $C = 1.02 \times 10^{-2}$  RB/psi which yields the dimensionless wellbore storage constant  $C_D = 965$ , and  $s = 7.7$ ; whereas using the type curves of Fig. 3.1.2, the authors of Ref. 6 obtained  $k = 10.89$  md,  $C = 9.3 \times 10^{-3}$  RB/psi ( $C_D = 879$ ) and  $s = 7.7$ . Interestingly, when we based our analysis on the equivalent time plots, we obtained the following values;  $[C_D \exp(2s)]_M = 10^{12}$ ,  $k = 12.8$  md,  $C = 8.49 \times 10^{-3}$  ( $C_D = 803$ ) and  $s=10.47$ .

Although the two sets of estimates we obtained do not differ greatly, the question is which set is most accurate? Noting that the estimates of Ref. 6 lie between our two sets of estimates, we used superposition to generate the analytical buildup solution for the case where  $C_D = 879$ ,  $s = 7.7$  ( $C_D \exp[2s] = 4 \times 10^9$ ) with a producing time given by  $t_D = 1.99 \times 10^5$ . (This value of producing time was computed based on the value  $k = 10.89$  md obtained in Ref. 6.) The results obtained for our derivative group are shown in Fig. 3.3.3 where the solid curve represents the drawdown solution; the circular and square data points, respectively, represent analytical buildup solution  $\Delta p/(2\Delta p')$  plotted versus  $\Delta t_D/C_D$  and  $t_{eD}/C_D$  respectively. Here,  $\Delta t_D$  represents dimensionless shut-in time and  $t_{eD}$  represents dimensionless equivalent time. Note neither method of plotting correlates the buildup solution with the corresponding drawdown solution which explains the two sets of answers we obtained and in fact indicates that the results obtained in Ref. 6 are the most accurate. Note, however, that the analysis results of Ref. 6 were obtained by refining the initial estimates obtained from type-curve matching with drawdown type curves by using buildup solutions generated analytically. The same refinement of our analysis results could be obtained by the same procedure. The most significant point is that, at least for this example, the use of equivalent time does not eliminate errors incurred in type curve matching when producing time effects are important.

### 3.3.2 Wellbore Storage and Skin; Drawdown Example

The drawdown example considered here is taken from Ref. 81. This example was previously analyzed in Ref. 81 and later analyzed in Ref. 82 using the automated type-curve matching technique. Table 3.3.1 lists the pertinent reservoir/well

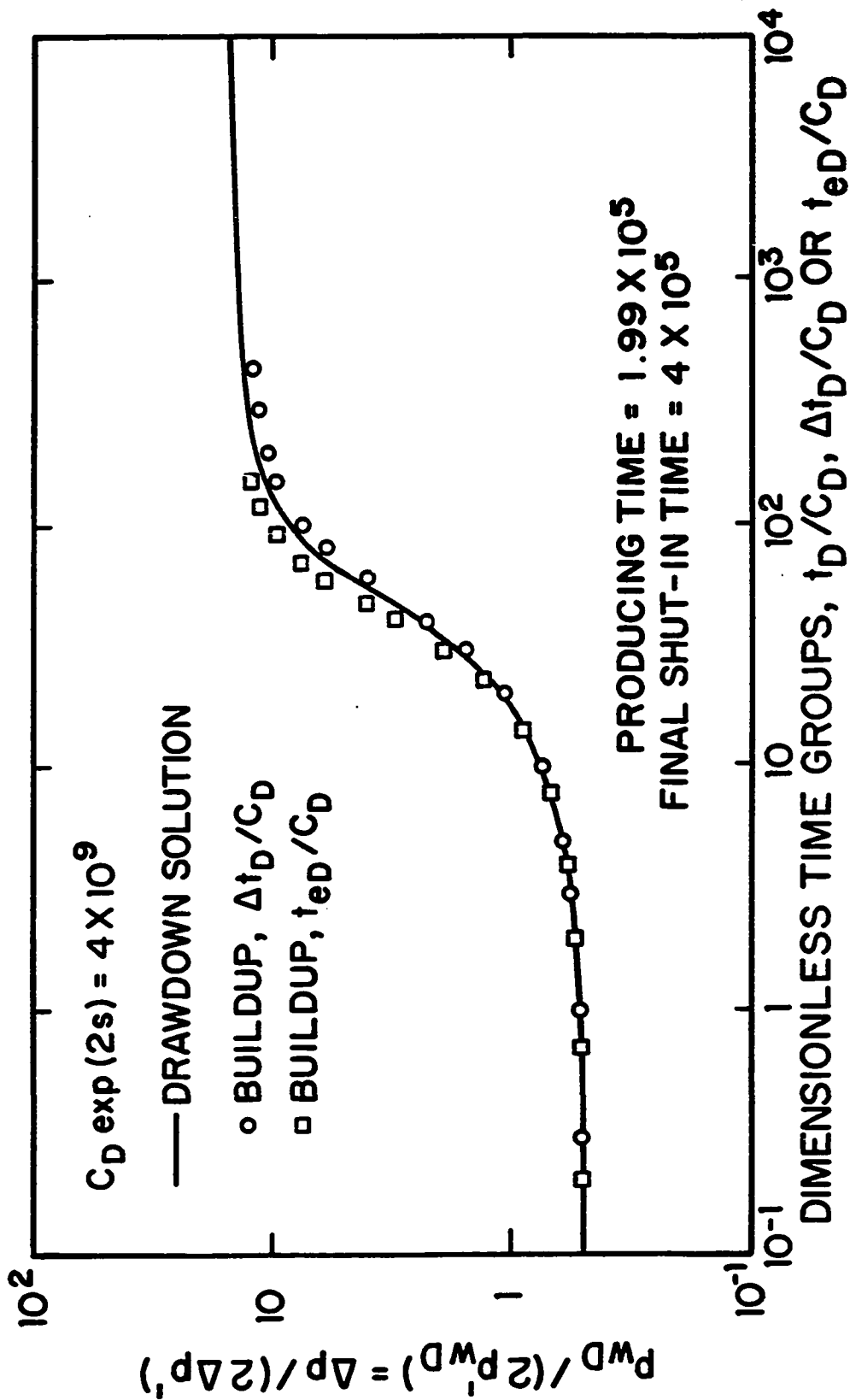


Fig. 3.3.3 - Effect of Producing Time - Wellbore Storage and Skin; Buildup Example

**Table 3.3.1****Wellbore Storage and Skin; Drawdown Example, Ref. 81****Reservoir/Well Parameters**

<b>Porosity (fraction)</b> . . . . .	<b>0.039</b>
<b>Thickness (ft)</b> . . . . .	<b>69</b>
<b>Wellbore Radius (ft)</b> . . . . .	<b>0.2</b>
<b>System Compressibility (1/psi)</b> . . . . .	<b>6.7E-06</b>
<b>Viscosity of Fluid (cp)</b> . . . . .	<b>0.9</b>
<b>Formation Volume Factor (RB/STB)</b> . . . . .	<b>1.325</b>
<b>Production Rate (STB/D)</b> . . . . .	<b>252</b>

data and Table 3.3.2 presents the pressure and derivative data as functions of flowing time. Fig. 3.3.4 presents type-curve match of a log-log plot of  $\Delta p/(2\Delta p')$  versus  $t$  obtained using the type curves of the form shown in Fig. 3.1.3. The circular data points represent the field data. The dashed curve on Fig. 3.3.4 represents the solution corresponding to  $C_D \exp(2s) = 8 \times 10^8$  with which the field data was matched. Clearly, the match shown in Fig. 3.3.4 indicates that early-time part of the field data, which corresponds to flowing time less than 2 hours, is influenced by wellbore storage and skin effects and the type curve-match of field data is good. However, the data beyond 2 hours do not match well to the  $C_D \exp(2s) = 8 \times 10^8$  solution. Therefore, it is expected that field data beyond 2 hours may not represent the model (wellbore storage and skin) on which the type type curve of Fig. 3.1.2 is based possibly due to a changing wellbore storage coefficient. As mentioned earlier, this is one distinct advantage of the type curves based on  $p_{wD}/(2p'_{wD})$  which give an indication whether the field data actually is represented by the model chosen for analysis.

Figure 3.3.5 shows a semilog plot of field  $\Delta p/(2\Delta p')$  data versus  $t$ . All data corresponding to  $t \geq 3$  hours is approximately on a semilog straight line of slope exactly equal to 1.151. According to the theory on the identification of semilog straight lines presented earlier in this work, the field data beyond 3 hours is free of wellbore storage effects and reflects radial flow, and thus, should be analyzable by standard semilog methods.

A conventional semilog plot of  $\Delta p$  versus  $t$  shown in Fig. 3.3.6 exhibits a well-defined semilog straight line of slope  $m = 78$  psi/cycle and  $(\Delta p)_{1hr} = 827$  psi. Using the standard computational procedure, the following estimates are obtained;  $k = 9.1$  md and  $s = 5.58$ . Using the match-point values recorded in Fig. 3.3.4 and the value of the wellbore storage coefficient obtained from unit slope line on a log-log plot of  $\Delta p$  versus  $t$  in the standard way (not shown here) as  $C = 8.6 \times 10^{-3}$  RB/psi ( $C_D = 1.1 \times 10^4$ ), one obtains the following estimates;  $k = 8.67$  md and  $s = 5.59$ . Note that these values of permeability and skin factor agree very closely with those obtained from conventional semilog analysis of the pressure data shown in Fig.

**Table 3.3.2**  
**Wellbore Storage and Skin; Drawdown Example, Ref. 81**  
**Pressure and Derivative versus Time Data**

Flowing Time, $t$ (Hours)	Pressure and Derivative Data		
	$\Delta p$ (psi)	$\Delta p'$ (psi)	$\Delta p/(2\Delta p')$
3.3000E-02	5.3000E+01	5.1134E+01	5.1070E-01
5.0000E-02	7.8000E+01	7.4541E+01	5.2368E-01
1.0000E-01	1.4800E+02	1.3234E+02	5.5746E-01
1.5000E-01	2.1000E+02	1.8165E+02	5.7774E-01
2.0000E-01	2.6700E+02	2.2093E+02	6.0450E-01
3.0000E-01	3.6900E+02	2.7890E+02	6.6218E-01
4.0000E-01	4.5400E+02	3.0400E+02	7.4516E-01
5.0000E-01	5.1900E+02	3.1102E+02	8.3346E-01
6.0000E-01	5.7200E+02	3.0183E+02	9.4454E-01
8.0000E-01	6.5400E+02	3.0026E+02	1.0890E+00
1.0000E+00	7.1900E+02	2.7576E+02	1.2887E+00
1.5000E+00	8.0400E+02	2.1404E+02	1.8786E+00
2.0000E+00	8.4900E+02	1.3800E+02	3.0683E+00
2.5000E+00	8.5900E+02	7.2500E+01	5.9389E+00
3.0000E+00	8.6400E+02	3.6000E+01	1.2006E+01
3.5000E+00	8.6900E+02	3.2200E+01	1.3496E+01
4.0000E+00	8.7400E+02	3.5200E+01	1.2407E+01
4.5000E+00	8.7700E+02	3.4873E+01	1.2586E+01
5.0000E+00	8.8200E+02	3.3934E+01	1.2983E+01
6.0000E+00	8.8700E+02	3.5184E+01	1.2613E+01
7.0000E+00	8.9300E+02	3.4057E+01	1.3104E+01
8.0000E+00	8.9700E+02	3.5719E+01	1.2559E+01
1.0000E+01	9.0500E+02	3.4328E+01	1.3183E+01
1.2000E+01	9.1100E+02	2.8810E+01	1.5809E+01

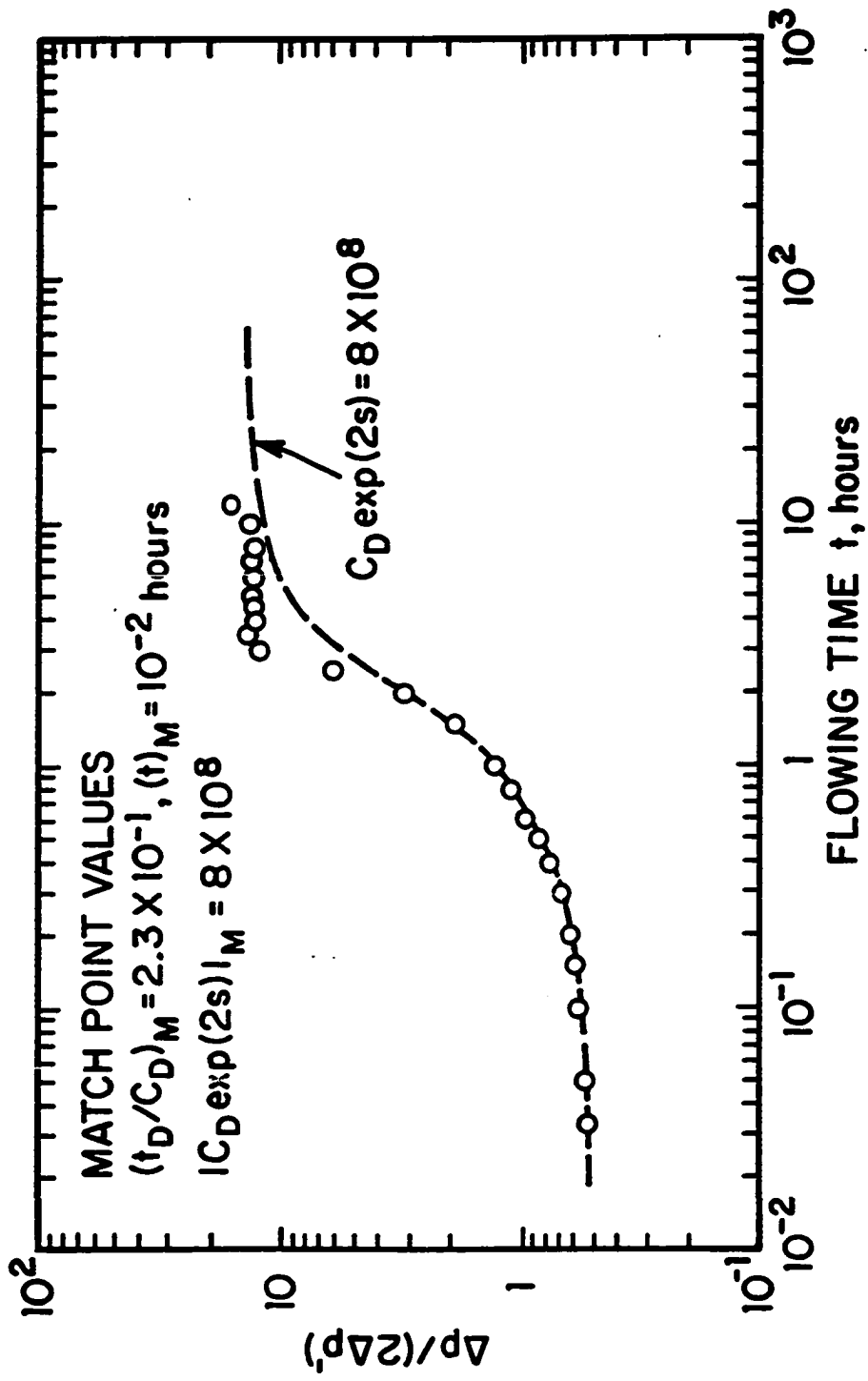


Fig. 3.3.4 - Type-Curve Match of Pressure/Pressure-Derivative Data - Wellbore Storage and Skin; Drawdown Example

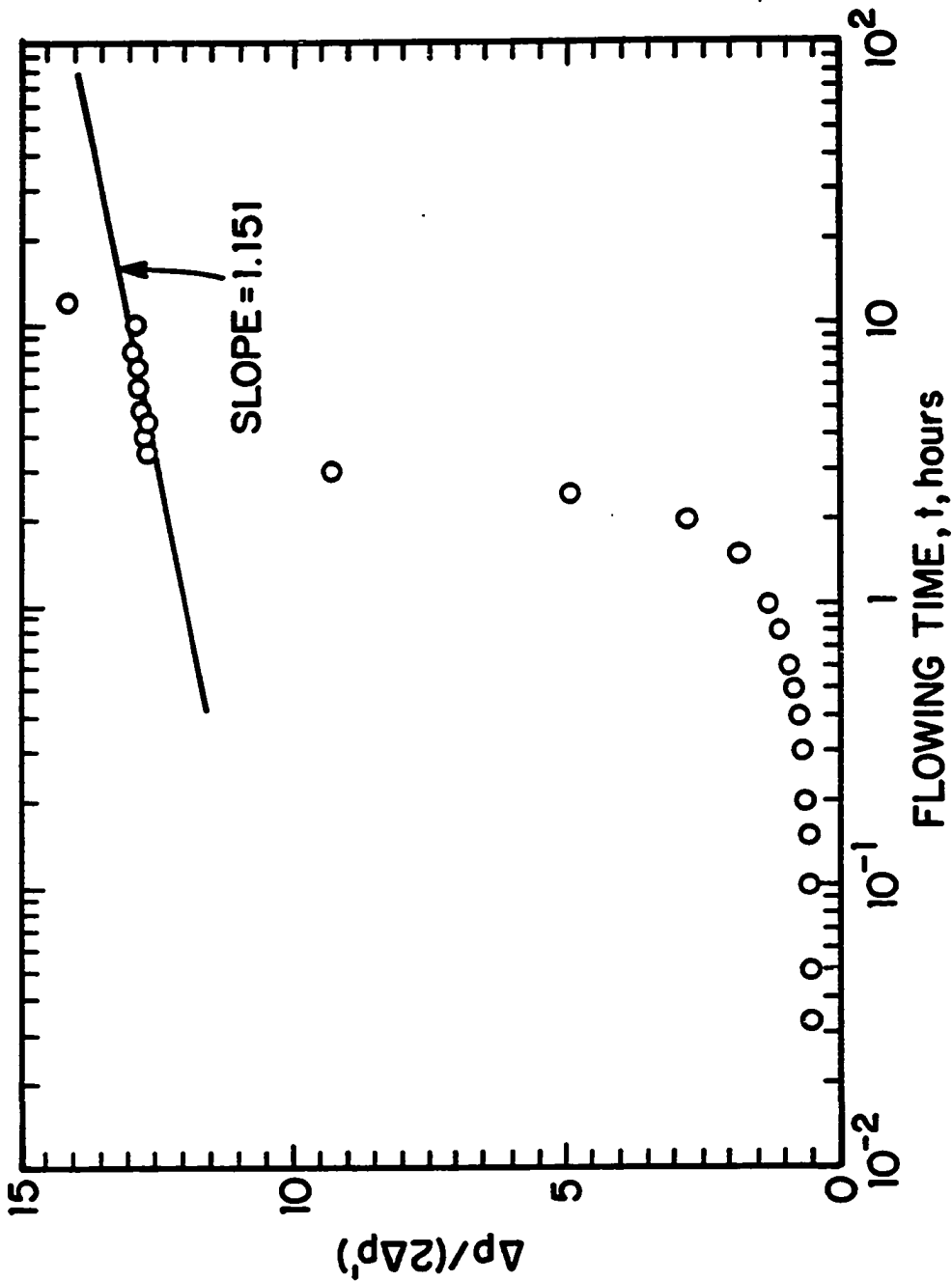


Fig. 3.3.5 - Semilog Plot of  $\Delta p / (2\Delta p')$  Versus Time - Wellbore Storage and Skin; Drawdown Example



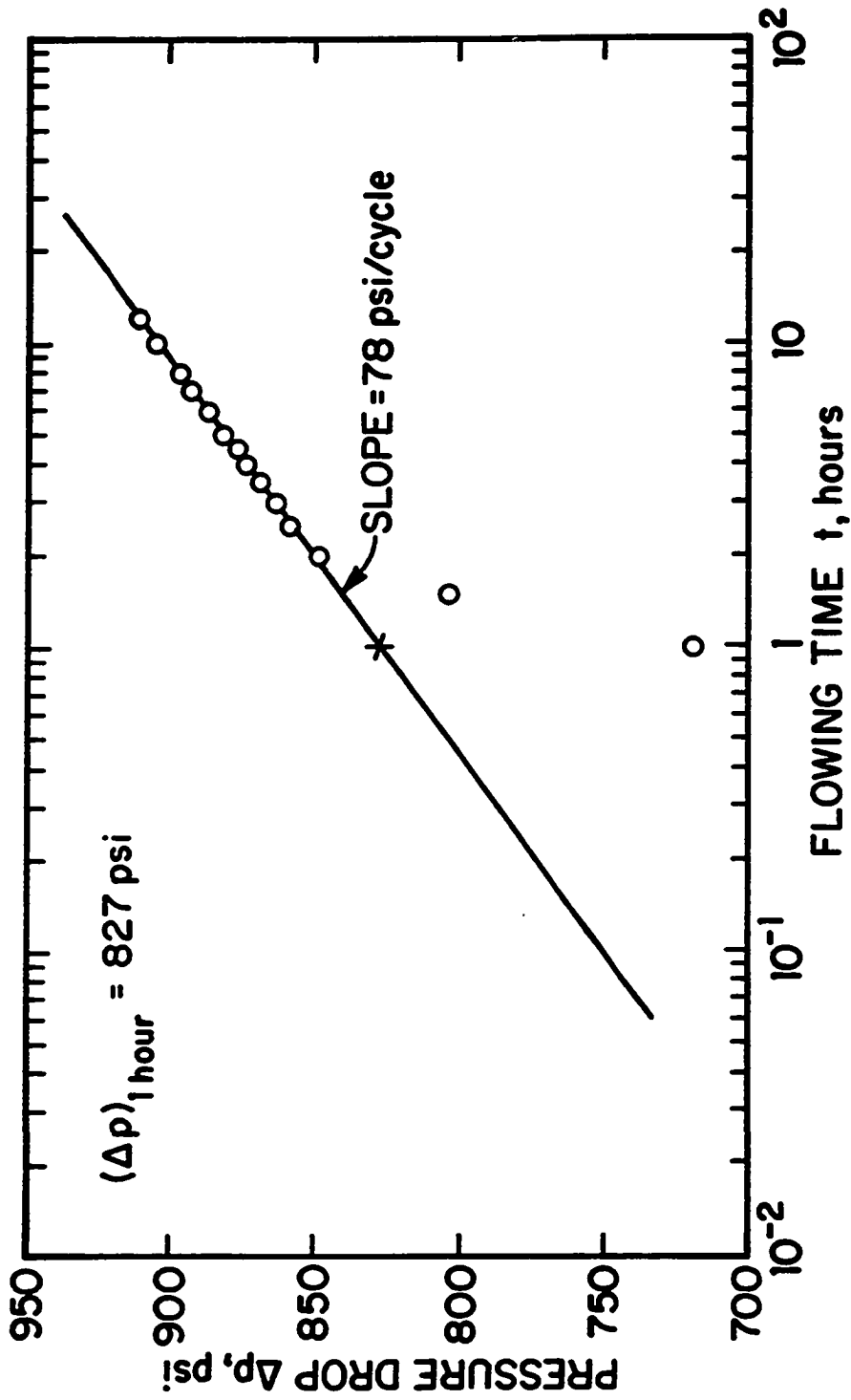


Fig. 3.3.6 - Semilog Plot of Pressure Change,  $\Delta p$ , Versus Time - Wellbore Storage and Skin; Drawdown Example

3.3.6. Therefore, one might think that the type-curve match of field data shown in Fig. 3.3.4 in which early-time data matches perfectly with wellbore storage-skin type curve of  $C_D \exp(2s) = 8 \times 10^8$  represents an acceptable and a consistent type curve match.

For this same data, both Refs. 81 and 82 obtained the following estimates (as the best-fit values):  $k = 15.5$  md,  $s = 14.9$ , and  $C = 8.5 \times 10^{-3}$  RB/psi ( $C_D = 1.05 \times 10^4$ ), by automated type-curve matching of the pressure data ( $\Delta p$  versus  $t$ ) using the wellbore storage and skin solutions of Agarwal *et al.*<sup>14</sup>. It is clear that our estimates of  $k$  and  $s$  obtained from the type-curve match of  $\Delta p/(2\Delta p')$  data as shown in Fig. 3.3.4 differ significantly from those of Refs. 81 and 82. To investigate this discrepancy in the two sets of estimates, first we type-curve matched the field data plot of  $\Delta p/(2\Delta p')$  versus  $t$  with the type curve corresponding to  $C_D \exp(2s) = 9.2 \times 10^{16}$  which one would have to match in order to obtain the parameter values given by Refs. 81 and 82. This match is shown in Fig. 3.3.7. Clearly, this match also does not represent an acceptable type-curve match for the late-time part of data; moreover, the estimates of  $k$  and  $s$  (estimates of Refs. 81 and 82) obtained from this match are not consistent with the estimates obtained from semilog straight line shown in Fig. 3.3.6. Second, since their technique is solely based on the automated type-curve matching of pressure data ( $\Delta p$  versus  $t$ ), we type-curve matched the  $\Delta p$  versus  $t$  data with the type curve corresponding to  $C_D \exp(2s) = 9.2 \times 10^{16}$  (match of Refs. 81 and 82) and the type curve corresponding to the  $C_D \exp(2s) = 8 \times 10^8$ . Both matches of  $\Delta p$  versus  $t$  data are shown in Fig. 3.3.8. The circular data points correspond to the match obtained with the  $C_D \exp(2s) = 9.2 \times 10^{16}$  solution, whereas the triangular data points correspond to the match obtained with the  $C_D \exp(2s) = 8 \times 10^8$  solution. It is apparent from Fig. 3.3.8 that visually the quality of the two corresponding pressure matches is not much different, although the match based on the parameters obtained in Refs. 81 and 82 looks slightly superior. However, as shown earlier, both matches gave two significantly different set of estimates for  $k$  and  $s$ ; thus, at least for this example, this indicates that type-curve matching of pressure data is difficult and subjective; that is, it can produce

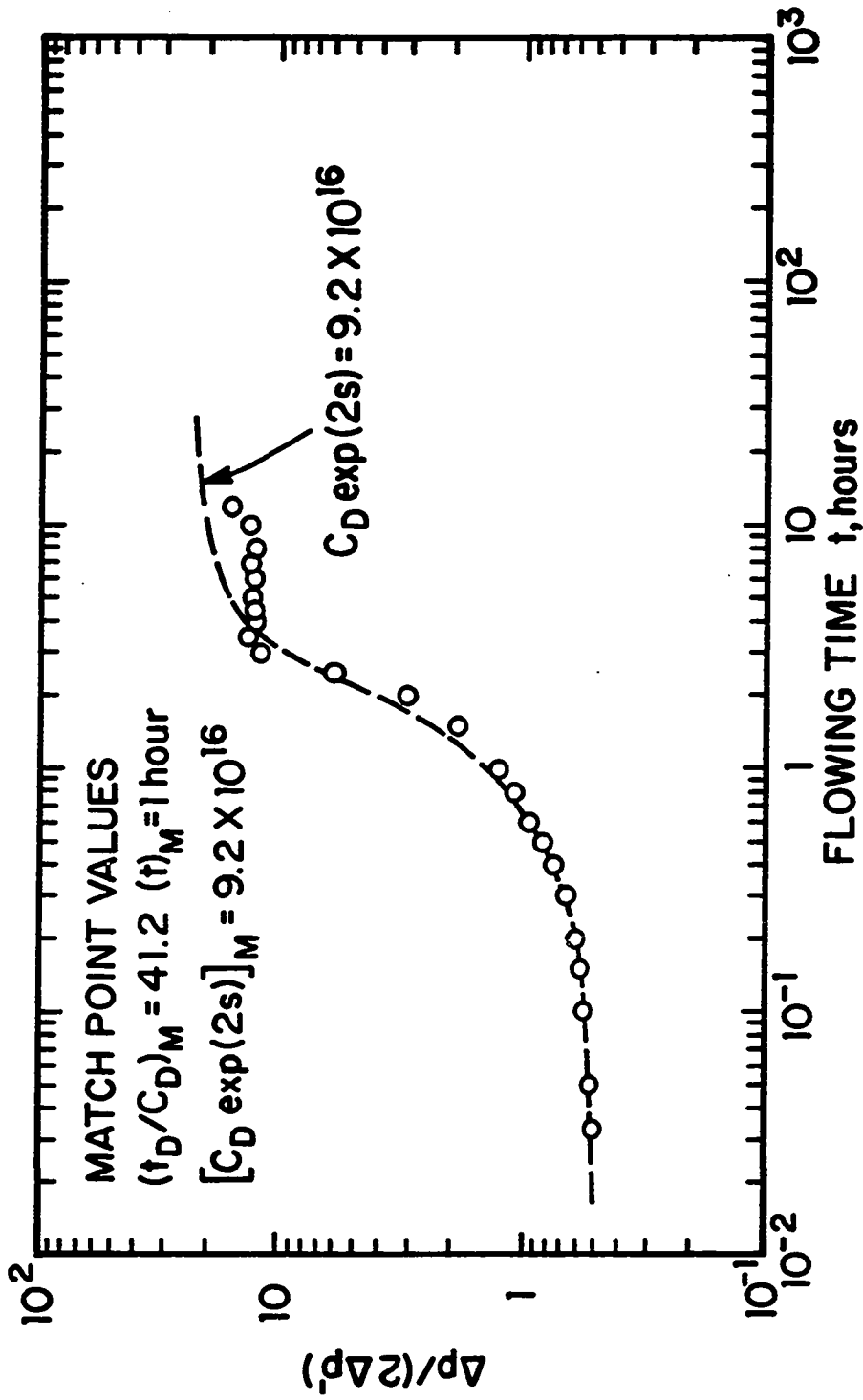


Fig. 3.3.7 - Attempted Type-Curve Match of Pressure/Pressure-Derivative Data Using Parameter Values of Ref. 82

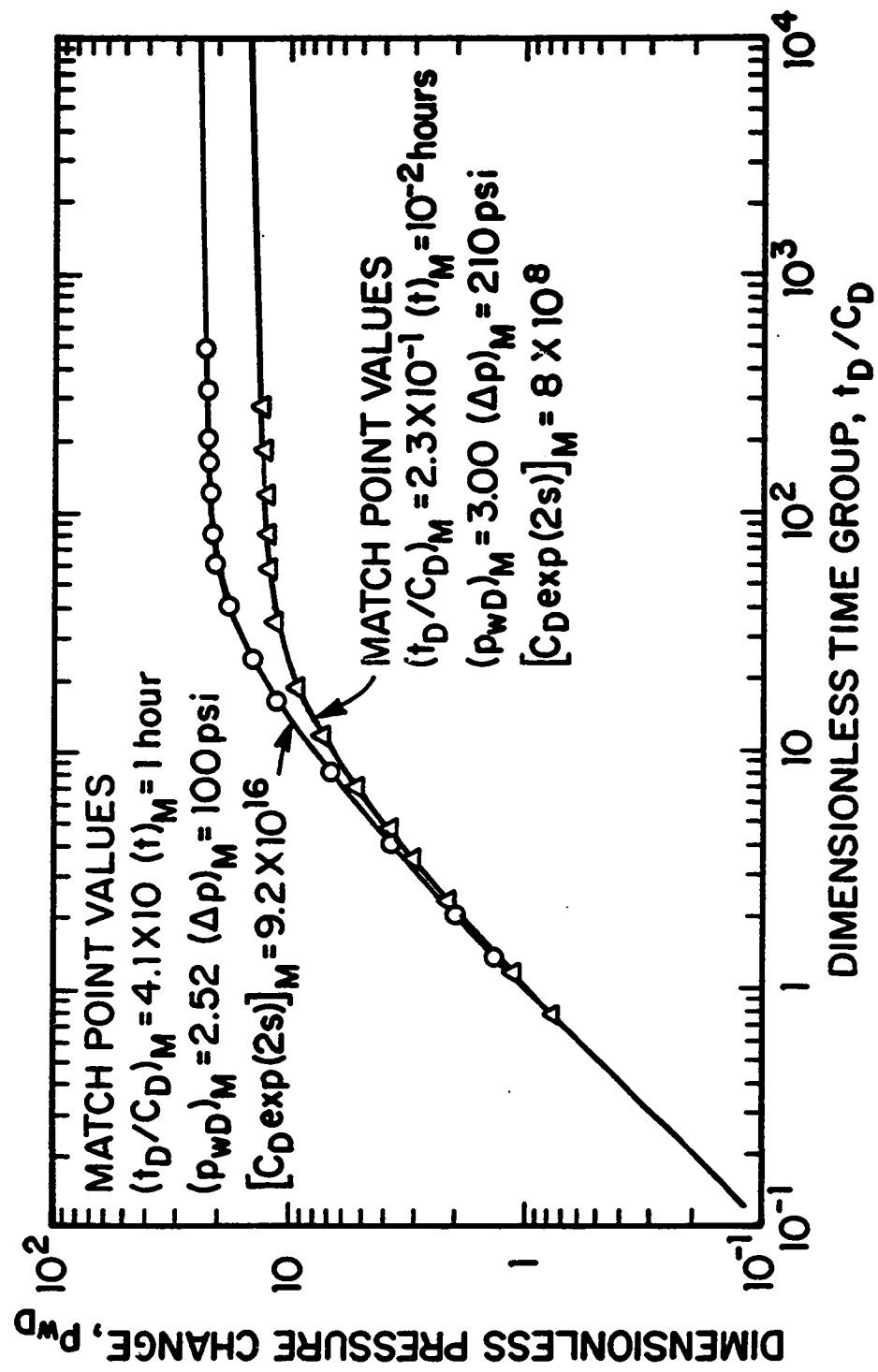


Fig. 3.3.8 - Type-Curve Match of Pressure Data - Wellbore Storage and Skin; Drawdown Example

nonunique results.

As illustrated above, since the type-curve matching of pressure data may suffer from uniqueness problem, the automated type-curve matching of well test data based on the  $\Delta p/(2\Delta p')$  solution could prove invaluable in eliminating the uniqueness problem involved in type-curve matching of pressure data alone.

### 3.3.3 Infinite-Conductivity Fracture; Buildup Example

The buildup field example considered here is the vertical fracture-buildup example of Ref. 18 and represents buildup pressure data from a hydraulically fractured well. As is well known, such pressure data can be analyzed with the infinite-conductivity type curves, provided that the fracture is well propped and that producing time effects are not significant. The pertinent reservoir/well data is listed in Table 3.3.3. Shut-in pressure change, its derivative and the pressure/pressure-derivative data as functions of shut-in time and equivalent time are summarized in Table 3.3.4. Because  $t_p \gg \Delta t$  for shut-in times considered, producing time effects are not important; nevertheless, we have chosen to graph the data in terms of equivalent time,  $t_e$ .

Figure 3.3.9 shows a log-log plot of the shut-in pressure change,  $\Delta p = p_{ws} - p_{wf,s}$ , and the two pressure/pressure derivative groups,  $\Delta p/(2\Delta p')$  and  $(2\Delta p')/\Delta p$  versus equivalent time,  $t_e$ . Recall that two pressure/pressure-derivative groups are type-curve matched by moving the field data plot only in the horizontal direction.

Figure 3.3.10 shows the match of derivative data obtained by moving the data plot, which was made on tracing paper, only in the horizontal direction. The two solid curves traced in Fig. 3.3.10 represent the two drawdown type curves of Fig. 3.1.6. As recorded in Fig. 3.3.10, the time match-point values obtained by matching the two sets of derivative data are  $(t_e)_M = 10$  hours and  $(t_{eD})_M = 0.6$ . Having fixed the correspondence between the time scales with the match of two pressure/pressure-derivative groups, the data plot was then moved only in the vertical direction to obtain the type-curve match of pressure data ( $\Delta p$  versus  $t_e$ ) shown in Fig. 3.3.11. The solid curve traced in Fig. 3.3.11 represents the dimensionless

**Table 3.3.3**  
**Infinite-Conductivity Fracture; Buildup Example, Ref. 18**  
**Reservoir/Well Parameters**

Porosity (fraction) . . . . .	0.12
Thickness (ft) . . . . .	82
Wellbore Radius (ft) . . . . .	0.28
System Compressibility (1/psi) . . . . .	2.1E-05
Viscosity of Fluid (cp) . . . . .	0.65
Formation Volume Factor (RB/STB) . . . . .	1.26
Production Rate prior to Shut-in (STB/D) . . . . .	419
Producing Time (hours) . . . . .	7800
Initial Reservoir Pressure (psi) . . . . .	3770
Flowing Pressure at the Instant of Shut-in (psi) . . . . .	3420

**Table 3.3.4**  
**Infinite-Conductivity Fracture; Buildup Example, Ref. 18**  
**Pressure and Derivative versus Time Data**

Shut-in Time, $\Delta t$ (Hours)	Equivalent Time, $t_e$ (Hours)	Pressure and Derivative Data		
		$\Delta p$ (psi)	$\Delta p'$ (psi)	$\Delta p/(2\Delta p')$
8.3300E-02	8.3299E-02	1.1000E+01	3.5504E+00	1.5491E+00
1.6700E-01	1.6700E-01	1.5000E+01	6.4357E+00	1.1654E+00
2.5000E-01	2.4999E-01	1.8000E+01	8.6219E+00	1.0439E+00
5.0000E-01	4.9997E-01	2.4500E+01	1.1353E+01	1.0790E+00
7.5000E-01	7.4993E-01	2.9000E+01	1.3275E+01	1.0923E+00
1.0000E+00	9.9987E-01	3.2000E+01	1.3129E+01	1.2186E+00
2.0000E+00	1.9995E+00	4.3000E+01	1.9079E+01	1.1269E+00
3.0000E+00	2.9989E+00	5.1000E+01	2.2206E+01	1.1483E+00
4.0000E+00	3.9979E+00	5.7000E+01	2.2809E+01	1.2495E+00
5.0000E+00	4.9968E+00	6.2000E+01	2.3514E+01	1.3184E+00
6.0000E+00	5.9954E+00	6.6000E+01	2.6420E+01	1.2490E+00
7.0000E+00	6.9937E+00	7.0000E+01	2.8725E+01	1.2184E+00
8.0000E+00	7.9918E+00	7.5000E+01	2.8827E+01	1.3009E+00
9.0000E+00	8.9896E+00	7.8000E+01	2.9338E+01	1.3293E+00
1.0000E+01	9.9872E+00	8.0000E+01	2.7123E+01	1.4784E+00
1.2000E+01	1.1982E+01	8.6000E+01	2.6973E+01	1.5942E+00
2.4000E+01	2.3926E+01	1.0800E+02	3.9317E+01	1.3734E+00
3.6000E+01	3.5835E+01	1.2400E+02	4.2422E+01	1.4615E+00
4.8000E+01	4.7706E+01	1.3500E+02	4.1391E+01	1.6308E+00
6.0000E+01	5.9542E+01	1.4300E+02	4.0758E+01	1.7542E+00
7.2000E+01	7.1341E+01	1.5000E+02	4.0679E+01	1.8437E+00
9.6000E+01	9.4833E+01	1.6200E+02	4.3372E+01	1.8676E+00
1.2000E+02	1.1818E+02	1.7000E+02	4.4867E+01	1.8945E+00
1.4400E+02	1.4139E+02	1.8000E+02	4.4241E+01	2.0343E+00
1.9200E+02	1.8739E+02	1.9000E+02	4.3310E+01	2.1935E+00
2.4000E+02	2.3284E+02	2.0000E+02	3.5000E+01	2.8571E+00

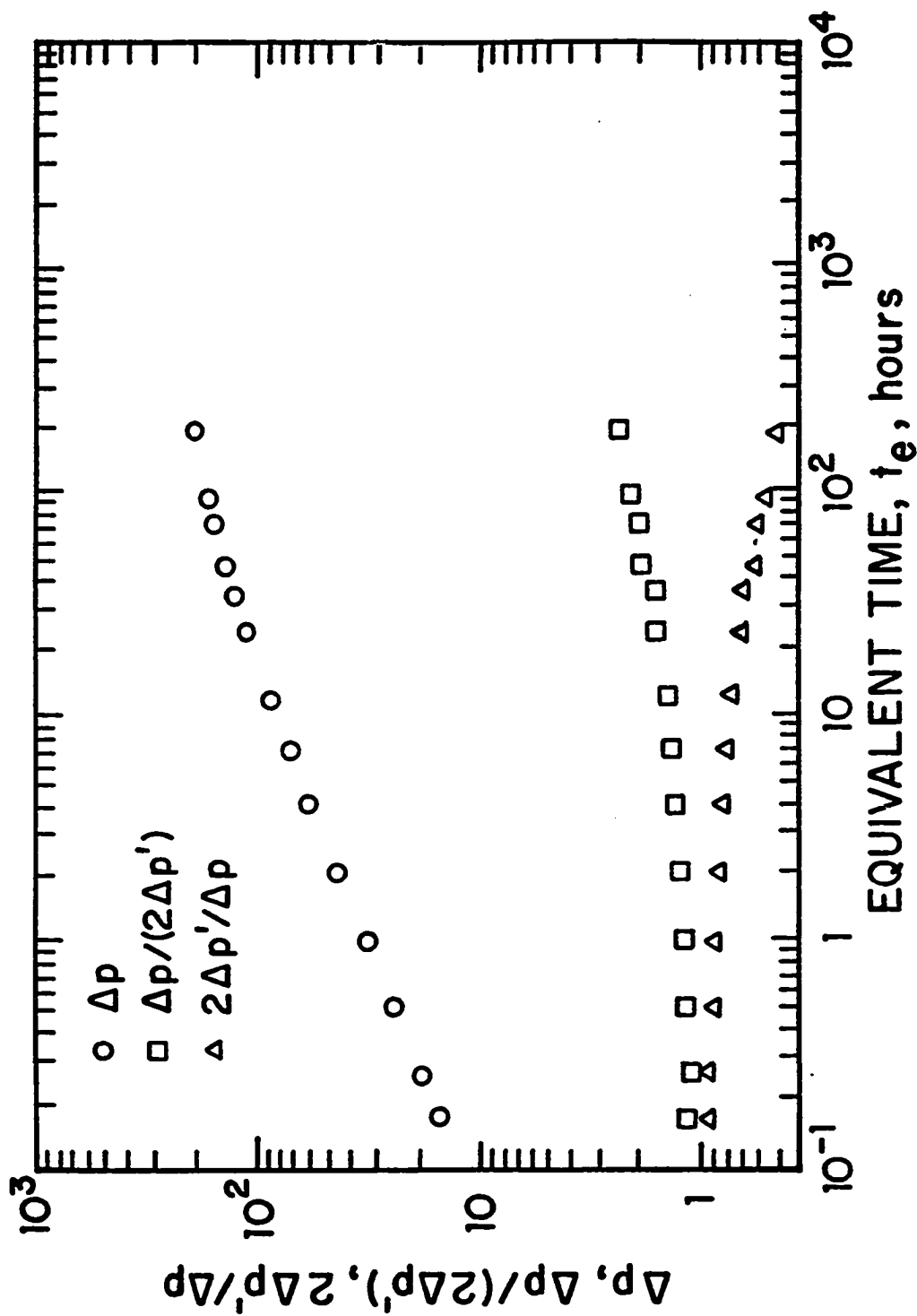


Fig. 3.3.9 - Pressure and Two Sets of Pressure/Pressure-Derivative Data - Infinite-Conductivity Fracture; Buildup Example



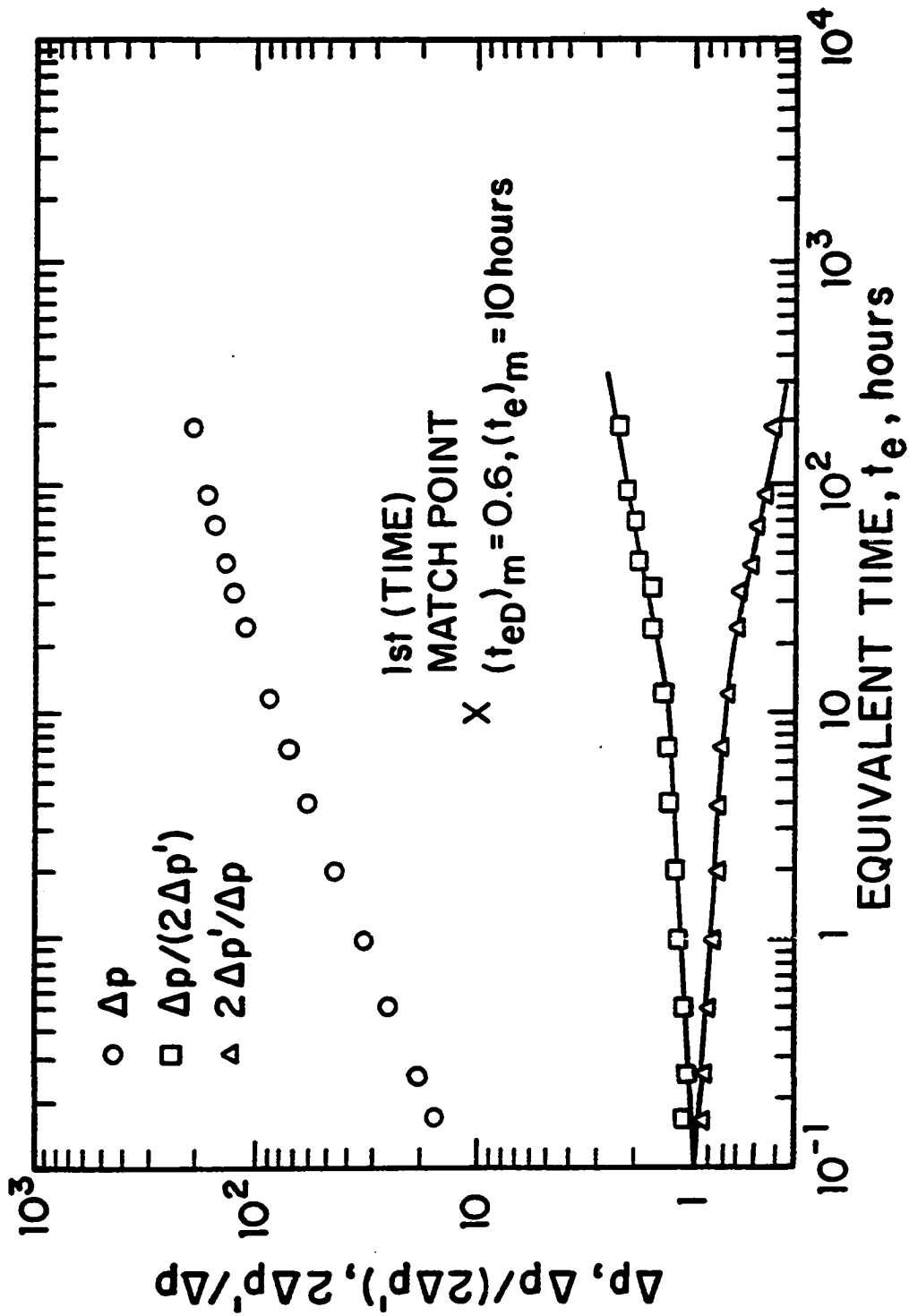


Fig. 3.3.10 - Type-Curve Match of Pressure/Pressure-Derivative Data - Infinite-Conductivity Fracture; Buildup Example

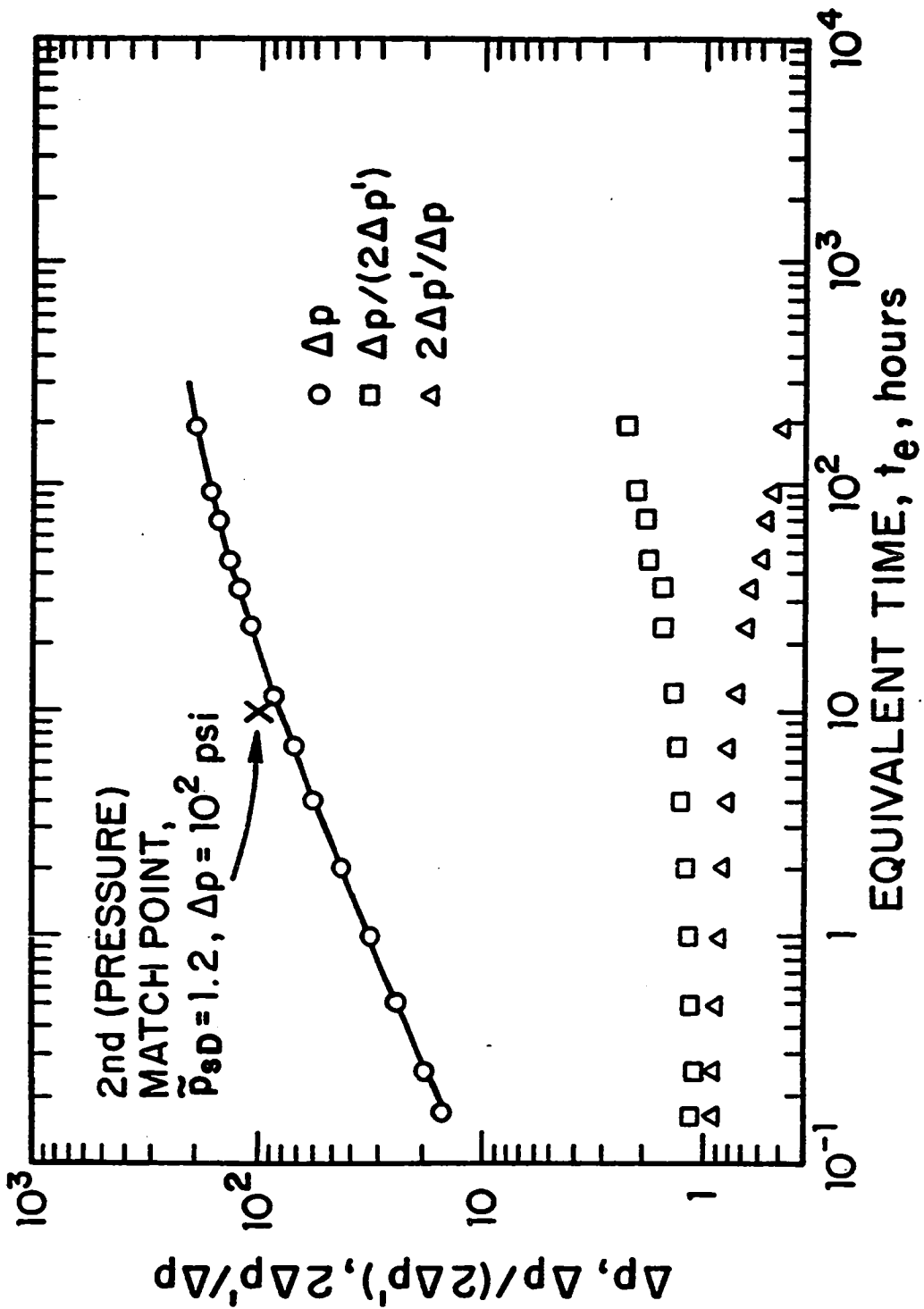


Fig. 3.3.11 - Type-Curve Match of Buildup Pressure Data - Infinite-Conductivity Fracture

drawdown pressure drop for an infinite-conductivity fracture; see Fig. 3.1.6. The pressure match-point values obtained from type-curve match of Fig. 3.3.11 are  $(\Delta p)_M = 100$  psi and  $(\tilde{p}_{eD})_M = 1.2$ . Using the pressure match-point values and data presented in Table 3.3.3 previously, one obtains

$$\begin{aligned} kh &= \frac{141.2qB\mu(\tilde{p}_{eD})_M}{(\Delta p)_M} \\ &= \frac{[141.2(419 \text{ STB/D})(1.26\text{RB/STB})0.65\text{cp}]1.2}{100\text{psi}}; \end{aligned} \quad (3.3.1)$$

therefore,  $kh = 581.45$  md-ft; thus,  $k = (kh)/h = 7.09$  md. From time match-point values, the fracture half-length can be computed from the following equation:

$$L_{x_f} = \sqrt{\frac{2.637 \times 10^{-4} k (t)_M}{\phi c_t \mu (t_{eD})_M}}. \quad (3.3.2)$$

Using the value of permeability obtained and data from Table 3.3.3, one obtains  $L_{x_f} = 137.9$  ft. As is well known, for an infinite-conductivity fracture, one can estimate the effective wellbore radius from  $r'_w = L_{x_f}/2$  and the skin factor due to existence of a vertical fracture from  $s = \ln(r_w/r'_w)$ . Use of the results of our analysis and given data in these equations gives  $r'_w = 68.95$  ft and  $s = -5.5$ . Noting that type-curve match of Fig. 3.3.11 indicates that we have pseudoradial flow pressure data, we also analyzed the data using conventional semilog analysis (Horner's method) and obtained  $k = 7.20$  md,  $s = -5.5$ , and  $L_{x_f} = 133$  ft. The semilog analysis results are in close agreement with the results obtained with our type curves. The results are also in close agreement with the results of Ref. 18.

### 3.3.4 Finite-Conductivity Fracture; Drawdown Example

The drawdown example given here is the drawdown oil well example of Ref. 20. Relevant reservoir/well data is recorded in Table 3.3.5 and pressure,  $\Delta p$ , logarithmic pressure derivative,  $\Delta p'$ , and the pressure/pressure-derivative,  $\Delta p/(2\Delta p')$ , data are shown in Table 3.3.6.

Figure 3.3.12 shows a type curve match of a semilog plot of  $\Delta p/(2\Delta p')$  versus  $t$  with the type curve of Fig. 3.1.17. The type curve match was obtained by moving

**Table 3.3.5**  
**Finite-Conductivity Fracture; Drawdown Example, Ref. 20**  
**Reservoir/Well Parameters**

Porosity (fraction) . . . . .	0.18
Thickness (ft) . . . . .	55
Wellbore Radius (ft) . . . . .	0.25
System Compressibility (1/psi) . . . . .	1.8E-05
Viscosity of Fluid (cp) . . . . .	1.8
Formation Volume Factor (RB/STB) . . . . .	1.4
Production Rate (STB/D) . . . . .	195

**Table 3.3.6**  
**Finite-Conductivity Fracture; Drawdown Example, Ref. 20**  
**Pressure and Derivative versus Time Data**

Flowing Time, $t$ (Hours)	Pressure and Derivative Data		
	$\Delta p$ (psi)	$\Delta p'$ (psi)	$\Delta p/(2\Delta p')$
1.0000E+00	8.1000E+01	2.8129E+01	1.4398E+00
2.0000E+00	1.0900E+02	4.6829E+01	1.1638E+00
3.0000E+00	1.2800E+02	5.6100E+01	1.1408E+00
4.0000E+00	1.4400E+02	6.0400E+01	1.1921E+00
5.0000E+00	1.5700E+02	6.7000E+01	1.1716E+00
6.0000E+00	1.7000E+02	7.2600E+01	1.1708E+00
7.0000E+00	1.8200E+02	7.7000E+01	1.1818E+00
8.0000E+00	1.9200E+02	7.4400E+01	1.2903E+00
9.0000E+00	2.0100E+02	7.4923E+01	1.3414E+00
1.0000E+01	2.0700E+02	7.5949E+01	1.3628E+00
1.2000E+01	2.2300E+02	8.2684E+01	1.3485E+00
1.4000E+01	2.3600E+02	8.8582E+01	1.3321E+00
1.6000E+01	2.4700E+02	8.7812E+01	1.4064E+00
2.0000E+01	2.6700E+02	9.2696E+01	1.4402E+00
2.4000E+01	2.8300E+02	9.8623E+01	1.4348E+00
3.0000E+01	3.0700E+02	1.0094E+02	1.5207E+00
4.0000E+01	3.3300E+02	1.0654E+02	1.5629E+00
5.0000E+01	3.5600E+02	1.1150E+02	1.5964E+00
6.0000E+01	3.7800E+02	1.1760E+02	1.6071E+00
7.0000E+01	3.9600E+02	1.1830E+02	1.6737E+00
8.0000E+01	4.1100E+02	1.2000E+02	1.7125E+00
9.0000E+01	4.2400E+02	1.2030E+02	1.7623E+00
1.0000E+02	4.3900E+02	1.2191E+02	1.8005E+00
1.2000E+02	4.5900E+02	1.1929E+02	1.9239E+00
1.5000E+02	4.8400E+02	1.2345E+02	1.9603E+00
2.0000E+02	5.2200E+02	1.2994E+02	2.0087E+00
2.5000E+02	5.4800E+02	1.2470E+02	2.1973E+00
3.0000E+02	5.7100E+02	1.0437E+02	2.7354E+00

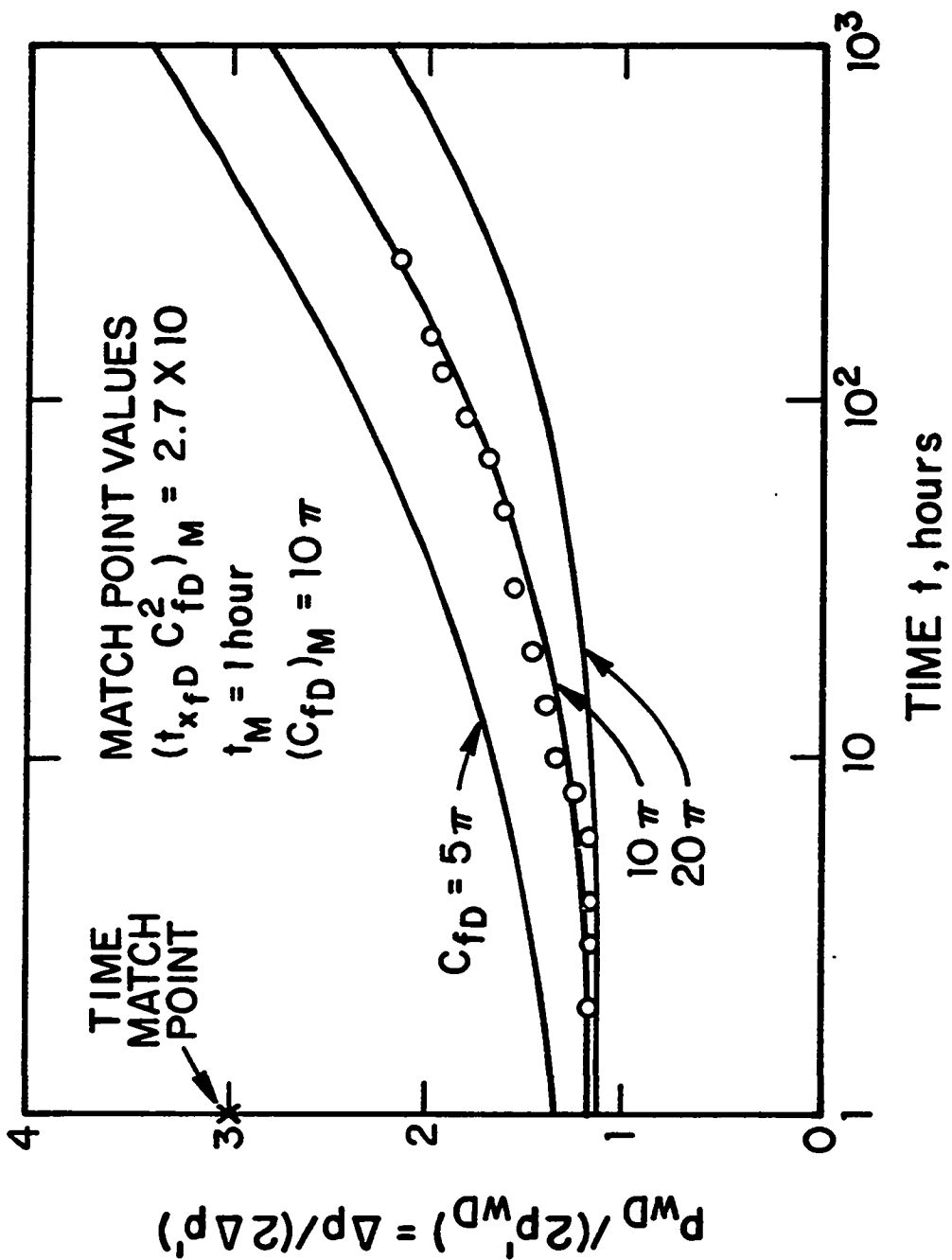


Fig. 3.3.12 - Type-Curve Match of Pressure/Pressure-Derivative Data - Finite-Conductivity Fracture; Drawdown Example

the data plot only in the horizontal direction since this is the fundamental advantage of the type curve of Fig. 3.1.17. The solid curves shown in Fig. 3.3.12 represent the dimensionless drawdown solutions for three values of  $C_{fD}$ ,  $5\pi$ ,  $10\pi$  and  $20\pi$ . Note that data were matched with the  $C_{fD} = 10\pi$  solution. (The dashed square shows the scales of the type curve of Fig. 3.1.17.) Note the match is reasonably good and yields the time match-point values  $(t_{x,D}C_{fD}^2)_M = 2.7 \times 10^1$  and  $(t_M) = 1$  hour as well as the match point value  $(C_{fD})_M = 10\pi$ . Keeping these match point values fixed, we then simultaneously matched  $\Delta p$  and  $\Delta p'$  versus  $t$  plots with the type curves of Fig. 3.1.16 to obtain the match shown in Fig. 3.3.13 which gives the pressure match-point values;  $(C_{fD}p_{wD})_M = 1.23 \times 10^2$  and  $(\Delta p)_M = 1000$  psi. Using these match point values, Eqs. 3.1.80, 3.1.81 and 3.1.69 yield the following results:  $k = 4.93$  md,  $L_{x_f} = 90.2$  ft and  $k_f b = 1.40 \times 10^4$  md-ft. From results of Barker and Ramey<sup>67</sup> or from Fig. 9 of Ref. 20, one can estimate  $n = 2.1$ . (The ordinate variable on Fig. 9 of Ref. 20 is equal to  $\ln(n)$ .) Using this values of  $n$ ,  $L_{x_f}$  and  $r_w = 0.25$  ft in Eq. 3.1.73 and solving for  $s_f$  gives  $s_f = -5.14$ . For this same example, Cinco-Ley and Samaniego-V.<sup>20</sup> obtained  $k = 5.05$  md,  $L_{x_f} = 83.2$  ft,  $k_f b = 1.32 \times 10^4$  md-ft and  $s_f = -5.06$  by type curve matching of pressure data and obtained  $k = 5.1$  md and  $s_f = -5.04$  by semilog analysis. Note that all results are in good agreement.

### 3.3.5 Finite-Conductivity Fracture; Buildup Example

The following gas well buildup example is from Table 6 of Ref. 83. The well had received an MHF treatment with a designed fracture length of 2500 ft. Water saturation is  $S_w = 0.5$  but Ref. 83 does not indicate whether the water flow rate was significant during the time period just prior to buildup. A very small amount of condensate was produced. The reservoir contains natural fractures and the type curves of Figs. 3.1.16 and 3.1.17 do not account for natural fractures. Based on the results of Ref. 84, one should not be able to match the early time data with the type curves of Figs 3.1.16 and 3.1.17 if the influence of the natural fractures is significant. From history matching using a reservoir simulator, Kozik and Holditch<sup>83</sup> obtained

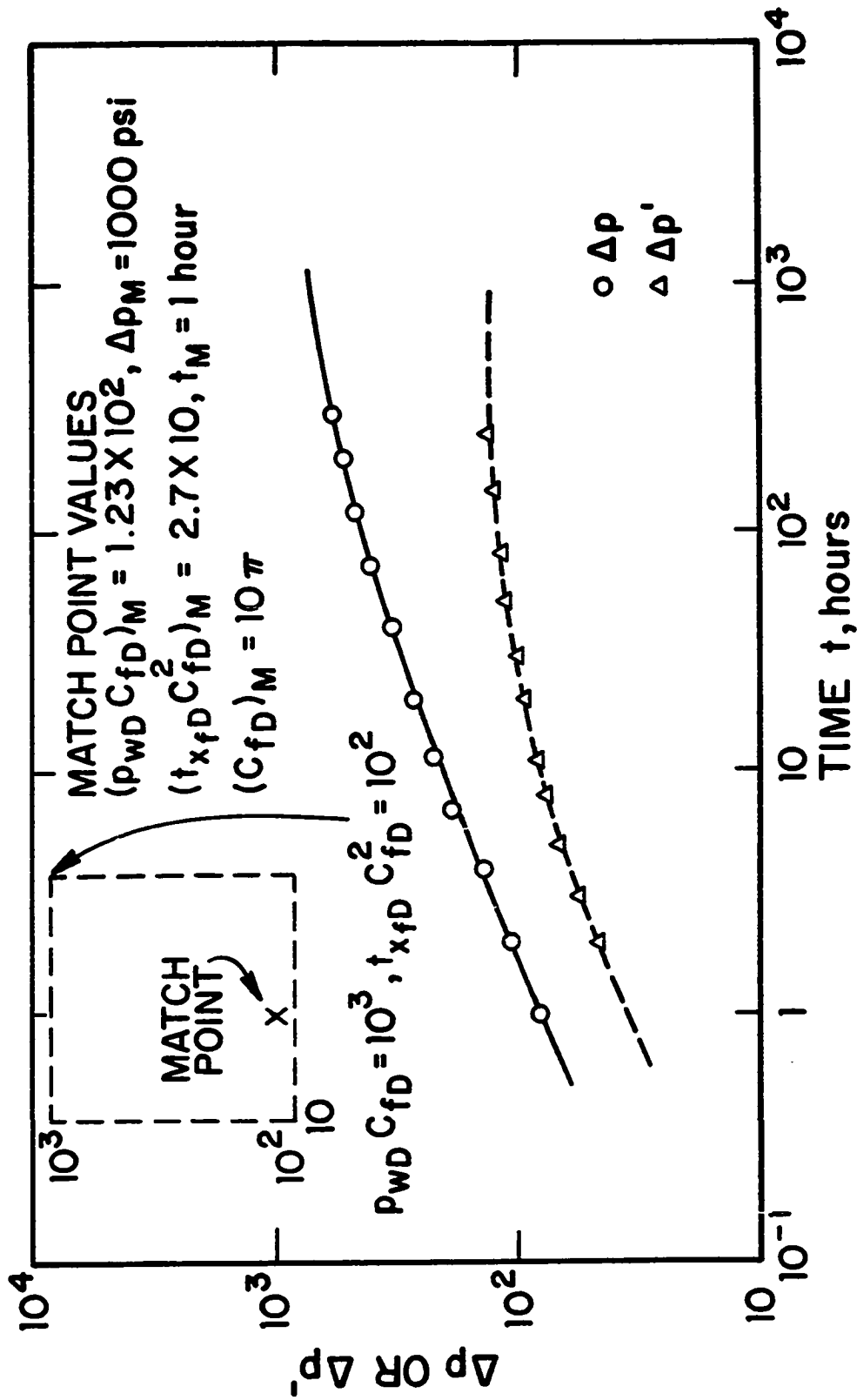


Fig. 3.3.13 - Type-Curve Match of Pressure and Derivative Data - Finite-Conductivity Fracture; Drawdown Example



$k = 0.022$  md,  $L_{xf} = 1500$  ft and  $C_{fD} = 30.3$ . Note that this value of  $C_{fD}$  is close to  $C_{fD} = 10\pi = 31.4$ ; thus, assuming the preceding parameters are correct, one should be able to match data to the appropriate type curves corresponding to  $C_{fD} = 10\pi$ . It is not clear whether their simulator used by Kozik and Holditch<sup>83</sup> accounts for natural fractures but their results do not appear to be unreasonable based on knowledge of the reservoir and the fracture design.

With knowledge of the inherent difficulties based on the complex reservoir/fracture system, we attempted to analyze the buildup data using real gas pseudopressure  $m(p)$ <sup>50</sup>

$$m(p) = \int_0^p \frac{2\tilde{p}}{\mu z} d\tilde{p}, \quad (3.3.3)$$

and equivalent pseudotime  $t_{ae}$  where

$$t_{ae} = \frac{t\Delta t_a}{t + \Delta t}; \quad (3.3.4)$$

see Refs. 51, 52 and 53. Here,  $t$  represents the producing time and  $\Delta t_a$  represents Agarwal's pseudotime<sup>51</sup>.

Table 3.3.7 summarizes shut-in pressure change, pseudopressure, and logarithmic derivative of pseudopressure and pseudopressure/pseudopressure-derivative versus  $t_{ae}$  data. In the results presented in Table 3.3.7,  $\Delta m(p)$  is the pseudopressure change defined by

$$\Delta m(p) = m(p_{ws}) - m(p_{wf}), \quad (3.3.5)$$

and  $\Delta m'(p)$  is the logarithmic derivative of  $\Delta m(p)$  with respect to  $t_{ae}$ ; i.e.,

$$\Delta m'(p) = \frac{d\Delta m(p)}{d \ln(t_{ae})}. \quad (3.3.6)$$

Figure 3.3.14 presents the best type curve match of  $\Delta m(p)/[2\Delta m'(p)]$  versus  $t_{ae}$  data obtained using the type curves of Fig. 3.1.17. The solid curve represents the curve matched and corresponds to the  $C_{fD} = 10\pi$  solution of Fig. 3.1.17. The match point values recorded in Fig. 3.3.14 correspond to this type curve match. The match is not good and leads one to expect that field data may not represent the reservoir/fracture system on which the type curve of Fig. 3.1.17 is

Table 3.3.7

Finite-Conductivity Fracture; Buildup Example, Ref. 83

Pseudopressure and Derivative versus Time Data

Shut-in Time, $\Delta t$ (Hours)	Equivalent Pseudotime, $t_{oe}$ (hrs psi/ cp)	Pseudopressure and Derivative Data		
		$\Delta m(p)$ (psi <sup>2</sup> / cp)	$\Delta m'(p)$ (psi <sup>2</sup> /cp)	$\Delta m(p)/[2\Delta m'(p)]$
2.5000E-01	3.9153E+04	2.4593E+07	6.0884E+06	2.0197E+00
5.0000E-01	8.0661E+04	3.1844E+07	1.0933E+07	1.4563E+00
7.5000E-01	1.2294E+05	3.5723E+07	1.4165E+07	1.2609E+00
1.0000E+00	1.6583E+05	4.0782E+07	1.5151E+07	1.3459E+00
1.5000E+00	2.5313E+05	4.7266E+07	1.8501E+07	1.2774E+00
2.0000E+00	3.4198E+05	5.2702E+07	1.9610E+07	1.3438E+00
2.5000E+00	4.3212E+05	5.7429E+07	2.1143E+07	1.3581E+00
3.0000E+00	5.2332E+05	6.1215E+07	2.1956E+07	1.3940E+00
4.0000E+00	7.0834E+05	6.8087E+07	2.3791E+07	1.4309E+00
6.0000E+00	1.0867E+06	7.8625E+07	2.8756E+07	1.3671E+00
8.0000E+00	1.4742E+06	8.7721E+07	3.1693E+07	1.3839E+00
1.0000E+01	1.8691E+06	9.5049E+07	3.4056E+07	1.3955E+00
1.2000E+01	2.2702E+06	1.0161E+08	3.5260E+07	1.4409E+00
1.6000E+01	3.0873E+06	1.1253E+08	4.0316E+07	1.3956E+00
2.0000E+01	3.9223E+06	1.2299E+08	4.1956E+07	1.4657E+00
2.4000E+01	4.7728E+06	1.3156E+08	3.9642E+07	1.6594E+00
3.3000E+01	6.7174E+06	1.4097E+08	5.1217E+07	1.3762E+00
4.1000E+01	8.4935E+06	1.6074E+08	6.3244E+07	1.2708E+00
4.9000E+01	1.0320E+07	1.7210E+08	6.9145E+07	1.2445E+00
5.3000E+01	1.1244E+07	1.7735E+08	6.4421E+07	1.3765E+00
6.1000E+01	1.3111E+07	1.8798E+08	6.8876E+07	1.3646E+00
6.9000E+01	1.5005E+07	1.9695E+08	7.3125E+07	1.3467E+00
7.7000E+01	1.6923E+07	2.0603E+08	7.5069E+07	1.3723E+00
8.5000E+01	1.8865E+07	2.1468E+08	7.9527E+07	1.3497E+00
9.3000E+01	2.0826E+07	2.2183E+08	8.0997E+07	1.3694E+00
1.0100E+02	2.2807E+07	2.3012E+08	8.5616E+07	1.3439E+00
1.0900E+02	2.4806E+07	2.3659E+08	8.8865E+07	1.3312E+00
1.1200E+02	2.5560E+07	2.4011E+08	8.8312E+07	1.3594E+00
1.2100E+02	2.7837E+07	2.4748E+08	9.3942E+07	1.3172E+00
1.3300E+02	3.0904E+07	2.5739E+08	9.6627E+07	1.3319E+00
1.4500E+02	3.4004E+07	2.6713E+08	1.0010E+08	1.3343E+00
1.5700E+02	3.7135E+07	2.7583E+08	1.0257E+08	1.3445E+00
1.6900E+02	4.0293E+07	2.8404E+08	1.0255E+08	1.3848E+00

Table 3.3.7 (Cont'd)

Finite-Conductivity Fracture; Buildup Example, Ref. 83

Pseudopressure and Derivative versus Time Data

Shut-in Time, $\Delta t$ (Hours)	Equivalent Pseudotime, $t_{ac}$ (hrs psi/ cp)	Pseudopressure and Derivative Data		
		$\Delta m(p)$ (psi <sup>2</sup> / cp)	$\Delta m'(p)$ (psi <sup>2</sup> /cp)	$\Delta m(p)/[2\Delta m'(p)]$
1.8100E+02	4.3478E+07	2.9231E+08	1.0399E+08	1.4054E+00
1.9300E+02	4.6686E+07	2.9920E+08	1.0909E+08	1.3714E+00
2.0500E+02	4.9915E+07	3.0643E+08	1.1393E+08	1.3449E+00
2.1700E+02	5.3167E+07	3.1458E+08	1.2463E+08	1.2620E+00
2.2900E+02	5.6441E+07	3.2161E+08	1.2825E+08	1.2539E+00
2.4100E+02	5.9738E+07	3.2986E+08	1.2769E+08	1.2917E+00
2.5300E+02	6.3056E+07	3.3609E+08	1.2798E+08	1.3130E+00
2.6500E+02	6.6391E+07	3.4265E+08	1.2757E+08	1.3430E+00
2.7700E+02	6.9743E+07	3.4894E+08	1.3400E+08	1.3020E+00
2.8900E+02	7.3113E+07	3.5556E+08	1.3654E+08	1.3020E+00
3.0100E+02	7.6499E+07	3.6192E+08	1.3670E+08	1.3237E+00
3.1300E+02	7.9901E+07	3.6769E+08	1.3490E+08	1.3628E+00
3.2500E+02	8.3317E+07	3.7318E+08	1.4135E+08	1.3201E+00
3.3700E+02	8.6745E+07	3.7869E+08	1.4177E+08	1.3356E+00
3.4900E+02	9.0189E+07	3.8546E+08	1.9076E+08	1.0103E+00
3.6000E+02	9.3357E+07	3.8917E+08	1.9564E+08	9.9461E-01
3.7400E+02	9.7423E+07	4.0501E+08	1.5711E+08	1.2889E+00
4.2200E+02	1.1144E+08	4.1033E+08	9.6357E+07	2.1292E+00
4.4600E+02	1.1844E+08	4.1756E+08	1.1093E+08	1.8821E+00
4.7000E+02	1.2546E+08	4.2387E+08	1.3200E+08	1.6056E+00
4.9400E+02	1.3251E+08	4.3338E+08	1.3541E+08	1.6002E+00
5.1800E+02	1.3958E+08	4.3943E+08	1.3780E+08	1.5945E+00
5.4200E+02	1.4666E+08	4.4582E+08	1.2986E+08	1.7166E+00
5.6600E+02	1.5376E+08	4.5256E+08	1.3419E+08	1.6862E+00
6.0200E+02	1.6443E+08	4.6126E+08	1.4915E+08	1.5462E+00
6.1400E+02	1.6799E+08	4.6417E+08	1.4414E+08	1.6102E+00
6.3800E+02	1.7512E+08	4.7162E+08	1.4948E+08	1.5776E+00
6.6200E+02	1.8227E+08	4.7650E+08	1.3394E+08	1.7788E+00
6.8600E+02	1.8942E+08	4.8172E+08	1.1670E+08	2.0639E+00

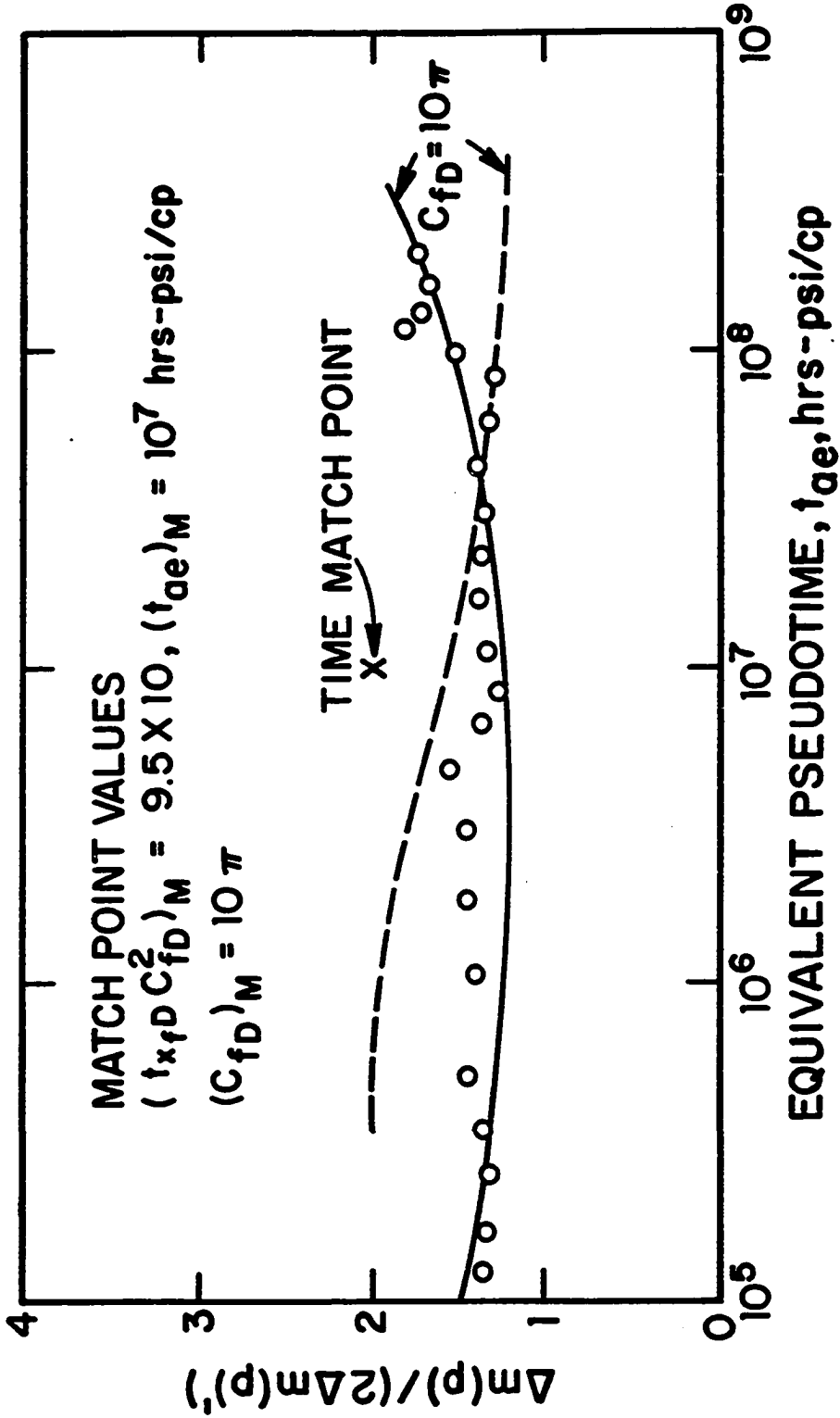


Fig. 3.3.14 - Attempted Type-Curve Match of Pseudopressure/Pseudopressure-Derivative Data - Finite-Conductivity; Buildup Example

based possibly due to the presence of natural fractures. The dashed curve of Fig. 3.3.14 corresponds to an earlier time part of the  $C_{fD} = 10\pi$  solution of Fig. 3.1.17. The plot of the buildup data compared to this dashed curve represents the type curve match that one would have to obtain in order to obtain the parameter values obtained by Ref. 80 by history matching. Clearly, this does not represent an acceptable type curve match.

For completeness, keeping the time match point-values recorded in Fig. 3.3.14 fixed, we simultaneously matched  $\Delta m(p)$  and  $\Delta m'(p)$  versus  $t_{ae}$  plots with the type curves of Fig. 3.1.16. This match is shown in Fig. 3.3.15 and represented by solid curves. As recorded in Fig. 3.3.15, this match determines the following pressure match-point values;  $(C_{fD}p_{wD})_M = 100$  and  $(\Delta m(p))_M = 10^9$  psi<sup>2</sup>/cp. Using these pressure match-point values and time match-point values recorded in Fig. 3.3.14, one obtains  $k = 0.181$  md and  $L_{x_f} = 525$  ft. For comparison purposes, the type curve match that one would obtain using the estimates of Ref. 83;  $k = 0.022$  md and  $L_{x_f} = 1500$  ft, is also shown in Fig. 3.3.15 by the dashed curves. Note that these results are not in good agreement because of the fact that field data plot may not represent the reservoir/fracture system on which type curves of Fig. 3.1.17 is based.

This example is intended to illustrate one of the advantages of the new type curves based on the  $p_{wD}/(2p'_{wD})$  pressure/pressure derivative group. Since type curve matching is accomplished by moving the data only in the horizontal direction, one should be able to use the type curves to obtain an indication of whether the field data actually represents the model assumed by the type curves.

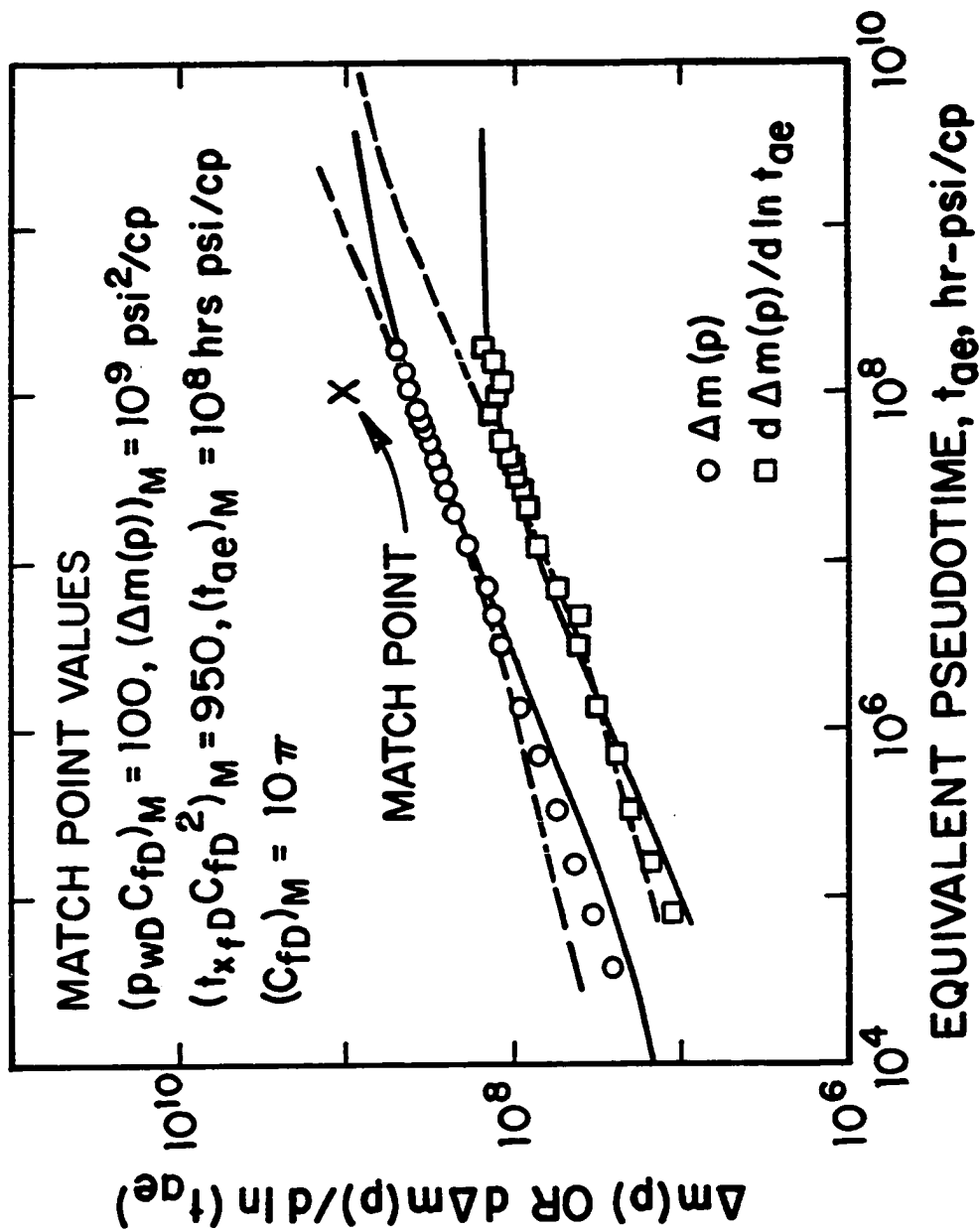


Fig. 3.3.15 - Attempted Type-Curve Match of Pseudopressure and Derivative Data

**CHAPTER IV**  
**ANALYSIS OF PRESSURE BUILDUP DATA**  
**USING THE PRESSURE DERIVATIVE**

The purpose of this chapter is to present new applications of the pressure derivative for analyzing the pressure buildup data obtained at a well located in a system of wells draining a closed bounded reservoir. Both unfractured and fractured wells are considered.

The well known Miller-Dyes-Hutchinson<sup>34</sup> and Matthews-Brons-Hazebroek<sup>35</sup> methods can be used to compute the volumetric average reservoir pressure from a buildup test under the following conditions: (i) permeability can be determined by semilog analysis; (ii) the drainage area of the well is known; and (iii) the well's location in the drainage area and the shape of the drainage area are known; i.e., the Dietz<sup>36</sup> shape factor is known. One of the primary contributions of this work is the presentation of a new method for determining the well's drainage area directly from the derivative of pressure buildup data.

The buildup response of a single well in a closed drainage area has been investigated by many researchers; see, for example, Refs. 34-37 and 85-90. For the most part, these references focus on the existence and duration of the Horner or MDH semilog straight lines and on methods for computing average reservoir pressure. For cases where pseudosteady-state flow exists at the instant of shut-in, the results of Ramey and Cobb<sup>85</sup>, and Larsen<sup>88</sup> indicate that the duration of the Horner and MDH semilog straight lines are essentially identical. In this work, it is shown that one can obtain a longer semilog straight line by using a modified MDH plot. This modified MDH plot is identical to one suggested by Codreanu<sup>90</sup> and also is conceptually similar to a method suggested by Slider<sup>87</sup>. However, Codreanu suggested a

trial and error procedure for determining the corrected shut-in pressure to use in the modified MDH plot. Our work removes this restriction. In addition, Ref. 90 considered only a single unfractured well in a closed drainage area whereas we consider general multi-well systems and also consider both fractured and unfractured wells.

It is worthwhile to note that Larsen<sup>88</sup> showed that the duration of Horner semilog straight line can be increased by replacing the actual producing time,  $t_p$ , by  $t'$  in the Horner time ratio, where  $t'$  corresponds to the time such that  $t'_{AD} = 0.08$ . In order to obtain  $t'$ , one must have a priori knowledge of the reservoir drainage area at the instant of shut-in and the permeability. Our method for computing drainage area and permeability directly from buildup data enables one to compute the value of  $t'$  necessary to apply Larsen's suggestion.

By using a method of analysis based on pressure derivatives, it is shown that the drainage area and permeability-thickness product can be obtained directly from a given pressure buildup test. The method uses the derivative of the shut-in pressure and does not require a priori knowledge of initial pressure,  $p_i$ , or the wellbore flowing pressure at the instant of shut-in,  $p_{wf,s}$ . Moreover, our method does not rely on the existence of the semilog straight line on a Horner or MDH plot. The method is applicable to both unfractured and fractured wells. The analysis procedure can be used to analyze the buildup pressures at a well located in any one of the following three systems: (i) a single well in a closed drainage area; (ii) a system of producing wells in a closed bounded reservoir; (iii) an infinite multi-well pattern. The basic assumption is that the buildup surveyed well has established a unique drainage area prior to shut-in. For the closed bounded reservoir cases (cases (i) and (ii)), this means pseudosteady-state flow is established throughout the reservoir prior to shut-in. For case (iii), our assumption is that prior to shut-in, pseudosteady-state flow has been established in the drainage area of the well under consideration. A method for determining the average reservoir pressure is also given. The method requires only the knowledge of the Dietz shape factor and is not highly sensitive to the estimate of the Dietz shape factor.



We also present a second method for estimating a well's drainage area from pressure buildup data. The second method relies on the fact that during buildup, the shut-in pressure of a well located in an infinite multi-well pattern or in a multi-well closed bounded reservoir increases to a maximum and then decreases when nearby producing wells start to affect the shut-in pressure of buildup surveyed well. When the maximum in the shut-in pressure is observed, it is shown that the drainage area (at the instant of shut-in) and the average pressure in this drainage area can be calculated from the maximum shut-in pressure and the shut-in time at which it occurs.

At end of this chapter, we investigate the validity of new analysis methods mentioned above to analyze pressure buildup data influenced by wellbore storage and skin effects. Moreover, we include the analysis of an actual field pressure buildup test to illustrate the use of new pressure derivative methods in estimating reservoir/well parameters.

#### 4.1 Assumptions and Definitions

Throughout this chapter, we assume single-phase flow of a slightly compressible fluid of constant viscosity in a homogeneous reservoir. Moreover, we assume that all wells in an infinite multi-well pattern and in a closed bounded system produce with a constant rate, but the production rate may vary from well to well. We define the dimensionless variables in the standard way and oil field units are used throughout.

The dimensionless wellbore pressure drop is defined by

$$p_{wD} = \frac{kh [p_i - p_{wf}]}{141.2qB\mu}. \quad (4.1.1)$$

It is important to note that throughout this chapter  $p_{wD}$  represents the dimensionless drawdown wellbore pressure solution for the well under consideration. The expression for  $p_{wD}$  depends on the well location in the drainage area, whether the well is fractured or unfractured and the flow regime under consideration (linear, radial, pseudosteady-state, etc.).

The dimensionless wellbore shut-in pressure,  $p_{sD}$ , is defined by

$$p_{sD} = \frac{kh [p_i - p_{ws}]}{141.2q_1 B \mu}. \quad (4.1.2)$$

Because we consider multi-well systems, well one and the subscript 1 refer to the buildup surveyed well.

The dimensionless times based on wellbore radius,  $r_w$ , fracture half length,  $L_{x_f}$ , well 1's drainage area,  $A_1$ , and the total reservoir drainage area,  $A_t$ , are defined, respectively, by

$$t_D = \frac{2.637 \times 10^{-4} kt}{\phi c_t \mu r_w^2}, \quad (4.1.3)$$

$$t_{x_f D} = \frac{2.637 \times 10^{-4} kt}{\phi c_t \mu L_{x_f}^2}, \quad (4.1.4)$$

$$t_{A_1 D} = \frac{2.637 \times 10^{-4} kt}{\phi c_t \mu A_1}. \quad (4.1.5)$$

and

$$t_{A_t D} = \frac{2.637 \times 10^{-4} kt}{\phi c_t \mu A_t}. \quad (4.1.6)$$

It follows from Eqs. 4.1.3, 4.1.4, 4.1.5 and 4.1.6 that

$$t_{A_t D} = \frac{r_w^2}{A_t} t_D = \frac{L_{x_f}^2}{A_t} t_{x_f D} = \frac{A_1}{A_t} t_{A_1 D}, \quad (4.1.7)$$

where  $A_1$  always represents the drainage area of well 1 at the instant of shut-in, and  $A_t$  represents the total reservoir drainage area for the closed bounded reservoir cases considered. For the case of a single well in a closed drainage area,  $A_t = A_1$ .

Throughout,  $t_p$  denotes the producing time in hours and the corresponding dimensionless values of  $t_p$  are defined as  $t_{pD}$ ,  $t_{p x_f D}$ ,  $t_{p A_1 D}$ , and  $t_{p A_t D}$ . They are obtained, respectively, by replacing  $t$  on the right hand sides of Eqs. 4.1.3, 4.1.4, 4.1.5 and 4.1.6 by  $t_p$ . Similarly,  $\Delta t$  denotes the shut-in time in hours and the corresponding dimensionless values of  $\Delta t$  are defined, respectively, as  $\Delta t_D$ ,  $\Delta t_{x_f D}$ ,  $\Delta t_{A_1 D}$ , and  $\Delta t_{A_t D}$  which are obtained by replacing  $t$  by  $\Delta t$  in Eqs. 4.1.3 through 4.1.6. Throughout,  $t_{pss}$  denotes the time at which pseudosteady-state flow begins.  $R_H$  denotes the well known Horner<sup>37</sup> time ratio and is defined as

$$R_H = \frac{t_p + \Delta t}{\Delta t} = \frac{t_{pD} + \Delta t_D}{\Delta t_D} = \frac{t_{p x_f D} + \Delta t_{x_f D}}{\Delta t_{x_f D}}. \quad (4.1.8)$$

The dimensionless distance based on wellbore radius,  $r_w$ , is defined by

$$r_D = \frac{r}{r_w}. \quad (4.1.9)$$

Throughout  $r$  is the radial distance measured from well 1 and  $x$  and  $y$  are the distances in  $x$  and  $y$  directions. The relationship between the radial coordinate system and the  $x - y$  coordinate system is given by

$$r^2 = x^2 + y^2. \quad (4.1.10)$$

#### 4.2 General Buildup Solution

The geometry for a system of producing wells completed in a  $x_e$  by  $y_e$  closed bounded rectangular reservoir is depicted in Fig. 4.2.1. The  $x - y$  coordinate system is centered at well 1 shown in Fig. 4.2.1 and  $(x_k, y_k)$  represents the coordinate of well  $k$ . In Fig. 4.2.1, the solid circles represent the producing wells. The relative location of well  $k$  in the closed rectangular reservoir shown in Fig. 4.2.1 is determined by two parameters  $\alpha_k$  and  $\beta_k$  which are defined, respectively, by

$$\alpha_k = \frac{x_{wk}}{x_e}, \quad (4.2.1)$$

and

$$\beta_k = \frac{y_{wk}}{y_e}, \quad (4.2.2)$$

where  $x_{wk}$  denotes the distance (in the  $x$  direction) between well  $k$  and the right boundary of the reservoir, and  $y_{wk}$  denotes the distance (in the  $y$  direction) between well  $k$  and the bottom boundary of the reservoir. For example,  $\alpha_k = \beta_k = 0.5$  indicates that well  $k$  is located at the center of the closed bounded rectangular reservoir.

For the system of Fig. 4.2.1, we assume that well  $k$  ( $2 \leq k \leq m$ ) produces at a rate  $q_k$  for all times and well 1 produces at a rate  $q_1$  for  $0 < t \leq t_p$  and then is shut-in for pressure buildup. Here,  $m$  denotes the number of wells in the closed bounded

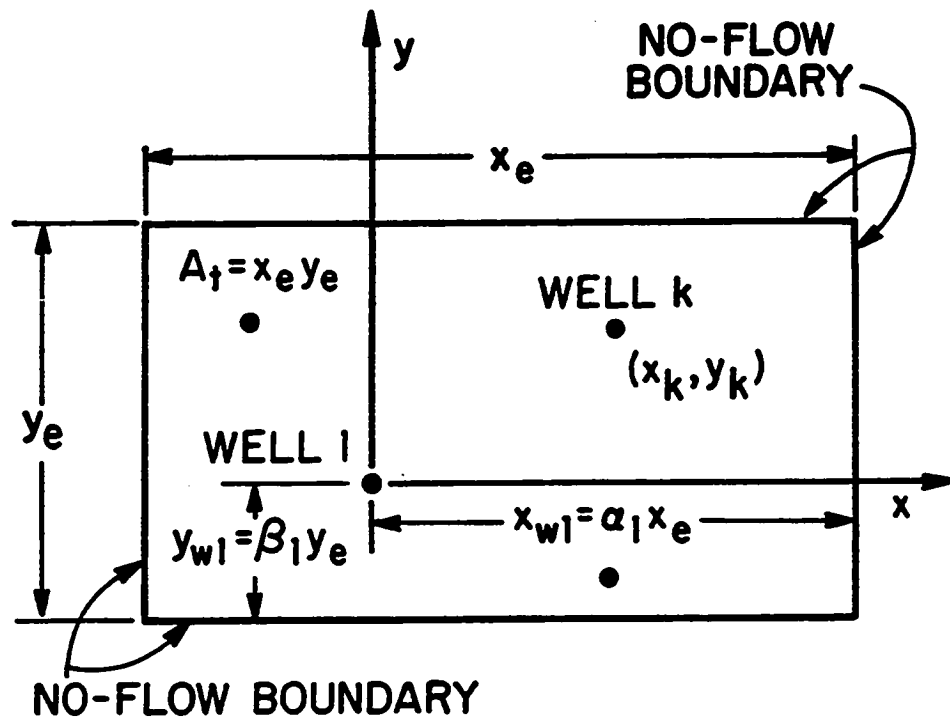


Fig. 4.2.1 - System of Producing Wells in a Closed Bounded Reservoir

system. Using the method of images and superposition, as shown in Appendix E, the dimensionless shut-in pressure at well 1 can be given by

$$\begin{aligned}
 p_{sD} = \frac{kh(p_i - p_{ws}(\Delta t))}{141.2q_1B\mu} = & \\
 & \left[ p_D(x_1, y_1, t_p + \Delta t) + \sum_{j=2}^{\infty} p_D(x_{1j}, y_{1j}, t_p + \Delta t) + s \right] \\
 & - \left[ \left[ p_D(x_1, y_1, \Delta t) + \sum_{j=2}^{\infty} p_D(x_{1j}, y_{1j}, \Delta t) + s \right] \right] \\
 & + \left( \sum_{k=2}^m \frac{q_k}{q_1} p_D(x_k, y_k, t_p + \Delta t) \right) \\
 & + \sum_{k=2}^m \sum_{j=2}^{\infty} \frac{q_k}{q_1} p_D(x_{kj}, y_{kj}, t_p + \Delta t). \quad (4.2.3)
 \end{aligned}$$

In Eq. 4.2.3,  $(x_{kj}, y_{kj})$  represents the coordinate of the  $j$ th image well of well  $k$ . The term  $p_D$  represents the dimensionless pressure drop that would be obtained at a single producing well with a zero skin factor in an infinite reservoir. We have used the standard assumption that skin factors associated with well  $k$ ,  $2 \leq k \leq m$ , do not affect the pressure change at well 1. Only the skin factor of the well 1 influences the pressure drop at well 1. Throughout,  $s$  denotes the skin factor of well 1. Note that skin factor can be canceled from Eq. 4.2.3 but we have chosen to include it for later reference. The first sum on the right hand side of Eq. 4.2.3 represents the pressure drop due to the image wells associated with well 1 and the double sum represents the pressure drop due to the image wells of well 2 through  $m$ . The sum in parentheses represents the pressure drop observed at well 1 due to production at wells 2 through  $m$ . The group of terms enclosed within double square brackets represents the pressure change caused by the shut-in of well 1. For all reservoir systems considered, we use the algorithms suggested by Larsen<sup>73</sup> to generate the buildup solution given by Eq. 4.2.3.

If we let  $p_{wD}$  be the dimensionless drawdown pressure drop associated with well 1 and its image wells, then Eq. 4.2.3 can be rewritten as

$$p_{sD} = \frac{kh(p_i - p_{ws}(\Delta t))}{141.2q_1B\mu} = p_{wD}(t_p + \Delta t) - p_{wD}(\Delta t)$$

$$\begin{aligned}
& + \left( \sum_{k=2}^m \frac{q_k}{q_1} p_D(x_k, y_k, t_p + \Delta t) \right) \\
& + \sum_{k=2}^m \sum_{j=2}^{\infty} \frac{q_k}{q_1} p_D(x_{kj}, y_{kj}, t_p + \Delta t). \tag{4.2.4}
\end{aligned}$$

For a single well system,  $m = 1$  and Eq. 4.2.4 reduces to the standard superposition equation; i.e.,

$$p_{sD} = p_{wD}([t_p + \Delta t]_D) - p_{wD}(\Delta t_D). \tag{4.2.5}$$

Equations 4.2.3 through 4.2.5 apply to both fractured and unfractured wells. For unfractured wells, we use the line source solution to represent each  $p_D$  term in Eqs. 4.2.3 and 4.2.4, whereas for fractured wells we use the appropriate infinite-acting solutions of Refs. 17 and 19.

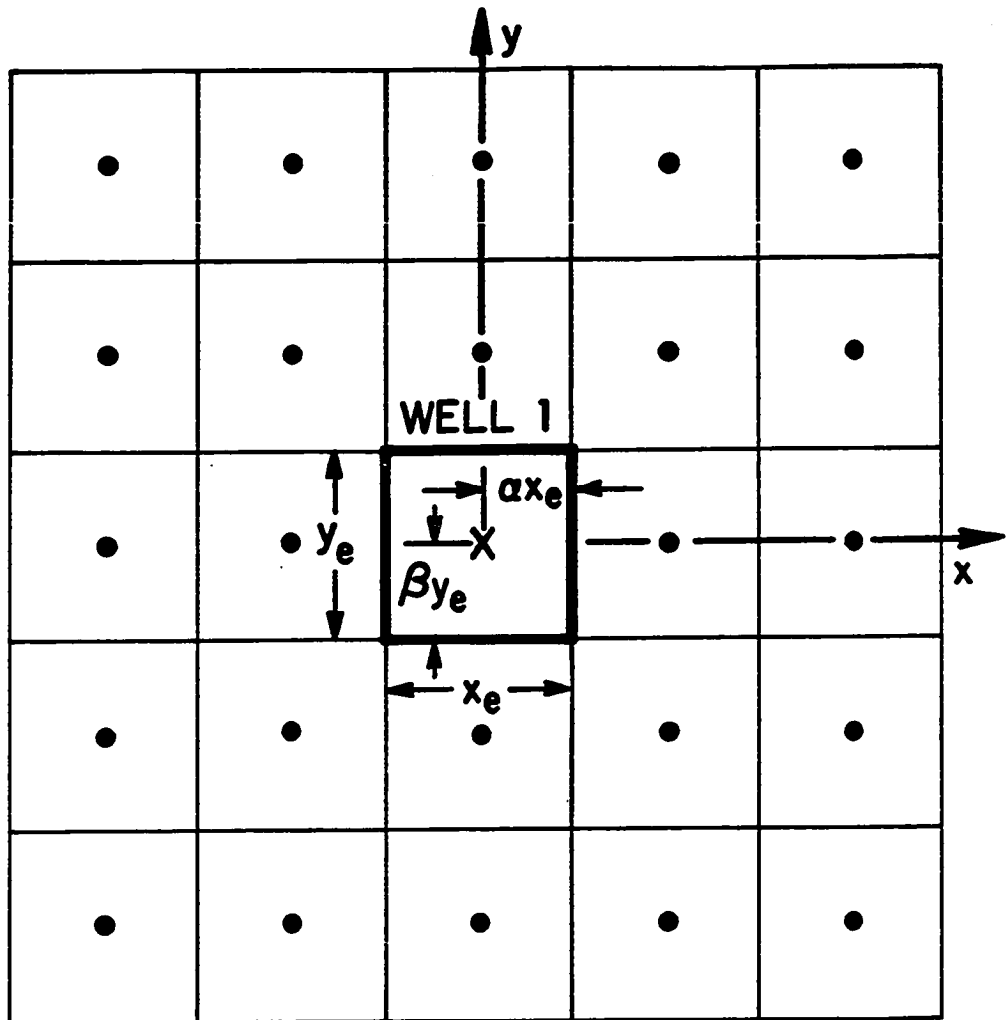
Assuming for simplicity that all wells produce at the same rate, it is easy to show that the buildup response at a well located in an infinite multi-well pattern is given by

$$\begin{aligned}
p_{sD} = \frac{kh[p_i - p_{ws}(\Delta t)]}{141.2q_1 B\mu} = [p_D(x_1, y_1, t_p + \Delta t) + \sum_{j=2}^{\infty} p_D(x_j, y_j, t_p + \Delta t)] \\
- p_D(x_1, y_1, \Delta t), \tag{4.2.6}
\end{aligned}$$

where  $(x_j, y_j)$  denotes the location of well  $j$ . Fig. 4.2.2 depicts one possible infinite multi-well pattern. In Fig. 4.2.2, the solid circles denote wells which are on production for all times and the cross denotes the location of well 1 which produces at a rate  $q_1$  for  $0 < t \leq t_p$  and then is shut-in. The closed square represents well 1's drainage area at the instant of shut-in. During buildup, the pressure at well 1 will initially increase but will eventually decline due to production at nearby producing wells.

### 4.3 Unfractured Wells

For an unfractured completely-penetrating well, all  $p_D$  terms in Eqs. 4.2.3 and 4.2.4 are given by the line source solution. Here, three cases are considered: the buildup response at a single well in a closed bounded reservoir; the buildup



X BUILDUP SURVEYED WELL  
• PRODUCING WELLS

Fig. 4.2.2 - Infinite Multi-Well Pattern

response at a well in a multi-well system located in a closed bounded reservoir and the buildup response at a well located in an infinite multi-well pattern.

#### 4.3.1 Single Well in a Closed Reservoir

In this subsection, we consider a single line source well located in a closed (bounded) rectangular drainage area. The well is produced at a rate  $q_1$  until  $t = t_p$  and is then shut-in for pressure buildup. For this system, well 1's dimensionless shut-in pressure,  $p_{sD}$ , can be obtained from Eq. 4.2.3 with both the double summation term and the summation term enclosed in parentheses deleted. Alternately, the dimensionless buildup pressure can be obtained from Eq. 4.2.5 by using the appropriate flow regime representation for  $p_{wD}$ . During transient flow,  $p_{wD}$  is given by

$$p_{wD}(t_D) = \frac{1}{2} \ln \left( \frac{4t_D}{e^{\gamma}} \right) + s, \quad (4.3.1)$$

and during pseudosteady-state flow,  $p_{wD}$  is given by

$$p_{wD}(t_D) = 2\pi t_{A_1D} + \frac{1}{2} \ln \left( \frac{4A_1}{e^{\gamma} C_{A_1} r_w^2} \right) + s. \quad (4.3.2)$$

Here,  $A_1$  denotes the drainage area of the well under consideration and  $C_{A_1}$  denotes the associated Dietz shape factor.

If  $t_p \geq t_{pss}$ ; i.e., if pseudosteady-state flow (see Eq. 4.3.2) exists at the instant of shut-in and  $\Delta t$  is sufficiently small so that  $p_{wD}(\Delta t_D)$  is given by its semilog approximation (see Eq. 4.3.1), then Eq. 4.2.4 can be rewritten as

$$p_{sD} = 2\pi(t_p + \Delta t)_{A_1D} - \frac{1}{2} \ln(\Delta t_{A_1D} C_{A_1}). \quad (4.3.3)$$

Eq. 4.3.3 holds for shut-in times such that  $\Delta t_D \leq t_{esa,D}$  where  $t_{esa,D}$  denotes the ending time of the semilog approximation; i.e., the time when the semilog approximation for  $p_{wD}(\Delta t_D)$  no longer applies. Taking the logarithmic derivative of  $p_{sD}$  given by Eq. 4.3.3 with respect to  $\Delta t_{A_1D}$  gives

$$\frac{dp_{sD}}{d \ln \Delta t_{A_1D}} = \Delta t_{A_1D} \frac{dp_{sD}}{d \Delta t_{A_1D}} = 2\pi \Delta t_{A_1D} - \frac{1}{2}, \quad (4.3.4)$$



where the first equality of Eq. 4.3.4 follows from the chain rule. Note that Eq. 4.3.4 is independent of the producing time,  $t_p$ , and applies for all shut-in times such that  $\Delta t_D \leq t_{esa,D}$  provided that  $t_p \geq t_{pss}$ .

Eq. 4.3.4 was established previously in Ref. 91 (also see Ref. 88). However, both Refs. 88 and 91 focused on the case where Eq. 4.3.4 can be approximated by  $-1/2$ ; i.e., the case where the  $2\pi\Delta t_{A_1,D}$  term in Eqs. 4.3.3 and 4.3.4 is negligible. In fact, when this approximation holds, for all practical purposes, a semilog straight line on a MDH or a Horner plot exists. As shown later, the right side of Eq. 4.3.4 is well approximated by  $-1/2$  only at very early shut-in times.

Here, we show that when Eq. 4.3.4 is used directly, it provides a way to compute the drainage area of the well (at the instant of shut-in) and the permeability-thickness product. In dimensional variables, Eq. 4.3.4 is equivalent to

$$-\frac{dp_{ws}}{d \ln \Delta t} = m_i \Delta t - b, \quad (4.3.5)$$

where  $m_i$  and  $b$  are given, respectively, as

$$m_i = \frac{0.2340q_1 B}{\phi c_i h A_1}, \quad (4.3.6)$$

and

$$b = \frac{141.2q_1 B \mu}{2kh}. \quad (4.3.7)$$

Eq. 4.3.5 indicates that a Cartesian plot of  $-dp_{ws}/d \ln \Delta t$  vs.  $\Delta t$  will yield a straight line with slope equal to  $m_i$  and intercept equal to  $b$ . The drainage area of the well can be obtained from the value of slope  $m_i$  by the obvious rearrangement of Eq. 4.3.6, provided we know the compressibility-porosity-thickness product,  $\phi c_i h$ . The flow capacity  $kh$  can be obtained from the intercept  $b$  by the obvious rearrangement of Eq. 4.3.7. Assuming that the reservoir thickness  $h$  is known, the value of permeability,  $k$ , can then be computed. This analysis procedure does not require knowledge of the initial pressure,  $p_i$ , the pressure at the instant of shut-in,  $p_{wf,s}$ , or the producing time,  $t_p$ .

Figure 4.3.1 shows a Cartesian plot of  $dp_{sD}/d \ln \Delta t_{A_1,D}$  vs.  $\Delta t_{A_1,D}$  for a well off center ( $\alpha_1 = 0.25, \beta_1 = 0.5$ ) in a 2 : 1 closed rectangular reservoir; see insert

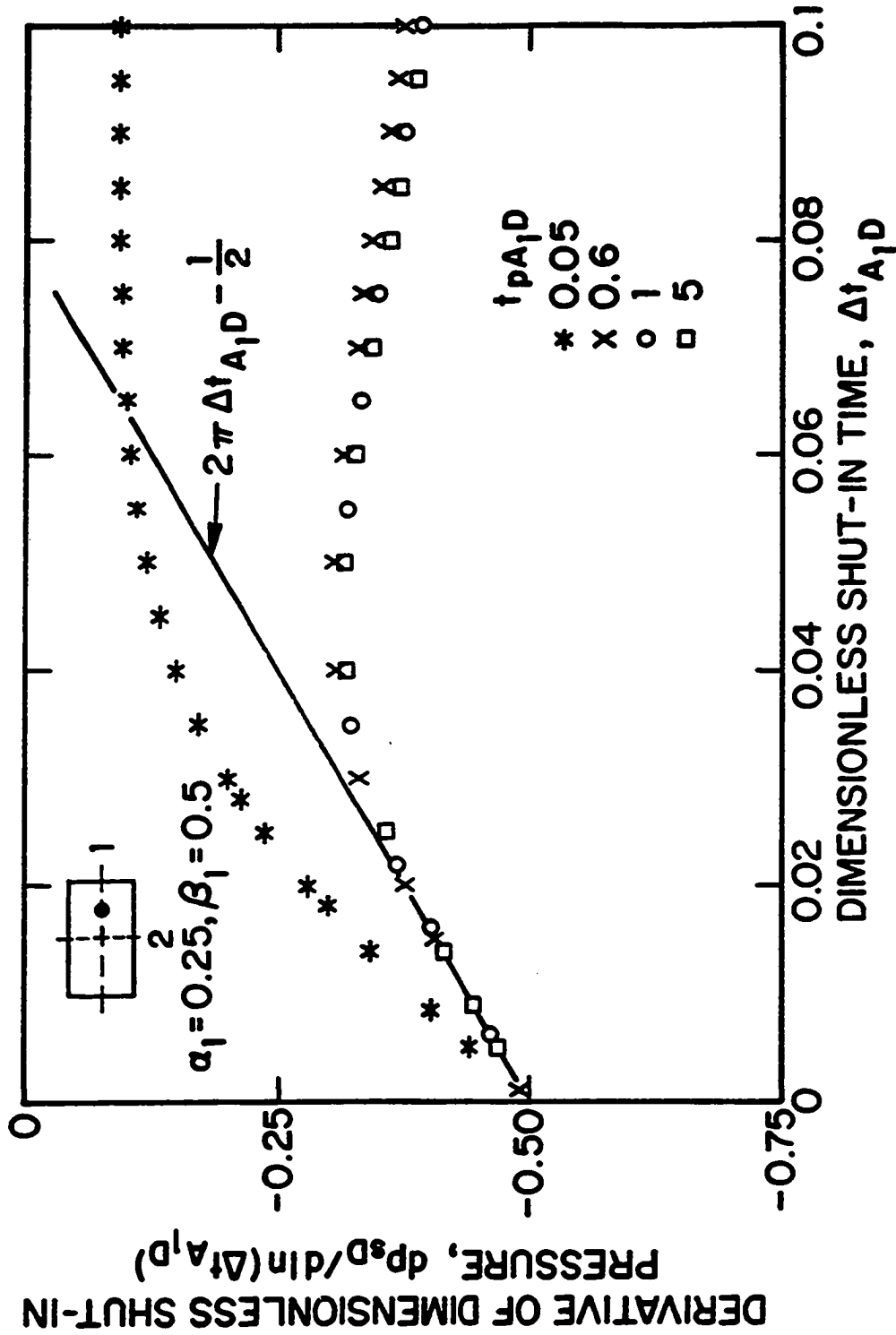


Fig. 4.3.1 - Effect of Producing Time on Derivative Response; Single Well in a Closed Bounded Reservoir

in Fig. 4.3.1. For this system, the time to reach pseudosteady-state flow period is  $t_{pss,A_1D} = 0.61$ . This value is based on a 5 percent difference between  $2\pi$  and the drawdown slope,  $dp_{wD}/dt_{A_1D}$ . In Fig. 4.3.1, the solid straight line with slope equal to  $2\pi$  and intercept equal to  $-1/2$  represents Eq. 4.3.4. Note that as we have predicted theoretically,  $dp_{eD}/d \ln \Delta t_{A_1D}$  follows Eq. 4.3.4 until  $\Delta t_{A_1D} = t_{esa,A_1D} = 0.028$  for all dimensionless producing times such that  $t_{pA_1D} \geq 0.6$ . Note that the short producing time case ( $t_{pA_1D} = 0.05$ ) shown in Fig. 4.3.1 does not follow the straight line predicted by Eq. 4.3.4. For producing and shut-in times such that both  $p_{wD}$  terms in Eq. 4.2.4 are given by the semilog approximations (see Eq. 4.3.1), it is easy show that

$$\frac{dp_{eD}}{d \ln \Delta t_{A_1D}} = -\frac{1}{2} \left( \frac{t_p}{t_p + \Delta t} \right). \quad (4.3.8)$$

Eq. 4.3.4 can be rewritten as

$$-\frac{dp_{eD}}{d \ln \Delta t_{A_1D}} + 2\pi \Delta t_{A_1D} = \frac{1}{2}. \quad (4.3.9)$$

Figure 4.3.2 illustrates the existence and the duration of the straight line predicted by Eq. 4.3.4, or, equivalently, the validity of Eq. 4.3.9, for three different well locations in a 2 : 1 rectangular drainage area. The geometries of the rectangular systems are depicted on Fig. 4.3.2. The dimensionless producing time is  $t_{pA_1D} = 3$  for all results shown in Fig. 4.3.2. Note that Fig. 4.3.2 presents a log-log plot of  $-(dp_{eD}/d \ln \Delta t_{A_1D}) + 2\pi \Delta t_{A_1D}$  vs.  $\Delta t_{A_1D}$ . The solid dots in Fig. 4.3.2 denote the ending time of Eq. 4.3.9 (equivalently, the ending time of Eq. 4.3.4) for the three cases based on a 5 percent difference between the two sides of Eq. 4.3.9. It is apparent from Fig. 4.3.2 that Eqs. 4.3.9 and 4.3.4 apply longer for cases 2 and 3 than for case 1. This is the expected theoretical result since Eqs. 4.3.4 and 4.3.9 cease to apply when the shut-in pressure is influenced by the closest reservoir boundary; i.e., when  $p_{wD}(\Delta t_D)$  is no longer given by its semilog approximation.

For long producing times ( $t_{pA_1D} > t_{pss,A_1D}$ ) and shut-in times such that  $\Delta t_{A_1D} \leq \Delta t_{esa,A_1D}$ , Eq. 4.3.3 applies. As is well known MDH semilog analysis assumes shut-in times sufficiently small so that  $t_p + \Delta t$  can be replaced by  $t_p$  in

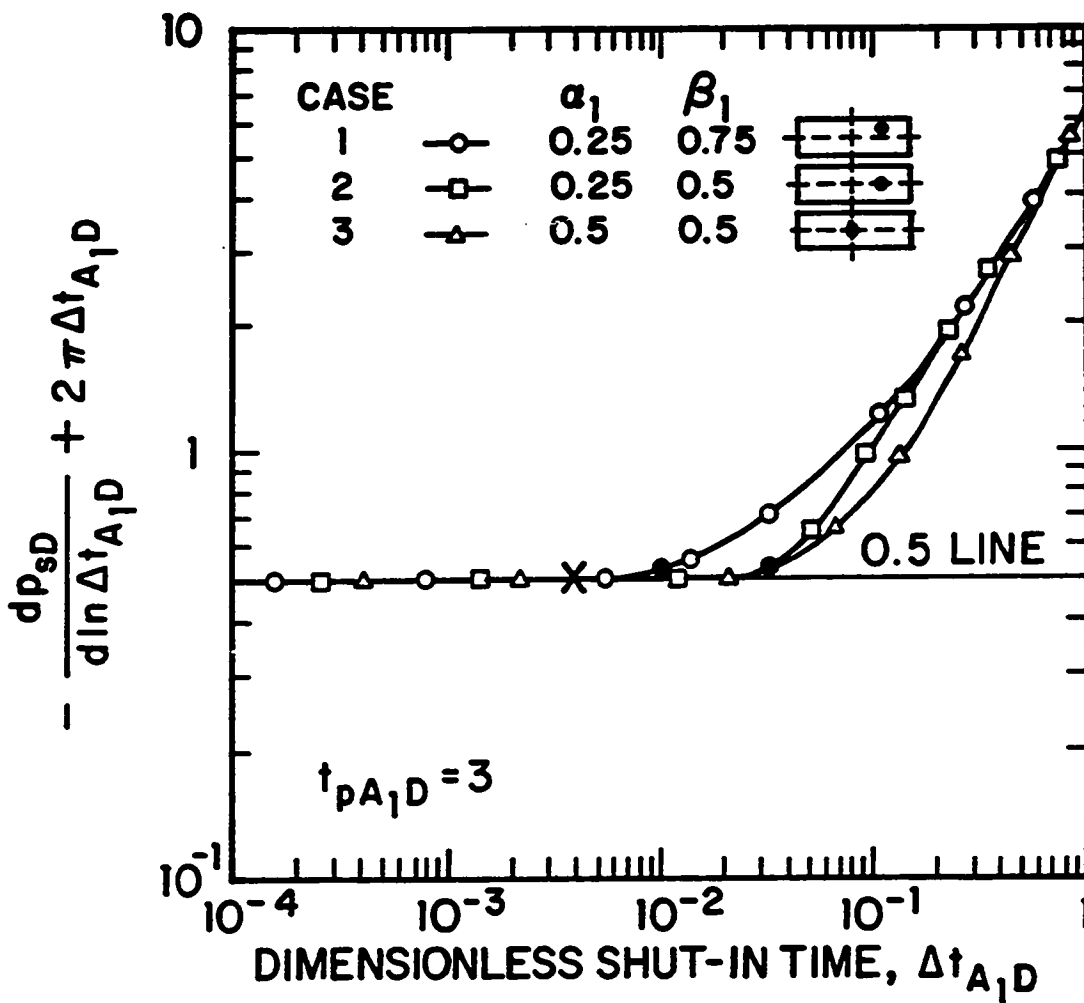


Fig. 4.3.2 - Effect of Well Location on Derivative Response; Single Well in a 2 : 1 Rectangular Reservoir

Eq. 4.3.3. In this case a semilog plot of  $p_{eD}$  vs.  $\Delta t_D$  will exhibit a semilog straight line of slope  $-1.151$ , or equivalently,

$$-\frac{dp_{eD}}{d \ln \Delta t_D} = -\frac{dp_{eD}}{d \ln \Delta t_{A_1D}} = \frac{1}{2}. \quad (4.3.10)$$

The MDH semilog straight line will end when the approximation  $t_p + \Delta t \approx t_p$  is no longer valid. On the other hand, Eq. 4.3.3 can be rearranged to yield

$$p_{eD} - 2\pi\Delta t_{A_1D} = 2\pi t_{pA_1D} - \frac{1}{2} \ln(\Delta t_{A_1D} C_{A_1}). \quad (4.3.11)$$

Taking the logarithmic derivative of Eq. 4.3.11 yields Eq. 4.3.9. These results suggest that the "modified" MDH semilog plot of  $p_{eD} - 2\pi\Delta t_{A_1D}$  vs.  $\Delta t_{A_1D}$  should yield a longer semilog straight line than the conventional MDH plot. The modified MDH plot will end when  $\Delta t_{A_1D} > \Delta t_{eoa,A_1D}$  and does not assume that  $t_p + \Delta t \approx t_p$ .

The point labeled with a cross in Fig. 4.3.2 denotes the time at which the MDH slope ( $-dp_{eD}/d \ln \Delta t_{A_1D}$ ) would deviate from  $1/2$  by more than 5 percent. This time corresponds to  $\Delta t_{A_1D} = 0.004$ . The solid circles represent the time at which the semilog straight line ends on the modified MDH plot. It is clear from Fig. 4.3.2 that Eq. 4.3.9 applies for a longer period of time than Eq. 4.3.10 does.

Figure 4.3.3 compares the duration of the conventional MDH slope of 0.5 (Eq. 4.3.10) with the modified MDH slope of 0.5 predicted by Eq. 4.3.9 for a case where the well is located off center ( $\alpha_1 = 0.25, \beta_1 = 0.5$ ) of a 2 : 1 closed rectangular drainage area. The dimensionless producing time is  $t_{pA_1D} = 3$  for all results shown in Fig. 4.3.3. Both  $-dp_{eD}/d \ln \Delta t_{A_1D}$  (MDH slope) and  $-(dp_{eD}/d \ln \Delta t_{A_1D}) + 2\pi\Delta t_{A_1D}$  (modified MDH slope) are plotted as a function of the dimensionless shut-in time,  $\Delta t_{A_1D}$  in Fig. 4.3.3. The cross denotes the earliest time where the left side of Eq. 4.3.10 differs from 0.5 by more than 5 percent and the solid circle indicates the earliest time such that the left side of Eq. 4.3.9 differs from 0.5 by more than 5 percent. An inspection of the results of Fig. 4.3.3 indicates that the left hand side of Eq. 4.3.9 agrees with 0.5 longer (about a log cycle more) than the MDH slope. Note the derivative response (MDH slope) decreases and then increases due to non-symmetry of the well location in the drainage area.

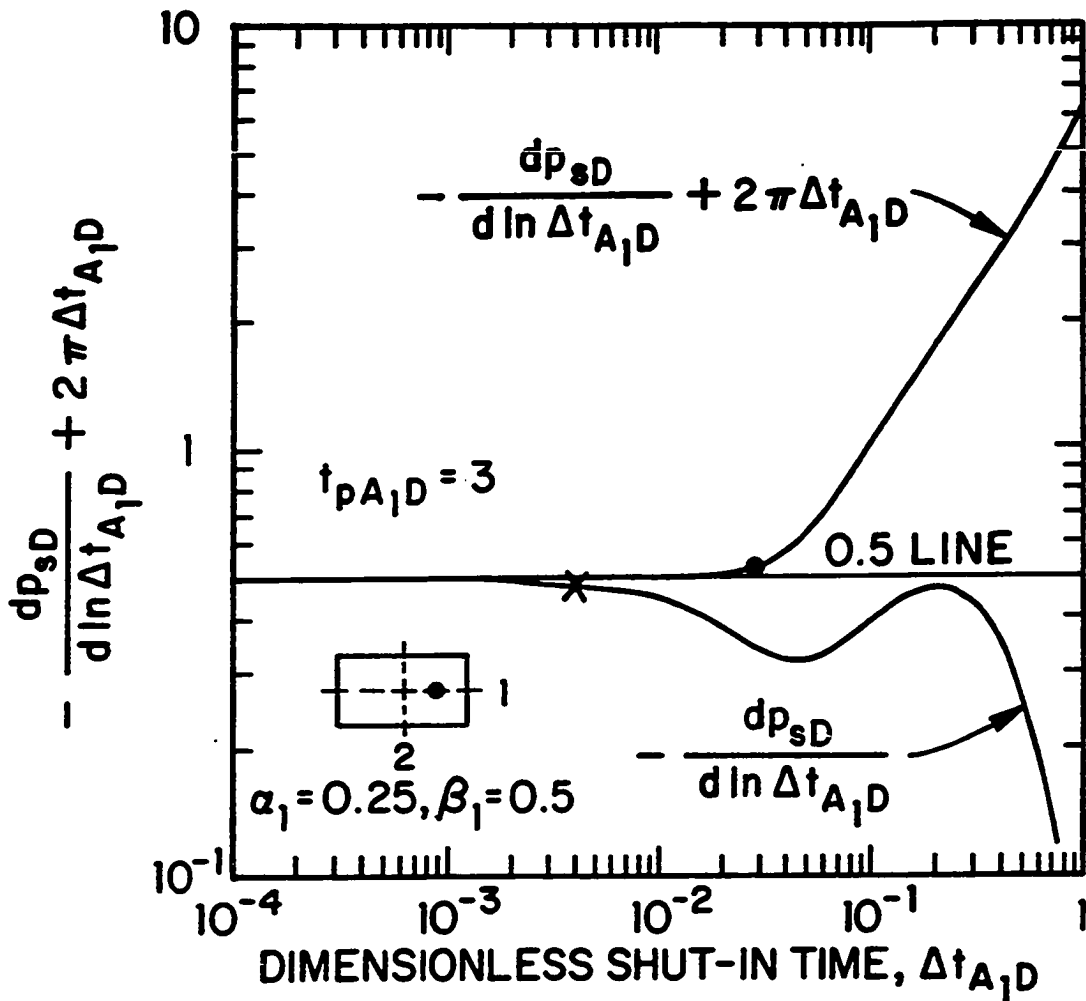


Fig. 4.3.3 - Comparison of Conventional and Modified MDH Slopes

The drainage area of the well (at the instant of shut-in) and the permeability-thickness product can be obtained from the derivative analysis procedure suggested by Eqs. 4.3.5 through 4.3.7. Rearranging Eq. 4.3.11 gives

$$\begin{aligned} p_{DMDH} &= \frac{kh[\bar{p} - p_{ws}]}{141.2q_1B\mu} = p_{sD} - 2\pi t_{pA_1D} \\ &= 2\pi\Delta t_{A_1D} - \frac{1}{2} \ln(\Delta t_{A_1D} C_{A_1}), \end{aligned} \quad (4.3.12)$$

where the first equality of Eq. 4.3.12 defines the dimensionless MDH function and the  $2\pi t_{pA_1D}$  term is given by the material balance equation; i.e.,

$$\bar{p}_D = \frac{kh[p_i - \bar{p}]}{141.2q_1B\mu} = 2\pi t_{pA_1D}. \quad (4.3.13)$$

Using Eq. 4.3.13 and the definition of  $p_{sD}$  in Eq. 4.3.12, and rearranging the resulting equation gives

$$\begin{aligned} p_{DMDH} - 2\pi\Delta t_{A_1D} &= \frac{kh[\bar{p} - p_{ws}]}{141.2q_1B\mu} - 2\pi\Delta t_{A_1D} \\ &= -\frac{1}{2} \ln(\Delta t_{A_1D} C_{A_1}). \end{aligned} \quad (4.3.14)$$

Multiplying Eq. 4.3.14 by  $141.2q_1B\mu/(kh)$  and rearranging the resulting equation, we obtain

$$\begin{aligned} p_{ws} + m_i\Delta t &= \bar{p} + m \log(\Delta t_{A_1D} C_{A_1}) \\ &= \bar{p} + m \left[ \log(\Delta t) + \log\left(\frac{m_i}{4\pi b} C_{A_1}\right) \right], \end{aligned} \quad (4.3.15)$$

where  $C_{A_1}$  is the Dietz shape factor,  $m_i$  is given by Eq. 4.3.6, and  $m$  is given by

$$m = \frac{162.6q_1B\mu}{kh} = 2.303b, \quad (4.3.16)$$

where  $b$  is given by Eq. 4.3.7.

Figure 4.3.4 is used to compare the existence and the duration of semilog straight lines predicted by Eqs. 4.3.12 and 4.3.14. Fig. 4.3.4 is a semilog plot of  $p_{DMDH}$  (conventional MDH plot) and  $p_{DMDH} - 2\pi\Delta t_{A_1D}$  (modified MDH plot) vs.  $\Delta t_{A_1D}$  for the same cases considered in Fig. 4.3.2. A cross represents the

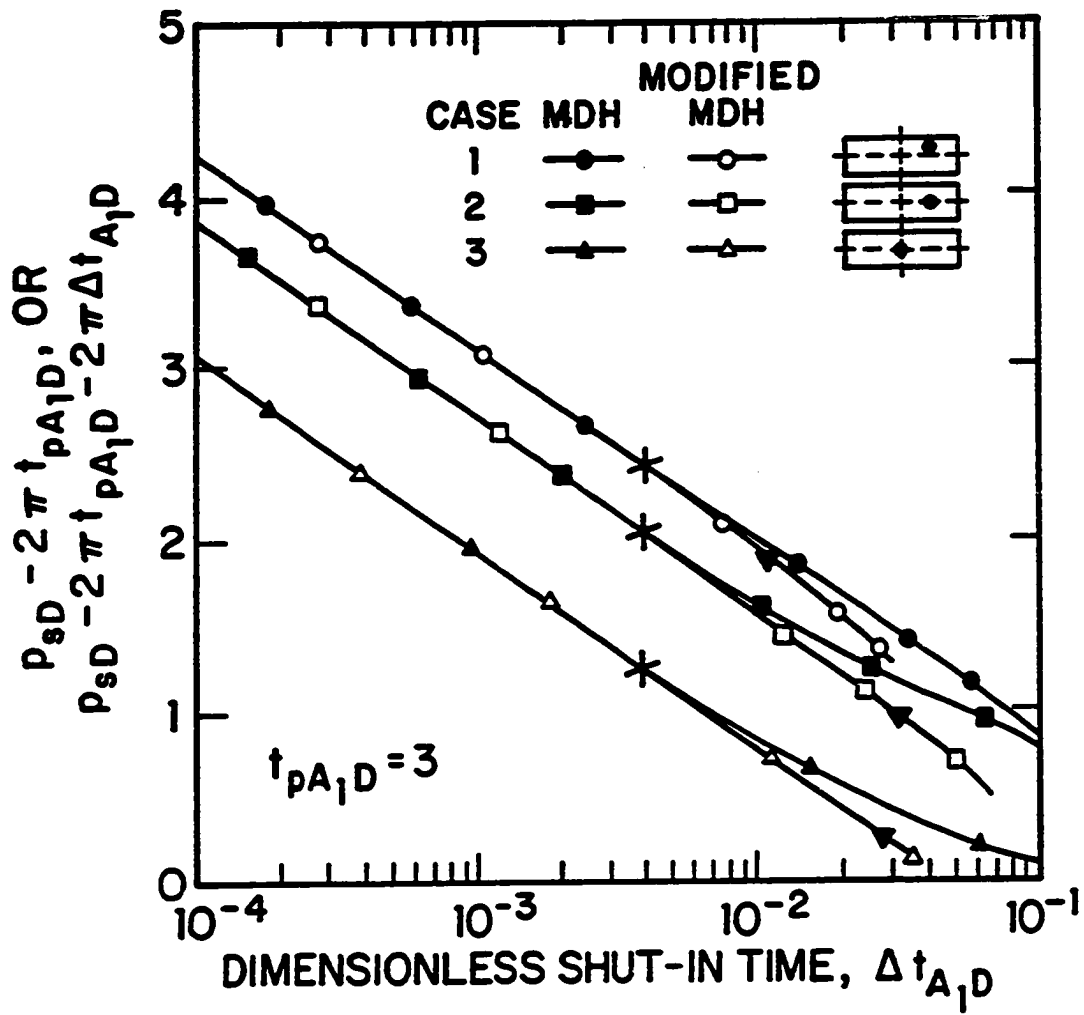


Fig. 4.3.4 - Comparison of Conventional and Modified MDH Semilog Plots



ending time of the semilog straight line on the conventional MDH plot, whereas the inverted solid triangles are used to denote the ending time of the semilog straight line on the modified MDH plots for each case. Fig. 4.3.4 shows that the modified MDH plot yields a longer semilog straight line than the conventional MDH plot does. For cases 2 and 3 the modified MDH semilog straight line is on the order of one log cycle longer.

#### 4.3.2 Analysis Procedure

Equation 4.3.15 indicates that a semilog plot of  $p_{ws} + m_i \Delta t$  vs.  $\Delta t$  will yield a semilog straight line with slope equal to  $m$ . This plot is referred to as a modified MDH plot. Note that preparation of this semilog plot requires that  $m_i$  can be determined as the slope of the straight line obtained on a Cartesian plot of  $-dp_{ws}/d \ln \Delta t$  vs.  $\Delta t$ . Codreanu's<sup>90</sup> analysis procedure is based on Eq. 4.3.15. However, his analysis is based on a trial and error procedure. In essence, his procedure requires that we guess values of  $m_i$  (or equivalently the drainage area  $A_1$ ) and then prepare semilog plots of  $p_{ws} + m_i \Delta t$  vs.  $\Delta t$  for various values of  $m_i$ . The procedure assumes that the value of  $m_i$  which gives the best (longest) semilog straight line represents the correct value of  $m_i$  or  $A_1$  (see Eq. 4.3.6). Our derivative analysis based on Eqs. 4.3.5 through 4.3.7 eliminates the trial and error procedure and gives a direct estimate of the well's drainage area as well as the flow capacity,  $kh$ . Since  $kh$  can also be determined from the slope  $m$  (see Eq. 4.3.16) of the semilog straight line obtained on a modified MDH plot suggested by Eq. 4.3.15, computation of  $kh$  from Eq. 4.3.15 provides a check for the value of  $kh$  computed from  $b$  by the obvious rearrangement of Eq. 4.3.7. We can also determine the average reservoir pressure from the semilog straight line predicted by Eq. 4.3.15. Extrapolating the semilog straight line obtained to the shut-in time of one hour and rearranging Eq. 4.3.15 gives

$$\bar{p} = (p_{ws} + m_i \Delta t)_{\Delta t=1\text{hour}} - m \left[ \log \left( \frac{m_i}{4\pi b} C_{A_1} \right) \right]. \quad (4.3.17)$$

The determination of the average pressure,  $\bar{p}$ , from Eq. 4.3.17 does not require

knowledge of the initial pressure and the producing time. It does, however, require an estimate of the Dietz shape factor,  $C_{A_1}$ . However, since  $C_{A_1}$  appears in the log term of Eq. 4.3.17, a highly accurate estimate of  $C_{A_1}$  is not required to obtain an accurate estimate of average reservoir pressure.

Results of Figs. 4.3.1 and 4.3.2 and other computational results not shown here indicate that the existence and the duration of the straight line on a Cartesian plot of  $dp_{eD}/d \ln \Delta t_{A_1D}$  vs.  $\Delta t_{A_1D}$  depend on the shape of the closed drainage region and the well's location in the closed drainage region. Therefore, it should be possible to estimate the Dietz shape factor from Table 4.3.1 which, for various well locations and drainage shapes, gives  $t_{pss,A_1D}$ , the starting time of pseudosteady-state flow, and  $\Delta t_{esa,A_1D}$ , the ending time of Cartesian straight line (Eq. 4.3.4), which is referred as the dimensionless departure time. In Table 4.3.1, these times are given for both 1% and 5% deviations, that is, the value of  $\Delta t_{esa,A_1D}$  represents the earliest shut-in time at which the left side of Eq. 4.3.9 differs from 0.5 by more than 5 percent (or more than 1 percent). The dimensionless starting times for pseudosteady-state flow,  $t_{pss,A_1D}$  are based on a criterion that the drawdown slope,  $dp_{wD}/dt_{A_1D}$ , differs from  $2\pi$  by more than 5 percent (or more than 1 percent). Shape factors are given for all the rectangular drainage/well geometries presented by Earlougher<sup>54</sup> (see Table C-1 of Ref. 54). In Table 4.3.1, the departure times are denoted by  $t_{esa,A_1D}$  and the starting times for the pseudosteady-state flow are denoted by  $t_{pss,A_1D}$ . Note that  $t_{esa,A_1D}$  also represent the time when the semilog approximation of Eq. 4.3.3 no longer applies; i.e., when  $p_{wD}(\Delta t_{A_1D})$  is no longer given by its semilog approximation. If a straight line is obtained on a Cartesian plot of  $-dp_{ws}/d \ln \Delta t$  versus  $\Delta t$  and the derivative response departs from this straight line, one first computes corresponding dimensionless values of the producing time and the departure time; i.e.,  $t_{pA_1D}$  and  $\Delta t_{esa,A_1D}$  using the values of  $m_i$  and  $b$  obtained from our derivative analysis procedure discussed earlier, and by comparing these dimensionless time values with times presented in Table 3.4.1, one can obtain an estimate of the shape factor.

If the initial pressure,  $p_i$ , is known, one can determine the average pressure

Table 4.3.1

Departure Times and Starting Times of PseudoSteady-State Flow For Various  
Closed Single-Well Drainage Shapes

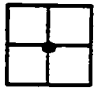
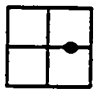
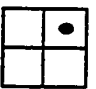
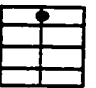



Well/Reservoir Configuration	$C_{\lambda_1}$	$t_{pss, \lambda_1 D}$		$t_{esa, \lambda_1 D}$	
		1%	5%	1%	5%
1 	30.883	0.152	0.113	0.0420	0.057
1 	12.985	0.467	0.304	0.0135	0.021
1 	4.513	0.511	0.378	0.0120	0.017
1 	3.335	0.526	0.359	0.0052	0.0034
2 	21.837	0.265	0.188	0.0240	0.0340
2 	10.837	0.285	0.209	0.0068	0.0110
2 	4.514	0.890	0.608	0.0240	0.0340

Table 4.3.1 (Cont'd)

Departure Times and Starting Times of PseudoSteady-State Flow For Various Closed Single-Well Drainage Shapes

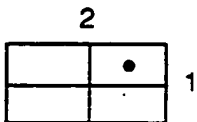
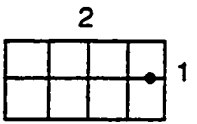
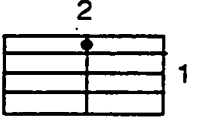
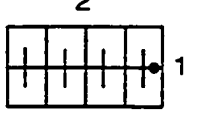
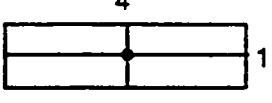
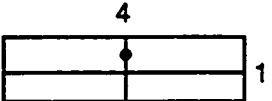

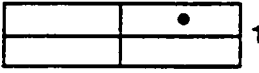

Well/Reservoir Configuration	$C_{A_1}$	$t_{psa, A_1 D}$		$t_{esa, A_1 D}$	
		1%	5%	1%	5%
	2.077	0.890	0.608	0.0068	0.011
	0.583	1.140	0.717	0.0068	0.011
	3.157	0.300	0.219	0.0017	0.0026
	0.111	1.100	0.741	0.0017	0.0026
	5.379	0.525	0.377	0.0120	0.0170
	2.699	0.525	0.377	0.0035	0.0053

Table 4.3.1 (Cont'd)

Departure Times and Starting Times of PseudoSteady-State Flow For Various Closed Single-Well Drainage Shapes

Well/Reservoir Configuration	$C_{A_1}$	$t_{pss, A_1 D}$		$t_{esa, A_1 D}$	
		1%	5%	1%	5%
<p style="text-align: center;">4</p> 	0.232	1.850	1.218	0.0120	0.0170
<p style="text-align: center;">4</p> 	0.116	1.850	1.218	0.0035	0.0053
<p style="text-align: center;">5</p> 	2.361	0.660	0.469	0.0095	0.0135

directly from the material balance equation (Eq. 4.3.13) after computing  $t_{pA_1D}$  from

$$t_{pA_1D} = \frac{m_1}{4\pi b} t_p, \quad (4.3.18)$$

where  $t_p$  is the actual producing time. After computing the average reservoir pressure, one can then obtain the shape factor,  $C_{A_1}$ , from Eq. 4.3.17.

The skin factor,  $s$ , can be obtained by extrapolating the semilog straight line (obtained on a plot  $p_{ws} + m_1 \Delta t$  vs.  $\Delta t$ ) to the shut-in time of one hour; i.e.,

$$s = 1.151 \left[ \frac{(p_{ws} + m_1 \Delta t)_{\Delta t=1 \text{ hour}} - p_{wf,s}}{m} - \log \left( \frac{k}{\phi c_t \mu r_w^2} \right) + 3.23 \right], \quad (4.3.19)$$

where  $p_{wf,s}$  is the wellbore flowing pressure at the instant of shut-in and  $m$  is the slope of a semilog straight line represented by Eq. 4.3.15. It should be noted that Eq. 4.3.19 assumes that  $t_p \geq t_{pss}$ . The derivation of Eq. 4.3.19 can be obtained from Eq. 4.3.15 and Eq. 4.3.2 (with  $t$  replaced by  $t_p$ ) by the standard procedure.

### 4.3.3 Well Located in an Infinite Multi-Well Pattern

Figure 4.2.2 shows one possible geometry for an infinite multi-well pattern. We consider a specific well (line source well) located in a multi-well pattern and this well (denoted by a cross in Fig. 4.2.2) produces at a rate  $q_1$  until time  $t_p$  and then is shut-in for a buildup test, whereas the other wells in the pattern continue to produce. Here, for simplicity, we consider the case where all wells produce with the same constant rate  $q_1$ . Our objective is to investigate the effect of interference due to continuous production of the offset wells on the buildup response of a specific well, well 1 in our notation.

As shown previously, the dimensionless shut-in pressure,  $p_{sD}$ , of a specific well (well 1) located in an infinite multi-well pattern is given by Eq. 4.2.6 where each  $p_D$  term is given by the exponential-integral solution (see Eq. 3.1.1).

For sufficiently short producing times such that the infinite sum in Eq. 4.2.6 is negligible and for sufficiently short shut-in times such that both  $p_D(t_p + \Delta t)$  and

$p_D(\Delta t)$  terms in Eq. 4.2.5 are given by their log approximations, Eq. 4.2.5 reduces to the standard Horner equation; that is,

$$p_{sD} = \frac{1}{2} \ln R_H. \quad (4.3.20)$$

Note that when Eq. 4.3.20 holds, as is well known<sup>37,85</sup>, one can only obtain the flow capacity and the skin factor by using a semilog plot of the shut-in pressure,  $p_{ws}$ , versus Horner time ratio,  $R_H$ , in the conventional manner.

Here, we assume  $t_p \geq t_{pss}$  so that the term in square brackets in Eq. 4.2.5 is given by its pseudosteady-state approximation (see Eq. 4.3.2). Replacing  $p_D(\Delta t)$  in Eq. 4.2.5 by its semilog approximation and the group of terms in square brackets by the pseudosteady-state equation, and rearranging the resulting equation, we obtain

$$p_{sD} = 2\pi(t_p + \Delta t)_{A_1D} - \frac{1}{2} \ln(\Delta t_{A_1D} C_{A_1}). \quad (4.3.21)$$

Note that Eq. 4.3.21 is the same as the buildup response equation of a single well in a closed system (see Eq. 4.3.3). The only difference between the two cases is that Eq. 4.3.21 represents the buildup solution at all shut-in times for an infinite multi-well pattern case, whereas, for the case of a single well in a closed system, Eq. 4.3.3 is valid only for shut-in times  $\Delta t_D \leq t_{esa,D}$ . However, both equations assume that  $t_p + \Delta t \geq t_{pss}$ . The difference in a physical sense can be explained as follows. After shutting-in well 1 in an infinite multi-well pattern, continued production at other wells causes well 1 to lose its drainage area. However, for a single well in a closed reservoir, the drainage area of the well is preserved because there is no interference effect due to other wells.

Taking the logarithmic derivative of Eq. 4.3.21 with respect to the dimensionless shut-in time  $\Delta t_{A_1D}$  gives

$$\frac{dp_{sD}}{d \ln \Delta t_{A_1D}} = 2\pi \Delta t_{A_1D} - \frac{1}{2}. \quad (4.3.22)$$

Equating the right hand side of Eq. 4.3.22 to zero gives

$$\Delta t_{A_1D} = \frac{1}{4\pi}. \quad (4.3.23)$$

Since it can be shown that  $d^2 p_{sD}/d\Delta t_{A_1D}^2 > 0$  at  $\Delta t_{A_1D} = 1/4\pi$ , then  $p_{sD}$  has a minimum at  $\Delta t_{A_1D} = 1/4\pi$ . Thus, interference effect on the buildup response of a specific well can be characterized by a maximum peak in the shut-in pressure,  $p_{ws}$ . This result is valid for all geometric shapes and well locations. It follows from Eqs. 4.3.13, 4.3.21 and 4.3.23 that the minimum of  $p_{sD}$  is given by

$$(p_{sD})_{min} = \bar{p}_D + \frac{1}{2} \left[ 1 - \ln \left( \frac{C_{A_1}}{4\pi} \right) \right]. \quad (4.3.24)$$

It follows from Eq. 4.3.23 that the drainage area of the well at the instant of shut-in can be obtained as

$$A_1 = \frac{3.3138 \times 10^{-9} k}{\phi c_t \mu} \Delta t_{max}. \quad (4.3.25)$$

where  $\Delta t_{max}$  denotes the time at which the shut-in pressure,  $p_{ws}$ , has a maximum ( $p_{sD}$  has a minimum).

Using the definition of  $p_{sD}$  given by Eq. 4.1.2, and replacing  $\bar{p}_D$  in Eq. 4.3.24 by its definition (see Eq. 4.3.13) and solving the resulting equation for the average pressure,  $\bar{p}$ , gives

$$\bar{p} = (p_{ws})_{max} + b \left[ 1 - \ln \left( \frac{C_{A_1}}{4\pi} \right) \right], \quad (4.3.26)$$

where  $b$  is given by Eq. 4.3.7 and  $(p_{ws})_{max}$  represents the maximum shut-in pressure which occurs at the value of  $\Delta t$  ( $\Delta t_{max}$ ) corresponding to  $\Delta t_{A_1D} = 1/4\pi$ .

Figure 4.3.5 shows a semilog plot of the dimensionless shut-in pressure,  $p_{sD}$ , versus  $\Delta t_{A_1D}$  for well off center ( $\alpha_1 = 0.25, \beta_1 = 0.75$ ) in a 2 : 1 closed rectangular drainage region which is created due to production of nearby producing wells in the infinite multi-well pattern. In Fig. 4.3.5, we consider three values of producing times,  $t_{pA_1D}$ , 0.6, 2.0, 5.0. For this system, the producing time to reach to pseudosteady-state flow period prior to shut-in is  $t_{pss,A_1D} = 0.61$  (see Table 4.3.1). It is apparent from the results of Fig. 4.3.5 that, for a given value of producing time, the dimensionless pressure decreases to a minimum and then increases as the shut-in time increases, and the minimum dimensionless shut-in pressure occurs at a shut-in time,  $\Delta t_{A_1D} = 1/(4\pi)$  as expected from our analytical observations. Computations



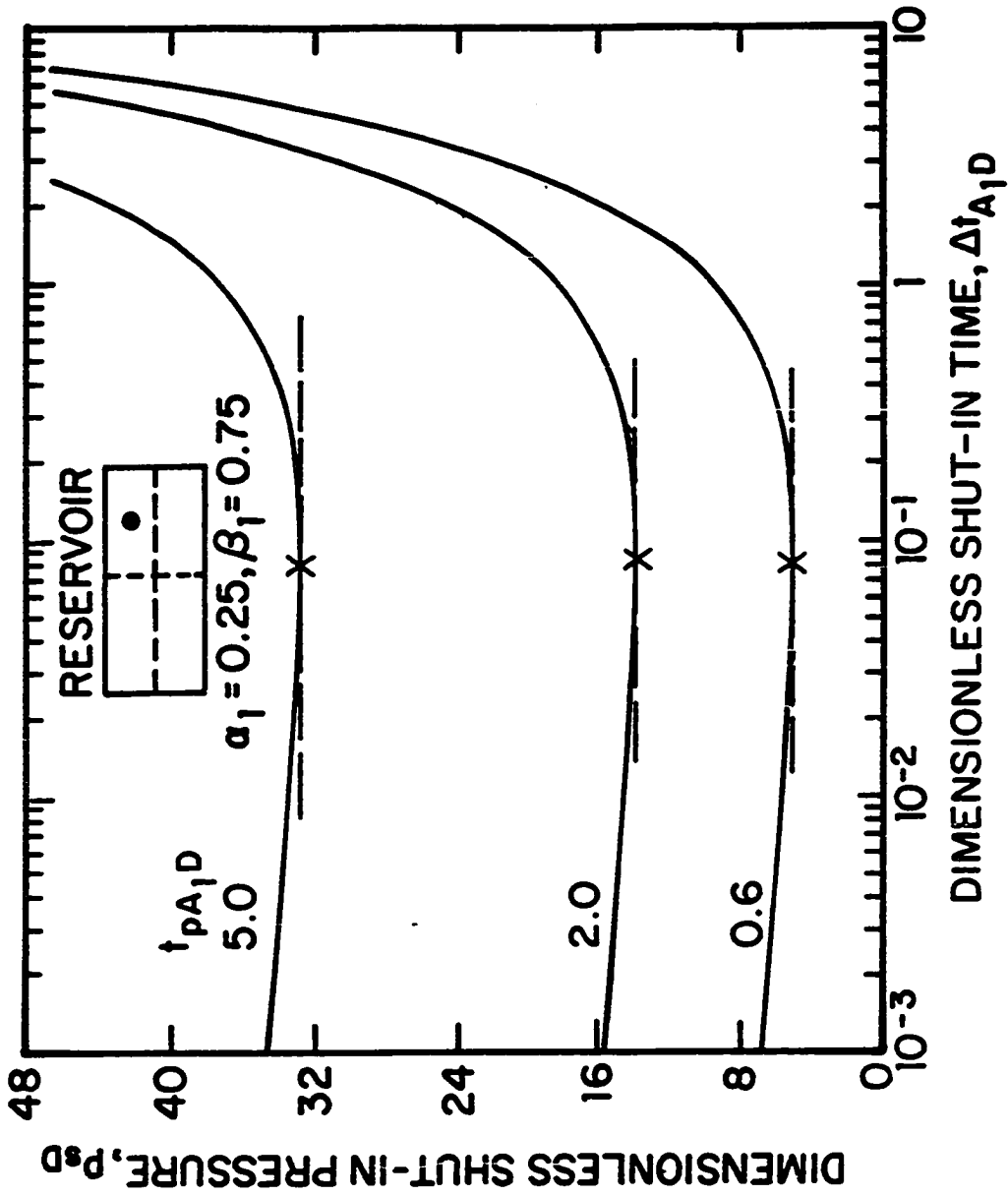


Fig. 4.3.5 - Effect of Producing Time on Pressure Response; Single Well in an Infinite Multi-Well Pattern

also indicate that the the minimum of  $p_{sD}$  is given by Eq. 4.3.24 for a given value of the producing time. For example, the value of  $(p_{sD})_{min} \approx 14$  for  $t_{A_1D} = 2$  in Fig. 4.3.5, whereas Eq. 4.3.24 predicts  $(p_{sD})_{min} = 13.97$  for this geometry and the producing time. They are in excellent agreement. Thus, the results of Fig. 4.3.5 and Eqs. 4.3.25 and 4.3.26 suggest that when the interference effect of the offset wells influences the buildup response of a specific well in an infinite multi-well pattern, the drainage area and the average reservoir pressure in this drainage area can be determined from the maximum shut-in pressure and from the time at which it occurs. As shown previously, the maximum of the shut-in pressure will occur if there are interference effects on the buildup response from the nearby producing wells. For shut-in times such that  $\Delta t_{A_1D} \leq 1/(4\pi)$ , Eqs. 4.3.21 and 4.3.22 hold. Hence, the analysis procedure suggested in the previous subsection (single well in a closed reservoir) to obtain the well's drainage area, the permeability-thickness product, the average reservoir pressure and the skin factor applies for a specific well located in an infinite multi-well pattern.

The determination of average pressure in the well's drainage area at the instant of shut-in from Eq. 4.3.26 requires knowledge of the shape factor  $C_{A_1}$  and the parameter  $b$  given by Eq. 4.3.7. Recall that  $b$  can be easily determined from the intercept of a Cartesian plot of  $-dp_{ws}/d \ln \Delta t$  vs.  $\Delta t$ . Note that only a rough estimate of the shape factor,  $C_{A_1}$ , is necessary for determining the average pressure from Eq. 4.3.26.

The above conclusion that the average pressure,  $\bar{p}$ , is related to the maximum shut-in pressure,  $(p_{ws})_{max}$ , has been observed empirically by Stein<sup>92</sup> for planar fractures in a multi-well pattern. His claim that  $(p_{ws})_{max}$  is close to  $\bar{p}$  was based purely on the numerical observations. He did not present Eq. 4.3.26 or derive the time at which the maximum of  $p_{ws}$  occurs. As can be seen from Eq. 4.3.24, the minimum of the dimensionless shut-in pressure,  $(p_{sD})_{min}$ , is always greater than the dimensionless average pressure,  $\bar{p}_D$ , for all geometric shapes (or, equivalently  $(p_{ws})_{max} < \bar{p}$ ; see Eq. 4.3.26) and the difference between the dimensionless average pressure,  $\bar{p}_D$ , and the dimensionless minimum shut-in pressure,  $(p_{sD})_{min}$ , increases

as the shape factor,  $C_{A_1}$ , decreases.

#### 4.3.4 Multi-Well System in a Closed Bounded Reservoir

In this subsection, we examine the buildup response of a specific well located in a system of producing wells completed in a closed bounded reservoir. Well 1 is the specific well where the buildup test is conducted, while the other wells continue to produce; see Fig. 4.2.1. For simplicity, we restrict our attention to the case where all wells start to produce at the same time. Our objective is to investigate the interference effects of nearby producing wells on the buildup response of well 1.

As shown previously, the dimensionless shut-in pressure,  $p_{sD}$ , at a well in a system of producing wells contained in a closed bounded reservoir is given by Eq. 4.2.3 where each  $p_D$  term is given by the exponential-integral solution (see Eq. 3.1.1). We again assume  $t_p \geq t_{pss}$  so that pseudosteady-state flow exists at the instant of shut-in. When pseudosteady-state flow exists, each of the  $m$  wells in the closed reservoir of Fig. 4.2.1 has its own drainage area. The drainage area of well 1 is  $A_1$  which is related to the total reservoir area<sup>35</sup> by

$$\frac{A_1}{A_t} = \frac{q_1}{\sum_{k=1}^m q_k}. \quad (4.3.27)$$

During pseudosteady-state flow, well 1 behaves as if it were a single well in the closed reservoir with drainage area  $A_1$ . Thus, the sum of all  $p_D(t_p + \Delta t)_D$  terms in Eq. 4.2.3 is equal to the pseudosteady-state equation for well 1 in its drainage area,  $A_1$ , so Eq. 4.2.3 can be reduced to

$$p_{sD} = 2\pi (t_p + \Delta t)_{A_1 D} + \frac{1}{2} \ln\left(\frac{4A_1}{e^{\gamma} C_{A_1} r_w^2}\right) - \frac{1}{2} \left[ -\text{Ei}\left[-\frac{1}{4\Delta t_D}\right] - \sum_{j=2}^{\infty} \text{Ei}\left[-\frac{r_{jD}^2}{4\Delta t_D}\right] \right], \quad (4.3.28)$$

where  $r_{jD}$  represents the radial distance (based on wellbore radius) between well 1 and its image well  $j$ ; i.e.,  $r_{jD} = r_j/r_w$ , where  $r_j$  is the distance between well 1 and well  $j$ . Note that in deriving Eq. 4.3.28 from Eq. 4.2.3, we have also replaced each

$p_D(\Delta t_D)$  term in Eq. 4.2.3 by the appropriate exponential-integral solution given by Eq. 3.1.1.

For early shut-in times ( $\Delta t_D \geq 25$ ), the first exponential integral term in Eq. 4.3.28 is given by its semilog approximation (see Eq. 4.3.1), then Eq. 4.3.28 can be written as

$$p_{sD} = 2\pi (t_p + \Delta t)_{A_1D} - \frac{1}{2} \ln(\Delta t_{A_1D} C_{A_1}) + \frac{1}{2} \sum_{j=2}^{\infty} \text{Ei} \left[ -\frac{a_{jD}^2}{4\Delta t_{A_1D}} \right], \quad (4.3.29)$$

where  $a_{jD}$  is the dimensionless radial distance (based on well 1's drainage area,  $A_1$ ) between well 1 and its image well  $j$ ; i.e.,

$$a_{jD} = \frac{r_j}{\sqrt{A_1}} = \frac{r_w}{\sqrt{A_1}} r_{jD}. \quad (4.3.30)$$

Except for the appearance of the infinite sum of the exponential terms, Eq. 4.3.30 is identical to the basic equation derived for a single well in a closed system (Eq. 4.3.3) and for a well in an infinite multi-well pattern (Eq. 4.3.21). The infinite sum of exponential-integral functions is due to the existence of physical (no flow) boundaries of the closed bounded reservoir.

Differentiating Eq. 4.3.29 with respect to natural log of  $\Delta t_{A_1D}$  gives

$$\frac{dp_{sD}}{d \ln \Delta t_{A_1D}} = 2\pi \Delta t_{A_1D} - \frac{1}{2} \left[ 1 + \sum_{j=2}^{\infty} \exp\left(-\frac{a_{jD}^2}{4\Delta t_{A_1D}}\right) \right]. \quad (4.3.31)$$

Since Eq. 4.3.31 holds for all shut-in times provided that  $t_p + \Delta t \geq t_{pss}$ , equating Eq. 4.3.31 to zero gives

$$\Delta t_{A_1D} = \frac{1}{4\pi} \left[ 1 + \sum_{j=2}^{\infty} \exp\left(-\frac{a_{jD}^2}{4\Delta t_{A_1D}}\right) \right]. \quad (4.3.32)$$

Note that the minimum of  $p_{sD}$  occurs at the shut-in time such that  $\Delta t_{A_1D} \geq 1/(4\pi)$ .

Here, we investigate the influence of infinite sum in Eq. 4.3.31 on the derivative response. We define  $2d$  to be the distance between the buildup surveyed well (well 1) and its nearest image well. Thus,  $d$  is the distance to the nearest reservoir

boundary. If in Eq. 4.3.31, the exponential term due to well 1's nearest image well is negligible compared to one, then from a physical viewpoint, it is reasonable to expect that the infinite sum of exponentials is negligible compared to one. If this is the case, then Eqs. 4.3.29 and 4.3.31 can be approximated by Eqs. 4.3.3 and 4.3.4, respectively. In this case, pressure buildup data obtained at well 1 can be analyzed by application of Eqs. 4.3.5-4.3.7, 4.3.17 and 4.3.19. Moreover, if the buildup test is run long enough to observe  $(p_{ws})_{max}$ , Eqs. 4.3.25 and 4.3.26 also can be applied to estimate the well's drainage area,  $A_1$ , and the average pressure in the well's drainage area at the instant of shut-in provided that the summation term in Eq. 4.3.32 is negligible at the time at which  $(p_{ws})_{max}$  occurs.

Retaining only the exponential term due to the nearest image well of the buildup surveyed well and neglecting the other exponential terms in the infinite sum in Eq. 4.3.31 gives the following approximation;

$$\frac{dp_{sD}}{d \ln \Delta t_{A_1D}} = 2\pi \Delta t_{A_1D} - \frac{1}{2} [1 + \delta], \quad (4.3.33)$$

where

$$\delta = \exp\left(-\frac{d_{A_1}^2}{\Delta t_{A_1D}}\right). \quad (4.3.34)$$

In Eq. 4.3.34,  $d_{A_1}$  is the dimensionless distance (based on the drainage area of the buildup surveyed well) between the buildup surveyed well and the nearest physical (no flow) boundary of the reservoir; i.e.,  $d_{A_1} = d/\sqrt{A_1}$ .

Equation 4.3.33 can be approximated by  $2\pi \Delta t_{A_1D} - 1/2$ , which is the derivative response of a buildup surveyed well in an infinite multi-well pattern, provided that  $\delta$  is negligible compared to the other terms on the right side of Eq. 4.3.33. If we assume that the effect of  $\delta$  in Eq. 4.3.33 is negligible whenever  $\delta \leq 0.0189$ , it follows from Eq. 4.3.34 that the effect of  $\delta$  is negligible for

$$\Delta t_{A_1D} < \frac{1}{4} d_{A_1}^2 = \frac{1}{4} \frac{A_t}{A_1} d_{A_t}^2, \quad (4.3.35)$$

where  $A_t$  represents the total reservoir area.

When  $\Delta t_{A_1D} > (1/4)d_{A_1}^2$  (or  $\Delta t_{A_tD} > (1/4)d_{A_t}^2$ ), the derivative response given by Eq. 4.3.33 will deviate from the derivative response of a well in an infinite multi-well pattern (see Eq. 4.3.22). If well 1 is the only well in a closed bounded reservoir

so that  $A_t = A_1$ , then the condition on the dimensionless shut-in time given by Eq. 4.3.35 should represent the ending time of the semilog approximation of  $p_{wD}(\Delta t_D)$  and hence the ending time of Eq. 4.3.3 for a well in a closed drainage area.

If we want Eq. 4.3.33 to be approximately equal to the derivative response of a buildup surveyed well in an infinite multi-well pattern (see Eq. 4.3.22) at a shut-in time  $\Delta t_{A_1D} = 1/(4\pi)$ , then the preceding discussion indicates that we must have  $1/(4\pi) < (1/4)d_{A_1}^2$ , which is equivalent to

$$d_{A_1} = \sqrt{\frac{A_t}{A_1}} d_{A_t} > \frac{1}{\sqrt{\pi}}. \quad (4.3.36)$$

When Eq. 4.3.36 holds, the derivative response given by Eq. 4.3.33 is approximately equal to the one for a well in an infinite multi-well pattern for shut-in times such that  $\Delta t_{A_1D} \leq 1/(4\pi)$ , and hence the minimum of the dimensionless shut-in pressure occurs at a dimensionless shut-in time approximately equal to  $1/(4\pi)$ . Thus,  $A_1$  and  $\bar{p}$ , respectively, can be computed from Eqs. 4.3.25 and 4.3.26. If the inequality of Eq. 4.3.36 is not satisfied, then the derivative response given approximately by Eq. 4.3.33 (or, exactly, by Eq. 4.3.31) will depart from the derivative response given by Eq. 4.3.22 at a shut-in time,  $\Delta t_{A_1D} = (1/4)d_{A_1}^2 < 1/(4\pi)$ , and hence, the minimum of the dimensionless shut-in pressure will occur at a shut-in time,  $\Delta t_{A_1D} > 1/(4\pi)$ . In this case, if the value of  $\Delta t_{A_1D}$  at which  $(p_{eD})_{min}$  occurs is much greater than  $1/4\pi (\approx 0.08)$ , Eqs. 4.3.25 and 4.3.26 will not yield accurate estimates of  $A_1$  and  $\bar{p}$ .

If all physical no-flow boundaries of the closed drainage area influence the buildup response at the well of interest (well 1), that is, "pseudosteady-state" flow prevails during buildup, from a semi-theoretical viewpoint, one expects that the term in braces, that is, the term containing exponential-integral functions, in Eq. 4.3.28 can be approximated by the following equation:

$$-\frac{1}{2} \left[ -\text{Ei} \left[ -\frac{1}{4\Delta t_D} \right] - \sum_{j=2}^{\infty} \text{Ei} \left[ -\frac{r_{jD}^2}{4\Delta t_D} \right] \right] = 2\pi \Delta t_{A_tD} + \frac{1}{2} \ln \left( \frac{4A_t}{e^{\gamma} C_{A_t} r_w^2} \right), \quad (4.3.37)$$

because of the fact that left hand side of Eq. 4.3.37 represents the pressure drops due to well 1 and its image wells necessary to keep no-flow boundaries for the whole

reservoir drainage area. Extensive numerical computations indicate that indeed the relation given by Eq. 4.3.37 is true. Using the relation given by Eq. 4.3.37 in Eq. 4.3.28, it can be easily shown that the buildup pressure change,  $p_{sD}$ , and its logarithmic derivative,  $dp_{sD}/d \ln \Delta t_{A_1D}$ , are given, respectively, by the following equations:

$$p_{sD} = 2\pi \left( t_{pA_1D} + \Delta t_{A_1D} \left[ 1 - \frac{A_1}{A_t} \right] \right) + \frac{1}{2} \ln \left( \frac{A_1 C_{A_1}}{A_t C_{A_t}} \right), \quad (4.3.38)$$

and

$$\begin{aligned} \frac{dp_{sD}}{d \ln \Delta t_{A_1D}} &= 2\pi \Delta t_{A_1D} \left( 1 - \frac{A_1}{A_t} \right) \\ &= 2\pi \Delta t_{A_1D} \left( 1 - \frac{q_1}{\sum_{k=1}^m q_k} \right). \end{aligned} \quad (4.3.39)$$

In Eq. 4.3.38,  $C_{A_t}$  represents the shape factor of well 1 with respect to its location in total closed reservoir drainage area, whereas  $C_{A_1}$  represents the shape factor of well 1 with respect to its drainage area existed at the moment of shut-in created by the production of other wells in the reservoir. It should be noted that Eqs. 4.3.38 and 4.3.39 apply only for shut-in times such that  $\Delta t \geq t_{pss}$ . Moreover, it should be noted that if there is only a single well in the reservoir drainage area, that is,  $A_1 = A_t$  and  $C_{A_1} = C_{A_t}$ , then Eqs. 4.3.38 and 4.3.39, respectively, reduce to the corresponding equations for a single well in a closed drainage area; i.e.,

$$p_{sD} = 2\pi t_{pA_1D}, \quad (4.3.40)$$

and

$$\frac{dp_{sD}}{d \ln \Delta t_{A_1D}} = 0. \quad (4.3.41)$$

Although Eqs. 4.3.38 and 4.3.39 are not of practical interest because they may require extremely long shut-in times to apply, they are very useful for verifying numerical simulators.

Figure 4.3.6 shows a two-well system in a closed square reservoir. In Fig. 4.3.6, the buildup surveyed well, which is shown by a cross, is located at the center of

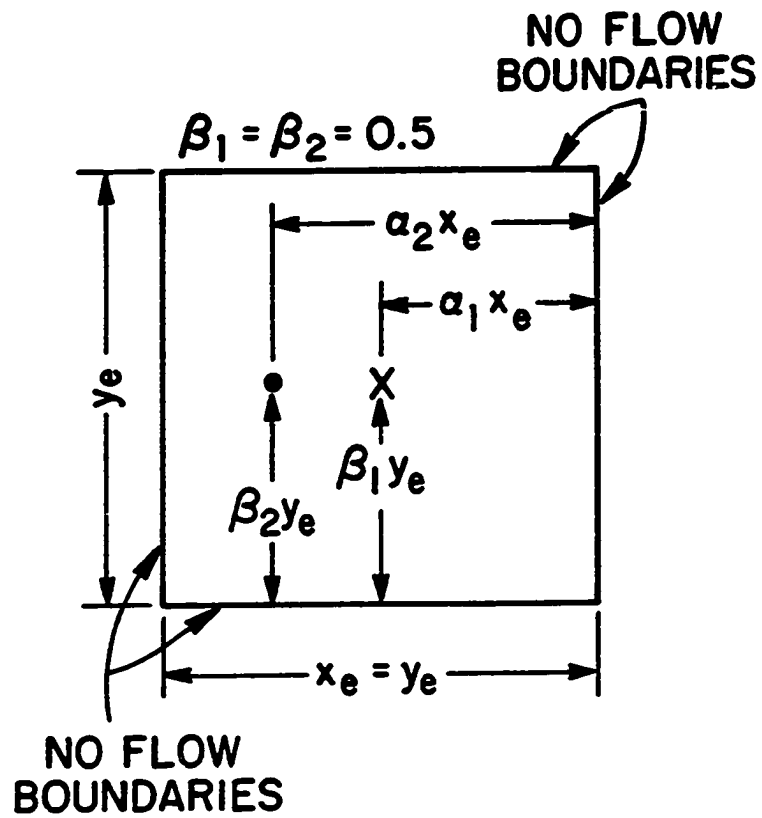


Fig. 4.3.6 - Two-Well System; Closed Square Reservoir



the closed square; i.e.,  $\alpha_1 = \beta_1 = 0.5$ , whereas the producing well (well 2), which is shown by a solid dot, is located at  $\alpha_2 = 0.75, \beta_2 = 0.5$ . Fig. 4.3.7 shows results obtained for the reservoir/well geometry of Fig. 4.3.6 for various ratios of  $q_1/q_2$ . The dimensionless producing time is  $t_{pA_1D} = 2$  for all results shown in Fig. 4.3.7. The top solid curve represents Eq. 4.3.22. Note that the derivative response for all cases correlates with Eq. 4.3.22 for shut-in times such that  $\Delta t_{A_1D} \leq 0.05$ . Thus, the analysis procedure based on Eqs. 4.3.5–4.3.7, 4.3.17 and 4.3.19 can be applied to analyze corresponding field data. For all cases,  $dp_{sD}/d \ln \Delta t_{A_1D} = 0$  at  $\Delta t_{A_1D} \approx 1/4\pi = 0.08$ . Thus,  $A_1$  and  $\bar{p}$  could also be determined from the maximum shut-in pressure and the shut-in time at which it occurs; see Eqs. 4.3.25 and 4.3.26.

Table 4.3.2 presents the multi-well cases considered to generate results shown in Figs. 4.3.8 and 4.3.9. Table 4.3.2 shows reservoir/well geometry of a closed square drainage region for six different cases. In Table 4.3.2, a solid dot is used to represent the producing well, whereas a cross mark is used to represent the buildup surveyed well. Here we assume that all wells produce at a same rate; that is,  $q_1/q_i = 1$  for  $i = 2, \dots, m$  where  $m$  denotes the total number of wells in the closed reservoir drainage area. Fig. 4.3.8 shows a semilog plot of the dimensionless shut-in pressure,  $p_{sD}$ , versus the shut-in time,  $\Delta t_{A_1D}$ , for the six different reservoir/well geometries of Table 4.3.2. Similarly, Fig. 4.3.9 presents a semilog plot of  $dp_{sD}/d \ln \Delta t_{A_1D}$  versus  $\Delta t_{A_1D}$ . For comparison purposes, the solid curve through open circular data points which represents the derivative response of a well located in an infinite multi-well pattern; i.e., Eq. 4.3.22, is also shown in Fig. 4.3.9. In Fig. 4.3.9, a solid circular data point denotes the time at which the derivative response deviates from the derivative response of a well in an infinite multi-well pattern. It is apparent that increasing the number of producing wells while keeping the position of the buildup surveyed well in the closed drainage area fixed makes the derivative response of buildup surveyed well agree longer with the derivative response for a well in an infinite multi-well pattern (shown by the solid curve through circular data points) and makes the derivative response become zero at a shut-in time closer to  $1/(4\pi)$ .

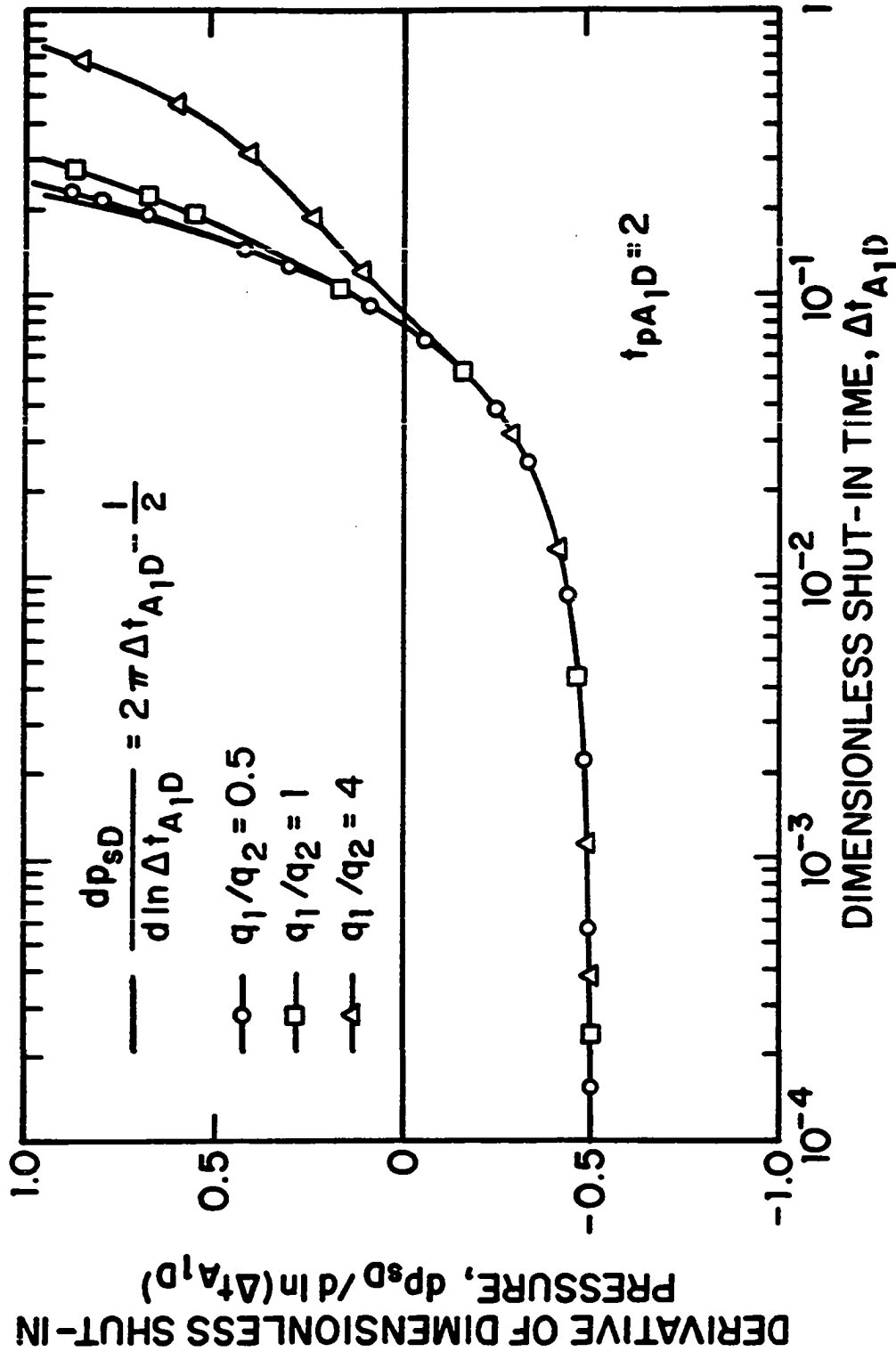
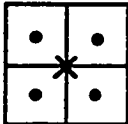
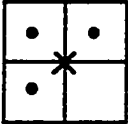
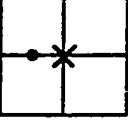
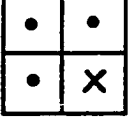
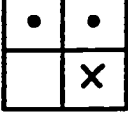
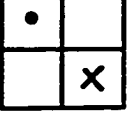


Fig. 4.3.7 - Influence of Individual Well Rates on Derivative Response

Table 4.3.2

Well/Reservoir Cases Considered for Results of  
Figs. 4.3.8 and 4.3.9

Well/Reservoir Configuration	Case	Number of Wells	$(\alpha_1, \beta_1)$
	1	5	0.5, 0.5
	2	4	0.5, 0.5
	3	2	0.5, 0.5
	4	4	0.25, 0.25
	5	3	0.25, 0.25
	6	2	0.25, 0.25

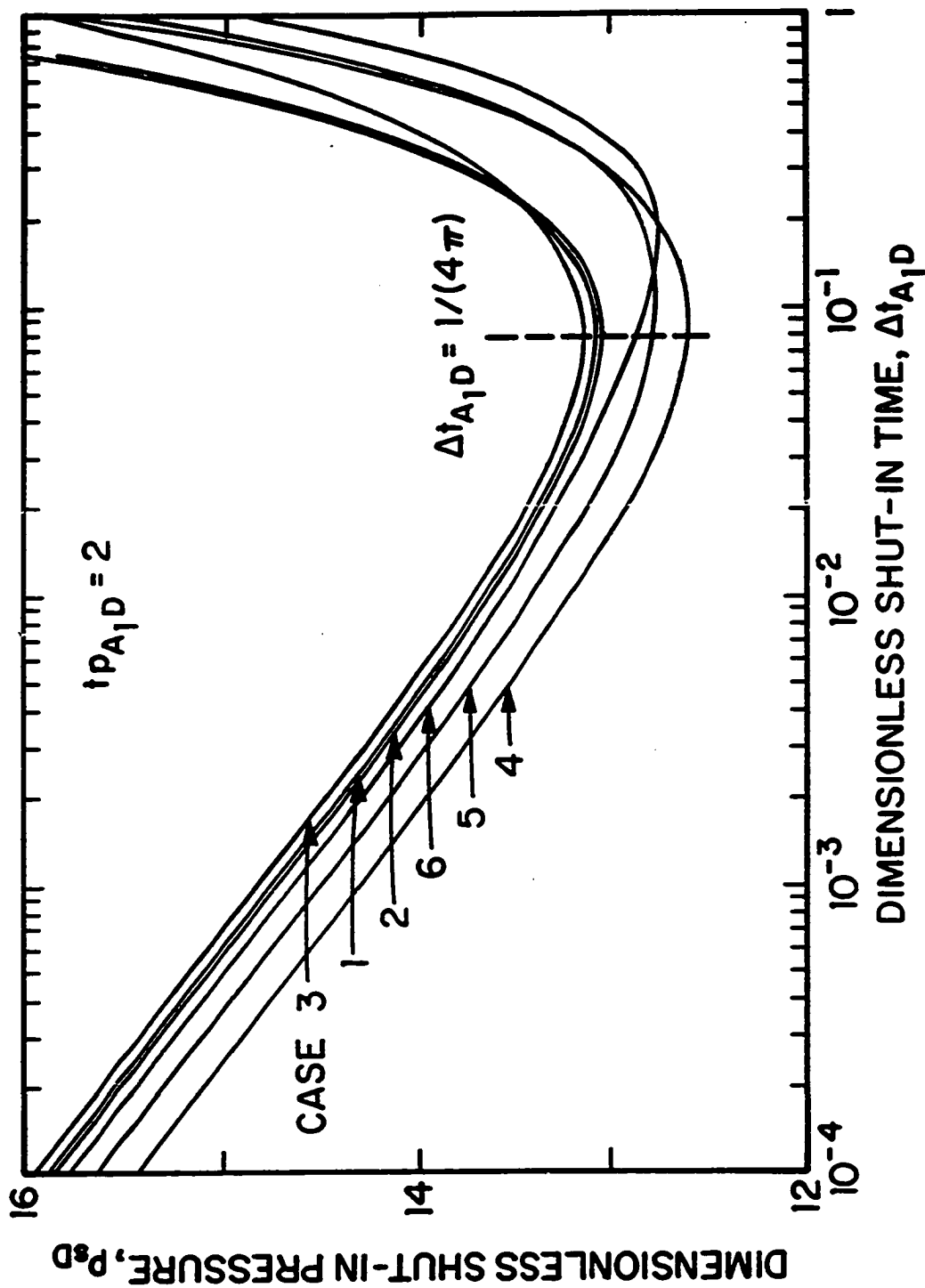


Fig. 4.3.8 - Effect of Number of Wells and Well Location on Pressure Response

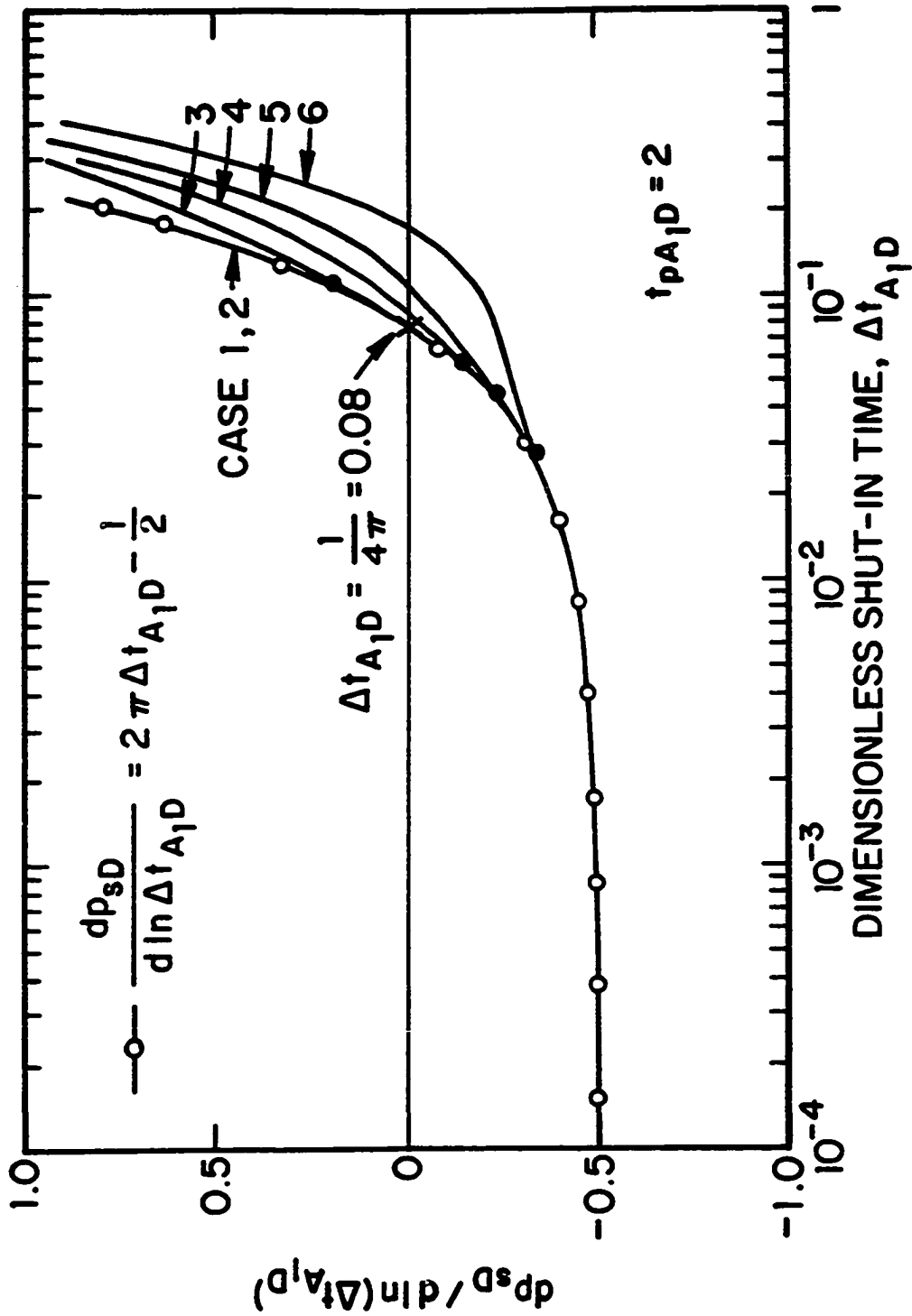


Fig. 4.3.9 - Effect of Number of Wells and Well Location on Derivative Response

For cases 1, 2 and 3, the derivative response,  $dp_{eD}/d \ln \Delta t_{A_1D}$ , departs from Eq. 4.3.22 at a shut-in time  $\Delta t_{A_1D} > 1/(4\pi)$  and  $dp_{eD}/d \ln \Delta t_{A_1D} = 0$ , that is, the minimum of shut-in pressure  $p_{eD}$  occurs (see Fig. 4.3.8) at  $\Delta t_{A_1D} = 1/(4\pi)$  because of the fact that the nearest distance between the buildup surveyed well and the physical boundary of the reservoir,  $d_{A_t}$ , is same and equals 0.5, and this value of  $d_{A_t}$  satisfies the criterion given by Eq. 4.3.36. However, for cases 4, 5, and 6, the derivative response departs from Eq. 4.3.22 at a shut-in time  $\Delta t_{A_1D} < 1/(4\pi)$  and the derivative become equal to zero (or, the shut-in pressure is minimum; see Fig. 4.3.8) (due to interference effect of nearby producing wells) at a shut-in time  $\Delta t_{A_1D} > 1/(4\pi)$ . This is not surprising because of the fact that for cases 4, 5 and 6,  $d_{A_t} = 0.25$  and this value of  $d_{A_t}$  does not satisfy the criterion given by Eq. 4.3.36.

Figure 4.3.10 shows the geometry of a two-well ( $q_1 = q_2$ ) system in a 2 : 1 closed rectangle. The location of the producing well ( $\alpha_2 = 0.75, \beta_2 = 0.5$ ) is fixed in the rectangle whereas the location of the buildup surveyed well denoted by a cross is fixed only in the  $y$ -direction; i.e.,  $\beta_1 = 0.5$  and  $\alpha_1$  is the parameter of interest. Fig. 4.3.11 is a semilog plot of  $dp_{eD}/d \ln \Delta t_{A_1D}$  versus  $\Delta t_{A_1D}$  as a function of the parameter  $\alpha_1$ . It is apparent that the shorter the distance between the buildup surveyed well and the right hand boundary of the rectangle, the earlier the derivative response deviates from the derivative response of a well in an infinite multi-well pattern (solid curve through circular data points in Fig. 4.3.11). It should be noted that for cases 1 and 2 where  $\alpha_1 = 0.5$  and  $\alpha_1 = 0.25$ , respectively, the derivative response departs from the infinite multi-well derivative response at the same shut-in time. This is not surprising because, in both cases, the nearest distance between the buildup surveyed well and the physical boundary of the reservoir is the same; i.e.,  $d_{A_t} = 0.25\sqrt{2}$ . For cases 3 and 4, the  $dp_{eD}/d \ln \Delta t_{A_1D} = 0$  at shut-in times such that  $\Delta t_{A_1D} \gg 1/4\pi$ ; i.e., the minimum of  $p_{eD}$  (maximum of  $p_{ws}$ ) occurs at a shut-in time significantly different than  $\Delta t_{A_1D} = 1/4\pi$ . Thus, Eqs. 4.3.25 and 4.3.26 cannot be applied to compute well's drainage area,  $A_1$ , and the average pressure in the well's drainage area,  $\bar{p}$ . However, in all cases, Eq. 4.3.22 applies for sufficiently small values of  $\Delta t_{A_1D}$ . Thus, Eqs. 4.3.5-4.3.7, 4.3.17 and 4.3.19 can be

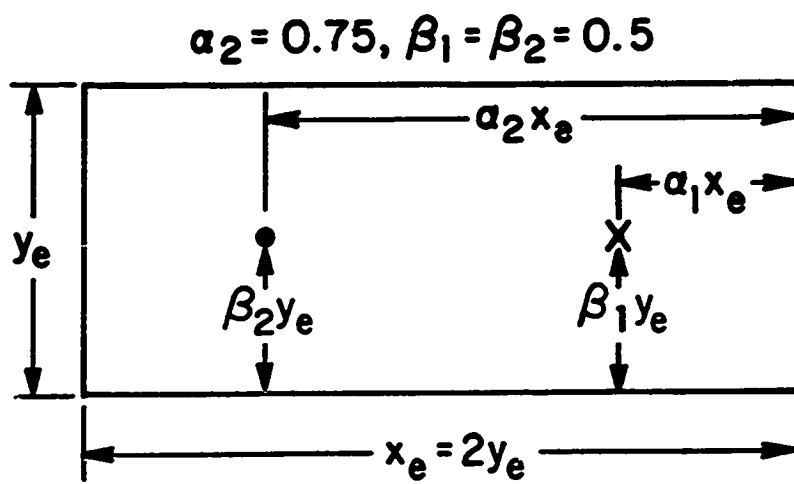


Fig. 4.3.10 - Two-Well System; Closed 2 : 1 Rectangular Reservoir

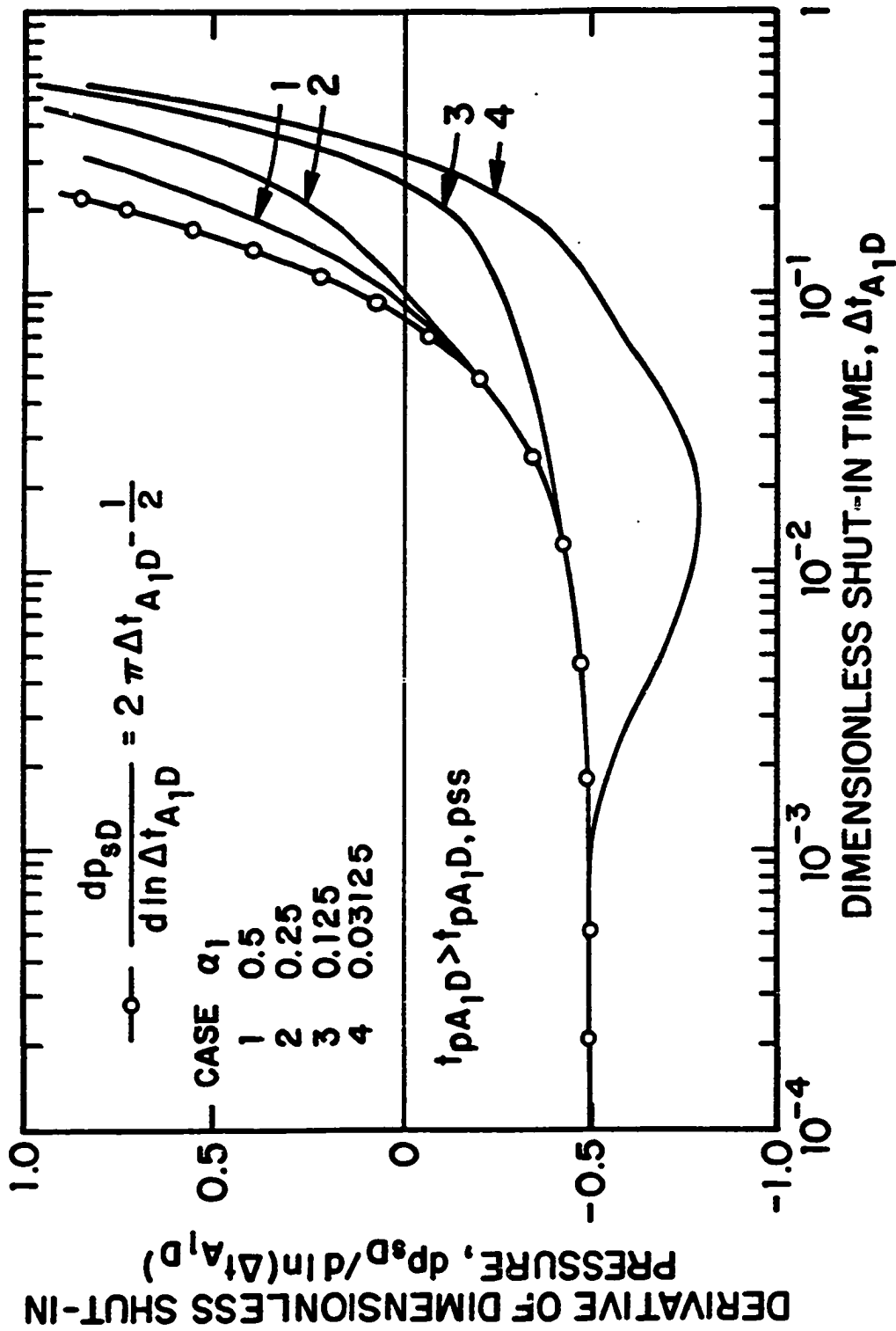


Fig. 4.3.11 - Effect of Parameter  $\alpha_1$  on Derivative Response



applied.

#### 4.4 Fractured Wells

Here, the basic results obtained for unfractured wells are extended to fractured wells. Only infinite-conductivity and uniform-flux fractures are considered in this section. Relevant equations to determine well's drainage area and well/reservoir parameters for finite-conductivity vertically fractured wells are presented in Appendix F. In the following, we investigate the buildup response at a fractured well located in a closed one-well rectangular reservoir and in an infinite multi-well pattern of fractured wells.

##### 4.4.1 Single Well in a Closed Reservoir

For a single well in a closed drainage area, the dimensionless buildup pressure,  $p_{sD}$ , is given by Eq. 4.2.5. If  $t_p + \Delta t \geq t_{pss}$ , the first term in Eq. 4.2.5 is given by its pseudosteady-state equation and Eq. 4.2.5 can be written as

$$p_{sD} = 2\pi(t_p + \Delta t)_{A_1D} + \frac{1}{2} \ln\left(\frac{4A_1}{e^{\gamma} C_{f_1} L_{x_f}^2}\right) - p_{wD}(\Delta t_{x_fD}), \quad (4.4.1)$$

where  $C_{f_1}$  is the shape factor of a fractured well<sup>19</sup>.

For early shut-in times such that  $p_{wD}(\Delta t_{x_fD})$  term is given by its well known linear flow approximation<sup>17</sup> (also see Eq. 3.1.30), using the linear flow approximation for  $p_{wD}(\Delta t_{x_fD})$  and the relation between  $\Delta t_{x_fD}$  and  $\Delta t_{A_1D}$  (Eq. 4.1.7), Eq. 4.4.1 can be rewritten as

$$p_{sD} = 2\pi(t_p + \Delta t)_{A_1D} + \frac{1}{2} \ln\left(\frac{4A_1}{e^{\gamma} C_{f_1} L_{x_f}^2}\right) - \sqrt{\pi \Delta t_{A_1D} \frac{A_1}{L_{x_f}^2}}. \quad (4.4.2)$$

Taking the derivative of Eq. 4.4.2 with respect to  $\sqrt{\Delta t_{A_1D}}$ , we obtain

$$\frac{dp_{sD}}{d\sqrt{\Delta t_{A_1D}}} = 4\pi\sqrt{\Delta t_{A_1D}} - \sqrt{\pi \frac{A_1}{L_{x_f}^2}}. \quad (4.4.3)$$

Using the definitions of  $p_{sD}$  and  $\Delta t_{A_1D}$  in Eq. 4.4.3 and rearranging the resulting equation gives

$$-\frac{dp_{ws}}{d\sqrt{\Delta t}} = m_{cl}\sqrt{\Delta t} - b_{cl}, \quad (4.4.4)$$

where  $m_{cl}$  and  $b_{cl}$  are given, respectively, by

$$m_{cl} = 2m_i = \frac{0.46790q_1B}{\phi c_t h A_1}, \quad (4.4.5)$$

and

$$b_{cl} = \frac{4.0641q_1B}{h} \sqrt{\frac{\mu}{\phi c_t k L_{x_f}^2}}. \quad (4.4.6)$$

Here,  $m_i$  is given by Eq. 4.3.6.

Equation 4.4.4 suggests that during linear flow period, a Cartesian plot of  $-dp_{ws}/d\sqrt{\Delta t}$  vs.  $\sqrt{\Delta t}$  will yield a straight line with a slope,  $m_{cl}$ , and an intercept,  $b_{cl}$ . From the slope,  $m_{cl}$ , the drainage area of the well at the instant of shut-in can be obtained as

$$A_1 = \frac{0.46790q_1B}{\phi c_t h m_{cl}}, \quad (4.4.7)$$

and from the intercept at  $\Delta t = 0$ ,  $b_{cl}$ , the product of permeability-fracture half-length,  $kL_{x_f}^2$ , can be obtained as

$$kL_{x_f}^2 = \left( \frac{4.0641q_1B}{hb_{cl}} \right)^2 \frac{\mu}{\phi c_t}. \quad (4.4.8)$$

When  $p_{wD}(\Delta t_{x_fD})$  term in Eq. 4.4.1 is given by its well known pseudoradial flow approximation<sup>12</sup> (also see Eq. 3.1.33), Eq. 4.4.1 becomes

$$p_{sD} = 2\pi(t_p + \Delta t)_{A_1D} + \frac{1}{2} \ln \left( \frac{4A_1}{e^{\gamma} C_{f_1} L_{x_f}^2} \right) - \frac{1}{2} (\ln \Delta t_{x_fD} + c), \quad (4.4.9)$$

where  $c = 2.80907$  for an uniform-flux fracture and  $c = 2.200$  for an infinite-conductivity fracture. Note that when Eq. 4.4.9 holds, we can use the effective wellbore radius concept. By using the effective wellbore radius, we can show that Eq. 4.4.9 can be written as

$$p_{sD} = 2\pi(t_p + \Delta t)_{A_1D} - \frac{1}{2} \ln(\Delta t_{A_1D} C_{A_1}), \quad (4.4.10)$$

where  $C_{A_1}$  is the shape factor of an unfractured well for the reservoir/well geometry under consideration.

Differentiating Eq. 4.4.10 with respect to  $\ln \Delta t_{A_1D}$  gives

$$\frac{dp_{sD}}{d \ln \Delta t_{A_1D}} = 2\pi \Delta t_{A_1D} - \frac{1}{2}. \quad (4.4.11)$$

Equations 4.4.10 and 4.4.11 are exactly the same as the equations for a single unfractured well (see Eqs. 4.3.3 and 4.3.4) in a closed drainage area. If Eqs. 4.4.10 and 4.4.11 hold, the analysis procedure (see Eqs. 4.3.5-4.3.7, 4.3.17 and 4.3.19) described for a single unfractured well in a closed drainage area can be used to obtain the well's drainage area, the permeability-thickness product, the average reservoir pressure and the skin factor,  $s_f$ , due to the existence of the fracture. The fracture half-length then can be estimated from

$$L_{x_f} = nr_w e^{-s_f}, \quad (4.4.12)$$

where  $n = c$  for a uniform-flux fracture and  $n = 2$  for an infinite-conductivity fracture.

When the  $p_{wD}(\Delta t_{x_fD})$  term in Eq. 4.4.1 is given by the pseudosteady-state approximation, that is, when  $\Delta t \geq t_{pss}$ , Eq. 4.2.5 simplifies to  $p_{sD} = 2\pi t_{pA_1D}$  so that

$$\frac{dp_{sD}}{d \ln \Delta t_{A_1D}} = 0. \quad (4.4.13)$$

Equation 4.4.3 can be rewritten as

$$\frac{dp_{sD}}{d\sqrt{\Delta t_{A_1D}}} + \sqrt{\pi \frac{A_1}{L_{x_f}^2}} = 4\pi \sqrt{\Delta t_{A_1D}}. \quad (4.4.14)$$

Eq. 4.4.14 suggests that a log-log plot of  $(dp_{sD}/d\sqrt{\Delta t_{A_1D}}) + \sqrt{(\pi A_1)/L_{x_f}^2}$  vs.  $\sqrt{\Delta t_{A_1D}}$  will yield a straight line with a slope equal to unity.

Figures 4.4.1 and 4.4.2, respectively, are used to illustrate the validity of Eq. 4.4.14 (or equivalently of Eq. 4.4.3) for an uniform-flux and an infinite-conductivity fractured well at the center of a closed square.  $L_{x_f}/\sqrt{A_1}$  is the parameter of interest in Figs. 4.4.1 and 4.4.2 and varies from 0.025 to 0.5. The dimensionless producing time  $t_{pA_1D} = 1$  was used to generate all results shown in Figs. 4.4.1 and 4.4.2.

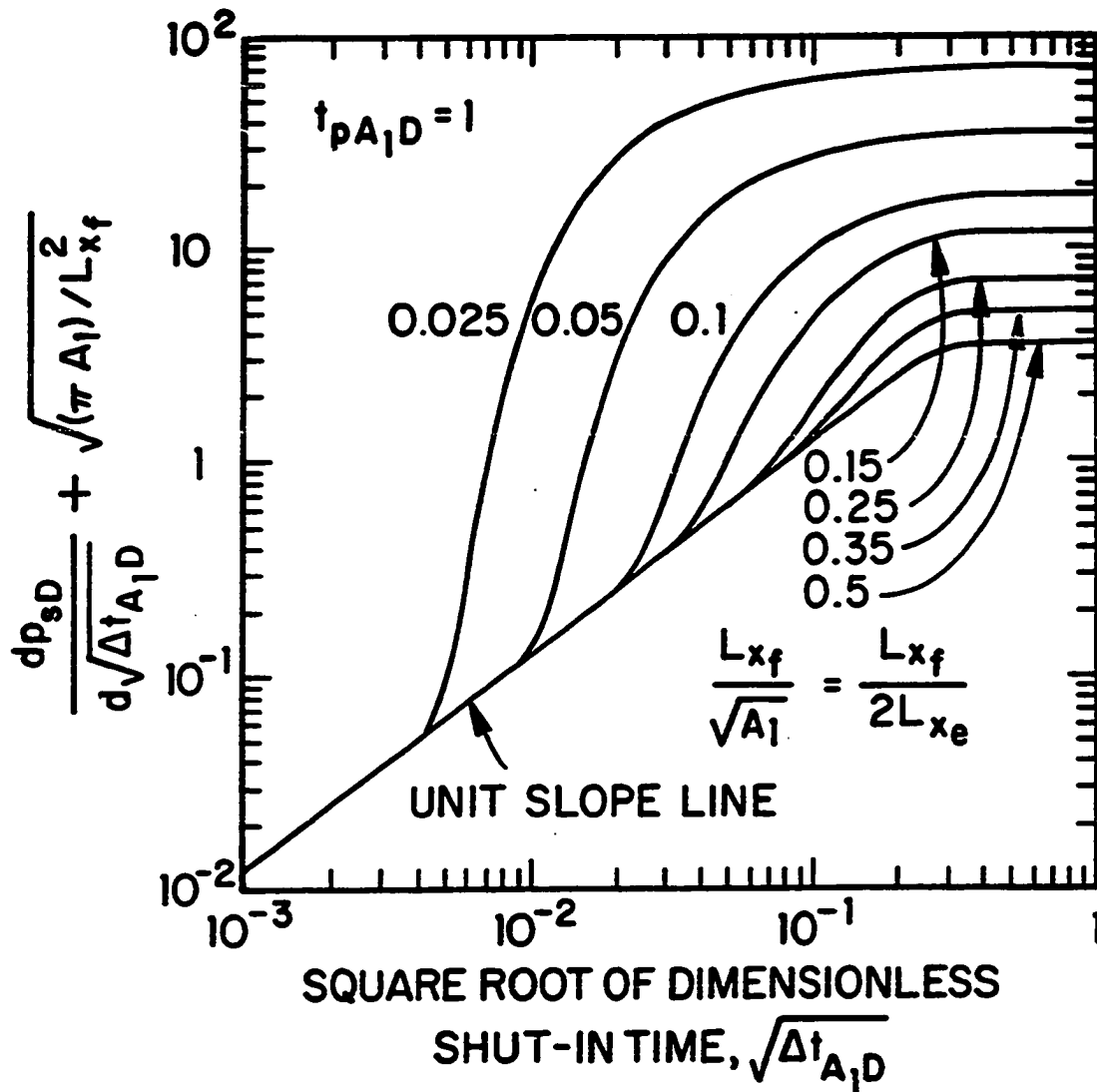


Fig. 4.4.1 - Effect of Penetration Ratio,  $L_{xf}/\sqrt{A_1}$ , on Derivative Response; Uniform-Flux Fracture

..

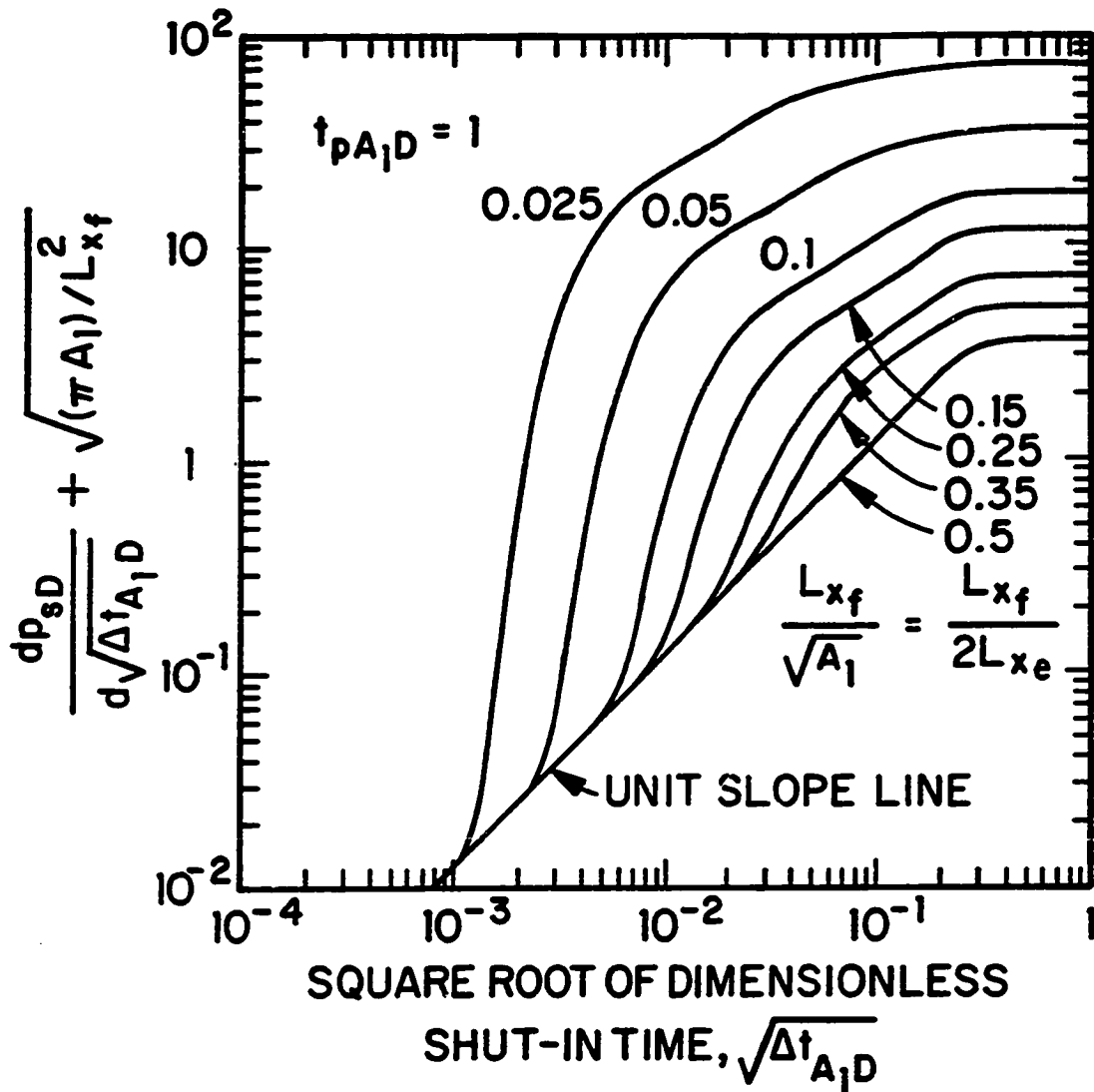


Fig. 4.4.2 - Effect of Penetration Ratio,  $L_{xf}/\sqrt{A_1}$ , on Derivative Response; Infinite-Conductivity Fracture

Figs. 4.4.1 and 4.4.2 show log-log plots of  $(dp_{eD}/d\sqrt{\Delta t_{A_1D}}) + \sqrt{(\pi A_1)/L_{x_f}^2}$  vs.  $\sqrt{\Delta t_{A_1D}}$ .

Figure 4.4.1 shows that when the fracture half-length increases; i.e.,  $L_{x_f}/\sqrt{A_1}$  increases toward the value of 0.5, the duration of Eq. 4.4.14 increases substantially. This is the expected result based on the work of Ref. 17. The bottom curve of Figs. 4.4.1 and 4.4.2, respectively, represent the uniform-flux and infinite-conductivity solutions for the case where  $L_{x_f}/\sqrt{A_1} = 0.5$ , i.e.,  $L_{x_f}/L_{x_e} = 1$ . Fig. 4.4.1 also shows that when  $\sqrt{\Delta t_{A_1D}} \geq \sqrt{t_{pss,A_1D}} = 0.32$ , Eq. 4.4.13 holds. When Eq. 4.4.13 holds, the left hand side of Eq. 4.4.13 is equal to  $\sqrt{(\pi A_1)/L_{x_f}^2}$ .

Figure 4.4.2 shows the duration of Eq. 4.4.14 for an infinite-conductivity fractured well at the center of a closed square for the same values of  $L_{x_f}/\sqrt{A_1}$  ( $= L_{x_f}/2L_{x_e}$ ) considered in Fig. 4.4.1. Comparing the results of Fig. 4.4.2 with the results of Fig. 4.4.1, it is apparent that for each value of  $L_{x_f}/\sqrt{A_1} < 0.5$ , the duration of the unit slope line for an infinite-conductivity fracture is shorter than the duration of the unit slope line for a uniform-flux fracture. Again, this is the expected result based on the results of Ref. 17.

Equations 4.4.3, 4.4.11 and 4.4.13, respectively, can be rearranged to obtain the following equations:

$$-\frac{dp_{eD}}{d \ln \Delta t_{A_1D}} + 2\pi \Delta t_{A_1D} = \frac{1}{2} \sqrt{\pi \Delta t_{A_1D} \frac{A_1}{L_{x_f}^2}}, \quad (4.4.15)$$

$$-\frac{dp_{eD}}{d \ln \Delta t_{A_1D}} + 2\pi \Delta t_{A_1D} = \frac{1}{2}, \quad (4.4.16)$$

and

$$-\frac{dp_{eD}}{d \ln \Delta t_{A_1D}} + 2\pi \Delta t_{A_1D} = 2\pi \Delta t_{A_1D}. \quad (4.4.17)$$

Eq. 4.4.15 applies during linear flow, i.e., when  $p_{wD}(\Delta t_{x_fD}) = \sqrt{\pi \Delta t_{x_fD}}$ . Eq. 4.4.16 applies during pseudoradial flow, i.e.,  $p_{wD}(\Delta t_{x_fD})$  is given by its pseudoradial flow approximation. Eq. 4.4.17 applies when  $p_{wD}(\Delta t_{x_fD})$  is given by its pseudosteady-state flow approximation, i.e., when  $\Delta t_{A_1D} \geq t_{pss,A_1D}$ .

When Eq. 4.4.15 holds, a log-log plot of the left hand side of Eq. 4.4.15 vs.  $\Delta t_{A_1D}$  will yield a 1/2 slope line. When Eq. 4.4.16 holds, the left hand side of Eq.

4.4.16 will be equal to 0.5 and the log-log plot will show a horizontal line. Finally, when Eq. 4.4.17 holds, a log=log plot of the left hand side of Eq. 4.4.17 versus  $\Delta t_{A_1D}$  will be a unit slope line.

Figure 4.4.3 presents results for an uniform-flux fractured well located at the center of a closed square drainage region. In Fig. 4.4.3,  $L_{x_f}/\sqrt{A_1} = L_{x_f}/(2L_{x_e})$  is the parameter of interest. Fig. 4.4.3 represents a log-log plot  $-(dp_{sD}/d \ln \Delta t_{A_1D}) + 2\pi \Delta t_{A_1D}$  vs.  $\Delta t_{A_1D}$ . It is clear from the results of Fig. 4.4.3 that; (i) for all values of  $L_{x_f}/\sqrt{A_1}$ , the 1/2 slope line (linear flow) exists. The points labeled with a solid circle represent the time at which linear flow ends. Note that the duration of the 1/2 slope line (linear flow period) decreases as  $L_{x_f}/\sqrt{A_1}$  decreases. The duration of linear flow is the longest for a value of  $L_{x_f}/\sqrt{A_1} = 0.5$  which corresponds to  $L_{x_e}/L_{x_f} = 1$ ; (ii) the 0.5 line (pseudo-radial flow) exists when  $L_{x_f}/\sqrt{A_1} \leq 0.1$  which corresponds to  $L_{x_e}/L_{x_f} \geq 5$ . Note that the duration of 0.5 line is almost a half log cycle for a value of  $L_{x_e}/L_{x_f} = 5$ ; and (iii) the unit slope line (pseudosteady-state) starts at  $\Delta t_{A_1D} = t_{pss,A_1D} = 0.11$  for all values of  $L_{x_f}/\sqrt{A_1}$ . The point labeled with a cross denotes the beginning of pseudosteady-state flow; i.e.,  $\Delta t_{A_1D} = 0.11$ .

#### 4.4.2 Analysis Procedure

Here, we present procedures for analyzing buildup data at a well located at the center of an uniform-flux or infinite-conductivity vertical fracture. The possible analysis procedures depend on the flow regimes exhibited by the data.

As noted previously, when the buildup data exhibits linear flow, Eq. 4.4.4 applies and the well's drainage area,  $A_1$ , and  $kL_{x_f}^2$  can be computed from Eqs. 4.4.7 and 4.4.8, respectively. Eq. 4.4.2 can be rearranged to obtain the following equation:

$$p_{sD} - 2\pi(t_p + \Delta t)_{A_1D} = \frac{1}{2} \ln \left( \frac{4A_1}{e^\gamma C_{f1} L_{x_f}^2} \right) - \sqrt{\pi \Delta t_{A_1D} \frac{A_1}{L_{x_f}^2}}. \quad (4.4.18)$$

Using the left hand side of material balance equation (Eq. 4.3.13) in Eq. 4.4.18, and rewriting the resulting equation in the dimensional form gives

$$p_{ws} + \frac{m_{cl}}{2} \Delta t = \bar{p} + b \ln \left( \frac{L_{x_f}^2 C_{f1} e^\gamma}{4A_1} \right) + b_{cl} \sqrt{\Delta t}, \quad (4.4.19)$$

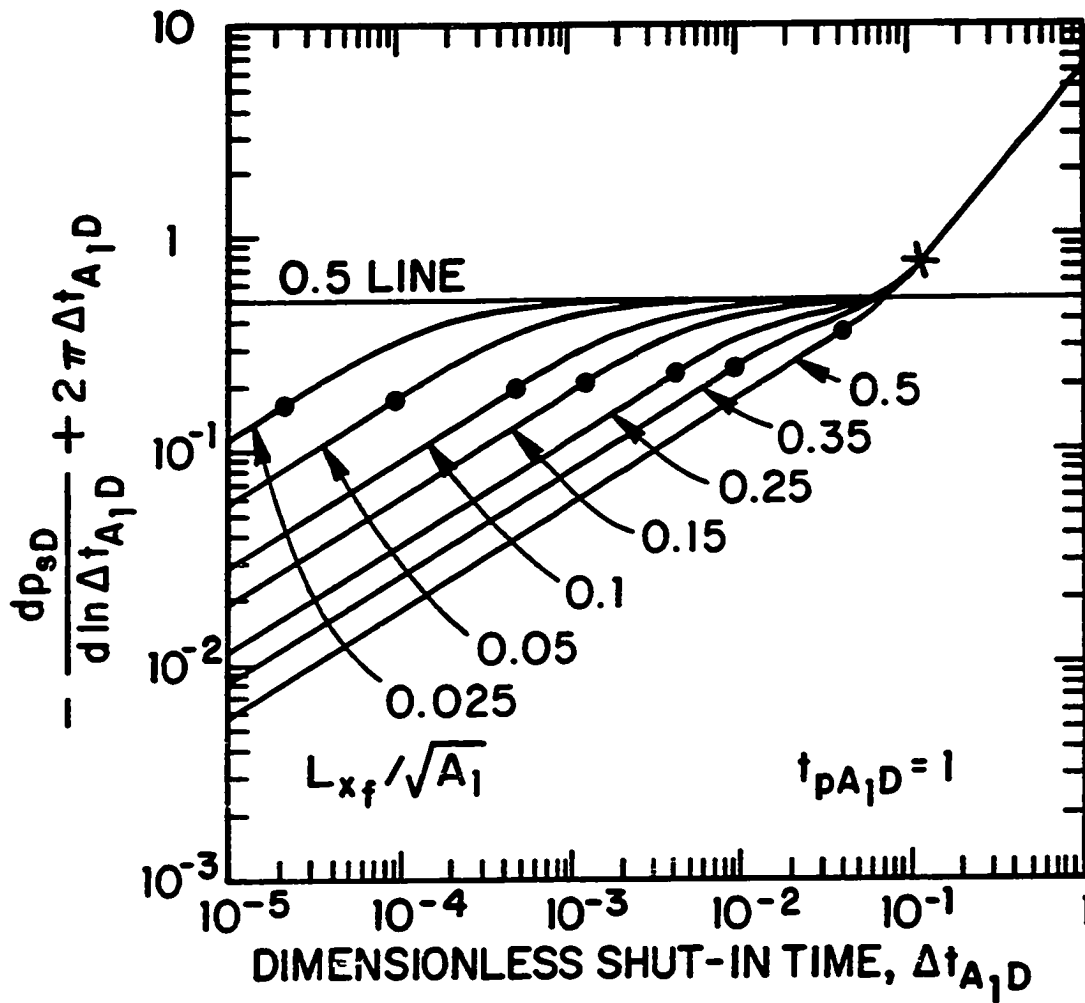


Fig. 4.4.3 - Log-Log Plot of Derivative Response Versus Shut-in Time; Uniform-Flux Fracture



where  $p_{ws}$  is the shut-in pressure,  $\bar{p}$  is the average pressure at the instant of shut-in, and  $A_1 (= 4L_x L_y)$  is the drainage area of the well at the instant of shut-in. In Eq. 4.4.19,  $b$  is given by Eq. 4.3.7, and  $b_{cd}$  is given by Eq. 4.4.6. During linear flow,  $m_{cd}$  can be computed from the  $\sqrt{\Delta t}$  plot suggested by Eq. 4.4.4. To determine the average reservoir pressure at the instant of shut-in, we extrapolate the straight line obtained in a Cartesian plot of  $p_{ws} + \frac{m_{cd}}{2} \Delta t$  vs.  $\Delta t$  to  $\Delta t = 0$ . From Eqs. 4.4.19 and 4.3.7, it follows that the intercept at  $\Delta t = 0$  is given by

$$\left( p_{ws} + \frac{m_{cd}}{2} \Delta t \right)_{\Delta t=0} = \bar{p} + \frac{141.2q_1 B \mu}{2kh} \ln \left[ \frac{L_{x_f}^2 C_{f_1} e^{\gamma}}{4A_1} \right]. \quad (4.4.20)$$

The determination of the average pressure from Eq. 4.4.20 requires the knowledge of three parameters, the permeability,  $k$ , the fracture half-length,  $L_{x_f}$ , and, the shape factor,  $C_{f_1}$ . If the buildup data also exhibits pseudo-radial flow, then the drainage area and the permeability-thickness product can be obtained from a Cartesian plot of  $-dp_{ws}/d \ln \Delta t$  vs.  $\Delta t$ ; see Eqs. 4.3.5 through 4.3.7. Using this estimate of  $k$  and the value of  $kL_{x_f}^2$  obtained from the linear flow analysis, (see Eqs. 4.4.4 through 4.4.8), one can estimate the fracture half-length,  $L_{x_f}$ . In this case, the determination of average reservoir pressure from Eq. 4.4.20 requires only that the shape factor is known.

If  $A_1$  can be determined by the derivative analysis of linear flow (Eqs. 4.4.4 through 4.4.8) or pseudo-radial flow (Eqs. 4.3.5 through 4.3.7), then a modified pressure change plot can be used to improve the reliability of type curve matching. The theoretical basis for this modified type curve matching procedure follows. From standard superposition results, it is well known that

$$\bar{p}_{s,D} = \frac{kh [p_{ws} - p_{wf,s}]}{141.2q_1 B \mu} = -p_{wD} [(t_p + \Delta t)_{x_f,D}] + p_{wD} (t_{px_f,D}) + p_{wD} (\Delta t_{x_f,D}). \quad (4.4.21)$$

If  $t_p \geq t_{pss}$ , then  $p_{wD} [(t_p + \Delta t)_{x_f,D}]$  and  $p_{wD} (t_{px_f,D})$  are both given by the appropriate pseudosteady-state approximations and Eq. 4.4.21 reduces to

$$\bar{p}_{s,D} = \frac{kh [p_{ws} - p_{wf,s}]}{141.2q_1 B \mu} = -2\pi \Delta t_{A_1,D} + p_{wD} (\Delta t_{x_f,D}). \quad (4.4.22)$$

Defining  $\Delta p_c$  by

$$\Delta p_c = p_{ws} - p_{wf,s} + m_i \Delta t, \quad (4.4.23)$$

Eq. 4.4.22 can be written as

$$p_{csD} = \frac{kh\Delta p_c}{141.2q_1 B\mu} = p_{wD}(\Delta t_{x_fD}), \quad (4.4.24)$$

where the first equality of Eq. 4.4.24 serves to define  $p_{csD}$ . Since  $p_{wD}(\Delta t_{x_fD})$  represents the drawdown solution, Eq. 4.4.24 indicates that a log-log plot of  $\Delta p_c$  vs.  $\Delta t$  can be type curve matched with the appropriate drawdown type curves for all values of shut-in time.

Figure 4.4.4 illustrates the validity of this type curve matching procedure based on the  $p_{csD}$  plot. In Fig. 4.4.4, solid curves represent the infinite-conductivity drawdown solution for a well at the center of a closed square reservoir for the specified values of  $L_{x_f}/\sqrt{A_1}$ . The modified buildup pressure change,  $p_{csD}$ , for the case  $L_{x_f}/\sqrt{A_1} = 0.25$  is plotted versus  $\Delta t_{x_fD}$  (circular data points). In addition, the buildup pressure change,  $\bar{p}_{sD}$ , for the same penetration ratio is graphed versus both Agarwal's equivalent time<sup>48</sup>,  $\Delta t_{ex_fD}$  (square data points) and  $\Delta t_{x_fD}$  (triangular data points). The dimensionless producing time  $t_{pA_1D} = 1$  was used to generate the buildup pressure changes;  $p_{csD}$  and  $\bar{p}_{sD}$ . As can be seen from Fig. 4.4.4, the  $p_{csD}$  vs.  $\Delta t_{x_fD}$  plot correlates with the drawdown solution for all shut-in times as expected from Eq. 4.4.24. On the other hand, the  $\bar{p}_{sD}$  vs.  $\Delta t_{ex_fD}$ , and the  $\bar{p}_{sD}$  vs.  $\Delta t_{x_fD}$  plots fail to correlate with drawdown solution except at early shut-in times. Before closing this subsection, we note that one can also use the drawdown type curves based on pressure/pressure-derivative presented in Chapter III to analyze the entire buildup data provided the buildup data is plotted as  $\Delta p_c/(2\Delta p'_c)$  versus  $\Delta t$  where  $\Delta p_c$  is given by Eq. 4.4.23 and  $\Delta p'_c$  denotes the derivative of  $\Delta p_c$  with respect to  $\ln \Delta t$ .

#### 4.4.3 Well Located in an Infinite Multi-Well Pattern

In this subsection, we investigate the buildup response of a planar (uniform-flux or infinite-conductivity) fractured well located in an infinite multi-well pattern.

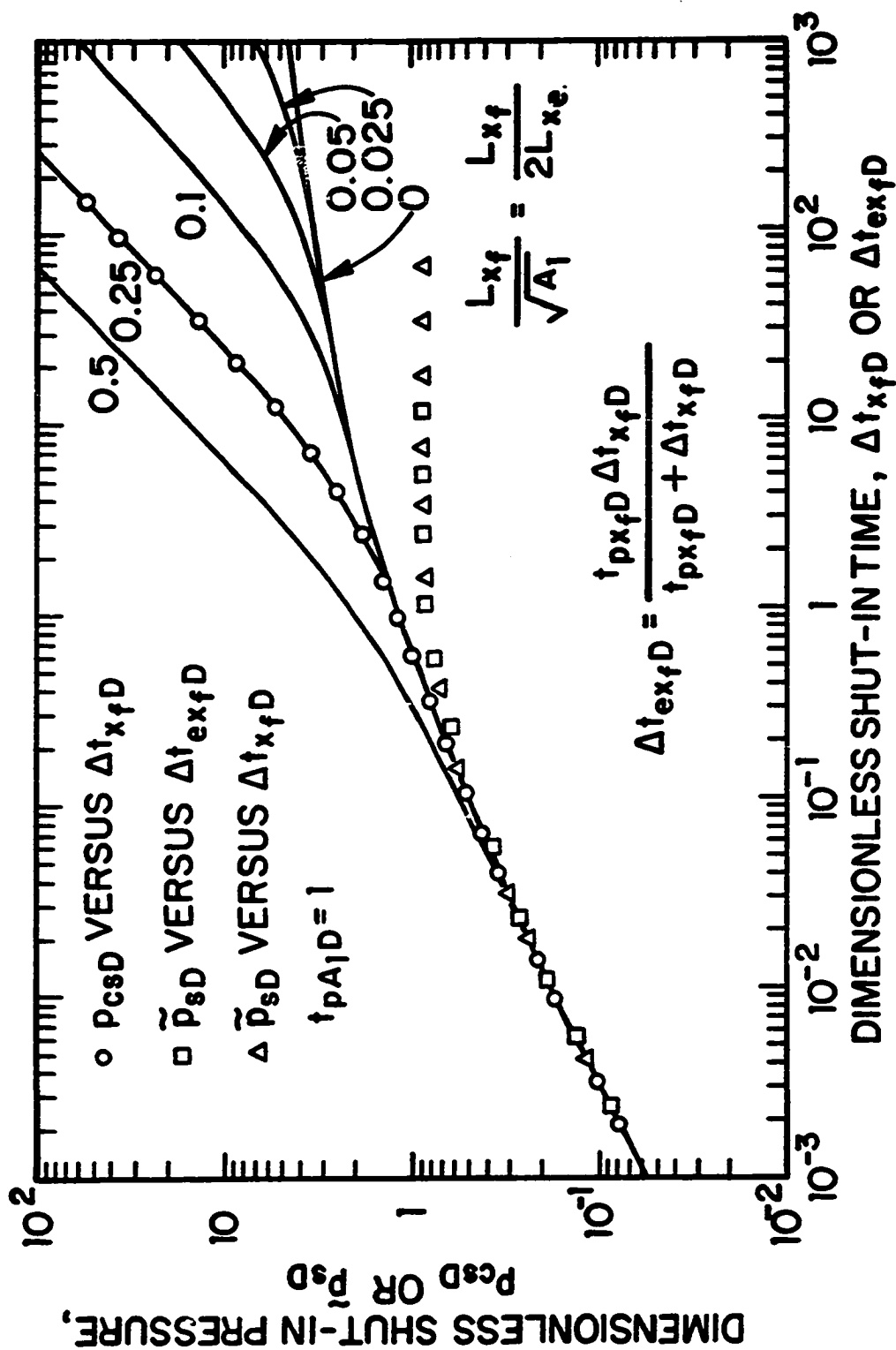


Fig. 4.4.4 - Correlation of Modified Buildup Pressure With Drawdown Solution; Infinite-Conductivity Fracture

Stein<sup>92</sup> has investigated type curve analysis of buildup pressure change at a specific well in an infinite multi-well pattern. He generated the buildup response of a specific fractured well by using superposition and the method of images in which the closed drainage area of the fractured well at the moment of shut-in is created by using line source offset wells. Based on the work of Ref. 17 and computational results not shown here, the procedure used by Ref. 92 is a good approximation provided that the parameter  $L_{x_j}/\sqrt{A_1}$  is sufficiently small. We do not pursue this procedure to generate the buildup response of a specific well. Instead we use the procedure in which all the offset wells are considered to be fractured so that the superposition and method of images principle can be used without any approximation. Note that in our procedure, all producing wells (offset wells) shown by solid dots and the buildup surveyed well shown by a cross mark in Fig. 4.2.2 are fractured wells, whereas in the procedure used by Stein only the buildup surveyed well is considered to be a fractured well and all the producing wells (offset wells) are considered to be line source wells. As shown previously, the dimensionless buildup pressure,  $p_{sD}$ , of specific well (well 1 in our notation) located in an infinite multi-well pattern depicted by Fig. 4.2.2 is given by Eq. 4.2.6 where each  $p_D$  term is given by the infinite acting solution of Ref. 17 (also see Eq. 3.1.22).

Since we are interested in long producing times,  $t_p \geq t_{pss}$ , the term in square brackets in Eq. 4.2.6 is given by its pseudosteady-state approximation. Moreover, for sufficiently short shut-in times, the  $p_D(\Delta t)$  term in Eq. 4.2.6 can be approximated by linear flow equation (see Eq. 3.1.30). Under these conditions, one obtains Eqs. 4.4.2 and 4.4.3. Therefore, one can apply Eqs. 4.4.4 through 4.4.6 and Eq. 4.4.19 to obtain estimates of  $A_1$  and  $kL_x^2$ , by the standard procedure described for a single fractured well in a closed drainage area during linear flow. For shut-in times such that  $p_D(\Delta t)$  term in Eq. 4.2.6 is given by pseudo-radial flow approximation (Eq. 3.1.33), one obtains Eqs. 4.4.10 and 4.4.11. Therefore, during the pseudoradial flow equation, one can use the analysis procedure given for a single fractured well in the previous subsection to analyze the buildup response of a specific well located in an infinite multi-well pattern. As shown for a single unfractured well

located in an infinite multi-well pattern, Eqs. 4.4.10 and 4.4.11 will be valid for all shut-in times because of the interference effect of nearby producing offset wells, and the dimensionless buildup pressure  $p_{sD}$  will have a minimum which is given by Eq. 4.3.24 at  $\Delta t_{A_1D} = 1/(4\pi)$ . Therefore, by using Eqs. 4.3.25 and 4.3.26, respectively, one can compute well's drainage area at the instant of shut-in and the average reservoir pressure in this drainage area. However, as shown later by results of Fig. 4.4.5, the minimum of  $p_{sD}$  will not occur at  $\Delta t_{A_1D} = 1/(4\pi)$  for all values of the penetration ratio  $L_{xf}/\sqrt{A_1}$ . Specifically, the minimum of  $p_{sD}$  will occur at  $\Delta t_{A_1D} = 1/(4\pi)$  if and only if the pseudo-radial flow prevails at a shut-in time  $\Delta t_{A_1D} < 1/(4\pi)$ , that is, Eq. 4.4.10 (or Eq. 4.4.11) holds at a shut-in time  $\Delta t_{A_1D} < 1/(4\pi)$ . The condition on  $L_{xf}/\sqrt{A_1}$  so that the minimum of  $p_{sD}$  occurs at  $\Delta t_{A_1D} = 1/(4\pi)$  can be derived using the fact that for all practical purposes, the pseudo-radial flow holds for shut-in times  $\Delta t_{A_1D} \geq c(L_{xf}^2/A_1)$  where  $c = 3$  for an uniform-flux fracture and  $c = 7$  for an infinite-conductivity fracture. Using this fact, one can show that Eq. 4.4.10 holds at a shut-in time  $\Delta t_{A_1D} < 1/(4\pi)$  if and only if  $L_{xf}/\sqrt{A_1} < 0.16$  for an uniform-flux fracture and  $L_{xf}/\sqrt{A_1} < 0.11$  for an infinite-conductivity fracture.

Figure 4.4.5 presents results for an uniform-flux fractured well with a closed square drainage area created by the production of nearby producing wells. Fig. 4.4.5 shows a semilog plot of the derivative response,  $dp_{sD}/d\sqrt{\Delta t_{A_1D}}$  versus  $\Delta t_{A_1D}$  as a function of the penetration ratio  $L_{xf}/\sqrt{A_1}$ . Note that when linear flow prevails during buildup,  $dp_{sD}/d\sqrt{\Delta t_{A_1D}}$  is given by Eq. 4.4.3; i.e.,

$$\frac{dp_{sD}}{d\sqrt{\Delta t_{A_1D}}} = 4\pi\sqrt{\Delta t_{A_1D}} - \sqrt{\pi\frac{A_1}{L_{xf}^2}}. \quad (4.4.25)$$

A cross mark shown in Fig. 4.4.5 is used to denote the ending time of Eq. 4.4.25 for a given value of  $L_{xf}/\sqrt{A_1}$ . When pseudoradial flow prevails during buildup,  $dp_{sD}/d\sqrt{\Delta t_{A_1D}}$  is given by the following equation:

$$\frac{dp_{sD}}{d\sqrt{\Delta t_{A_1D}}} = 4\pi\sqrt{\Delta t_{A_1D}} - \frac{1}{\sqrt{\Delta t_{A_1D}}}. \quad (4.4.26)$$

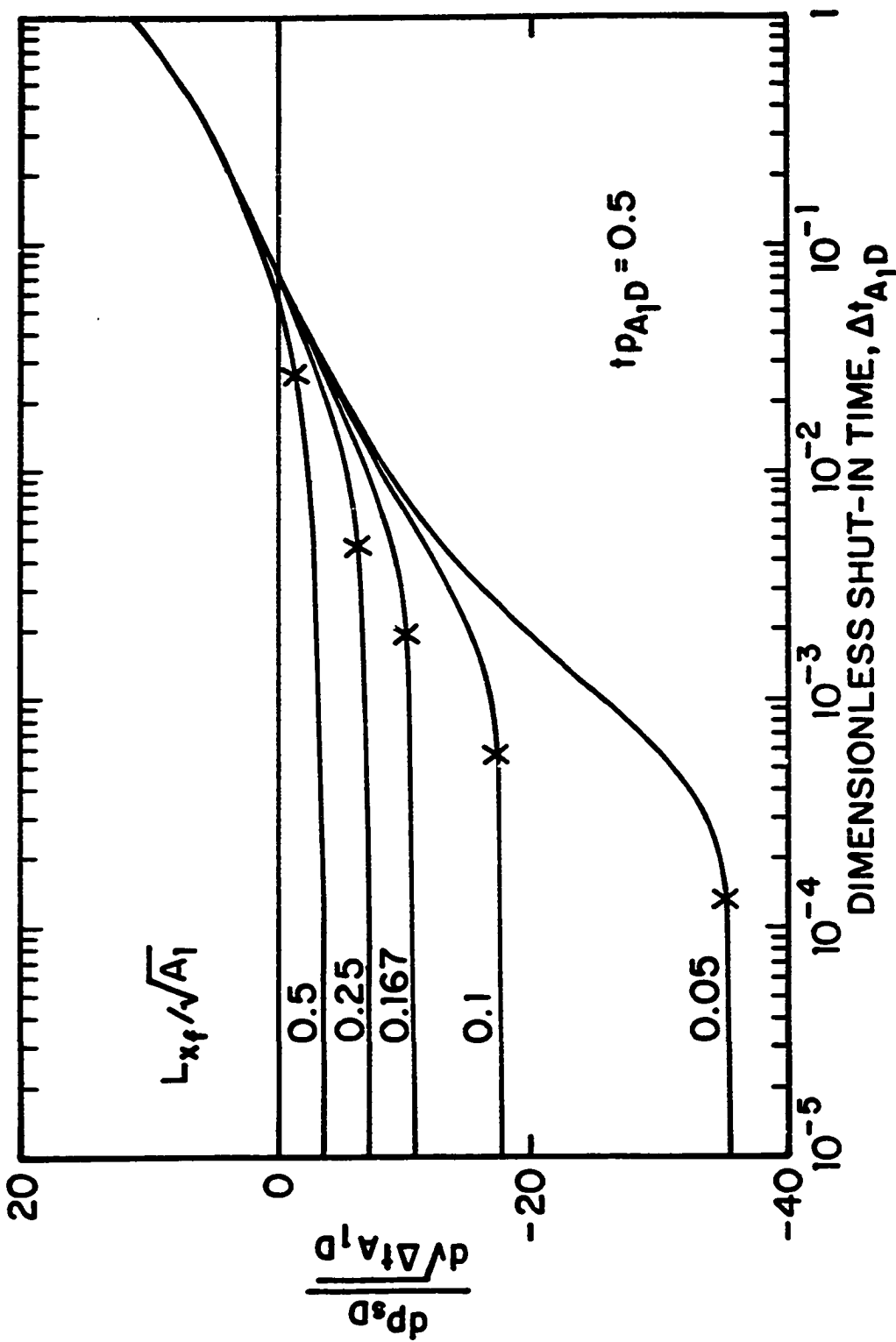


Fig. 4.4.5 - Derivative Response in an Infinite Multi-Well Pattern; Uniform-Flux Fracture

Eq. 4.4.26 follows from Eq. 4.4.11 using the chain rule. Eq. 4.4.26 holds at an earliest time when  $\Delta t_{A_1D} \geq c(L_{e_f}^2/A_1)$  where  $c = 3$  and  $L_{e_f}^2/A_1 = 0.0025$ , that is, when  $\Delta t_{A_1D} = 0.0075$ . Thus, the bottom curve in Fig. 4.4.5 represents Eq. 4.4.26, or equivalently, Eq. 4.4.11. It is apparent from results of Fig. 4.4.5 that for values of  $L_{e_f}/\sqrt{A_1} < 0.5$ , Eq. 4.4.11 holds for all values of shut-in time when  $\Delta t_{A_1D} \geq 3(L_{e_f}^2/A_1)$  and  $dp_{eD}/d\sqrt{\Delta t_{A_1D}}$  is zero for all practical purposes at the shut-in time  $\Delta t_{A_1D} = 1/(4\pi)$ . For the case where  $L_{e_f}/\sqrt{A_1} = 0.5$ ,  $dp_{eD}/d\sqrt{\Delta t_{A_1D}}$  is zero at shut-in time  $\Delta t_{A_1D} \approx 0.058$  which is earlier than  $1/(4\pi)$  and Eq. 4.4.26 does not hold unless  $\Delta t_{A_1D} \geq 0.15$ .

Finally, we note that one can use the drawdown type curves to analyze the buildup pressure change obtained at a specific well in a multi-well pattern provided a modified buildup pressure change plot is used as shown in the previous subsection for a single fractured well in a closed drainage area. In this case, due to interference effect of nearby producing offset wells, the modified buildup pressure change will correlate with the infinite-acting solution (see curve labeled with  $L_{e_f}/\sqrt{A_1} = 0$  in Fig. 4.4.4) for all shut-in times, whereas for a single well in a closed drainage area, the modified buildup pressure change will deviate from infinite-acting solution when no-flow boundaries of the closed drainage region are felt during buildup; see Fig. 4.4.4.

#### 4.5 Wellbore Storage and Skin Effects

Here, we consider wellbore storage and skin effects on the buildup response of a single unfractured well in a closed drainage area. It is assumed that no wellbore storage and skin effects exist prior to shut-in and the well is produced long enough so that pseudosteady-state flow is established prior to shut-in. The results presented here are generated by using Eq. 4.2.5 where each  $p_{wD}$  term is computed in Laplace space using the well known superposition result<sup>13,14</sup>, i.e.,

$$\bar{p}_{wD} = \frac{u\bar{p}_{bD}(u) + s}{u + C_D u^2 [u\bar{p}_{bD}(u) + s]}, \quad (4.5.1)$$

and then inverted numerically using the Stehfest algorithm. In Eq. 4.5.1,  $u$  rep-

resents the Laplace transform variable with respect to appropriate dimensionless time based on wellbore radius in Eq. 4.2.5,  $C_D$  represents the dimensionless wellbore storage coefficient as defined by Eq. 3.1.13,  $s$  represents the skin factor and  $p_{bD}$  represents the Laplace space solution for a line source well producing at a constant rate in a closed bounded reservoir without wellbore storage and skin effects, that is,

$$p_{bD}(r_D = 1, t_D) = p_D(r_D = 1, t_D) + \sum_{j=2}^{\infty} p_D(r_{Dj}, t_D), \quad (4.5.2)$$

where  $r_{Dj}$  is the dimensionless radial distance defined by Eq. 4.1.9 between the producing well and its image well  $j$  and  $p_D$  represents the dimensionless pressure drop obtained due to a line source well produced at constant rate in an infinite reservoir, that is, the exponential integral solution (see Eq. 3.1.1). Eq. 4.5.2 can be obtained using superposition and the method of images principle.

Previously, the buildup response of a single unfractured well (line source well) in a closed square drainage area under wellbore storage and skin effects was investigated by Chen and Brigham<sup>93</sup>. They investigated the existence and the duration of a semilog straight line on a conventional Horner and MDH plot of the dimensionless buildup pressure,  $p_{sD}$ , influenced by wellbore storage and skin effects during buildup. Our objective is to investigate the effect of wellbore storage and skin on the existence and duration of a straight line on a Cartesian plot of  $dp_{sD}/d \ln \Delta t_{A_1D}$  versus  $\Delta t_{A_1D}$  and to delineate the conditions under which the analysis procedure given by Eqs. 4.3.5 through 4.3.7, Eq. 4.3.17 and 4.3.19 can be applied.

Here, we are only interested in long producing times such that  $t_p \geq t_{pss}$ . For small values of shut-in time, the buildup response is controlled by wellbore storage effects, that is, the  $p_{wD}(\Delta t)$  term in Eq. 4.2.5 is equal to  $\Delta t_D/C_D$ . In this case, Eq. 4.2.5 is given by the following equation:

$$p_{sD} = 2\pi (t_p + \Delta t)_{A_1D} + \frac{1}{2} \ln \left[ \frac{4A_1}{e^{\gamma} C_{A_1} r_w^2} \right] - \frac{\Delta t_D}{C_D}. \quad (4.5.3)$$

Differentiating Eq. 4.5.3 with respect to  $\ln \Delta t_{A_1D}$  gives

$$\frac{dp_{sD}}{d \ln \Delta t_{A_1D}} = \frac{dp_{sD}}{d \ln \Delta t_D} = \left( 2\pi - \frac{A_1}{r_w^2 C_D} \right) \Delta t_{A_1D} = \left( 2\pi \frac{r_w^2}{A_1} - \frac{1}{C_D} \right) \Delta t_D. \quad (4.5.4)$$



For a 40 acre drainage area and  $r_w = 0.35$  ft,  $2\pi(r_w^2/A_1) = 4.4 \times 10^{-7}$ , whereas values of  $C_D$  are in the range of  $0 < C_D \leq 10^5$ . Thus, for most practical situations,  $1/C_D \gg 2\pi(r_w^2/A_1)$ , and Eq. 4.5.4 can be approximated well by the following equation:

$$\frac{dp_{sD}}{d \ln \Delta t_{A_1D}} = \frac{dp_{sD}}{d \ln \Delta t_D} = -\frac{\Delta t_D}{C_D} = -\frac{A}{r_w^2} \frac{\Delta t_{A_1D}}{C_D}. \quad (4.5.5)$$

Eq. 4.5.5 can be written in dimensional form as

$$\frac{dp_{ws}}{d \ln \Delta t} = \frac{qB}{24C} \Delta t; \quad (4.5.6)$$

that is, during wellbore storage dominated flow, one can determine the wellbore storage coefficient,  $C$ , from the slope of a straight line on a Cartesian plot of  $dp_{ws}/d \ln \Delta t$  versus  $\Delta t$  in the conventional manner.

If wellbore storage effects become negligible so that the  $p_{wD}(\Delta t_D)$  term in Eq. 4.2.5 can be replaced by the radial flow equation (see Eq. 4.3.1), then the dimensionless buildup pressure change,  $p_{sD}$ , and its derivative with respect to  $\ln \Delta t_{A_1D}$  are given, respectively, by the following equations:

$$p_{sD} = 2\pi (t_p + \Delta t)_{A_1D} - \frac{1}{2} \ln (\Delta t_{A_1D} C_{A_1}), \quad (4.5.7)$$

and

$$\frac{dp_{sD}}{d \ln \Delta t_{A_1D}} = 2\pi \Delta t_{A_1D} - \frac{1}{2}. \quad (4.5.8)$$

Note that Eqs. 4.5.4 and 4.5.8 can be rearranged, respectively, to obtain the following equations:

$$-\frac{dp_{sD}}{d \ln \Delta t_{A_1D}} + 2\pi \Delta t_{A_1D} = \frac{A_1}{r_w^2} \frac{\Delta t_{A_1D}}{C_D}, \quad (4.5.9)$$

and

$$-\frac{dp_{sD}}{d \ln \Delta t_{A_1D}} + 2\pi \Delta t_{A_1D} = \frac{1}{2}. \quad (4.5.10)$$

Figure 4.5.1 illustrates the existence and the duration of the straight line predicted by Eq. 4.5.8, or, equivalently, the validity of Eq. 4.5.10, for a well located at the center of a closed square drainage area with wellbore storage effects. The

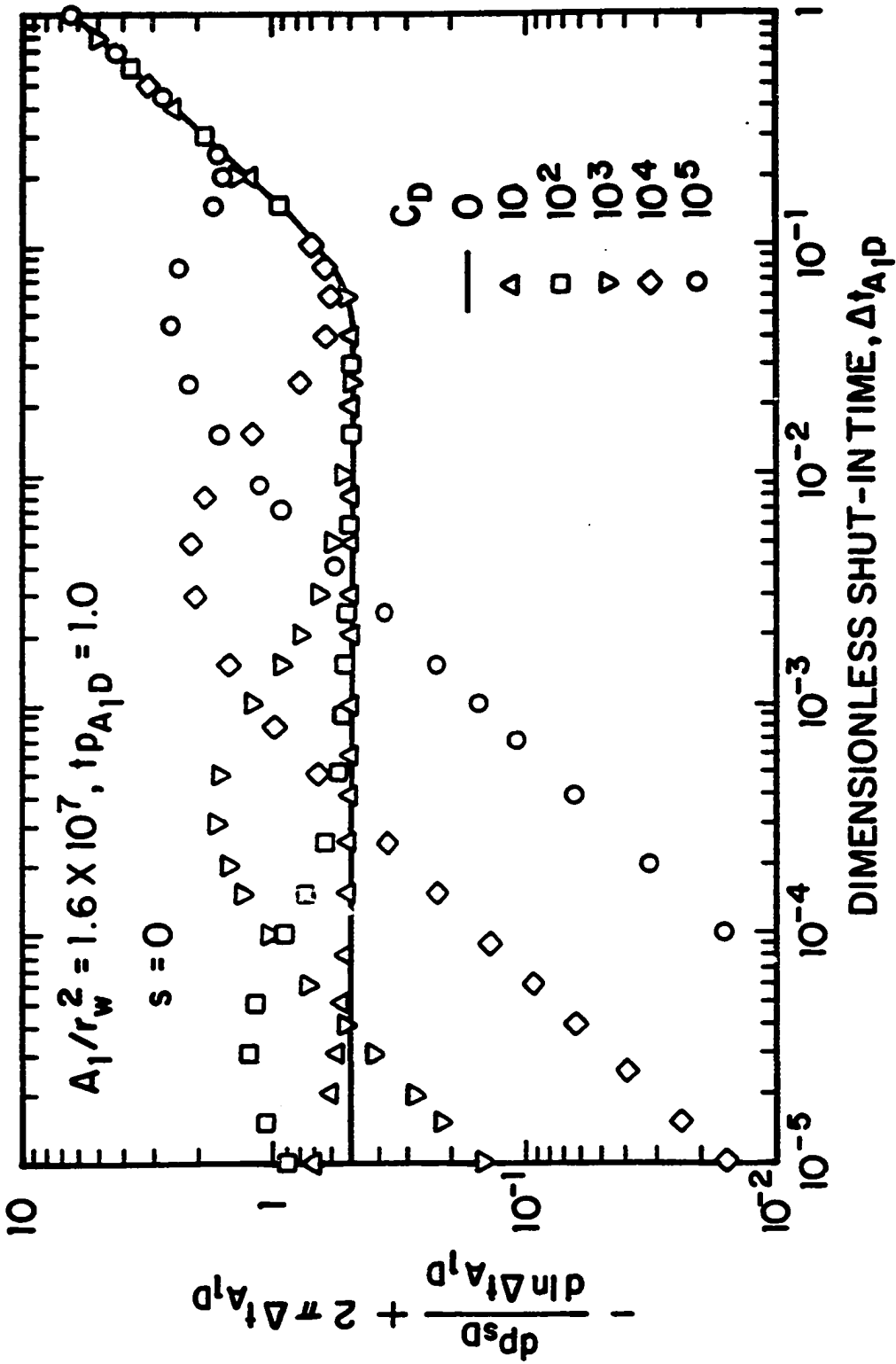


Fig. 4.5.1 - Effect of Wellbore Storage on Derivative Response; Closed Square Reservoir

dimensionless wellbore coefficient,  $C_D$ , is the parameter of interest. For the results of Fig. 4.5.1,  $t_{pA_1D} = 1$ ,  $A_1/r_w^2 = 1.6 \times 10^7$  and  $s = 0$ . Fig. 4.5.1 shows a log-log plot of  $-(dp_{sD}/d \ln \Delta t_{A_1D}) + 2\pi \Delta t_{A_1D}$  versus  $\Delta t_{A_1D}$ . The solid curve corresponds to a case where the dimensionless wellbore storage coefficient is zero. Note for this case, as noted in Section 4.3.1, the derivative response equals 0.5 for all shut-in times such that  $\Delta t_{A_1D} \leq 0.05$  and displays a unit-slope line for shut-in times  $\Delta t_{A_1D} \geq 0.1$ ; that is, pseudosteady-state flow is reached during buildup. It is apparent from results of Fig. 4.5.1 that the larger the value of  $C_D$ , the shorter the duration of Eq. 4.5.10. Note for values of  $C_D \geq 10^4$ , Eq. 4.5.10 never applies and for  $C_D = 10^3$ , the duration of Eq. 4.5.10 is only about one-half of a log cycle. For sufficiently small values of the shut-in time, the derivative response displays a unit-slope line as predicted by Eq. 4.5.9 during wellbore storage dominated flow. Note that for the cases where  $C_D \leq 10^3$ , Eq. 4.5.10 holds and thus, for these cases, Eqs. 4.3.5 through 4.3.7 and Eq. 4.3.17 can be applied to determine the well's drainage, the permeability, and the average reservoir pressure.

Figure 4.5.2 shows the effect of skin on the duration of Eq. 4.5.10 for a well at the center of a closed square drainage area for a case where  $t_{pA_1D} = 1$ ,  $A_1/r_w^2 = 4 \times 10^8$  and  $C_D = 10^3$ . In Fig. 4.5.2, the solid curve through circular data points represents the case where  $C_D = 0$ . It is apparent that increasing the magnitude of the skin factor delays the starting time of Eq. 4.5.10. However, for all practical purposes, for the cases considered in Fig. 4.5.2, Eq. 4.5.10 applies for shut-in times such that  $0.003 \leq \Delta t_{A_1D} \leq 0.05$ . Therefore, one can apply the analysis procedure described earlier for a well with no wellbore storage effects to determine the well's drainage area, the permeability, the average reservoir pressure and the skin factor. Note that if the dimensionless wellbore storage coefficient is zero, Eq. 4.5.10 applies for all shut-in times prior to pseudosteady-state flow and the skin factor plays no role on the duration and the existence of Eq. 4.5.10.

Next, we examine the effect of drainage area on the derivative response obtained at a well with wellbore storage effects in a closed square reservoir. Fig. 4.5.3 shows a log-log plot of  $-(dp_{sD}/d \ln \Delta t_{A_1D}) + 2\pi \Delta t_{A_1D}$  versus  $\Delta t_{A_1D}$ . For the results of

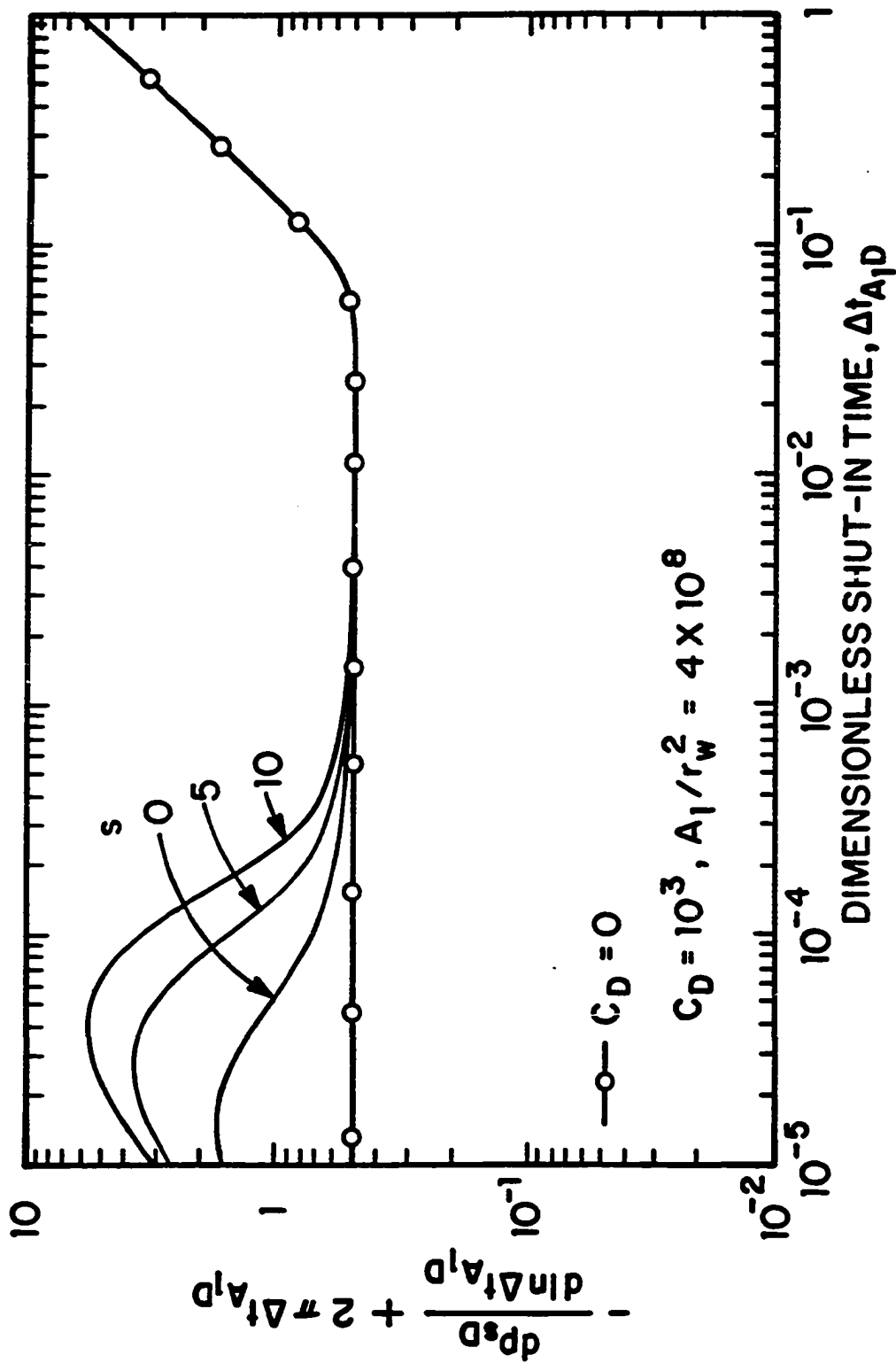


Fig. 4.5.2 - Effect of Wellbore Storage and Skin on Derivative Response; Closed Square Reservoir

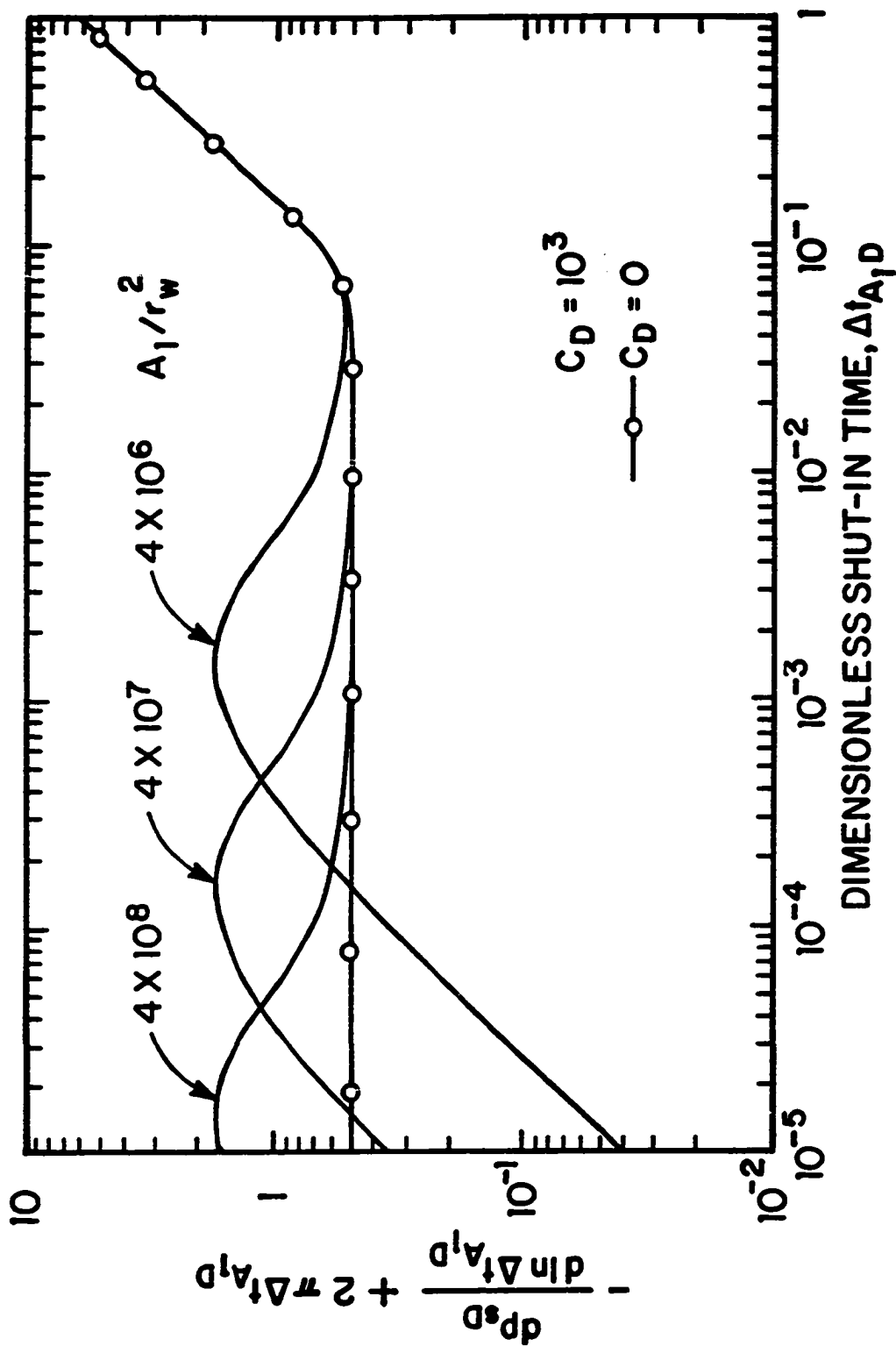


Fig. 4.5.3 - Effect of Drainage Area and Wellbore Storage on Derivative Response; Closed Square Reservoir

Fig. 4.5.3,  $t_{pA_1D} = 0.5$ ,  $C_D = 1000$  and  $A_1/r_w^2$  is the parameter of interest. It is important to note that increasing the drainage area of the well at the instant of shut-in increases the duration of Eq. 4.5.10. For example, for the case where  $A_1/r_w^2 = 4 \times 10^7$ , Eq. 4.5.10 applies for shut-in times  $0.01 \leq \Delta t_{A_1D} \leq 0.05$ , whereas for the case where  $A_1/r_w^2 = 4 \times 10^6$ , Eq. 4.5.10 does not hold because of the fact that when the wellbore storage effects no longer control the derivative response, pseudosteady-state is reached during buildup.

As far as the determination of beginning of a straight line on a Cartesian plot of  $-dp_{ws}/d \ln \Delta t$  versus  $\Delta t$  under wellbore storage effects is concerned, one can use the tabulated values of Ref. 94 (see Table 2 of Ref. 94). Strictly speaking, tabulated values given by Ref. 94 are based on the infinite-acting drawdown solutions. Therefore, it is reasonable to expect that these beginning times do not hold for some values of the dimensionless wellbore storage coefficient,  $C_D$ , and  $A_1/r_w^2$ . Moreover, it should be noted in order to use these tabulated values to determine the beginning of a straight line on a Cartesian plot, a priori knowledge of the wellbore storage coefficient  $C$ , the skin factor  $s$ , and the value of permeability  $k$  is required. One may be able to determine these parameters from a preliminary type-curve match of buildup pressure change  $\Delta p$  ( $= p_{ws} - p_{wf,s}$ ) and  $\Delta p/(2\Delta p')$  data using the drawdown wellbore storage and skin type curves presented in Chapter III. If these values cannot be determined from such a type curve matching, one can apply the well known 1 1/2-cycle rule. As far as the ending time of the straight line on a Cartesian plot of the derivative response is concerned, one can use the values presented in Table 4.3.1.

Before closing this section, we note that even though results concerning the buildup response of a specific well with wellbore storage and skin effects in an infinite multi-well pattern are not presented, one can expect that the buildup response of a well in a closed drainage area differ from the buildup response of a well in an infinite multi-well pattern at late shut-in times. For a well in an infinite multi-well pattern, when the effect of wellbore storage storage coefficient is negligible on the buildup response, Eq. 4.5.10 holds for all shut-in times due to depletion of the well's drainage

area by nearby producing wells. Therefore, one can apply the analysis procedure discussed above based on Eqs. 4.5.6 and 4.5.8 for a well with wellbore storage and skin effects for the infinite multi-well pattern case in the straightforward way.

#### 4.6 Field Example

Here, a field buildup test for an unfractured well in a closed drainage area is presented to show how one can use the analysis procedures given in this work. The data for the example considered is from Ref. 95. Relevant reservoir/well data is recorded in Table 4.6.1. The buildup pressure change and its derivative as functions of shut-in time are presented in Table 4.6.2.

Figure 4.6.1 shows a preliminary type-curve match of  $\Delta p/(2\Delta p')$  versus  $\Delta t$  obtained using the drawdown wellbore storage and skin type curves infinite-acting reservoirs presented in Fig. 3.1.3. Here,  $\Delta p$  denote the buildup pressure change, that is,  $\Delta p = p_{ws} - p_{wf,s}$  and  $\Delta p'$  is the derivative of  $\Delta p$  with respect to  $\ln \Delta t$ . The solid curves shown in Fig 4.6.1 represent the drawdown solutions for three values of  $C_D \exp(2s)$ ,  $10^6$ ,  $10^7$  and  $10^{10}$ . Note that data were matched with  $C_D \exp(2s) = 10^7$  solution. By using the standard computational procedures given in Chapter III, the following estimates were obtained from the match point values recorded in Fig. 4.6.1;  $k = 3.85$  md,  $C = 2.15 \times 10^{-3}$  ( $C_D = 1126$ ) RB/psi, and  $s = 4.55$ . Here, we determined the wellbore storage coefficient  $C$  from a unit slope on a log-log plot of  $\Delta p$  versus  $\Delta t$  (not shown here) in the conventional manner. Figure 4.6.2 is a Cartesian plot of the logarithmic derivative of shut-in pressure,  $-dp_{ws}/d \ln \Delta t$ , vs. the shut-in time,  $\Delta t$ . As shown by results of Fig. 4.6.1, the early-time data reflect wellbore storage effects. Therefore, in order to determine a beginning time for the straight line, we used Table 2 of Ref. 93 for a tolerance of 10% using the value of  $C_D \exp(2s) = 10^7$  obtained from the preliminary type-curve match shown in Fig. 4.6.1. This time corresponds to a shut-in of  $\Delta t \geq 25$ . The solid straight line shown on Fig. 4.6.2 shows the best straight line fitted through the data points beyond  $\Delta t \geq 25$  using a least-squares procedure. This straight line has a slope,  $m_l = 0.205$  psi/hr, and an intercept at  $\Delta t = 0$  of  $-b = -71.2$  psi. Using the slope

**Table 4.6.1**  
**Reservoir/Well Parameters; Field Example**

Porosity (percent) . . . . .	0.13
Thickness (ft) . . . . .	15
Wellbore Radius (ft) . . . . .	0.25
System Compressibility (1/psi) . . . . .	14E-06
Viscosity of Fluid (cp) . . . . .	0.72
Formation Volume Factor (RB/STB) . . . . .	1.30
Production Rate Prior to Shut-in (STB/D) . . . . .	60
Flowing Pressure at the Instant of Shut-in (psi) . . . . .	1203
Producing Time (hrs) . . . . .	1730
Permeability (From Core Data) (md) . . . . .	2 - 8
Estimated Well's Drainage area (acres) . . . . .	80



**Table 4.6.2**  
**Pressure and Derivative versus Time Data; Field Example**

Shut-in Time, $\Delta t$ (Hours)	Pressure and Derivative Data		
	$\Delta p$ (psi)	$\Delta p'$ (psi)	$\Delta p/(2\Delta p')$
1.0800E-01	1.6900E+02	1.6418E+02	5.1466E-01
1.3000E-01	2.0100E+02	1.9058E+02	5.2733E-01
1.7300E-01	2.6200E+02	2.3529E+02	5.5676E-01
2.1600E-01	3.1900E+02	2.7474E+02	5.8054E-01
2.6000E-01	3.7100E+02	3.0737E+02	6.0350E-01
3.4600E-01	4.6700E+02	3.6299E+02	6.4327E-01
4.3200E-01	5.5100E+02	4.0412E+02	6.8173E-01
6.5000E-01	7.2700E+02	4.8658E+02	7.4705E-01
8.6000E-01	8.7300E+02	5.0981E+02	8.5620E-01
1.0800E+00	9.8200E+02	4.9926E+02	9.8346E-01
1.3000E+00	1.0610E+03	4.4486E+02	1.1925E+00
1.7300E+00	1.1700E+03	3.9184E+02	1.4930E+00
2.1600E+00	1.2420E+03	3.2024E+02	1.9392E+00
3.4600E+00	1.3570E+03	2.4722E+02	2.7446E+00
5.4100E+00	1.4260E+03	1.8784E+02	3.7959E+00
8.6500E+00	1.4640E+03	1.1869E+02	6.1673E+00
1.1670E+01	1.4880E+03	8.7273E+01	8.5250E+00
1.7300E+01	1.5170E+03	7.5194E+01	1.0087E+01
1.9500E+01	1.5150E+03	7.2586E+01	1.0505E+01
2.2900E+01	1.5340E+03	6.9020E+01	1.1127E+01
2.5900E+01	1.5440E+03	6.8186E+01	1.1322E+01
2.8500E+01	1.5490E+03	6.5992E+01	1.1751E+01
3.5500E+01	1.5640E+03	6.5042E+01	1.2023E+01
3.9800E+01	1.5720E+03	6.2464E+01	1.2583E+01
4.3200E+01	1.5770E+03	6.2015E+01	1.2715E+01
5.1900E+01	1.5870E+03	5.8267E+01	1.3618E+01
6.0500E+01	1.5960E+03	5.8702E+01	1.3594E+01
6.9200E+01	1.6040E+03	5.8186E+01	1.3783E+01
8.6500E+01	1.6160E+03	5.3158E+01	1.5200E+01
1.0380E+02	1.6240E+03	4.7824E+01	1.6979E+01
1.3000E+02	1.6340E+03	3.4983E+01	2.3354E+01

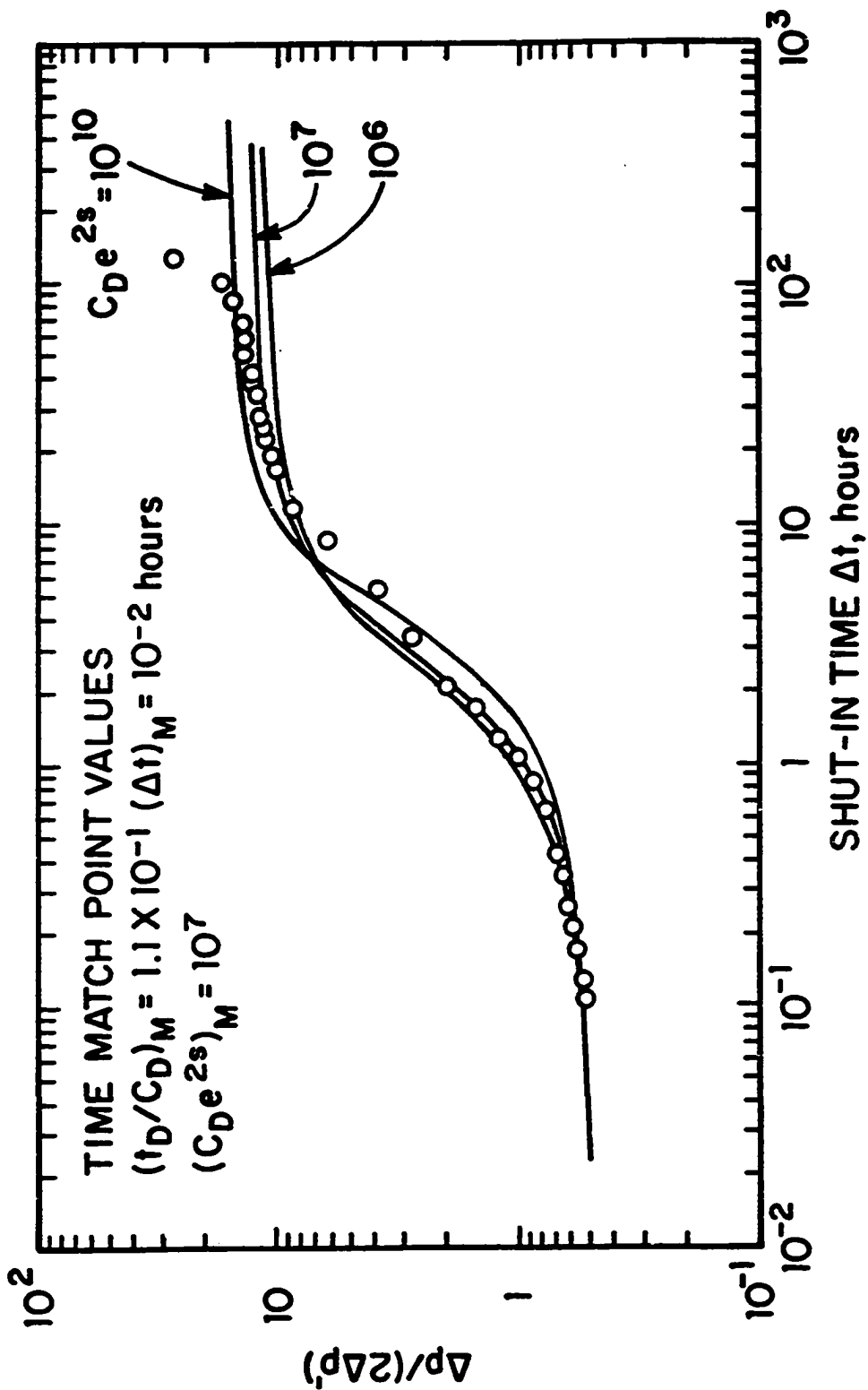


Fig. 4.6.1 - Preliminary Type-Curve Match of Pressure/Pressure-Derivative Data; Field Example

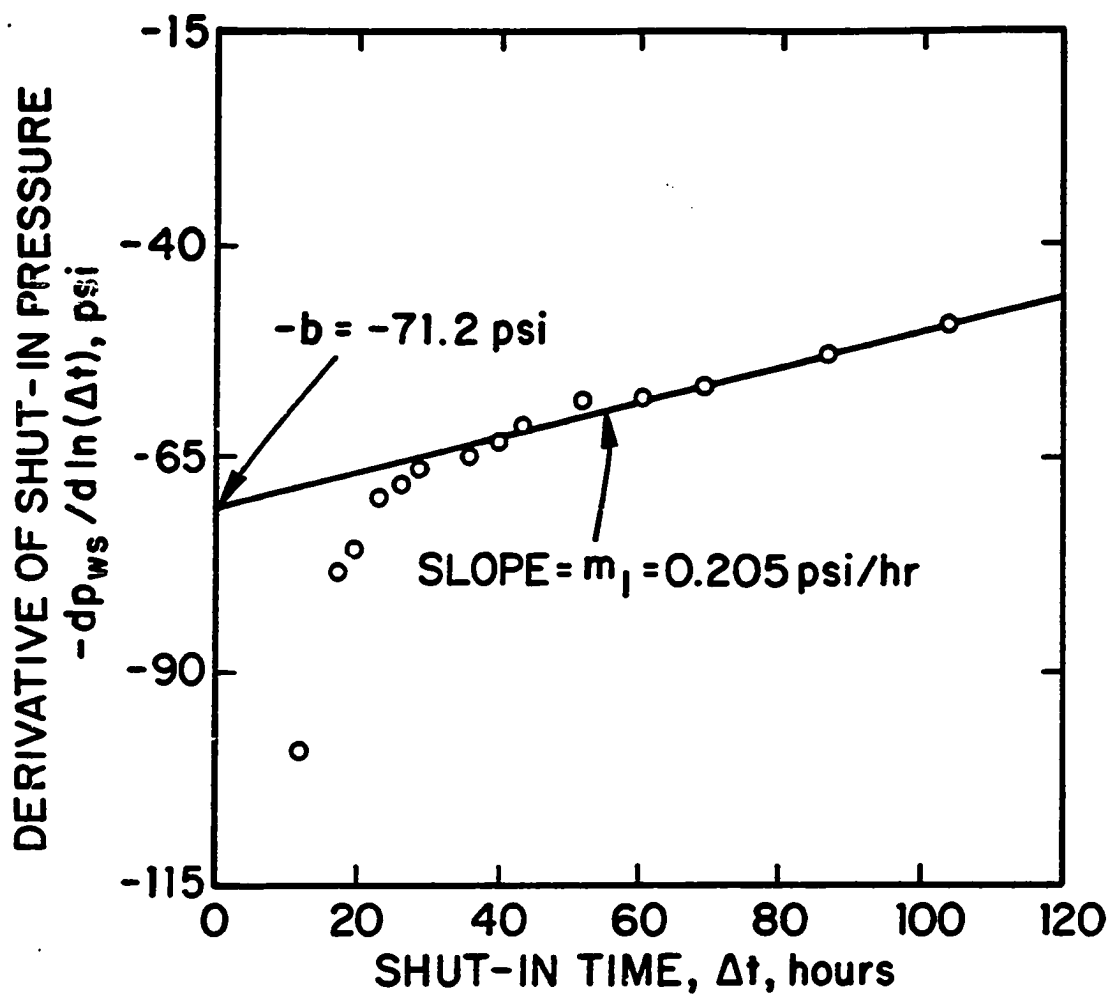


Fig. 4.6.2 - Cartesian Plot of Derivative of Shut-in Pressure; Field Example

and the intercept values in Eqs. 4.3.6 and 4.3.7, the drainage area of the well and the permeability-thickness product were obtained, respectively, as  $A = 75$  acres, and  $kh = 55.7$  md-ft ( $k = 3.71$  md.).

Figure 4.6.3 shows a semilog plot of the shut-in pressure,  $p_{ws}$  (MDH plot) and  $p_{ws} + m_i \Delta t$  (modified MDH plot), where  $m_i$  was obtained from the slope of the straight line shown on Fig. 4.6.2, versus the shut-in time,  $\Delta t$ . It is apparent from Fig. 4.6.3 that the plot of  $p_{ws} + m_i \Delta t$  versus  $\Delta t$  yields a well-defined semilog straight line for  $\Delta t \geq 25$  hours, whereas the conventional MDH plot of data shows no well-defined semilog straight line. The slope of modified MDH semilog straight line is  $m = 160$  psi/log cycle. From Eqs. 4.3.16 and 4.3.19, respectively, we find  $kh = 57.1$  md-ft ( $k = 3.81$  md.) and the skin factor,  $s = 4.42$ . Note that the  $kh$  value obtained from the intercept at  $\Delta t = 0$  on Fig. 4.6.2 is in good agreement with the  $kh$  value obtained from the slope of the modified MDH semilog straight line in Fig. 4.6.3. Also note that the values of permeability and skin factor obtained from our new procedure are in good agreement with the values obtained from type curve analysis. Because neither the initial pressure nor the geometry of the system is known, an estimate of a shape factor is needed to compute the average pressure from Eq. 4.3.17. As can be seen from the results of Figs. 4.6.2 and 4.6.3, all points corresponding to  $\Delta t \geq 25$  hours lie on the appropriate straight line. Thus, the shut-in pressure is not influenced by the drainage area boundary or the reservoir boundary. Thus, the final shut-in time must correspond to  $\Delta t_{A_1 D} < t_{esa, A_1 D}$  and moreover, we must have  $t_{pA_1 D} > t_{pes, A_1 D}$ . Using the estimates of  $A_1$  and  $k$  obtained, the dimensionless values of the last shut-in time and the producing time correspond, respectively, to  $\Delta t_{A_1 D} = 0.03$  and  $t_{pA_1 D} = 0.396$ . Since we must have  $0.03 < t_{esa, A_1 D}$  and  $0.396 > t_{pes, A_1 D}$ , Table 4.3.1 indicates that  $C_{A_1} = 30.88$  is a good candidate. Using this value in Eq. 4.3.17, Eq. 4.3.17 predicts an average pressure of  $\bar{p} = 2879.5$  psi.

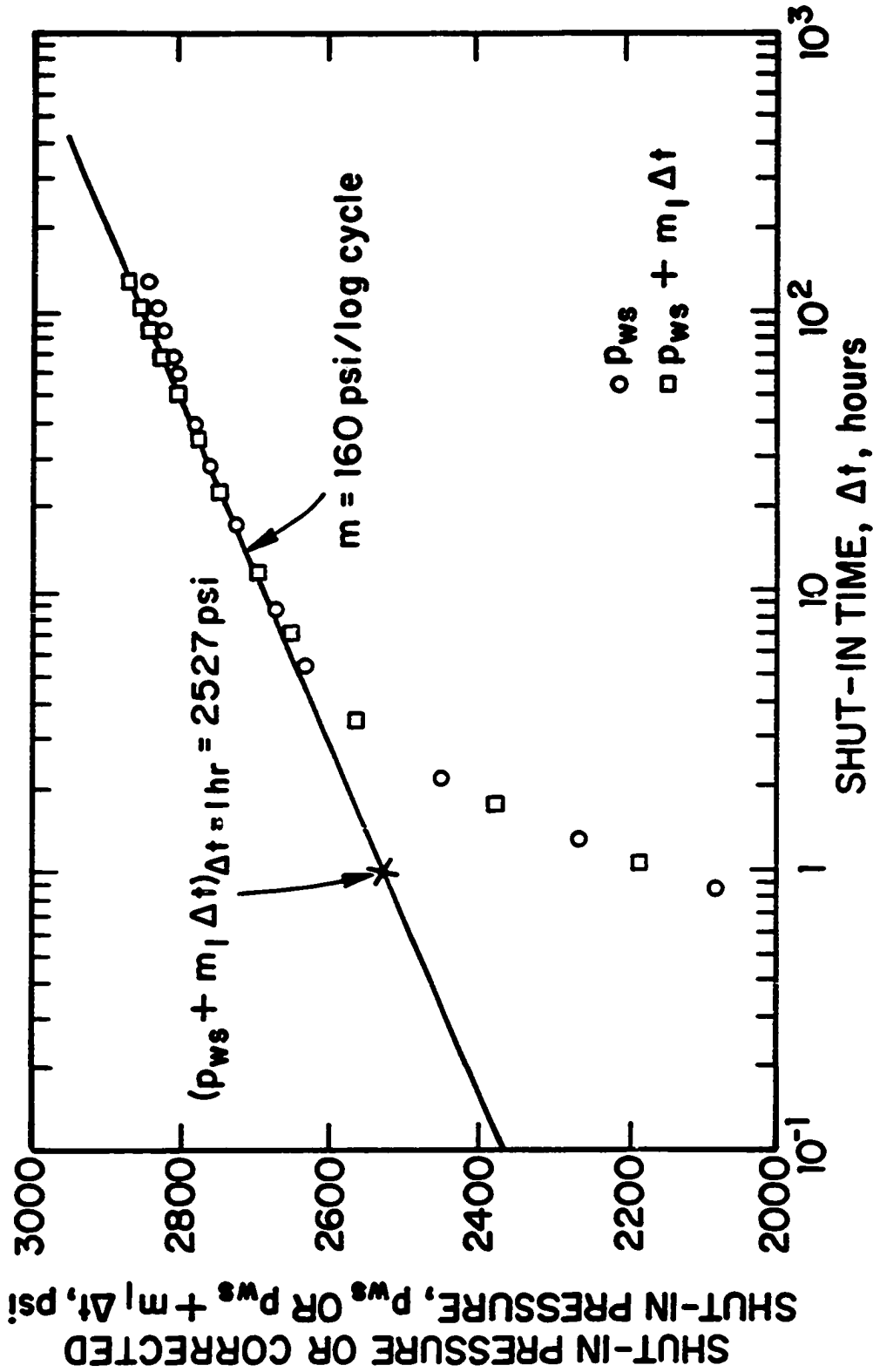


Fig. 4.6.3 - Semilog Plots of Shut-in Pressure and Corrected Shut-in Pressure; Field Example

## CHAPTER V

### CONCLUSIONS

The major objectives of this work were to develop new procedures for constructing type curves utilizing the pressure derivative, which simplify the interpretation and the analysis of well-test data, and to present new analysis procedures based on the pressure derivative, which can be used to analyze well-test data even in cases where type-curve analysis and conventional semilog analysis of well pressure data are not appropriate.

A new general method for constructing type curves based on both pressure and its logarithmic derivative has been presented. The type curves involve graphs of the dimensionless pressure and a new pressure/pressure-derivative group which is equal to dimensionless pressure divided by its logarithmic derivative. By using this pressure/pressure-derivative group, new type curves have been presented for the following well/reservoir problems: classical line source solution, wellbore storage and skin, fractured wells (either planar or finite-conductivity), naturally fractured reservoirs, and composite reservoirs. Type curves were presented for both infinite-acting reservoirs and closed bounded reservoirs. It has been shown that the drawdown type curves based on the pressure/pressure-derivative group can be used to analyze buildup data prior to the time when producing times become important. If producing time effects become important, we showed that the use of equivalent time does not always eliminate the errors incurred in type-curve matching buildup data with the new drawdown type curves presented in this work. In these cases, we showed that new buildup type curves utilizing the buildup pressure/pressure derivative group can be constructed to analyze such buildup data. The major advantage of the new type curves presented in this work over previous derivative type

curves is that the the dimensionless pressure/pressure-derivative group used can be constructed exactly from actual field data. Thus, type-curve matching of the field pressure/pressure-derivative data can be accomplished by moving the field data plot only in the horizontal direction and the new derivative type curves give an excellent indication of whether the field case actually represents the well/reservoir model assumed by the type-curve solution.

It has also been shown that the basic idea of plotting the pressure change over its logarithmic derivative can be used effectively to identify proper semilog straight lines, that is, to determine time periods where pressure data can be analyzed by conventional semilog methods. We have shown that a semilog plot of the pressure/pressure-derivative group versus time will always exhibit a 1.151 slope during plane radial flow in a homogeneous reservoir and this slope will be independent of reservoir properties. Moreover, we showed that this semilog identification method can be also used for nonhomogeneous reservoir such as composite and naturally fractured reservoirs.

Finally, we investigated the buildup response of a well (either fractured or unfractured) located in a system of producing wells completed in a closed bounded reservoir. We have presented new analysis procedures based on the pressure derivative to determine well/reservoir parameters. Specifically, we showed that a well's drainage area can be directly determined from buildup tests by using the pressure derivative and we showed that this observation is applicable to both fractured and unfractured wells.

From the results of this work, the following conclusions are warranted:

- (i) Type curves based on the pressure/pressure-derivative not only simplify interpretation of well-test data but also are advantageous in identifying whether given field data are representative of the solution assumed by a particular type-curve solution.
- (ii) A semilog plot of pressure/pressure-derivative data versus time can be used to identify proper semilog straight lines and to determine time periods where conventional semilog analysis methods can be applied with confidence to determine well/reservoir parameters.

(iii) Using an appropriate plot of the pressure derivative, the well's drainage area at the instant of shut-in and the permeability-thickness product can be obtained from a build test for a well producing to pseudosteady-state prior to shut-in. The determination of the drainage area does not require the knowledge of initial pressure, the producing time or the flowing wellbore pressure at the instant of shut-in.

(iv) For a well located in a system of producing wells in an infinite multi-well pattern or in a closed bounded reservoir, the shut-in pressure reaches a maximum at a dimensionless shut-in time (based on the well's drainage area) of  $1/(4\pi)$  due to depletion of the well's drainage region by nearby producing wells. From the maximum shut-in time and the shut-in time at which the maximum shut-in pressure occurs, both the well's drainage area and the average reservoir pressure in this drainage area can be computed.

(v) In cases where the buildup response is influenced by wellbore storage and skin effects, the well's drainage area and the permeability-thickness product can be computed from a Cartesian plot of the derivative of shut-in pressure versus time provided the wellbore storage coefficient is sufficiently small, and/or the well's drainage area is sufficiently large so that a Cartesian plot of the derivative of shut-in pressure versus time exhibits a straight line.

(vi) Once the well's drainage area is obtained from the buildup pressure-derivative analysis (see Conclusions (iv) and (v)), the shut-in pressure and its derivative can be corrected to analyze the entire buildup response by using a modified MDH semilog plot, which provides estimates of the skin factor and average reservoir pressure and a check on the permeability-thickness product obtained from derivative analysis, or by using drawdown type curves. The determination of the drainage area requires a priori knowledge of the shape factor but a highly accurate estimate of the shape factor is not required to obtain an accurate estimate of average reservoir pressure from a modified MDH semilog plot.



## NOMENCLATURE

### Symbol

$A$	= reservoir drainage area, ft <sup>2</sup>
$A_1$	= well's drainage area, ft <sup>2</sup>
$b$	= intercept defined by Eq. 4.3.7, psi/hr
$b_{bi}$	= intercept defined by Eq. F-5, psi/hr <sup>1/4</sup>
$b_{cd}$	= intercept defined by Eq. 4.4.6, psi/hr <sup>1/2</sup>
$B$	= formation volume factor, RB/STB
$c_t$	= compressibility factor, psi <sup>-1</sup>
$C$	= wellbore storage constant, RB/psi
$C_A$	= Dietz shape factor for an unfractured well
$C_D$	= dimensionless wellbore storage constant
$C_f$	= shape factor for a vertically fractured well
$C_{fD}$	= dimensionless fracture conductivity
$C_{x_fD}$	= dimensionless wellbore storage constant defined by Eq. 3.1.64
$h$	= total reservoir thickness, ft
$h_{ft}$	= total thickness of fracture system, ft
$h_{mt}$	= total thickness of matrix system, ft
$k$	= reservoir permeability, md
$k_f$	= fracture absolute permeability, md
$L_{xe}$	= distance to the external boundary in x direction, ft
$L_{xf}$	= fracture half-length, ft
$L_{ye}$	= distance to the external boundary in y direction, ft
$m$	= slope defined by Eq. 4.3.16, psi/log cycle
$m(p)$	= real gas pseudopressure defined by Eq. 3.3.3, psi <sup>2</sup> /cp

$m_l$	= slope defined by Eq. 4.3.6, psi/hr
$m_{bi}$	= slope defined by Eq. F-4, psi/hr
$m_{ci}$	= slope defined by Eq. 4.4.5, psi/hr
$\Delta m(p)$	= pseudopressure change defined by Eq. 3.3.5, psi <sup>2</sup> /cp
$\Delta m'(p)$	= logarithmic derivative of $\Delta m(p)$ , psi <sup>2</sup> /cp
$p$	= pressure, psi
$\bar{p}$	= average reservoir pressure, psi
$p_i$	= initial pressure, psi
$p_D$	= dimensionless pressure defined by Eq. 3.1.3
$p_{s,D}$	= dimensionless shut-in pressure drop defined by Eq. 2
$p_{wD}$	= dimensionless wellbore pressure drop
$p_{wf}$	= flowing wellbore pressure, psi
$p_{ws}$	= shut-in pressure, psi
$p_{csD}$	= corrected dimensionless shut-in pressure, Eq. 4.4.24
$p_{w,f,D}$	= dimensionless pressure based on fracture properties, Eq. 3.2.14
$p_{wf,s}$	= wellbore pressure at the instant of shut-in, psi
$\tilde{p}_{s,D}$	= dimensionless shut-in pressure defined by Eq. 4.4.21
$p'_{wD}$	= logarithmic derivative of $p_{wD}$ defined Eq. 2.1.5
$\tilde{p}'_{s,D}$	= logarithmic derivative of $\tilde{p}_{s,D}$ defined by Eq. 3.1.44
$\Delta p$	= change in wellbore pressure during a drawdown or buildup test, psi
$\Delta p_c$	= corrected shut-in pressure defined by Eq. 4.4.23, psi
$\Delta p'$	= logarithmic derivative of $\Delta p$ , psi
$\Delta p'_c$	= logarithmic derivative of $\Delta p_c$ , psi
$q$	= flow rate, STB/Day
$q_D$	= dimensionless flow rate defined Eq. 3.1.100
$q'$	= logarithmic derivative of flow rate, STB/day
$q'_D$	= logarithmic derivative of $q_D$
$r$	= radial distance, ft
$r_D$	= dimensionless radial distance
$r_e$	= external reservoir radius, ft

$r_o$	= radius of inner zone; composite reservoir, ft
$r_w$	= wellbore radius, ft
$R_H$	= Horner time ratio defined by Eq. 4.1.8
$r'_w$	= effective wellbore radius, ft
$s$	= skin factor due to damage or stimulation
$s_f$	= skin factor due to the existence of a fracture
$t$	= time, hours
$t_D$	= dimensionless time based on wellbore radius
$t_c$	= equivalent time defined by Eq. 2.3.8, hours
$t_p$	= producing time, hours
$t_{ac}$	= equivalent pseudotime defined by Eq. 3.3.4, psi-hr/cp
$t_{AD}$	= dimensionless time based on reservoir drainage area
$t_{D2}$	= dimensionless time based on outer zone; composite reservoir
$t_{cD}$	= dimensionless equivalent time defined by Eq. 3.1.42
$t_{fD}$	= dimensionless time based on fracture properties; fractured reservoir
$t_{z,D}$	= dimensionless time based on fracture half-length
$t_{Dr'_w}$	= dimensionless time based on effective wellbore radius
$t_{pz,D}$	= dimensionless producing time based on fracture half-length
$\Delta t$	= shut-in time, hours
$\Delta t_a$	= pseudotime, psi-hr/cp
$\Delta t_D$	= dimensionless shut-in time based on wellbore radius
$\Delta t_{AD}$	= dimensionless shut-in time based on reservoir drainage area
$\Delta t_{z,D}$	= dimensionless shut-in time based on fracture half-length
$\alpha$	= dimensionless parameter defined by Eq. 4.2.1
$\beta$	= dimensionless parameter defined by Eq. 4.2.2
$\delta$	= Dirac delta function
$\nabla$	= gradient operator
$\eta$	= diffusivity
$\eta_r$	= diffusivity ratio defined by Eq. 3.2.4
$\lambda$	= mobility defined by Eq. 3.2.1

- $\lambda_r$  = mobility ratio defined by Eq. 3.2.3  
 $\omega'$  = matrix storativity defined by Eq. 3.2.16  
 $\lambda'$  = fracture transfer coefficient defined by Eq. 3.2.17  
 $\mu$  = viscosity, cp  
 $\gamma$  = Euler's constant  
 $\phi$  = porosity, fraction

Subscripts

- $e$  = external  
 $f$  = fracture  
 $m$  = matrix  
 $t$  = total  
 $w$  = wellbore  
 $A$  = drainage area  
 $D$  = dimensionless

## REFERENCES

1. Tiab, D. and Crichlow, H. B.: "Pressure Analysis of Multiple-Sealing-Fault Systems and Bounded Reservoirs by Type-Curve Matching," *SPEJ* (Dec. 1979) 378-392.
2. Tiab, D. and Kumar, A.: "Application of  $p'_D$  Function to Interference Analysis," *JPT* (Aug. 1980) 1465-70.
3. Hurst, W.: "Water Influx into a Reservoir and Its Application to the Equation of Volumetric Balance," *Trans., AIME* (1943) 151, 263-278.
4. Carter, R. D. and Tracy, G. W.: "An Improved Method for Calculating Water Influx," *Trans., AIME* (1960) 219, 415-417.
5. Agarwal, R. G., Al-Hussainy, R. and Ramey, H. J.: "The Importance of Water Influx in Gas Reservoirs," *JPT* (Nov. 1965) 1336-1342; *Trans., AIME* (1965) 234.
6. Bourdet, D., Whittle, T. M., Douglas, A. A., and Pirard, Y. M.: "A New Set of Type Curves Simplifies Well Test Analysis," *World Oil* (May 1983) 95-106.
7. Bourdet, D., Ayoub, J. A., Whittle, T. M., Pirard, Y. M., and Kniazeff, V.: "Interpreting Well Tests in Fractured Reservoirs," *World Oil* (Oct. 1983) 77-87.
8. Bourdet, D., Alagoa, A., Ayoub, J. A., and Pirard, Y. M.: "New Type Curves Aid Analysis of Fissured Zone Well Tests," *World Oil* (April 1984) 111-124.
9. Wong, D. W., Harrington, A. G., and Cinco-Ley, H.: "Application of the Pressure Derivative Function in the Pressure-Transient Testing of Fractured Wells," *SPEFE* (Oct. 1986) 470-80.
10. Suresh, P. K. and Tiab, D.: "Pressure-Derivative Type Curves for Vertically Fractured Wells," *SPEFE* (March 1988) 156-158.

11. Yeh, N. and Reynolds, A. C.: "Analysis of Pressure Data From a Restricted-Entry Well in a Multilayered Reservoir," paper SPE 15584 presented at the 1986 SPE Annual Technical Conference and Exhibition, New Orleans, Oct. 5-8, to appear *SPEFE*.
12. Theis, C. V.: "The Relation Between the Lowering of Piezometric Surface and the Rate and Duration of Discharge of a Well Using Ground-Water Storage," *Trans.*, AGU (1935) 519-524.
13. van Everdingen, A. F. and Hurst, W.: "Application of the Laplace Transformation to Flow Problems in Reservoirs," *Trans.*, AIME (1949) 186, 305-24.
14. Agarwal, R. G., Al-Hussainy, R., and Ramey, H. J. Jr.: "An Investigation of Wellbore Storage and Skin Effects in Unsteady Liquid Flow: I. Analytical Treatment," *SPEJ* (Sept. 1970) 278-290.
15. Earlougher, R. C. Jr. and Kersch, K. M.: "Analysis of Short-Time Transient Test Data by Type-Curve Matching," *JPT* (July 1974) 793-800; *Trans.*, AIME, 257.
16. Gringarten, A. C., Bourdet, D., Landel, P. A., Kniazeff, V. J.: "A Comparison Between Different Skin and Wellbore Storage Type-Curves for Early-Time Transient Analysis," paper SPE 8205 presented at the 1979 SPE Annual Technical Conference and Exhibition, Las Vegas, Sept. 23-26.
17. Gringarten, A. C., Ramey, H. J. Jr., and Raghavan, R.: "Unsteady State Pressure Distribution Created by a Well With a Single Infinite-Conductivity Vertical Fracture," *SPEJ* (Aug. 1974) 347-60; *Trans.*, 257.
18. Gringarten, A. C., Ramey, H. J. Jr., and Raghavan, R.: "Applied Pressure Analysis for Fractured Wells," *JPT* (July 1975) 887-92; *Trans.*, AIME, 259.
19. Gringarten, A. C.: "Reservoir Limit Testing for Fractured Wells," paper SPE 7452 presented at the 1978 SPE Annual Technical Conference and Exhibition, Houston, Oct. 1-3.
20. Cinco, H., Samaniego, F. and Domingues, N.: "Transient Pressure Behavior for a Well With a Finite-Conductivity Vertical Fracture," *SPEJ* (Aug. 1978) 253-264.

21. Agarwal, R., Carter, R. and Pollock, C.: "Evaluation and Performance Prediction of Low-Permeability Gas Wells Stimulated by Massive Hydraulic Fracturing," *JPT* (March 1979) 362-372.
22. Cinco-L., H., Samaniego-V., F.: "Transient Pressure Analysis for Fractured Wells," *JPT* (Sept. 1981) 253-264.
23. Rosato, N., Bennett C., Reynolds, A. C., and Raghavan, R.: "Analysis of Short-Time Buildup Data For Finite Conductivity Fracture," *JPT* (Oct. 1982) 2413-22.
24. Bennett, C., Camacho-V., R., Reynolds, A. C., and Raghavan, R.: " Approximate Solutions for Fractured Wells Producing Layered Reservoirs," *SPEJ* (Oct. 1985) 729-742.
25. Hurst, W.: "Interference Between Oil Fields," *Trans.*, AIME (1960) 219, 175-92.
26. Loucks, T. L. and Guerrero, E. T.: "Pressure Drop in a Composite Reservoir," *SPEJ* (Sept. 1961) 170-76.
27. Larkin, B. K.: "Solutions to the Diffusion Equation for a Region Bounded by a Circular Discontinuity," *SPEJ* (June 1963) 113-15.
28. Carter, R. D.: "Pressure Behavior of a Limited Circular Composite Reservoir," *SPEJ* (Dec. 1966) 328-34.
29. Kazemi, H.: "Pressure Transient Analysis of Naturally Fractured Reservoirs with Uniform Fracture Disribution," *SPEJ* (Dec. 1969) 451-61; *Trans.*, AIME 246.
30. de Swaan-O., A.: "Analytical Solutions for Determining Naturally Fractured Reservoir properties by Well Testing," *SPEJ* (June 1976) 117-22; *Trans.*, AIME 261.
31. Najurieta, H. L.: "A Theory of Pressure Transient Analysis in Naturally Fractured Reservoirs," *JPT* (July 1980) 1241-50.
32. Kucuk, F. and Sawyer, W. K.: "Transient Flow in Naturally Fractured Reservoirs and Its Application to Devonian Gas Shales," paper SPE 9397 presented at the 1980 SPE Annual Fall Technical Conference and Exhibition, Dallas,

Sept. 21-24.

33. Serra, K., Reynolds A. C., and Raghavan, R.: "New Pressure Transient Analysis Methods for Naturally Fractured Reservoirs," *JPT* (Dec. 1983) 2271-83; *Trans.. AIME* 275.
34. Miller, C. C., Dyes, A. B., and Hutchinson, C. A., Jr.: "The Estimation of Permeability and Reservoir Pressure from Bottom Hole Pressure Buildup Characteristics," *Trans., AIME* (1950) 189, 91-104.
35. Matthews, C. S., Brons, F., and Hazebroek, P.: "A Method for Determination of Average Pressure in a Bounded Reservoir," *Trans., AIME* (1954) 201, 182-91.
36. Dietz, D. N.: "Determination of Average Reservoir Pressure from Buildup Surveys," *JPT* (Aug. 1965) 955-59.
37. Horner, D. R.: "Pressure Buildup In Wells," *Proc., Third World Pet. Cong., E. J. Brill, Leiden* (1951) II, 503.
38. Onur, M. and Reynolds, A. C.: "A New Approach for Constructing Derivative Type Curves," SPE paper 16473 (Feb. 1987) Richardson, TX.
39. Ozkan, E., Raghavan, R., and Joshi, S. D.: "Horizontal Well Pressure Analysis," paper SPE 16378 presented at the 1987 SPE California Regional Meeting, Ventura, April 8-10.
40. Onur, M., Yeh, N., and Reynolds, A. C.: "New Applications of the Pressure Derivative in Well Test Analysis," paper SPE 16810 presented at the 1987 SPE Annual Technical Conference and Exhibition, Dallas, Sept. 27-30, to appear *SPEFE*.
41. Duong, A. N.: "A New Set of Type-Curves for Well Test Interpretation Using the Pressure Derivative Ratio," paper SPE 16812 presented at the 1987 SPE Annual Technical Conference and Exhibition, Dallas, Sept. 27-30.
42. Onur, M., Serra, K., and Reynolds, A. C.: "Analysis of Pressure Buildup Data Obtained at a Well Located in a Multi-Well System," paper SPE 18123 presented at the 1988 SPE Annual Technical Conference and Exhibition, Houston, Oct. 2-5.



43. Bilhartz, H. H., Jr. and Ramey, H. J., Jr.: "The Combined Effects of Storage, Skin and Partial Penetration on Well Test Analysis," paper SPE 6753 presented at the 1977 SPE Annual Technical Conference and Exhibition, Denver, Oct. 9-12.
44. Hamming, R. W.: *Numerical Methods for Scientists and Engineers*, 2<sup>nd</sup> ed., Mc Graw-Hill Book Co., Inc., New York, N. Y., (1973), 227-495.
45. Dorn, W. S. and McCracken, D.: *Numerical Methods With Fortran IV Case Studies*, John Wiley & Sons, Inc., New York, N. Y., (1972), 219-56.
46. Burden, R. L., Faires, J. D., and Reynolds, A. C.: *Numerical Analysis*, 2<sup>nd</sup> ed., Prindle, Weber & Schmidt, Boston, Massachusetts, (1981), 124-172.
47. Bourdet, D., Ayoub, J. A., and Pirard, Y. M.: "Use of Pressure Derivative in Well Test Interpretation," paper SPE 12777 presented at the 1987 California Regional Meeting, Long Beach, April 11-13.
48. Agarwal, R. G.: "A New Method to Account for Producing Time Effects When Drawdown Type Curves Are Used to Analyze Pressure Buildup and Other Test Data," paper SPE 9289 presented at the 1980 SPE Annual Technical Conference and Exhibition, Dallas, Sept. 21-24.
49. Raghavan, R.: "The Effects of Producing Time on Type Curve Analysis," *JPT* (June 1980) 1053-1064.
50. Al-Hussainy, R., Ramey, H. J. Jr., and Crawford, P. M.: "The Flow of Real Gases Through Porous Media," *JPT* (May 1966) 624-636.
51. Agarwal, R. G.: "Real Gas Pseudo-Time - A New Function for Pressure Buildup of MHF Gas Wells," paper SPE 8270 presented at the 1979 SPE Annual Technical Conference and Exhibition, Las Vegas, Sept. 23-26.
52. Reynolds, A. C., Bratvold, R. and Ding, W.: "Semilog Analysis of Gas Well Drawdown and Buildup Data," *SPEFE* (Dec. 1987) 657-670.
53. Spivey, J. P. and Lee, W. J.: "A Comparison of the Use of Pseudotime and Normalized Time for Gas Well Buildup Analysis in Various Geometries," paper SPE 15580 presented at the 1986 SPE Annual Technical Conference and Exhibition, New Orleans, Oct. 5-8.

54. Earlougher, R. C., Jr.: *Advances in Well Testing*, Monograph Series, SPE, Richardson, TX (1977) 5.
55. Chow, V. T.: "On the Determination of Transmissibility and Storage Coefficients From Pumping Test Data," *Trans.*, AGU (June 1952) 397-404.
56. Jargon, J. R.: "Effect of Wellbore Storage and Well Damage at the Active Well on the Interference Test Analysis," *JPT* (Aug. 1976) 851-858.
57. Tongpenyai, J. and Raghavan, R.: "The Effect of Wellbore Storage and Skin on Interference Test Data," *JPT* (Jan. 1981) 151-160.
58. Peres, A. Serra, K. and Reynolds, A. C.: "Towards a Unified Theory of Well Testing for Nonlinear Radial Flow Problems With Applications to Interference Tests," paper SPE 18113 presented at 1988 SPE Annual Technical Conference and Exhibition, Houston, Oct. 2-5.
59. Stehfest, H.: "Algorithm 368, Numerical Inversion of Laplace Transforms," *Communications of the ACM* (Jan. 1970) 13, No. 1, 47-49.
60. Soliman, M. Y.: "Analysis of Buildup Tests With Short Producing Time," *SPEFE* (Aug. 1986) 353-357.
61. Ozkan, E., Vo, D. T., and Raghavan, R.: "Some Applications of Pressure Derivative Analysis Procedure," paper SPE 16811 presented at the 1987 SPE Annual Technical and Exhibition, Dallas, Sept. 27-30.
62. Fraim, M. L. and Lee, W. J.: "Determination of Formation Properties From Long-Term Gas Well Production Affected by Non-Darcy Flow," paper SPE 16934 presented at the 1987 SPE Annual Technical Conference and Exhibition, Dallas, Sept. 27-30.
63. Ramey, H. J., Jr., and Gringarten, A. C.: "Effect of High-Volume Vertical Fractures on Geothermal Steam Well Behavior," paper presented at Second United Nations Symposium on Geothermal Energy, San Francisco, May 20-29, 1975.
64. Raghavan, R.: "Some Practical Considerations in the Analysis of Pressure Data," *JPT* (Oct. 1976) 1256-1268.
65. Bennett, C. O.: *Analysis of Fractured Wells*, Ph.D. Dissertation, University of

- Tulsa (1982).
66. Cinco-L., H., Samaniego-V., F. and Rodriguez, F.: "Application of Pseudo-Linear Flow Model to the Pressure Transient Analysis of Fractured Wells," paper SPE 13059 presented at the 1984 SPE Annual Technical Conference and Exhibition, Houston, Sept. 16-19.
  67. Barker, B. J. and Ramey, H. J., Jr.: "Transient Flow to Finite-Conductivity Vertical Fractures," paper SPE 7489 presented at the 1978 SPE Annual Technical Conference and Exhibition, Houston, Oct. 1-3.
  68. Bennett, C., Rosato, N., Reynolds, A. and Raghavan, R.: "Effect of Fracture Heterogeneity and Wing Length on the Response of Fractured Wells," *SPEJ* (April 1983) 219-230.
  69. Bennett, C., Reynolds, A., Raghavan, R. and Elbel, J.: "Performance of Finite-Conductivity, Vertically Fractured Wells in Single Layer Reservoirs," *SPEFE* (Aug. 1986) 399-412.
  70. Bennett, C., Raghavan, R. and Reynolds, A.: "Analysis of Finite-Conductivity Vertical Fracture Intercepting Multi-Layer Commingled Reservoirs," *SPEFE* (June 1986) 259-274.
  71. Camacho-V., R., Raghavan, R. and Reynolds, A.: "Response of Wells Producing Layered Reservoirs: Unequal Fracture Length," *SPEFE* (March 1987) 9-28.
  72. Earlougher, R. C., Jr., Ramey, H. J., Jr., Miller, F. G., and Mueller, T. D.: "Pressure Distributions in Rectangular Reservoirs," *JPT* (Feb. 1968) 199-208; *Trans., AIME*, **243**.
  73. Larsen, L.: "A Simple Approach to Pressure Distributions in Geometric Shapes," *SPEJ* (Feb. 1985) 113-120.
  74. Proano, E. A. and Lilley, I. J.: "Derivative of Pressure: Application to Bounded Reservoir Interpretation," paper SPE 15861 presented at the 1986 SPE European Petroleum Conference, London, Oct. 20-22
  75. Brons, F. and Miller, W. C.: "A Simple Method for Correcting Spot Pressure Readings," *JPT* (Aug. 1961) 803-805; *Trans., AIME* **222**.

76. Locke, C. D. and Sawyer, W. K.: "Constant Pressure Injection Test in a Fractured Reservoir - History Match Using Numerical Simulation and Type Curve Analysis," paper SPE 5594 presented at the 1975 SPE Annual Technical Conference and Exhibition, Dallas, Sept. 28 - Oct. 1.
77. Streltsova, T. D.: "Well Pressure Behavior of a Naturally Fractured Reservoir," *SPEJ* (Oct. 1983) 769-780.
78. Barenblatt, G. E., Zheltov, I. P. and Kochina, I. N.: "Basic Concepts in the Theory of Seepage of Homogeneous Liquids in Fissured Rocks," *J. Appl. Math. Mech.* (May 1960) 24, 1286-1303.
79. Warren, J. E. and Root, P. J.: "The Behavior of Naturally Fractured Reservoirs," *SPEJ* (Sept. 1963) 245-255; *Trans.*, AIME, 228.
80. Bourdet, D. and Gringarten, A. C.: "Determination of Fissured Volume and Block Size in Fractured Reservoirs by Type-Curve Analysis," paper SPE 9293 presented at the 1980 SPE Annual Technical Conference and Exhibition, Dallas, Sept. 21-24.
81. Rosa, A. J.: *Automated Type Curve Matching in Well Test Analysis*, M.S. Thesis, Stanford University (1983).
82. Barua, J., Horne, R. N., Greenstadt, J. L. and Lopez, L.: "Improved Estimation Algorithms for Automated Type-Curve Analysis of Well Tests," *SPEFE* (March 1988) 186-196.
83. Kozik, H. G. and Holditch, S. A.: "A Case History for Massive Hydraulic Fracturing the Cotton Valley Lime Matrix, Fallon and Personville Fields," *JPT* (Feb. 1981) 229-244.
84. Yeh, N. S., Davison, M. J. and Raghavan, R.: "Fractured Well Responses in Heterogeneous Systems: Application to Devonian Shale and Austin Chalk Reservoirs," *J. Energy Res. Tech.* (June 1986) 120-130.
85. Ramey, H. J., Jr. and Cobb, W. M.: "A General Buildup Theory for a Well in a Closed Drainage Area," *JPT* (Dec. 1971) 1493-1505.
86. Odeh, A. S. and Al-Hussainy, R.: "A Method for Determining the Static Pressure of a Well from Buildup Data," *JPT* (May 1971) 621-624.

87. Slider, H. C.: "A Simplified Method of Pressure Buildup Analysis for a Stabilized Well," *JPT* (Sept. 1971) 1155-1160; *Trans.*, AIME 251.
88. Larsen, L.: "Limitations on the Use of Single and Multiple Horner, Miller-Dyes-Hutchinson, and Matthews-Brons-Hazebroek Analysis," paper SPE 12135 presented at the 1983 SPE Annual Technical Conference and Exhibition, San Francisco, CA, Oct. 5-8.
89. Denson, A. H., Smith, J. T. and Cobb, W. M.: "Determining Well Drainage Pore Volume and Porosity from Pressure Buildup Tests," *SPEJ* (Aug. 1976) 209-216.
90. Codreanu, D. B.: "A Simple Buildup Analysis (CPM) Method that Allows the Determination of Well Drainage Area and Drawdown Pressure for a Stabilized Well," paper SPE 15977, Richardson, TX, (July 1986).
91. Odeh, A. S. and Nabor, G. W.: "The Effect of Production History on Determination of Formation Characteristics from Flow Tests," *JPT* (Oct. 1966) 1343-1350.
92. Stein, M. H.: "Dimensionless Pressure of a Vertically Fracture Well Surrounded by Offset Wells," paper SPE 15639 presented at the 1986 SPE Annual Technical Conference and Exhibition, New Orleans, Oct. 5-8.
93. Chen, H. K. and Brigham, W. E.: "Pressure Buildup for a Well With Storage and Skin in a Closed Square," *JPT* (Jan. 1978) 141-46; *Trans.*, AIME, 265.
94. Vongvuthipornchai, S. and Raghavan, R.: "A Note on the Duration of the Transitional Period of Responses Influenced by Wellbore Storage and Skin," *SPEFE* (March 1988) 207-14.
95. Raghavan, R.: *Well Testing I Class Notes*, The University of Tulsa, OK, Fall 1984.
96. Schapery, R. A.: "Approximate Methods of Transform Inversion for Viscoelastic Stress Analysis," Proc. Fourth U.S National Congress of Applied Mechanics (1961) 1075-1085.

**APPENDIX A**  
**SHORT AND LONG TIME APPROXIMATIONS**  
**PLANAR FRACTURES; DRAWDOWN**

Here, we derive short and long time approximations for the dimensionless pressure drop  $p_{wD}$  (Eq. 3.1.22) and its logarithmic derivative  $p'_{wD}$  (Eq. 3.1.25) for a planar (either uniform-flux or infinite-conductivity) fractured well.

Recalling Eqs. 3.1.22 and 3.1.25, respectively, give

$$p_{wD} = \frac{1}{2} \sqrt{\pi t_{x,D}} \left[ \operatorname{erf} \left( \frac{1-x_D}{2\sqrt{t_{x,D}}} \right) + \operatorname{erf} \left( \frac{1+x_D}{2\sqrt{t_{x,D}}} \right) \right] - \frac{1-x_D}{4} \operatorname{Ei} \left[ -\frac{(1-x_D)^2}{4t_{x,D}} \right] - \frac{1+x_D}{4} \operatorname{Ei} \left[ -\frac{(1+x_D)^2}{4t_{x,D}} \right], \quad (A-1)$$

and

$$p'_{wD} = \frac{1}{4} \sqrt{\pi t_{x,D}} \left[ \operatorname{erf} \left( \frac{1-x_D}{2\sqrt{t_{x,D}}} \right) + \operatorname{erf} \left( \frac{1+x_D}{2\sqrt{t_{x,D}}} \right) \right], \quad (A-2)$$

where  $x_D = 0.0$  for an uniform-flux fracture and  $x_D = 0.732$  for an infinite-conductivity fracture.

#### Short Time Approximations

Dividing both sides of Eqs. A-1 and A-2 by  $\sqrt{\pi t_{x,D}}$  give, respectively,

$$\frac{p_{wD}}{\sqrt{\pi t_{x,D}}} = \frac{1}{2} \left[ \operatorname{erf} \left( \frac{1-x_D}{2\sqrt{t_{x,D}}} \right) + \operatorname{erf} \left( \frac{1+x_D}{2\sqrt{t_{x,D}}} \right) \right] - \frac{1-x_D}{4\sqrt{\pi t_{x,D}}} \operatorname{Ei} \left[ -\frac{(1-x_D)^2}{4t_{x,D}} \right] - \frac{1+x_D}{4\sqrt{\pi t_{x,D}}} \operatorname{Ei} \left[ -\frac{(1+x_D)^2}{4t_{x,D}} \right], \quad (A-3)$$

and

$$\frac{p'_{wD}}{\sqrt{\pi t_{x,D}}} = \frac{1}{4} \left[ \operatorname{erf} \left( \frac{1-x_D}{2\sqrt{t_{x,D}}} \right) + \operatorname{erf} \left( \frac{1+x_D}{2\sqrt{t_{x,D}}} \right) \right]. \quad (A-4)$$

Taking the limits of Eqs. A-3 and A-4 as  $t_{x,D}$  approaches zero, we obtain

$$\lim_{t_{x,D} \rightarrow 0} \frac{p_{wD}}{\sqrt{\pi t_{x,D}}} = \frac{1}{2} \lim_{t_{x,D} \rightarrow 0} \left[ \operatorname{erf} \left( \frac{1-x_D}{2\sqrt{t_{x,D}}} \right) + \operatorname{erf} \left( \frac{1+x_D}{2\sqrt{t_{x,D}}} \right) \right] + \lim_{t_{x,D} \rightarrow 0} \left\{ -\frac{1-x_D}{4\sqrt{\pi t_{x,D}}} \operatorname{Ei} \left[ -\frac{(1-x_D)^2}{4t_{x,D}} \right] - \frac{1+x_D}{4\sqrt{\pi t_{x,D}}} \operatorname{Ei} \left[ -\frac{(1+x_D)^2}{4t_{x,D}} \right] \right\}, \quad (A-5)$$

and

$$\lim_{t_{x,D} \rightarrow 0} \frac{p'_{wD}}{\sqrt{\pi t_{x,D}}} = \frac{1}{4} \lim_{t_{x,D} \rightarrow 0} \left[ \operatorname{erf} \left( \frac{1-x_D}{2\sqrt{t_{x,D}}} \right) + \operatorname{erf} \left( \frac{1+x_D}{2\sqrt{t_{x,D}}} \right) \right]. \quad (A-6)$$

Since,

$$\begin{aligned} \lim_{t_{x,D} \rightarrow 0} \operatorname{erf} \left( \frac{1 \pm x_D}{2\sqrt{t_{x,D}}} \right) &= \frac{2}{\sqrt{\pi}} \lim_{t_{x,D} \rightarrow 0} \int_0^{\frac{1 \pm x_D}{2\sqrt{t_{x,D}}}} \exp(-r^2) dr \\ &= \frac{2}{\sqrt{\pi}} \int_0^{\infty} \exp(-r^2) dr = 1, \end{aligned} \quad (A-7)$$

for  $0 \leq x_D < 1$ , it follows that

$$\lim_{t_{x,D} \rightarrow 0} \left[ \operatorname{erf} \left( \frac{1 - x_D}{2\sqrt{t_{x,D}}} \right) + \operatorname{erf} \left( \frac{1 + x_D}{2\sqrt{t_{x,D}}} \right) \right] = 2. \quad (A-8)$$

Since,

$$\frac{-\operatorname{Ei} \left[ -\frac{(1 \pm x_D)^2}{4t_{x,D}} \right]}{\sqrt{\pi t_{x,D}}} = \frac{\int_0^{\infty} \frac{(1 \pm x_D)^2}{4t_{x,D}} \frac{\exp(-r)}{r} dr}{\sqrt{\pi t_{x,D}}} \equiv L, \quad (A-9)$$

by taking the limit of Eq. A-9 as  $t_{x,D}$  approaches zero and applying l'Hôpital's rule, we obtain

$$\lim_{t_{x,D} \rightarrow 0} L = \frac{\exp \left[ -\frac{(1 \pm x_D)^2}{4t_{x,D}} \right] (1/t_{x,D})}{\frac{\sqrt{\pi}}{2} (1/\sqrt{t_{x,D}})},$$

or

$$= \frac{2}{\sqrt{\pi}} \lim_{t_{x,D} \rightarrow 0} \frac{(1/\sqrt{t_{x,D}})}{\exp \left[ \frac{(1 \pm x_D)^2}{4t_{x,D}} \right]}. \quad (A-10)$$

Since Eq. A-10 is in indeterminate form of  $\infty/\infty$ , applying l'Hôpital's rule once more, it can be shown that

$$\lim_{t_{x,D} \rightarrow 0} L = \frac{4}{\sqrt{\pi} (1 \pm x_D)^2} \lim_{t_{x,D} \rightarrow 0} \sqrt{t_{x,D}} \exp \left[ -\frac{(1 \pm x_D)^2}{4t_{x,D}} \right] = 0; \quad (A-11)$$

thus, it follows that

$$\lim_{t_{x,D} \rightarrow 0} \frac{-\operatorname{Ei} \left[ -\frac{(1 \pm x_D)^2}{4t_{x,D}} \right]}{\sqrt{\pi t_{x,D}}} = 0. \quad (A-12)$$

It follows easily from Eq. A-12 that

$$\lim_{t_{x,D} \rightarrow 0} \left\{ -\frac{1 - x_D}{4\sqrt{\pi t_{x,D}}} \operatorname{Ei} \left[ -\frac{(1 - x_D)^2}{4t_{x,D}} \right] - \frac{1 + x_D}{4\sqrt{\pi t_{x,D}}} \operatorname{Ei} \left[ -\frac{(1 + x_D)^2}{4t_{x,D}} \right] \right\} = 0. \quad (A-13)$$



Using Eqs. A-8 and A-13 in Eq. A-5 gives

$$\lim_{t_{x,D} \rightarrow 0} \frac{p_{wD}}{\sqrt{\pi t_{x,D}}} = 1, \quad (A-14)$$

and similarly using Eq. A-8 in Eq. A-6, we obtain

$$\lim_{t_{x,D} \rightarrow 0} \frac{p'_{wD}}{\sqrt{\pi t_{x,D}}} = \frac{1}{2}, \quad (A-15)$$

or

$$\lim_{t_{x,D} \rightarrow 0} \frac{2p'_{wD}}{\sqrt{\pi t_{x,D}}} = 1. \quad (A-16)$$

### Long Time Approximations

As is well known, the exponential-integral function,  $-\text{Ei}(-x)$ , is well approximated by

$$-\text{Ei}(-x) = -\ln(e^\gamma x) \quad (A-17)$$

provided that  $x$  is sufficiently small. Thus it follows directly from Eq. A-17 that for sufficiently large values of  $t_{x,D}$ , the following holds

$$-\text{Ei} \left[ -\frac{(1 \pm x_D)^2}{4t_{x,D}} \right] = \ln \left[ \frac{4t_{x,D}}{e^\gamma (1 \pm x_D)^2} \right]. \quad (A-18)$$

Replacing each exponential-integral function in Eq. A-1 with its appropriate logarithmic approximation given by the right side of Eq. A-18, Eq. A-1 can be written as

$$p_{wD} = \frac{1}{2} \sqrt{\pi t_{x,D}} \left[ \text{erf} \left( \frac{1-x_D}{2\sqrt{t_{x,D}}} \right) + \text{erf} \left( \frac{1+x_D}{2\sqrt{t_{x,D}}} \right) \right] + \frac{1}{2} \ln(t_{x,D}) + \sigma(x_D), \quad (A-19)$$

where  $\sigma(x_D)$  is given by

$$\sigma(x_D) = -\frac{(1-x_D)}{2} \ln(1-x_D) - \frac{(1+x_D)}{2} \ln(1+x_D) + 0.404544. \quad (A-20)$$

Since,

$$\frac{\frac{\sqrt{\pi}}{2} \text{erf}(x)}{x} = \frac{\int_0^x \exp(-r^2) dr}{x} \equiv R, \quad (A-21)$$

by taking the limit of Eq. A-21 as  $x$  approaches zero and applying l'Hôpital's rule, it can be shown that

$$\lim_{x \rightarrow 0} R = \lim_{x \rightarrow 0} \frac{\exp(-x^2)}{1} = 1; \quad (A-22)$$

thus, for sufficiently small values of  $x$ , the following approximation holds:

$$\frac{\sqrt{\pi}}{2} \operatorname{erf}(x) \approx x. \quad (A-23)$$

For sufficiently large values of  $t_{x,D}$ , it follows directly from Eq. A-23 that

$$\frac{\sqrt{\pi}}{2} \operatorname{erf}\left(\frac{1 \pm x_D}{2\sqrt{t_{x,D}}}\right) \approx \frac{(1 \pm x_D)}{2\sqrt{t_{x,D}}}, \quad (A-24)$$

or

$$\sqrt{\pi t_{x,D}} \operatorname{erf}\left(\frac{1 \pm x_D}{2\sqrt{t_{x,D}}}\right) \approx (1 \pm x_D). \quad (A-25)$$

Using the approximation given by Eq. A-23, Eq. A-16 can be approximated by

$$p_{wD} = \frac{1}{2} [\ln(t_{x,D}) + 2(\sigma(x_D) + 1)], \quad (A-26)$$

or defining  $c$  by

$$c = 2[\sigma(x_D) + 1], \quad (A-27)$$

$$p_{wD} = \frac{1}{2} [\ln(t_{x,D}) + c], \quad (A-28)$$

where  $c = 2.80907$  for  $x_D = 0$  (uniform-flux fracture), and  $c = 2.2$  for  $x_D = 0.732$  (infinite-conductivity fracture).

Finally, it follows from Eq. A-28 that

$$\lim_{t_{x,D} \rightarrow \infty} \frac{p_{wD}}{0.5 [\ln(t_{x,D}) + c]} = 1, \quad (A-29)$$

and replacing each  $\sqrt{\pi t_{x,D}}$  erf term in Eq. A-2 by the approximation given by Eq. A-23, and taking the limits of the resulting equation as  $t_{x,D} \rightarrow \infty$ , one can easily establish the following long time approximation for  $p'_{wD}$ :

$$\lim_{t_{x,D} \rightarrow \infty} 2p'_{wD} = 1. \quad (A-30)$$

**APPENDIX B**  
**SHORT AND LONG TIME APPROXIMATIONS**  
**PLANAR FRACTURES; BUILDUP**

The purpose of this appendix is to present the derivations of short and long time asymptotic formulas reported in Section 3.1.4 for the dimensionless buildup pressure change,  $\tilde{p}_{sD}$ , and its logarithmic derivative with respect to Agarwal's equivalent time<sup>48</sup>,  $\tilde{p}'_{sD}$ . The results presented apply to uniform-flux and infinite-conductivity fractures.

As noted in Section 3.1.4, from a well known superposition result, the dimensionless buildup pressure change,  $\tilde{p}_{sD}$ , can be expressed in terms of the dimensionless drawdown pressure change,  $p_{wD}$ , as

$$\tilde{p}_{sD} = p_{wD} (\Delta t_{x_f D}) + [-p_{wD} (t_{px_f D} + \Delta t_{x_f D}) + p_{wD} (\Delta t_{x_f D})], \quad (B-1)$$

and the logarithmic derivative of Eq. B-1 with respect to Agarwal's dimensionless equivalent time<sup>48</sup>,  $t_{eD}$  (Eq. 3.1.42) is given by

$$\begin{aligned} \frac{\tilde{p}'_{sD}}{\sqrt{\pi t_{eD}}} &= \frac{(\Delta t_{x_f D})^2}{4\sqrt{t_{eD} t_{eD}}} \left[ \frac{\sqrt{\Delta t_{x_f D}}}{\Delta t_{x_f D}} \left[ \operatorname{erf} \left( \frac{1-x_D}{2\sqrt{\Delta t_{x_f D}}} \right) + \operatorname{erf} \left( \frac{1+x_D}{2\sqrt{\Delta t_{x_f D}}} \right) \right] \right. \\ &\quad \left. - \frac{\sqrt{t_{px_f D} + \Delta t_{x_f D}}}{(t_{px_f D} + \Delta t_{x_f D})} \left[ \operatorname{erf} \left( \frac{1-x_D}{2\sqrt{t_{px_f D} + \Delta t_{x_f D}}} \right) + \operatorname{erf} \left( \frac{1+x_D}{2\sqrt{t_{px_f D} + \Delta t_{x_f D}}} \right) \right] \right], \quad (B-2) \end{aligned}$$

where  $x_D = 0.0$  for an uniform-flux fracture and  $x_D = 0.732$  for an infinite-conductivity fracture.

### Short Time Approximations

If  $\Delta t_{x_f D} \ll t_{px_f D}$  so that  $t_{eD} \approx \Delta t_{x_f D}$ , and the terms within the square brackets of Eq. B-1 can be neglected, then Eq. B-1 can be well approximated by the following equation:

$$\tilde{p}_{sD} = p_{wD} (\Delta t_{x_f D}) = p_{wD} (t_{eD}). \quad (B-3)$$

For sufficiently small values of time  $t_{eD} = t_{px_f D} \Delta t_{x_f D} / (\Delta t_{x_f D} + t_{px_f D}) \approx \Delta t_{x_f D}$  and  $p_{wD} (\Delta t_{x_f D}) \approx p_{wD} (t_{eD}) \approx \sqrt{\pi t_{eD}}$ . Thus,

$$\lim_{t_{eD} \rightarrow 0} \frac{\tilde{p}_{sD}}{\sqrt{\pi t_{eD}}} = \lim_{t_{eD} \rightarrow 0} \frac{p_{wD} (t_{eD})}{\sqrt{\pi t_{eD}}} = 1. \quad (B-4)$$

Applying the same underlying assumptions stated above to Eq. B-2 and taking the limits of the resulting equation as  $t_{eD}$  approaches zero, one can establish the following equation:

$$\lim_{t_{eD} \rightarrow 0} \frac{\tilde{p}'_{sD}}{\sqrt{\pi t_{eD}}} = \frac{1}{4} \lim_{t_{eD} \rightarrow 0} \left[ \operatorname{erf} \left( \frac{1-x_D}{2\sqrt{t_{eD}}} \right) + \operatorname{erf} \left( \frac{1+x_D}{2\sqrt{t_{eD}}} \right) \right] - \frac{1}{4\sqrt{t_{pxjD}}} \left[ \operatorname{erf} \left( \frac{1-x_D}{2\sqrt{t_{pxjD}}} \right) + \operatorname{erf} \left( \frac{1+x_D}{2\sqrt{t_{pxjD}}} \right) \right] \lim_{t_{eD} \rightarrow 0} \sqrt{t_{eD}}. \quad (B-5)$$

Since the first limit on the right side of Eq. B-4 is equal to 2 (see Appendix A) and the second limit is zero, it follows that

$$\lim_{t_{eD} \rightarrow 0} \frac{\tilde{p}'_{sD}}{\sqrt{\pi t_{eD}}} = \frac{1}{2}, \quad (B-6)$$

or

$$\lim_{t_{eD} \rightarrow 0} \frac{2\tilde{p}'_{sD}}{\sqrt{\pi t_{eD}}} = 1. \quad (B-7)$$

Note that Eq. 3.1.55 (or Eq. 3.1.56) can be obtained directly from Eqs. B-4 and B-7.

### Long Time Approximations

For sufficiently large values of shut-in time,  $\Delta t_{xjD}$ , so that drawdown terms  $p_{wD}(\Delta t_{xjD})$  and  $p_{wD}(t_{pxjD} + \Delta t_{xjD})$  can be replaced by their logarithmic approximations as given by Eq. A-21, Eq. B-1 can be approximated by the following equation:

$$\tilde{p}_{sD} = \frac{1}{2} \ln(t_{eD}) + p_{wD}(t_{pxjD}) - \frac{1}{2} \ln(t_{pxjD}). \quad (B-8)$$

Taking limits as  $\Delta t_{xjD} \rightarrow \infty$ ; that is,  $t_{eD}$  approaches  $t_{pxjD}$  (see Eq. 3.1.42), we can establish the following equation:

$$\lim_{t_{eD} \rightarrow t_{pxjD}} \tilde{p}_{sD} = p_{wD}(t_{pxjD}). \quad (B-9)$$

For sufficiently large values of  $\Delta t_{xjD}$  so that the approximation given by the right side of Eq. A-20 can be applied to each "erf" function term on the right side of Eq. B-2, the following equation for  $\tilde{p}'_{sD}$  applies:

$$2\tilde{p}'_{sD} = \frac{\Delta t_{xjD}}{t_{eD}} \left[ \frac{t_{pxjD}}{(t_{pxjD} + \Delta t_{xjD})} \right], \quad (B-10)$$

or

$$2\tilde{p}'_{eD} = 1. \quad (B-11)$$

Taking the limits in both sides of Eq. B-11 as  $t_{eD}$  approaches  $t_{px,D}$ , one obtains Eq. 3.1.58. Moreover, dividing Eq. B-9 by Eq. 3.1.58 gives Eq. 3.1.59.

**APPENDIX C**  
**DERIVATIONS OF EQS. 3.1.116 THROUGH 3.1.118**  
**CONSTANT PRESSURE PRODUCTION**

In this appendix, we derive the dimensionless rate expressions given by Eqs. 3.1.116, 3.1.117 and 3.1.118 for a planar fractured (either uniform-flux or infinite-conductivity) well produced at a constant wellbore pressure in a closed square reservoir.

For a planar fractured well produced at a constant rate in a closed square reservoir, we have noted that there exist three distinct flow regimes exhibited by the dimensionless well pressure drop  $p_{wD}$ . These are linear flow period at which the dimensionless pressure drop,  $p_{wD}$  is given by

$$p_{wD} = \sqrt{\pi t_{x_f D}}, \quad (C-1)$$

pseudoradial flow period at which  $p_{wD}$  is given by

$$p_{wD} = \frac{1}{2} [\ln(t_{x_f D}) + c], \quad (C-2)$$

and pseudosteady-state flow period at which  $p_{wD}$  is given by

$$p_{wD} = 2\pi t_{AD} + a_{c_f}, \quad (C-3)$$

where  $a_{c_f}$  is defined by Eq. 3.1.118.

The Laplace space solutions of Eqs. C-1, C-2 and C-3 with respect to dimensionless time  $t_{x_f D}$  are given, respectively, by the following equations:

$$\bar{p}_{wD} = \frac{\pi}{2} \frac{1}{u\sqrt{u}}, \quad (C-4)$$

$$\bar{p}_{wD} = \frac{1}{2u} [-\ln(u) + c - \gamma], \quad (C-5)$$

and

$$\bar{p}_{wD} = 2\pi \frac{L_{x_f}^2}{A} \frac{1}{u^2} + \frac{1}{u} a_{c_f}. \quad (C-6)$$

Here  $\bar{p}_{wD}$  denotes the Laplace transform of the dimensionless pressure drop,  $p_{wD}$ , defined by Eq. 2.1.1,  $u$  denotes the Laplace transform variable with respect to  $t_{x_f D}$ , and  $\gamma (= 0.57722)$  is the Euler's constant.



From the well known superposition result of van Everdingen and Hurst<sup>13</sup>, It follows that the Laplace space solution of dimensionless pressure for the constant rate case; i.e.,  $\bar{p}_{wD}$  is related to the Laplace space solution of the dimensionless rate for the constant wellbore pressure case by the following relation:

$$\bar{q}_D(u) \bar{p}_{wD}(u) = \frac{1}{u^2}, \quad (C-7)$$

where  $q_D$  is the dimensionless well rate defined by Eq. 3.1.100. Thus, using Eqs. C-4, C-5 and C-6 in Eq. C-7, the following Laplace space solutions for the dimensionless rate  $q_D$ , respectively, can be obtained:

$$\bar{q}_D(u) = \frac{2}{\pi} \frac{1}{\sqrt{u}}, \quad (C-8)$$

$$\bar{q}_D(u) = \left[ \frac{u}{2} (-\ln u + c - \gamma) \right]^{-1}. \quad (C-9)$$

and

$$\bar{q}_D(u) = \left[ 2\pi \frac{L_{x_f}^2}{A} + u a_{c_f} \right]^{-1}. \quad (C-10)$$

Inverting Eq. C-7 gives

$$q_D(t_{x_fD}) = \frac{2}{\pi} \frac{1}{\sqrt{\pi t_{x_fD}}}, \quad (C-11)$$

which applies during linear flow period. Inversion of Eq. C-9 can be accomplished by using the Schapery<sup>96</sup> approximation as modified by Najurieta<sup>31</sup>; i.e., the inverse Laplace transform of  $\bar{q}_D$  can be approximated by

$$q_D(t_{x_fD}) = (u\bar{q}_D)_{u=\frac{1}{0.5t_{x_fD}}}. \quad (C-12)$$

Applying Eq. C-12 to Eq. C-9, we obtain

$$q_D(t_{x_fD}) = \frac{1}{0.5 [\ln(t_{x_fD}) + c]}, \quad (C-13)$$

which applies during pseudoradial flow period. Finally inverting Eq. C-10, we obtain

$$q_D = \frac{1}{a_{c_f}} \exp \left[ -\frac{2\pi t_{AD}}{a_{c_f}} \right], \quad (C-14)$$

which applies during pseudosteady-state flow period.

**APPENDIX D**  
**DERIVATIONS OF EQS. 3.2.11 THROUGH 3.2.13**  
**COMPOSITE RESERVOIR**

In this appendix, we derive Eqs. 3.2.11 through 3.2.13. The Laplace space analytical solution of dimensionless well pressure drop due to a line source well producing at a constant rate in a composite infinite-acting reservoir was given by Hurst<sup>35</sup> as

$$\bar{p}_{wD1}(u) = \frac{1}{u} [K_0(\sqrt{u}) + I_0(\sqrt{u}) \Lambda(u)], \quad (D-1)$$

where  $\Lambda(u)$  is given by

$$\Lambda(u) = \frac{K_0(r_{sD}\sqrt{\eta_r u}) K_1(r_{sD}\sqrt{u}) - (\sqrt{\eta_r}/\lambda_r) K_0(r_{sD}\sqrt{u}) K_1(r_{sD}\sqrt{\eta_r u})}{K_0(r_{sD}\sqrt{\eta_r u}) I_1(r_{sD}\sqrt{u}) + (\sqrt{\eta_r}/\lambda_r) I_0(r_{sD}\sqrt{u}) K_1(r_{sD}\sqrt{\eta_r u})}. \quad (D-2)$$

Here  $\bar{p}_{wD1}$  denotes the Laplace transform of dimensionless well pressure drop defined in terms of the properties of inner zone (see Eq. 3.2.7),  $u$  denotes the Laplace transform variable with respect to dimensionless time  $t_{D1}$  defined in terms of the properties of inner zone, and  $r_{sD}$ ,  $\lambda_r$  and  $\eta_r$ , respectively, denote the dimensionless radius of inner zone defined by Eq. 3.2.2, the mobility ratio defined by Eq. 3.2.3 and the diffusivity ratio defined by Eq. 3.2.4. In Eqs. D-1 and D-2,  $I_0$  and  $K_0$  denote, respectively, the modified Bessel's functions of the first and second kind of order zero, and  $I_1$  and  $K_1$  denote, respectively, the modified Bessel's functions of the first and second kind of order one.

The long time approximation to Eq. D-1 can be obtained by assuming that Laplace variable  $u$  is sufficiently small so that various Bessel's functions in Eq. D-1 can be approximated by their following asymptotic formulas:

$$K_0(z) \approx -\ln\left(\frac{e^\gamma z}{2}\right), \quad (D-3)$$

$$zK_1(z) \approx 1, \quad (D-4)$$

$$I_0(z) \approx 1, \quad (D-5)$$

and

$$I_1(z) \approx 0. \quad (D-6)$$

Using the limiting forms of Bessel's functions given above in Eq. D-1 and simplifying the resulting equation, one obtains

$$\bar{p}_{wD1} = \frac{1}{u} \left[ -\ln \left( \frac{e^\gamma \sqrt{u}}{2} \right) + (1 - \lambda_r) \ln \left( \frac{e^\gamma r_{sD} \sqrt{u}}{2} \right) - \frac{\lambda_r}{2} \ln(\eta_r) \right]. \quad (D-7)$$

Inverting Eq. D-7 to real space gives

$$p_{wD1} = \frac{1}{2} \ln \left( \frac{4t_{D1}}{e^\gamma} \right) - \frac{(1 - \lambda_r)}{2} \ln \left( \frac{4t_{D1}}{e^\gamma r_{sD}^2} \right) - \frac{\lambda_r}{2} \ln(\eta_r). \quad (D-8)$$

Eq. D-8 further can be reduced to

$$\frac{p_{wD1}}{\lambda_r} = \frac{1}{2} \ln \left( \frac{4t_{D1}}{e^\gamma \eta_r} \right) + \frac{(1 - \lambda_r)}{\lambda_r} \ln(r_{sD}). \quad (D-9)$$

Since  $(p_{wD1}/\lambda_r) = p_{wD2}$ ,  $(t_{D1}/\eta_r) = t_{D2}$ , and  $\lambda_r = (\lambda_1/\lambda_2)$ , Eq. D-9 can be written as

$$\begin{aligned} p_{wD2} &= \frac{1}{2} \ln \left( \frac{4t_{D2}}{e^\gamma} \right) + \left( \frac{\lambda_2}{\lambda_1} - 1 \right) \ln(r_{sD}) \\ &= 1.151 [\log(t_{D2}) + 0.351] + \left( \frac{\lambda_2}{\lambda_1} - 1 \right) \ln(r_{sD}), \end{aligned} \quad (D-10)$$

which is Eq. 3.2.11. Differentiating Eq. D-10 with respect to  $\ln(t_{D2})$  and then multiplying the resulting equation by 2 gives

$$2p'_{wD2} = 2 \frac{dp_{wD2}}{d \ln(t_{D2})} = 1. \quad (D-11)$$

Furthermore, dividing Eq. D-10 by Eq. D-11 gives Eq. 3.2.13.

**APPENDIX E**  
**DERIVATION OF BUILDUP PRESSURE EQUATION**  
**FOR A WELL LOCATED IN A**  
**MULTI-WELL SYSTEM**

The purpose of this appendix is to provide a rigorous derivation of the buildup pressure equation given in Chapter IV for a well located in a system of producing wells completed in a closed bounded reservoir, i.e., Eq. 4.2.3.

A typical multi-well system in a closed bounded rectangular reservoir is shown in Fig. 4.2.1. For the system of Fig. 4.2.1, it is assumed that well  $k$  ( $2 \leq k \leq m$ , where  $m$  denotes the total number of wells in a closed bounded reservoir) is produced at a constant rate  $q_k$  for all times and well 1, the well of interest, is produced at a constant rate  $q_1$  for times  $0 < t \leq t_p$  and a constant rate  $q_0$  for times  $t \geq t_p$ . The diffusivity equation for a three dimensional flow of a slightly compressible, single phase fluid of constant viscosity in a homogeneous, isotropic, closed bounded reservoir containing  $m$  wells, produced at the rates specified above, can be given as

$$\frac{\phi c_t}{5.615B} \frac{\partial p}{\partial t} = 1.127 \times 10^{-3} \frac{k}{B\mu} \nabla^2 p - q(t) \delta(\underline{x} - \underline{x}_1) - \sum_{k=2}^m q_k \delta(\underline{x} - \underline{x}_k), \quad (E-1)$$

where

$$q(t) = \begin{cases} q_1, & \text{for } 0 < t \leq t_p; \\ q_0, & \text{for } t \geq t_p. \end{cases} \quad (E-2)$$

Here,  $\delta(\underline{x} - \underline{x}_k)$  is the Dirac-Delta function located at  $\underline{x}_k = (x_k, y_k, z_k)$ , that is,

$$\delta(\underline{x} - \underline{x}_k) = \delta(x - x_k) \delta(y - y_k) \delta(z - z_k), \quad (E-3)$$

$\nabla$  denotes the gradient operator in a Cartesian coordinate system and  $\nabla^2 p$  is given by

$$\nabla^2 p = \frac{\partial^2 p}{\partial x^2} + \frac{\partial^2 p}{\partial y^2} + \frac{\partial^2 p}{\partial z^2}. \quad (E-4)$$

Note that in Eq. E-1, the Dirac-Delta function,  $\delta$ , is in  $1/ft^3$ , the production rate,  $q$ , is in  $STB/DAY$  and the rate is positive for production.

We wish to solve Eq. E-1 subject to following initial and boundary conditions:

$$p(\underline{x}_k, t = 0) = p_i, \quad (E-5)$$

and

$$\nabla p \cdot \underline{n} = 0. \quad (E-6)$$

Here,  $p_i$  is the initial pressure and  $\underline{n}$  is the unit outward normal vector to the reservoir boundary. Note that the boundary condition specified by Eq. E-6 is the Neumann condition; that is, there is no flux across the boundary surfaces of the reservoir.

Defining  $\Delta p$  by

$$\Delta p = p_i - p(\underline{x}_k, t), \quad (E-7)$$

and dividing both sides of Eq. E-1 by the flow rate  $q_1$ , we can rewrite the IBVP (initial boundary value problem) specified by Eqs. E-1, E-5 and E-6, respectively, as

$$\begin{aligned} \frac{\phi c_t}{5.615 q_1 B} \frac{\partial \Delta p}{\partial t} &= 1.127 \times 10^{-3} \frac{k}{q_1 B \mu} \nabla^2 (\Delta p) \\ &+ \frac{q(t)}{q_1} \delta(\underline{x} - \underline{x}_1) + \sum_{k=2}^m \frac{q_k}{q_1} \delta(\underline{x} - \underline{x}_k), \end{aligned} \quad (E-8)$$

$$\Delta p(\underline{x}, t = 0) = 0, \quad (E-9)$$

$$\nabla(\Delta p) \cdot \underline{n} = 0; t > 0. \quad (E-10)$$

Note that the units in Eq. E-8 are  $1/ft^3$ .

Letting  $A_1$  be some characteristic area,  $h$  be the total reservoir thickness and introducing the following dimensionless variables:

$$\underline{x}_D = \frac{\underline{x}}{\sqrt{A_1}} = (x/\sqrt{A_1}, y/\sqrt{A_1}, z/\sqrt{A_1}), \quad (E-11)$$

$$p_{D1} = \frac{kh\Delta p}{141.2 q_1 B \mu}, \quad (E-12)$$

and

$$t_{D1} = \frac{6.33 \times 10^{-3} kt}{\phi c_t \mu A_1}, \quad (E-13)$$

the IBVP specified by Eqs. E-8 through E-10, respectively, can be written in the dimensionless form as

$$\frac{\partial p_{D1}}{\partial t_{D1}} = \nabla^2 p_{D1} + \frac{q(t_{D1})}{q_1} \delta_D(\underline{x}_D - \underline{x}_{1D}) + \sum_{k=2}^m \frac{q_k}{q_1} \delta_D(\underline{x}_D - \underline{x}_{kD}), \quad (E-14)$$

$$p_{D1}(\underline{x}_D, t_{D1} = 0) = 0, \quad (E-15)$$

$$\nabla(p_{D1}) \cdot \underline{n} = 0; t_{D1} > 0. \quad (E-16)$$

In Eq. E-14,  $\nabla^2 p_{D1}$  is given by

$$\nabla^2 p_{D1} = \frac{\partial^2 p_{D1}}{\partial x_{1D}^2} + \frac{\partial^2 p_{D1}}{\partial y_{1D}^2} + \frac{\partial^2 p_{D1}}{\partial z_{1D}^2}, \quad (E-17)$$

and

$$\delta_D(\underline{x}_D - \underline{x}_{kD}) = 2\pi A_1 h \delta(\underline{x}_D - \underline{x}_{kD}). \quad (E-18)$$

Let  $\tilde{p}_D$  be the solution of the following IBVP:

$$\frac{\partial \tilde{p}_D}{\partial t_{D1}} = \nabla^2 \tilde{p}_D + \frac{q_1}{q_1} \delta_D(\underline{x}_D - \underline{x}_{1D}) + \sum_{k=2}^m \frac{q_k}{q_1} \delta_D(\underline{x}_D - \underline{x}_{kD}), \quad (E-19)$$

$$\tilde{p}_D(\underline{x}_D, t_{D1} = 0) = 0, \quad (E-20)$$

$$\nabla(\tilde{p}_D) \cdot \underline{n} = 0; t_{D1} > 0, \quad (E-21)$$

and let  $\hat{p}_D$  be the solution of the following IBVP:

$$\frac{\partial \hat{p}_D}{\partial t_{D1}} = \nabla^2 \hat{p}_D + \left( \frac{q_0 - q_1}{q_1} \right) \delta_D(\underline{x}_D - \underline{x}_{1D}); t_{D1} > t_{pD1} \quad (E-22)$$

$$\hat{p}_D = 0; t_{D1} \leq t_{pD1} \quad (E-23)$$

$$\nabla(\hat{p}_D) \cdot \underline{n} = 0. \quad (E-24)$$

Since  $\hat{p}_D \equiv 0$  for  $t_{D1} < t_{pD1}$ , then it can be easily shown that  $p_{D1} = \tilde{p}_D + \hat{p}_D$  satisfies

$$\frac{\partial p_{D1}}{\partial t_{D1}} = \nabla^2 p_{D1} + \frac{q_1}{q_1} \delta_D(\underline{x}_D - \underline{x}_{1D}) + \sum_{k=2}^m \frac{q_k}{q_1} \delta_D(\underline{x}_D - \underline{x}_{kD}), \quad (E-25)$$

for  $0 < t_{D1} \leq t_{pD1}$ , and satisfies

$$\frac{\partial p_{D1}}{\partial t_{D1}} = \nabla^2 p_{D1} + \left( \frac{q_0 - q_1}{q_1} \right) \delta_D(\underline{x}_D - \underline{x}_{1D}), \quad (E-26)$$

for  $t_{D1} \geq t_{pD1}$ . Therefore,  $p_{D1} = \tilde{p} + \hat{p}_D$  is the solution of the IBVP specified by Eqs. E-14, E-15 and E-16.



By using superposition and method of images, one can obtain the solution to the IBVP given by Eqs. E-19, E-20 and E-21 as

$$\begin{aligned} \tilde{p}_D(t) = & \left[ p_D(x_{1D}, t) + \sum_{j=2}^{\infty} p_D(x_{1jD}, t) + s \right] \\ & + \sum_{k=2}^m \frac{q_k}{q_1} p_D(x_{kD}, t) + \sum_{k=2}^m \frac{q_k}{q_1} \sum_{j=2}^{\infty} p_D(x_{kjD}, t), \end{aligned} \quad (E-27)$$

where  $x_{kjD}$  denotes the location of the  $j^{\text{th}}$  image well for well  $k$  for  $1 \leq k \leq m$ . Similarly, the solution of the IBVP specified by Eqs. E-22, E-23 and E-24 can be given as

$$\begin{aligned} \hat{p}_D(t - t_p) = & \left( \frac{q_0 - q_1}{q_1} \right) p_D(x_{1D}, t - t_p) + \left( \frac{q_0 - q_1}{q_1} \right) s \\ & + \left( \frac{q_0 - q_1}{q_1} \right) \sum_{j=2}^{\infty} p_D(x_{1jD}, t - t_p). \end{aligned} \quad (E-28)$$

In Eqs. E-27 and E-28,  $s$  denotes the skin factor associated with well 1, and the  $p_D$  term represents the dimensionless pressure drop that would be obtained at a single producing well with zero skin factor in an infinite reservoir.

As shown previously,  $p_{D1} = \tilde{p}_D + \hat{p}_D$  is the solution of the IBVP given by Eqs. E-14 through E-16. Thus, it follows from Eqs. E-27 and E-28 that

$$\begin{aligned} p_{D1} = & \left[ p_D(x_{1D}, t) + \sum_{j=2}^{\infty} p_D(x_{1jD}, t) + s \right] \\ & + \sum_{k=2}^m \frac{q_k}{q_1} p_D(x_{kD}, t) + \sum_{k=2}^m \frac{q_k}{q_1} \sum_{j=2}^{\infty} p_D(x_{kjD}, t) \\ & + \left[ \left( \frac{q_0 - q_1}{q_1} \right) p_D(x_{1D}, t - t_p) + \left( \frac{q_0 - q_1}{q_1} \right) s \right] \\ & + \sum_{j=2}^{\infty} \left( \frac{q_0 - q_1}{q_1} \right) p_D(x_{1jD}, t - t_p). \end{aligned} \quad (E-29)$$

If we let  $\Delta t$  be

$$\Delta t = t - t_p, \quad (E-30)$$

then

$$t = t_p + \Delta t. \quad (E - 31)$$

If well 1 is shut-in at a time  $t = t_p$  for a buildup test; i.e.,  $q_0 = 0$ , then  $p_{D1} = p_{sD}$ , the dimensionless shut-in pressure, and Eq. E-29 can be written as

$$\begin{aligned} p_{sD} = & \left[ p_D(x_{1D}, t_p + \Delta t) + \sum_{j=2}^{\infty} p_D(x_{1jD}, t_p + \Delta t) + s \right] \\ & - \left[ p_D(x_{1D}, \Delta t) + \sum_{j=2}^{\infty} p_D(x_{1jD}, \Delta t) + s \right] \\ & + \sum_{k=2}^m \frac{q_k}{q_1} p_D(x_{kD}, t_p + \Delta t) + \sum_{k=2}^m \frac{q_k}{q_1} \sum_{j=2}^{\infty} p_D(x_{kjD}, t_p + \Delta t) \end{aligned} \quad (E - 32)$$

which is Eq. 4.2.3 of the text and applies for any well/reservoir model.

**APPENDIX F**  
**BUILDUP RESPONSE OF A FINITE-CONDUCTIVITY**  
**VERTICALLY FRACTURED WELL DURING**  
**BILINEAR FLOW REGIME**

Here, we show that the analysis procedures given in Chapter IV can be extended to finite-conductivity vertically fractured wells. Specifically, we consider the buildup response of a finite-conductivity fractured well which is produced long enough to reach pseudosteady-state prior to shut-in and consider only the bilinear flow regime during buildup.

If the pseudosteady-state is reached prior to shut-in, then Eq. 4.2.4 can be written as,

$$p_{sD} = 2\pi (t_p + \Delta t)_{A_1D} + \frac{1}{2} \ln \left( \frac{4A_1}{e^{\gamma} C_{A_1} (r'_w)^2} \right) - p_{wD}(\Delta t), \quad (F-1)$$

where  $C_{A_1}$  is the shape factor and  $r'_w$  is the effective wellbore radius as defined by Eq. 3.1.73.

For sufficiently small values of shut-in time such that the drawdown term,  $p_{wD}(\Delta t)$ , is approximated well by the bilinear flow equation (see Eq. 3.1.76), Eq. F-1 becomes

$$p_{sD} = 2\pi (t_p + \Delta t)_{A_1D} + \frac{1}{2} \ln \left( \frac{4A_1}{e^{\gamma} C_{A_1} (r'_w)^2} \right) - \frac{\pi (\Delta t_{A_1D})^{1/4}}{\Gamma(5/4) \sqrt{2C_{fD}}} \left( \frac{A_1}{L_{x,f}^2} \right)^{1/4} \quad (F-2)$$

where  $C_{fD}$  represents fracture conductivity and is given by Eq. 3.1.69.

Differentiating Eq. F-2 with respect to  $(\Delta t_{A_1D})^{1/4}$  and rearranging the resulting equation in a dimensional form gives

$$-\frac{dp_{ws}}{d(\Delta t)^{1/4}} = m_{bi} (\Delta t)^{3/4} - b_{bi} \quad (F-3)$$

where

$$m_{bi} = 4m_i = \frac{0.9340qB}{\phi c_t h A_1} \quad (F-4)$$

and

$$b_{bi} = \frac{40}{\Gamma(5/4)} \frac{qB\mu}{(\phi c_t \mu)^{1/4} (k)^{1/4} h (k_f b)^{1/2}} \quad (F-5)$$

In Eq. F-4,  $m_i$  is given by Eq. 4.3.6.

Equation F-3 suggests that during bilinear flow period, a Cartesian plot of  $-dp_{ws}/d(\Delta t^{1/4})$  versus  $\Delta t^{3/4}$  will yield a straight line with slope equal to  $m_{bi}$  given by Eq. F-4 from which the well's drainage at the instant of shut-in can be obtained. The intercept at  $\Delta t = 0$  is given by Eq. F-5 from which the product  $k^{1/4}h(k_f b)^{1/2}$  can be obtained.

Using the left hand side of material balance equation in Eq. F-2 and rewriting the resulting equation in the dimensional form gives

$$p_{ws} + \frac{m_{bi}}{4} \Delta t = \bar{p} + b \ln \left( \frac{C_{A_1} e^{\gamma} (r'_w)^2}{4A_1} \right) + b_{bi} \Delta t^{1/4}, \quad (F-6)$$

where  $b$  is given by Eq. 4.3.7. During bilinear flow,  $m_{bi}$  can be computed from the analysis procedure of Eq. F-3 described above; Eqs. F-3 through F-5. To determine the average reservoir pressure, we extrapolate the straight line obtained in a Cartesian plot of  $p_{ws} + (m_{bi}/4)\Delta t$  versus  $(\Delta t)^{1/4}$  to  $\Delta t = 0$ . The intercept at  $\Delta t = 0$  is given by the following equation:

$$\left( p_{ws} + \frac{m_{bi}}{4} \Delta t \right)_{\Delta t=0} = \bar{p} + b \ln \left( \frac{C_{A_1} e^{\gamma} (r'_w)^2}{4A_1} \right); \quad (F-7)$$

that is, the average pressure  $\bar{p}$  can be determined from Eq. F-7 provided that we know the shape factor, the permeability and the fracture half-length.